



**IAHR**  
**2017**

**37th IAHR**  
**WORLD CONGRESS**  
13-18 August, 2017  
Kuala Lumpur, Malaysia

URBAN FLOOD MANAGEMENT



## OGEE WEIR CREST DEFINITION: HISTORICAL ADVANCE

WILLI H. HAGER<sup>(1)</sup> & OSCAR CASTRO-ORGAZ<sup>(2)</sup>

<sup>(1)</sup> ETH Zurich, Laboratory of Hydraulics, Hydrology and Glaciology (VAW), Zurich, Switzerland,  
hager@vaw.baug.ethz.ch

<sup>(2)</sup> University of Córdoba, Spain,  
ag2caoro@uco.es

### ABSTRACT

The design of the standard spillway crest geometry is considered based on the various advances in hydraulics from the early 20<sup>th</sup> century. Muller and Creager realized that this shape should be based on the lower nappe profile of the sharp-crested weir, so that the experimental data of Bazin served as reference. The shape was improved as the overflow depths of spillways increased, to finally reach values of up to 20 m. For these large depths, aspects of cavitation damage had to be considered, which was successfully implemented by the Spanish Abecasis in 1970. This study sketches the various elements necessary to design standard spillways in the modern dam environment; it also describes the main actors who gave their inputs with short biographies.

**Keywords:** Cavitation damage; hydraulic experimentation; Ogee-spillway; pressure distribution; standard spillway.

### 1 INTRODUCTION

Spillways count to the important elements of hydraulic engineering, given their hydraulic characteristics for upstream flow depths below the weir crest, followed by an over-proportional discharge for overflow water depths above the weir crest. The entire spillway structure is composed of various elements, including the upstream reservoir portion, the crest zone, and the tailwater reach, typically in the form of a spillway chute, but also possible as a free jet impacting the tailwater rock, or even in the form of a Morning Glory overflow. The following is restricted to the fundamental, frontal overflow structure within a rectangular crest reach and an upstream vertical spillway wall, given its basic arrangement and the widespread application in hydraulic engineering.

The fixed overflow structure has a long history, given the particular head-discharge feature. Until the early 20<sup>th</sup> century, its shape was selected mainly based on economic and constructional reasons, given that the crest shape has only a secondary effect on the discharge characteristics for relatively small heads. As the heads on the spillway crest increase to, say, above 5 m, the aspect of crest geometry becomes important, so that means were sought to hydraulically define an adequate crest shape. The foundation of this concept were determined by Frenchman Henry Bazin (1829-1917) in the late 19<sup>th</sup> century, who provided excellent test data on the lower nappe geometry of fully-aerated, sharp-crested frontal weir flow. However, Bazin did not advance the idea of using his test data for the definition of the spillway crest shape.

Currently, this idea is often related to the American William P. Creager (1878-1953), a notable hydraulic engineer who was involved in many dam projects, and is remembered by his books *Engineering for masonry dams* (1917) and *Hydro-electric handbook* (1927), written with Joel D. Justin (1881-1950). The Creager spillway crest shape is a misnomer, however, given that this idea was originally proposed in 1908 by Richard O. Muller (1881-1940), a German who moved in the early years of the 20<sup>th</sup> century to the USA. His 1908 paper deals with the "Development of a practical type of concrete spillway dam", based on the data of Bazin. Assuming that the identical crest profile is measured for the sharp-crested weir flow, atmospheric bottom pressure conditions along the spillway crest are guaranteed. This paper details these developments and compares the results with these of Creager. Figure 1 compares the flows over the sharp-crested weir with that over the corresponding standard spillway, referred to also as Ogee spillway.

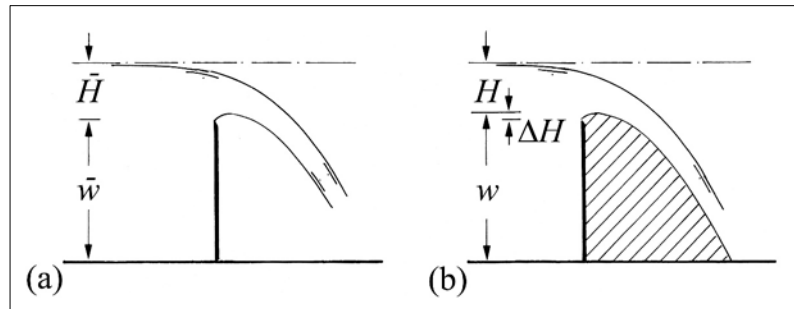


**Figure 1.** Frontal overflow structure (a) sharp-crested weir of weir height,  $w$ ; and overflow head,  $H$ ; (b) corresponding standard spillway with  $w$  as weir height up to fixed crest, and  $H$  as overflow depth so that  $H; + w; = H + w$  under design conditions.

## 2 EARLY DEVELOPMENTS

Muller (1908) states that his study is based on the work of Bazin (1898), in which six research papers are summarized in book form, detailing the (1) discharge characteristics of free weir flow, (2) upper and lower nappe geometries, (3) submerged sharp-crested weir flow, (4) details of submerged weir flow, (5) effect of crest thickness, and (6) effects of weir face slope and rounded crest. Muller further states that the crest shape is important to 'exclude all possibility of a vacuum between the face of the dam and the falling sheet of water when the discharge is at maximum'. He also noted about problems with vibrations affecting structural stability. He continues: 'Therefore, if the face is shaped in such a way as to extend inside of the lower nappe, as plotted by Bazin, it shall be safe to admit that a vacuum is impossible.' Muller noted that Bazin's data do not allow for a large range of nappe coordinates, so that his data had to be expanded to allow for a larger range of vertical extension. Figure 2a shows the upper and lower nappe profiles as given by Bazin (1898), whereas Fig. 2b shows the lower spillway profile based on the previous plot. Note that Muller (1908) also added results from Boussinesq (1887) relative to his theoretical weir flow study. Considering the crest section OA in Fig. 2a, the relative velocities  $v/(2gh)^{1/2}$  were determined to be 0.475 for the upper, and 0.946 for the lower nappe. Here,  $h$  is the head on the weir in which effects of the approach flow velocity were considered small, and  $g$  is the gravity acceleration. Muller further admitted that the average velocity in each section is located at one third of the local flow thickness, a hypothesis allowing for the plot in Fig. 2b. Muller's result is that the crest shape is defined by the dimensionally inhomogeneous curve  $y^2 = 2.3hx$ , with  $x$  as vertical, and  $y$  as horizontal coordinate. Thus, the 'practical standard spillway shape' has its origin at the maximum of the lower nappe,  $0.112h$  above the sharp weir crest, and  $0.25h$  downstream of its location. Further details can be referred to the forces and moments exerted onto the standard spillway, as well as on the reduction of horizontal pressure onto the dam. However, these are not further considered here.

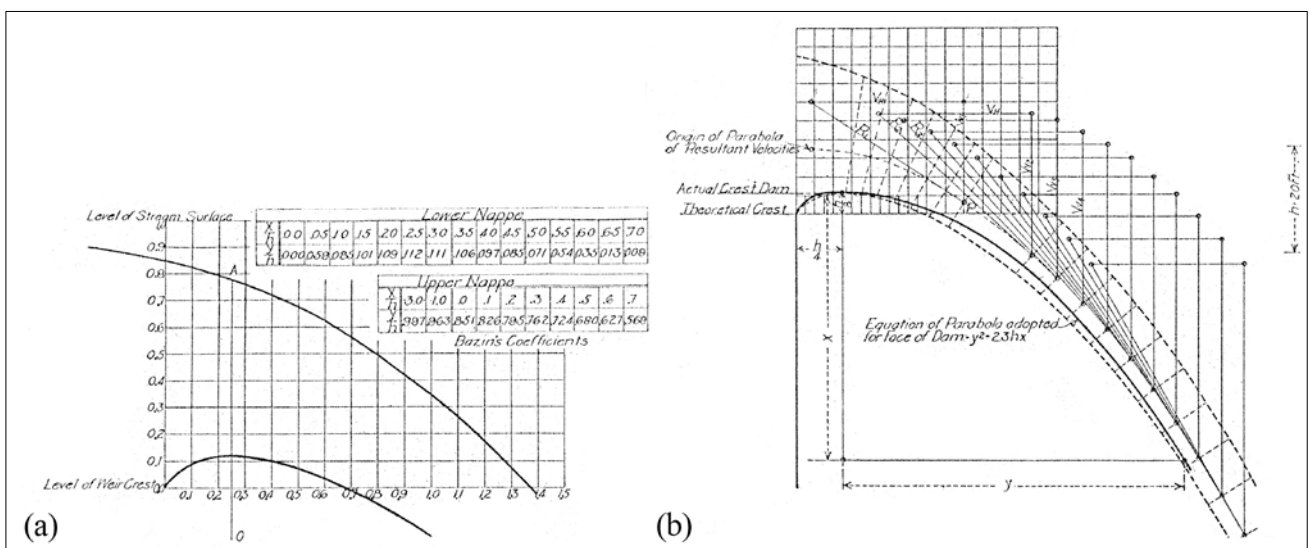


**Figure 2.** (a) Dimensionless upper and lower nappes (Bazin 1898), (b) crest zone of standard spillway (Muller 1908).

Creager (1917), without referring to Muller (1908), also noted that the crest shape of a spillway is essential to avoid low pressure zones causing structural vibrations, thereby endangering the stability of the entire dam. Referring also to the data of Bazin (1898), these are extended to define a larger range of the

overflowing jet. Upon letting the coordinate system ( $x'$ ;  $y'$ ) define the streamline of average velocity located again at one-third of the local jet thickness of the sharp-crested weir, and ( $x$ ;  $y$ ) that relating to the standard spillway, the vertical location is given as  $x' = (1/2)gt^2$ , with  $t$  as time measured from the coordinate origin. With  $v_h$  as the horizontal velocity at the origin, the horizontal distance is given as  $y' = v_h t$ . Eliminating time between these two relations defines the average jet trajectory as  $y'^2 = (2v_h^2/g)x'$ . Then, by applying the concept of Muller (1908) allows equally defining the standard spillway crest shape (Fig. 3). Note that the 'theoretical nappe' is located slightly below the dam surface crest zone for reasons of safety against low pressures. It is unclear to the present authors whether Creager adopted 'his approach' from Muller, or if this was independently obtained. Notably, both authors defined the crest profile of the standard spillway only by a plot, without any attempt to present a mathematical function. Creager and Justin (1927) took over the approach of Creager (1917), and proposed a circular arc transition of radius  $0.352h$  for the upstream quadrant.

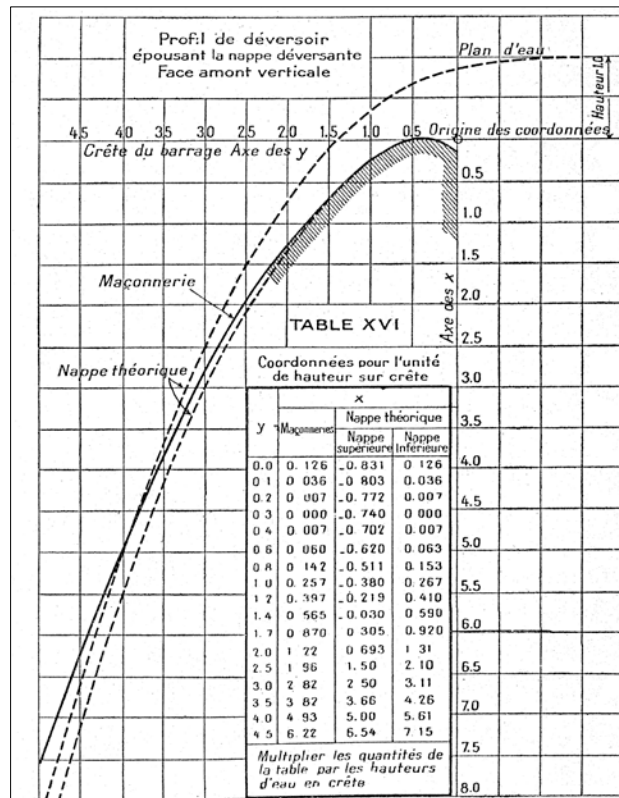


Figure 3. Crest shape of standard spillway for vertical upstream dam face (Creager 1917).

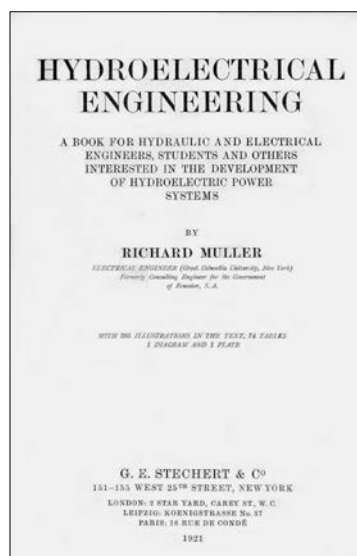


Figure 4. Title page of Muller (1921) (Hager 2015).

Richard O. Muller was born on October 17, 1881, at Stendal, Germany, and he passed away at age 63 on June 4, 1944, in New York NY. He was a graduate of Hannover University, Germany, and associated with the steam turbine industry all through his life. He initiated his career with the British Thompson-Houston Co., and the Westinghouse Co. He moved to the USA and was employed as turbine pioneer at Brooklyn NY. He was also a consultant at Washington DC. He was a consulting engineer for the Government of Ecuador, and professor of electrical engineering at University of Quito afterwards. He joined the Terry Steam Turbine Co., Hartford CT, in 1915, becoming chief engineer in 1926. Due to poor health, he retired from active work in 1943.

Muller was the true engineer having proposed to design spillways based on the lower nappe profile of sharp-crested rectangular weirs. This idea is commonly attributed to William P. Creager (1878-1953), yet Muller made this proposal as early as in 1908, when the first larger dams were erected. Muller authored in 1921 the book *Hydro-electrical engineering*, combining both civil and electrical engineering aspects. The chapters cover Stream measurement, Hydrology, Canals, Pipes, Dams, Turbines, Power house, Transmission lines, Water power projects, Hydro-electric plants, and Legislation. He was a ASME Member.



**Figure 5.** William P. Creager (Hager 2015).

William Pitcher Creager was born on September 21, 1878, in Baltimore MD, and passed away at age 75 on April 4, 1953, at Buffalo NY. He graduated in 1901 as civil engineer from the Rensselaer Polytechnic Institute, Troy NY. He was a provincial supervisor for the Philippine Government until 1904, designer of the New York State Barge Canal until 1906, draughtsman to the chief hydraulic engineer of the White Engineering Company until 1922, from when he acted as chief engineer of the New York Power Corporation. From 1931, Creager was consultant at Baltimore MD. He also served as member of the Advising Engineering Council, the Princeton University. He was a member of the American Society of Civil Engineers ASCE, and the American Institute of Consulting Engineers AICE.

Creager is particularly known for his books *Engineering for masonry dams* (1917), and the *Hydro-electric handbook* (1927) published with Joel Justin (1881-1950). Creager's name is retained for the surface profile of standard spillways ensuring practically atmospheric pressure conditions under the design discharge. Whereas up to 1900, the spillway crest profile was abrupt in curvature, Richard Muller (1881-1944) was the first to propose a crest profile of continuous curvature, to avoid local sub-pressures resulting in cavitation damage. Creager overlooked Muller's earlier proposal. Both designs are based on detailed observations of the lower nappe profile of sharp-crested 2D weir flow. Creager was a successful general engineer not involved in detailed hydraulic computations. His books may be regarded as excellent examples prior to World War II having had a large influence on the golden years in dam engineering.

### **3 ADVANCES UNTIL AFTER WWII**

The famous hydraulic engineer Rouse investigated with a colleague the question of dam crest shape in one of his first research projects (Rouse and Reid 1935). The three main criteria for spillway design are stated to be: (1) Maximum discharge passes with the least reservoir elevation increase, (2) structure be both stable and economic under all flow conditions, and (3) effect of crest geometry should be better known. Based on Rouse's thesis for the advanced engineering degree (Rouse 1932), the optimum design of the dam crest geometry was analytically studied. The research conclusions were experimentally verified by Reid (1934) in the River Hydraulics Laboratory of MIT. The purpose of the paper of Rouse and Reid (1935) was stated to check the proposal of Creager relative to the crest shape of standard spillways. The questions posed include: (1) Will the discharge really be uninfluenced by the presence of the solid bottom boundary?, (2) Is the pressure between the spillway face and the nappe really atmospheric?, (3) Under what conditions would the falling sheet spring free?, (4) Does the selected lower nappe profile provide the maximum discharge coefficient?, and (5) How much leeway in design is possible without seriously affecting the flow conditions?

Figure 6a shows a spillway conforming to the ventilated nappe of a sharp-crested weir. It is noted that the flow is affected by the weir geometry and the three independent forces gravity, viscosity and surface tension.

The gravity effect becomes relevant if the head on the weir is sufficiently large, yet at that time to an unknown absolute length. Experiments were conducted with a sharp-crested, vertical weir 0.40 m high under a head of 0.08 m, to study the pressure and velocity distributions. Based on the measured lower nappe of this set-up, the corresponding spillway was accurately reproduced in concrete and provided with 11 pressure tapings along the crest zone. It was noted that the discharge was by 3% lower than that over the weir, and that positive pressures prevailed along the crest zone, as shown in Fig. 6b (Profile I). This effect was removed by rubbing down the near vertical upstream face of the spillway by an amount equal to the weir crest width of 0.5 mm. The resulting boundary pressure heads were significantly different for Profiles I and II. For the latter, the discharge was only 0.7% smaller than the corresponding weir, and the pressure was almost exactly atmospheric. The authors stated that these conditions apply exclusively for the so-called spillway design (subscript  $d$ ) head,  $H_d$ , whereas for  $H < H_d$  the discharge coefficient is smaller and the pressure larger than that for  $H/H_d=1$ , and vice-versa for  $H/H_d > 1$ .

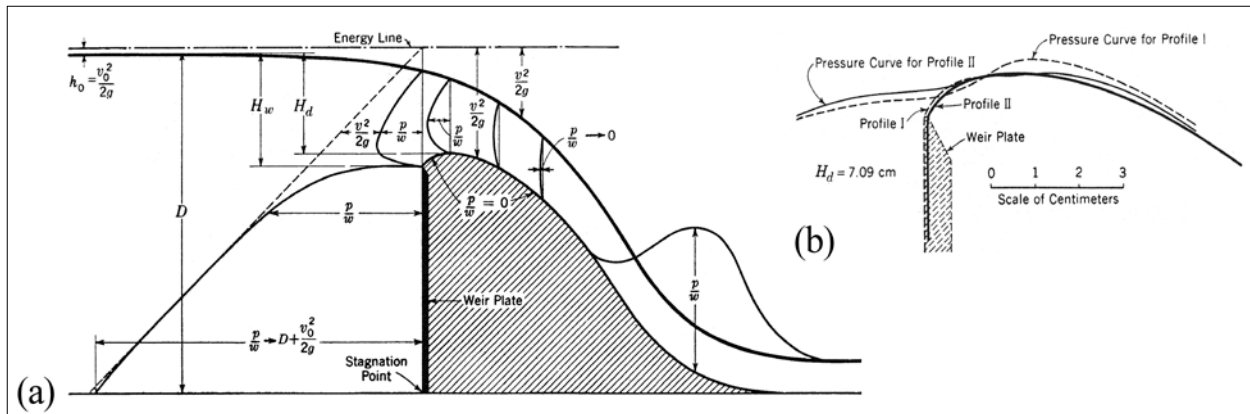


**Figure 6.** (a) Schematic view of spillway conforming to ventilated lower nappe of sharp-crested weir, (b) crest zone of model spillway and measured pressure distributions for Profiles I and II (Rouse and Reid 1935).

Figure 7 shows the free surface and pressure head profiles for the crest Profile II and six different discharges, for  $H_d=0.0709$  m. The relative heads thus varied between  $0.154 \leq H/H_d \leq 1.564$ . Note that the stagnation point at the bottom of the weir (Fig. 6a), so that the corresponding pressure is equal to the total approach flow energy head. As the weir crest is approached, the pressure on the weir reduces to exactly 0 at the crest for  $H/H_d=1$ .

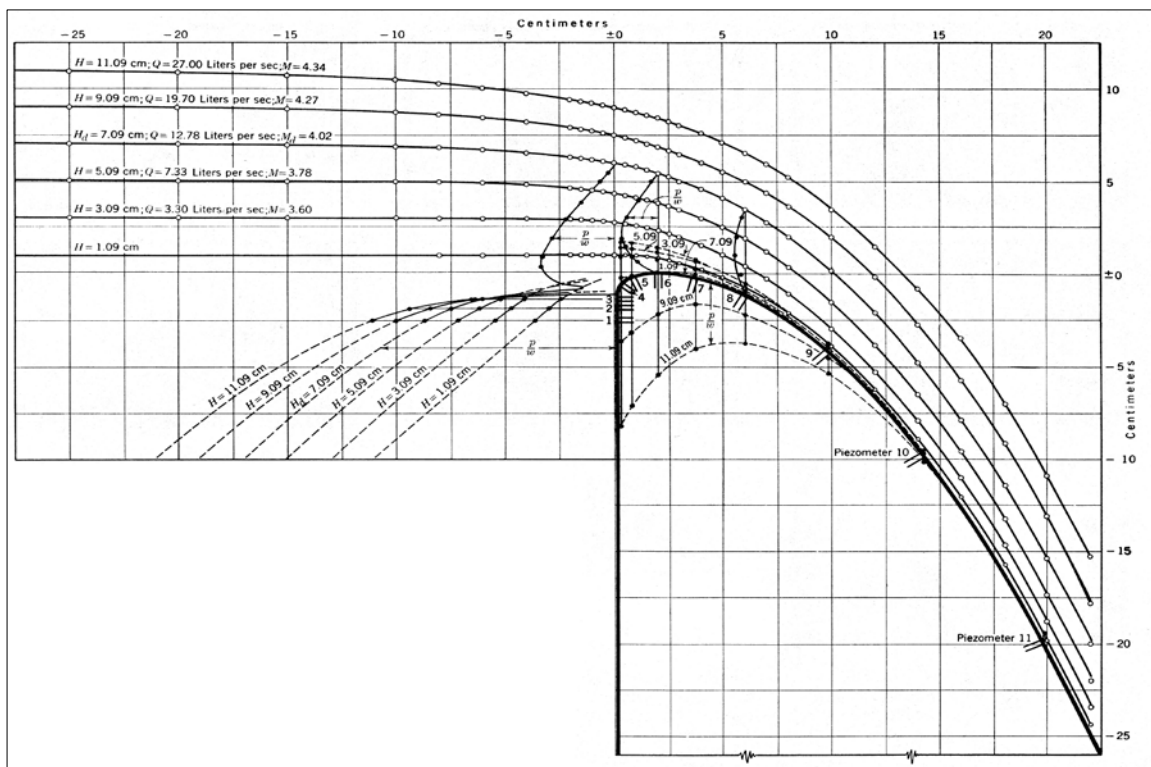


**Figure 7.** Free surface and pressure head profiles for six discharges (Rouse and Reid 1935).

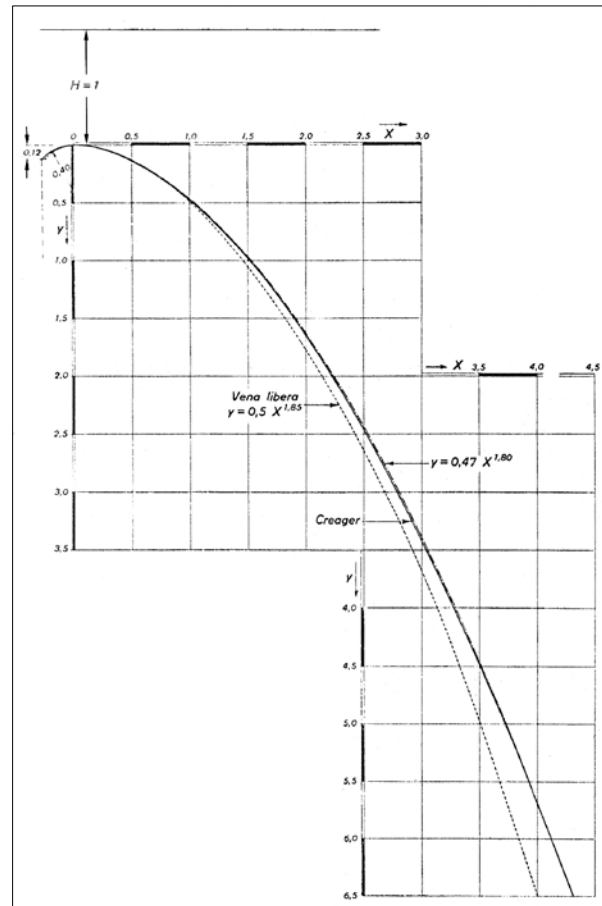


**Figure 8.** Lower nappe profile and Creager's spillway profile along with upper quadrant circular arc (Scimemi 1937).

The (dimensional) coefficient of discharge  $M$  of the weir flow formula  $Q=MBH^{3/2}$  with  $Q$  as discharge,  $B$  as weir width and  $H$  as head on the spillway was of primary importance. The measured  $M$ -values are indicated in Fig. 7. The  $M$ -value of  $3.89 \text{ [ft}^{1/2}/\text{s]}$  for the design condition was almost exactly that of the corresponding weir flow test, and agreed well with the data of Bazin (1898). The effect of the relative head  $H/H_d$  on the  $M$ -value was also successfully compared with the data of Creager (1917) and of Dillmann (1933), referred to as Munich. According to the latter observations, the flow separates from the spillway crest if the relative head is increased above  $H/H_d=3$ . Note that these indications only apply for almost zero approach flow conditions, i.e. the head on the spillway is much smaller than the spillway depth  $D-H_w$  (Fig. 6a). Rouse and Reid (1935) concluded that a spillway should be designed for  $H/H_d>1$  to take advantage of the increased discharge coefficient, yet without a final proposal. This effect will be discussed below. However, they stated that the critical pressure head zone is located upstream of the spillway crest, because it is where extremely low pressure occurs at larger values of  $H/H_d$  (Fig. 7). It is further stated that flow separation from the spillway crest by blowing air into the crest zone never occurred for  $H/H_d\leq 1.6$ , so that this is of no concern if the crest zone is designed according to Profile II. In conclusion, the study of Rouse and Reid (1935) is considered as an outstanding work in hydraulics.

Scimemi (1937) studied the spillway crest profile based on his earlier observations of the lower nappe profiles of rectangular, 2D weirs (Hager and Boes 2015). Let the Cartesian coordinate system be defined with  $(x; z)$  whose origin is located at the sharp weir crest, with  $y$  measured positively downwards. Scimemi's data cover relative horizontal coordinates from  $x/h=-0.5$  to 4, and relative vertical coordinates from  $y/h=-1$  to 5, i.e. much larger than until then available. His weir height was  $4h$ ; absolute heads of 0.044, 0.088 and 0.132 m were tested. The data relating to the upper and lower nappes do not reveal scale effects, so that the currently adopted minimum head of 40 to 50 mm appears sufficient to avoid scale effects (Castro-Orgaz and Hager 2014). Upon transforming the weir nappe data to these of the standard spillway, whose head is equal to  $H_d$ , and using the dimensionless coordinates  $X=x/H_d$  and  $Y=y/H_d$ , the lower nappe profile is reproduced as  $Y=0.50X^{1.85}$ , whereas the numerical values of Creager (1917) follow the curve  $Y=0.47X^{1.80}$ . The latter curve is located slightly above the former for safety reasons, to assure a slightly positive crest pressure at the spillway design condition. The bottom pressure curves were carefully measured on the model spillway for relative heads from  $H/H_d=0.68$  to 1.10. The latter value then had an atmospheric bottom pressure at  $x/H_d\approx 0.70$  locally, confirming the above safety criterion. Scimemi (1937) proposed to design the upstream quadrant with

a curvature radius of  $0.40H_d$ , from the coordinate origin to  $Y=0.12$ , i.e. the location of the corresponding sharp weir crest. Figure 8 shows both the two lower nappe profiles, and the details of the upstream quadrant. Scimemi thus was the first to propose analytically the entire crest geometry. His work is also contained as Discussion of Randolph (1938), who conducted tests both on models and on the prototype of Madden Dam at Panama Canal. He proposed a two-arc curve for the upstream quadrant, of radii  $0.50H_d$  and  $0.20H_d$ , respectively. The effect of a sloping upstream weir face was considered, and an expression for the coefficient of discharge was provided. Castro-Orgaz and Hager (2017) explain the shape of the spillway crest profile based on the non-hydrostatic Boussinesq equations by resorting to the critical flow theory.

Another experimental study on the effect of both the up- and downstream weir face slopes on the coefficient of discharge was conducted by the Russian, Offtizeroff (1940). The upstream weir face angle varied from  $15^\circ$  to  $90^\circ$  (vertical), whereas the downstream angle ranged from  $56^\circ$  to  $10^\circ$ . The test data are available in Tables, yet no data fit equations were proposed. The effect of spillway submergence on the discharge features was also discussed. The discussers of this work had doubts on various findings, yet the author provided no Closure.

Ferroglio (1941) repeated the tests of Scimemi (1937) with a model spillway 0.363 m high, of design head 0.1066 m and of vertical front face. A total of 16 pressure tapings were provided along the vertical face, the spillway crest zone and the tailwater face. A second model of reduced spillway height of 0.08 m was tested to detect possible effects of the approach flow velocity. The discharge coefficient  $\mu = Q/[B(gH^3)^{1/2}]$  was found to vary considerably between the two models, with the smaller spillway height by about 10% higher than for 0.363 m. As to the bottom pressure distributions, similar findings as these of Rouse and Reid (1935), and Scimemi (1937) resulted. At design head, the pressure head was almost exactly atmospheric in both models.

The knowledge on spillway design was summarized in a Symposium (1944) organized by the American Society of Civil Engineers (ASCE). On a total of 117 pages, 10 papers were presented. Here, the following are relevant: Spillway discharge coefficients for Norris Dam by G.H. Hickox, Pressure heads on Bonneville Dam by J.C. Stevens and R.B. Cochrane, and Meter measurements of discharge for the University Dam by E. Soucek. Hickox studied the effect of drum gate presence on the discharge coefficient, finding a reasonable agreement between model and prototype data. However, a similar task was attempted by Stevens and Cochrane, who used vertical plate gates. Given the large velocities below the gate, they were unable to measure the pressure head at the spillway crest zone. The study of Soucek mainly explored the submergence effect. A comparison between model and prototype data was successful yet no fit equations to the data were provided. The discussion to these papers is extensive, as was typical for the era. The results of the original studies were often complimented by these discussions, a fact that is almost completely forgotten today in favor of the Journal Impact Factor.

Given that the short biographies of Hunter Rouse (1906-1996) and Ettore Scimemi (1895-1952) are included in Hager and Boes (2015), these will not be repeated here.



**Figure 9.** Luigi Ferroglio (Hager, 2003).

Luigi Ferroglio was born on May 25, 1905, in Torino, Italy, and passed away at age 68 on May 16, 1970, at Villastellone, Piedmont, Italy. He was educated as a civil engineer at the *Università di Torino* and obtained his PhD title in the mid-1930s. His first works were on Venturi meters for discharge measurement, weir flows during World War II, and siphons by the end of the war. In 1946, he submitted an experimental work on V-notches for discharge measurement. This, in a way complimented earlier work on so-called circular weirs, which have not turned out valuable because of constructional difficulties. Ferroglio was an outstanding experimental engineer contributing to various aspects of hydraulic engineering. His observations on the pressure distribution of standard spillway flows were conducted at about the same time as in the USA. He advanced the condition of design head of these hydraulic structures, for which the pressure distribution on the

solid surface is exactly atmospheric. Ferroglia was a Lecturer at the Engineering Faculty of Torino University from 1935, and was appointed professor of hydraulic structures in 1940. He was also involved with public works, and had a passion for agricultural hydraulics.

#### 4 POST-WAR ADVANCES

At the end of WWII, the principles of standard spillway design were clarified, yet several details had to be studied, including for instance, the effects of gate or pier presence at the crest zone, and also the more complete definition of the final crest shape to be adopted. The location of the absolute minimum pressure heads along the crest zone was also not clear, therefore, additional research was conducted to fill in these research gaps.

The research of Smetana attempted to solve both questions relating to the lower nappe profile of a sharp-crested rectangular weir (not to be further detailed here), and the shape of the standard spillway crest (Smetana 1949). He notes that the proposal of Creager (1917) compares well with the accurate model data of Scimemi (1937). For additional safety against low-pressure zones, Smetana includes a supplementary 10% margin, although Creager (1917) has already added a similar increase. Smetana (1949) then discusses three cases of large dams (Dams A, B, C) studied at the Prague Hydraulic Laboratory of height 29, 39 and 18 m above the dam foundation. The overflow depth for Dam A was 1.55 m, without further details. Dam B had an average overflow depth of 1.17 m. Detailed model observations again resulted in positive pressures along the entire crest zone when adopting Creager's crest shape. Dam C had a maximum overflow depth of 4.95 m for the design discharge of 2,400 m<sup>3</sup>/s. The 100 m wide crest zone was subdivided into five passes, each 20 m wide.

Smetana (1949) then details the discharge coefficient as a function of the relative head  $H/H_d$ , as previously attempted, yet again without proposing an analytical relation. He also addresses the question of optimum dam crest width and maximum overflow depth, yet without a final proposal. As to the material to be used for the spillway, concrete is favored to create the least cracks and to obtain the best surface smoothness. Gates positioned on the spillway crests are stated to be a risk for maximum overflows, so that they should be avoided except for cases when they represent a significant gain for reservoir operation. Model observations revealed that the gate presence does not affect the pressure conditions along the spillway bottom. This study therefore does not only include the hydraulic, but also the constructional principles for successful dam crests.

Grzywiński (1950, 1951) studied the 'overhanging' overflow structure because it represents the optimum spillway shape to be adopted. Figure 10 shows his model weir, whose height was 0.50 m, and the design head was 0.10 m. The overhanging profile has advantages relative to the standard crest, but differences remain small. Figure 11 shows the model findings relative to the free surface profiles, the pressure head profiles and the discharge coefficients for various unit discharges, as noted in the plot, whose details are described as below.

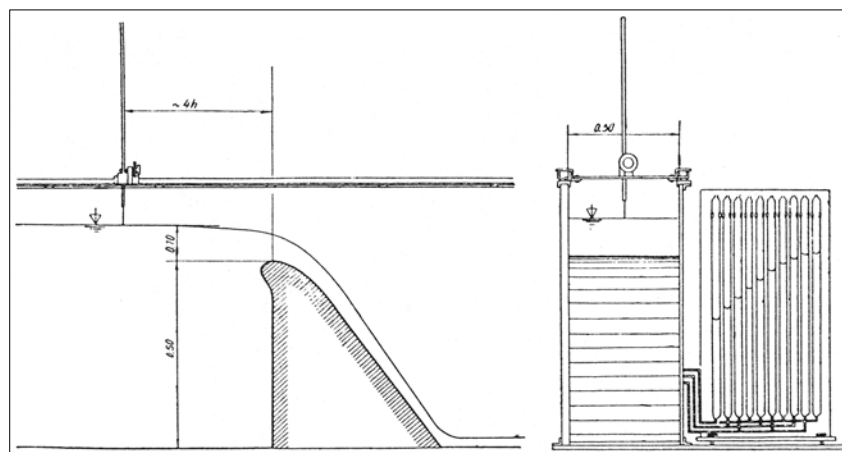
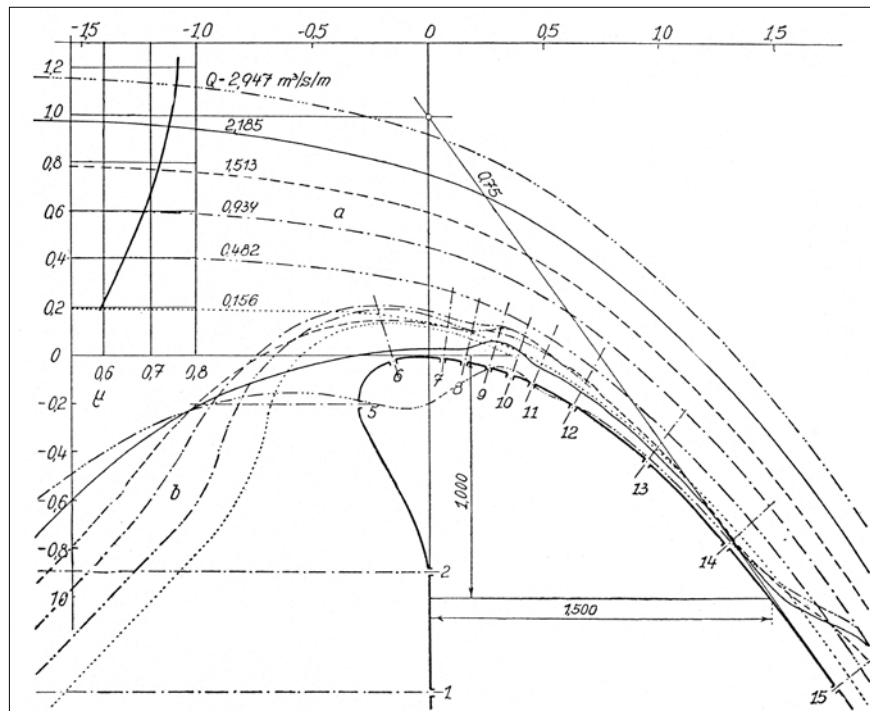


Figure 10. Scheme of model setup of Grzywiński (1950) with streamwise view (left) and cross-section view (right).

Grzywiński found no submergence effect if the tailwater elevation is below 75% of the weir height. Next, the effect of the approach flow velocity is found to be small if the weir height is more than double the overflow depth. The effect of surface roughness on the discharge coefficient depends on the ratio of sand roughness height to overflow depth, which should be below 1/100. As to the discharge coefficients for the overhanging spillway profile, minute differences with the previous results were found. Similar comments apply for the two spillway profiles, yet the overhanging profile was described as the hydraulic and economic optimum. These indications support earlier findings, leading to a safe design basis of spillway crests of large dams.



**Figure 11.** Free surface and pressure head profiles for overhanging spillway profile (Grzywnski 1950).

Escande (1951, 1953) supported the Creager spillway crest shape given that it corresponds to the optimum in terms of both crest pressure distribution and discharge coefficient,  $m$ . Tests were conducted at the Toulouse Hydraulic Laboratory, involving a channel 1 m wide and 2.05 m deep, in which a 1.7 m high Creager spillway profile of design head 0.14 m was inserted. The relation between  $m$  and the relative head  $H/H_d$  increases almost linearly up to  $H/H_d=1$ , from when it tends to a maximum at  $H/H_d=2$ , some 10% higher than that for  $H/H_d=1$ . Next, the free surface and bottom pressure head profiles are specified for relative heads  $H/H_d$  ranging from 0.25 to 2.25. It was noted that the flow does not separate from the spillway bottom even if air is injected for  $H/H_d < 1.6$ . For higher relative heads, flow separation occurred so that these should be avoided. These conditions occur if large logs of wood pass over the crest, or by the presence of piers supporting gates or bridges. A systematic test procedure on the prolongation of sills into the upstream portion revealed that, for  $H/H_d \leq 1.65$ , these should at least be equal to the design head,  $H_d$ . Next, the effect of a sector gate placed on the spillway crest was studied using the same model, attached to a pier 0.06 m wide, of frontal radius of 0.03 m, and projecting 0.30 m into the upstream portion. The test program involved relative gate openings and relative heads, to study the bottom pressure distributions under gate presence. It was found that the gate presence has no negative effect on the bottom pressure distribution if the above criterion  $H/H_d \leq 1.65$  is adhered. As mentioned previously, Escande's study thus mainly added to the design practice of dam overfall structures.

Cassidy (1970) and the many discussions to his paper led to a temporarily completed state-of-the-art. The notions 'standard shape' and 'standard spillway' were introduced describing the dam profile of atmospheric pressure distribution at design head. According to Cassidy (1970), the US Army Corps of Engineers (1965) have provided by then the last equations for the entire crest profile, including the Creager curve, and a complicated expression for the upstream quadrant. Cassidy's purpose was to present an approach for 'under-designing' spillway crests to take advantage of increased discharge capacity. It is stated that both the discharge coefficient and the minimum pressure head along the spillway crest depend exclusively on the relative spillway height, and the relative head,  $H/H_d$ . As previously, the spillway height was found to have no effect on these parameters if it is  $> 5H_d$ . The relative pressure head,  $h_p/H$  was found to be linearly reduce with increasing  $H/H_d$ .

The discussion of this paper is relevant, particularly that of Abecasis (1970). He proposed a three circular arc profile for the upstream quadrant instead of the one- or two-arc transitions, of radii 0.5, 0.2 and  $0.04H_d$  from the spillway crest to the upstream direction, to counter problems with cavitation damage. Abecasis appears to be the first with a definite proposal to reduce this risk. He also stated that the incipient vapor pressure head in prototype applications is around  $-7.6$  m due to impurity of water, instead of  $-10$  m for pure water. The proposed design procedure for high standard spillways thus includes both hydraulic and cavitation aspects. Based on the bottom pressure distribution for the improved spillway crest shape, involving the three-arc and the Creager transition for the up- and downstream quadrants, a plot is presented relating the relative head on the spillway to the absolute head to exclude cavitation damage. Typical values are  $H < 2$  m for

$H/H_d=2$ ,  $H<10$  m for  $H/H_d=1.6$ , and  $H<20$  m for  $H/H_d=1.4$ . These indications complete the design of the basic standard spillway with a vertical upstream wall, negligible velocity of approach, and absence of piers and gates on the crest zone.



**Figure 12.** Jan Smetana (Hager, 2003).

Jan Smetana was born on May 12, 1883, at Svobodne Dvory, and passed away at age 79 on August 13, 1962, at Prague. He graduated from the Czech Technical College at Prague and was a Lecturer at the Prague Hydraulic Engineering Institute from 1905 to 1911. He was then active in both the Bohemian River Regulation Commission and the Hydrographical Department, Prague Municipal Authority. He headed from 1920 to 1936 the State Hydrological Institute in Prague, setting up its engineering research station. He was a professor at the Czech University of Technology, Prague from 1936 to 1958. He was elected to the Czech Academy of Sciences in 1938, becoming a full member in 1946. Smetana founded the National Institute for Hydrology and Hydrotechnics (VUV). Known for his works in hydraulic structures, he developed the surface profile of gate flow in rectangular channels. He also studied submerged hydraulic jumps downstream of gates. Smetana presided over the technical section of the Czechoslovak Academy of Sciences since 1955, was an IAHR founding member and an honorary president of the International Association of Scientific Hydrology IASH. He was awarded the Klement Gottwald state prize in 1958, and the Order of the Czech Republic.



**Figure 13.** Anton Grzywienski (Hager, 2003).

Anton Grzywienski was born on October 3, 1898, at Truava in today's Czech Republic, and passed away at aged 84 years on April 8, 1982, at Baden/Vienna. He obtained his civil engineering degree from the Vienna Technical University in 1920, was a practicing engineer in Dutch India until 1924, returned to Vienna and was a consultant from 1931 to 1938. He submitted a PhD-thesis to his Alma Mater in 1929, and started lecturing in 1935. After World War II, he was appointed hydraulic professor at TU Vienna, from where he retired in 1971. Grzywienski was also concerned with hydraulic practice. He collaborated for the power plants Schwabeck and Maribor on Drau River, and Ybbs-Persen-beug on Danube River. His research interests included gates and spillways. He received the Fermat Medal from Toulouse University and was a corresponding member of Toulouse Academy. He was honorary member of the German Water Resources and Water Power Association since 1961, recipient of Prix Mahyer of *Académie des Sciences*, Paris, IAHR Council Member, and awarded in 1964 the honorary doctorate from Toulouse University.



**Figure 14.** Léopold Escande (Hager, 2003).

Léopold Escande studied at Toulouse University mechanical engineering, receiving the PhD degree in physics in 1929, from when he was a professor there, and from 1941 to 1972 as Director of *Ecole Nationale Supérieure*. In 1954, he took over as Secretary General of the *Conseil Supérieure de la Recherche Scientifique et Technique*. He has largely published in hydraulics, mainly on open channel hydraulics and losses in pipe flows. He collaborated with Charles Camichel (1871-1966) on the hydraulic similitude and on weir flow as early justifications for the applicability of hydraulic modelling. His books on open channel flows with a discussion of various hydraulic experiments such as the types of gate flow, or water hammer effects have received attention. Escande was a member of *Académie des Sciences, Institut de France* from 1954, received honorary doctorates from seventeen foreign universities, and the honorary professorship from three South-American universities. He was, among other, president of the International Association for Hydraulic Research IAHR. He was awarded the Chevalier's Cross of *Légion d'Honneur* in 1948, and was an Officer of the Order from 1956.

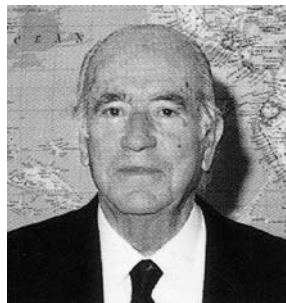


**Figure 15.** Fernando M.M. Abecasis (Hager, 2009).

Fernando Maria Manzanares Abecasis was born on August 30, 1922, in Madrid, and passed away at age 81 on October 12, 2003, in Lisbon. He was educated as a civil engineer at the Lisbon Instituto Superior Técnico IST and was a professor of hydraulic engineering from 1956. From 1948, he headed the Hydraulic Division of the LNEC Laboratory. Abecasis was a Member of the PIANC Committee on waves and seiches action, and also of the coastal hydraulics Committee of IAHR. He also served as consultant for the Hidrotécnica Portuguesa. Abecasis had a career similar to his brother's, both in research and consulting, therefore, both were leading hydraulic engineers of Portugal. Abecasis investigated the morning glory spillway in 1955, which have a potential for large under-pressure along with flow instability and cavitation damage. From then, only free flow was recommended for the design discharge so that no dangerous low-pressure zones occur along the entire hydraulic structure, from the intake usually in a reservoir to the outlet upstream from a stilling basin. Abecasis proposed an alternative design for the spillway crest geometry of the standard overflow structure in 1961. He observed large under-pressures upstream from the crest section and therefore proposed the three-radius design for the upstream quadrant, so that the limit unit discharge could be increased.

## 5 CONCLUSIONS

The design of the standard spillway crest as a main element of hydraulic engineering is considered based on the various proposals from the early 20<sup>th</sup> century up to 1970. Aspects including the safety and economy of design are highlighted, along with questions of the optimum crest shape in terms of discharge capacity and particularly means to control negative bottom pressures. It is noted that the optimum crest shape should closely follow the lower nappe profile of the sharp-crested weir, and that the minimum crest pressures

occur in its rising portion, so that the three-arc upstream quadrant crest shape appears to be an adequate design basis. In parallel, the researchers having advanced this problem are presented with short biographies, in which their educational background, their career highlights, their interests in hydraulic research, and their decorations are listed.

## REFERENCES

- Abecasis, F.M. (1970). Discussion of Designing Spillway Crests for High-Head Operation. *Journal of the Hydraulics Division*, ASCE, 96(12), 2654-2658.
- Bazin, H. (1898). *Expériences sur l'écoulement en déversoir exécutées à Dijon de 1886 à 1895 (Tests on weir flow executed at Dijon from 1886 to 1895)*. Dunod: Paris (in French).
- Boussinesq, J. (1887). *Sur la théorie de l'écoulement par un déversoir en mince paroi, quand il n'y a pas de contraction latérale et que la nappe déversante est libre en dessous (On the theory of sharp-crested weir flow, without lateral contraction and for free overflow)*. Comptes Rendus, Académie des Sciences, Paris 105, 17-22. (In French).
- Cassidy, J.J. (1970). Designing Spillway Crests for High-Head Operation. *Journal of the Hydraulics Division*, 96(3), 745-753.
- Castro-Organ, O. & Hager, W.H. (2014). Scale Effects of Round-Crested Weir Flow. *Journal of Hydraulic Research* 52(5), 653-665.
- Castro-Organ, O. & Hager, W.H. (2017). *Non-hydrostatic free surface flows*. Advances in Geophysical and Environmental Mechanics and Mathematics., Springer: Berlin, 1-696. (In press).
- Creager, W.P. (1917). *Engineering for Masonry Dams*. John Wiley and Sons, New York, U.S.A., 1-281.
- Creager, W.P., Justin, J.D. (1927). *Hydroelectric Handbook*. John Wiley and Sons, New York, U.S.A.,
- Dillmann, O. (1933). Untersuchungen an Überfällen (Weir investigations). *Mitteilung* 7, 26-52. Hydraulisches Institut, Technische Hochschule München: München (in German).
- Escande, L. (1951). Barrages-déversoirs à seuil Creager déprimé (Dam Overflows of Depressed Creager Shape). *Le Génie Civil* 128(4), 69-72, 128(5), 86-89. (In French).
- Escande, L. (1953). Nouveaux compléments d'hydraulique (New Complements of Hydraulics). *Publications Scientifiques et Techniques du Ministère de l'Air* 280. Magasin SDIT: Paris (In French).
- Ferroglio, L. (1941). Alcune osservazioni sul deflusso sopra le dighe tracimanti (Observations on the Overflow of Dams). *L'Energia Elettrica* 18(7), 455-459. (In Italian).
- Grzywnski, A. (1950). Über die Wahl des Profils bei vollkommenen Überfällen (On the profile selection of free overfalls). *Österreichische Bauzeitschrift*, 5(7), 111-114, 5(8), 130-136. (In German).
- Grzywnski, A. (1951). Anti-Vacuum Profiles for Spillways of Large Dams. *Proceeding 4<sup>th</sup> ICOLD Congress*, New Delhi 12(19), 105-124.
- Hager, W.H. (2015). *Hydraulicians in the USA*. Taylor & Francis, London.
- Hager, W.H., Boes, R.M. (2015). Spillway Jet: Historical Advance from Weir toward Standard Spillway. *Proceeding 36<sup>th</sup> IAHR World Congress the Hague* (79815), 1-8.
- Muller, R. (1908). Development of a Practical Type of Concrete Spillway Dam. *The Engineering Record* 58(17), 461-462, Discussion 59(3), 83-84.
- Muller, R. (1921). *Hydroelectrical engineering*. New York, G. E. Stechert & Co, 1-457.
- Offitzeroff, A.S. (1940). Model Studies of Overflow Spillway Sections. *Civil Engineering* 10(8), 523-526.
- Randolph, Jr., R.R. (1938). Hydraulic Tests on the Spillway of the Madden Dam. *Transaction in ASCE*, 103, 1080-1132.
- Reid, L. (1934). An Experimental Study of a Spillway Conforming to the Measured Lower Surface Nappe of Flow over a Rectangular, Suppressed, Sharp-Crested Weir. *MSc Thesis*, Dept. of Civil Engineering, Massachusetts Institute of Technology, Cambridge MA.
- Rouse, H. (1932). The Distribution of Hydraulic Energy in Weir Flow with Relation to Spillway Design. *MSc Thesis*, Massachusetts Institute of Technology, Cambridge MA.
- Rouse, H., Reid, L. (1935). Model Research on Spillway Crests. *Civil Engineering* 5(1), 10-14.
- Scimemi, E. (1937). Il profilo delle dighe sfioranti (The Profile of Overflow Structures). *L'Energia Elettrica* 14(12), 937-940. (In Italian).
- Smetana, J. (1949). Etude de la surface d'écoulement des grands barrages (Study on the Flow Surface of Large Dams). *Revue Générale de l'Hydraulique* 15(46), 19-32. (In French).
- Symposium (1944). Conformity Between Model and Prototype. *Transaction ASCE* 109, 2-193.
- US Army Corps of Engineers (1965). *Hydraulic Design of Spillways*. Engineer Manual EM 1110-2-1603. Department of the Army, Office of the Chief of Engineers, Washington DC.

## POTENTIALS AND CONSTRAINTS OF URBAN POLDER DEVELOPMENT IN JAKARTA, INDONESIA. CASE STUDY: RAWA BADAK POLDER

HARYO ISTIANTO <sup>(1)</sup>, FRANSISCUS X. SURYADI <sup>(2)</sup> & SUMI AMARIENA HAMIM <sup>(3)</sup>

<sup>(1)</sup>Ministry of Public Works and Housing, Jakarta, Indonesia  
Haryoistianto@gmail.com

<sup>(2)</sup>Department of Water Science and Engineering, UNESCO-IHE Institute for Water Education, Delft, the Netherlands;  
f.suryadi@unesco-ihe.org

<sup>(3)</sup>IGM University, Palembang, Indonesia  
sumi\_amariena@uigm.ac.id

### ABSTRACT

Jakarta as the capital city of Indonesia has developed urban polder systems to solve inundation problems in Jakarta. However, the inundation still occurred due to inadequate polder components, lack of the maintenance and land availability for polder development. The capacity of the polder system in Jakarta needs to be analyzed by investigating its potentials and constraints. Based on the analysis, conclusion and recommendations are proposed. Rawa Badak Polder in the north of Jakarta bay was selected as the study area. It is used to represent the polder issues in Jakarta. Polder components such as, dikes pumps or the open water storage were evaluated. Moreover, to deal with land availability for the demand of the open water storage in the dense area, Sustainable Urban Development System (SUDs) application of temporary retention basin was used. Based on the analysis, urban polder in Jakarta has met with many constraints during the development process such as lack of operation and maintenance, inadequate polder component and unavailability of space for polder component expansion. In the other side, the development of urban polder in Jakarta has been supported by topographical condition, road and river networks. In the existing condition, inundation still occurs in Rawa Badak Polder due to inadequate polder water management components. Dike does not cover the entire service area, pump capacity and open water storage were too small in comparison with the total service area. Dike utilization in Rawa Badak Polder reduce 40% of the inundation area. It shows that the independent hydrological condition in polder system is absolutely needed. Lower initial water levels at 1.5 m below the surface reduce the inundation area and bring the dynamic storage effect, thus the retention capacity is increased. By using the graphic relation between pump capacity and open water area, one of the solution to cope inundation is to increase the pump capacity up to 16 m<sup>3</sup>/s or increase the open water area up to 2.5%. SUDs application can be used as an approach to reduce the demand of the open water storage in Rawa Badak Polder. The combination between proper polder water management components design (dikes, open water storage, pumping and outlet capacity), good operation (proper initial condition) and the maintenance and SUDs application will solve the Inundation problem in Rawa Badak Polder. Based on this study, it can be concluded that urban polder development can be considered as one of the options to manage the flood problems especially in the northern part of Jakarta. With proper polder components design and SUDs application, the constraints of polder development can be overcome. Nevertheless, final solution should also consider about the economy and environmental analysis of the area.

**Keywords:** Urban Polder; water management components; flood protection; drainage; SUDs.

### 1 INTRODUCTION

Jakarta as the capital city of Indonesia and the central of economy needs to be protected from any inundation; where the characteristic of topography with low-laying flat lands and low gravitational drainage ability has potentials and is appropriate for urban polder development. Even though polders have been established in Jakarta, inundation still occurs annually. This condition happens due to some of the urban polder constructions in Jakarta is often not conducted based on a well-planning or approach between land use utilization and required polder components. Development of polder in Jakarta has constraints such as inadequate polder components, lack of operation and maintenance of the drainage systems, making inundation problems more complicated.

Most of the existing polders system in Jakarta cannot solve the inundation problem due to lack of polder components such as small retention area in the large service area, dikes do not cover all service area and small canals. The requirement of polder component expansion in order to deal with inundation problem has met with the problem of land availability. With the situation in Jakarta, expansion spaces of polder component are not easy to provide. Most of the areas have been occupied by inhabitants for residential, commercial and industrial purposes. Meanwhile, the utilization of the public space like park or garden to expand the polder component in these area are not proper. Inundation area in 2012 is shown in Figure 1.

Based on the potential and constraints of urban polder development, Rawa Badak Polder at the northern part of Jakarta is used to represent polder's development issues. Water management components inside the polder will be analyzed using the DUFLOW model. SUDs application will also be taken into account to enhance the water management. The most appropriate solution to deal with polders development in Jakarta will be discussed.

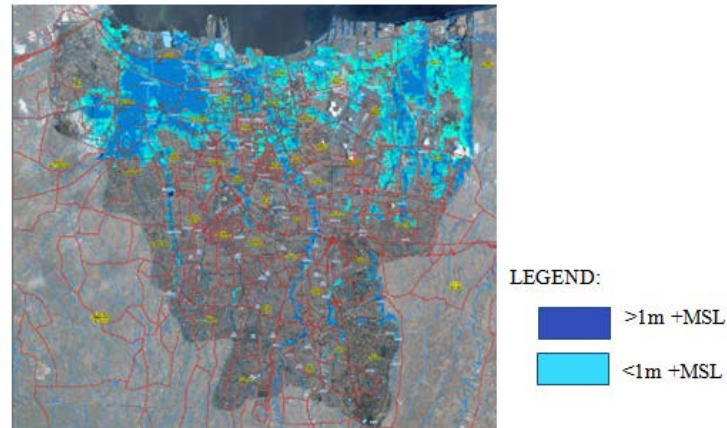


**Figure 1.** Inundation area in 2012. Blue color indicates inundated areas (BNPB, 2012).

## 2 POTENTIAL AND CONSTRAINTS OF URBAN POLDER DEVELOPMENT IN JAKARTA

Jakarta as the capital city of Indonesia has an important role in the development of Indonesia. Central government buildings, central offices of industry, commerce, international harbor and airport are placed around the city of Jakarta. These areas are a central of economic development of Indonesia. However, Jakarta as deltaic city cannot be free from some natural disasters such as flood (from the sea or from the excessive run off from upstream areas and also due to the land subsidence). Jakarta as the most important city in Indonesia should not have any inundations, where these conditions will hinder the global economy of Indonesia and also threaten the safety of the residents. Thus, the cost of polders development compared with the damage in this area is understandable.

Moreover, topographical condition of the northern part of Jakarta is dominated by lowland area and also affected by land subsidence which was predicted around 8.5 mm/year (Rochman Djaja et al, 2004). This condition will decrease the drainage ability and lead to inundation in northern part of Jakarta. The Central Government has given serious response to it and proposed a polder system to overcome that problem. Around 69 existing and proposed polders are built in the northern part of Jakarta. This situation shows that the polder water management system can be considered in Jakarta.

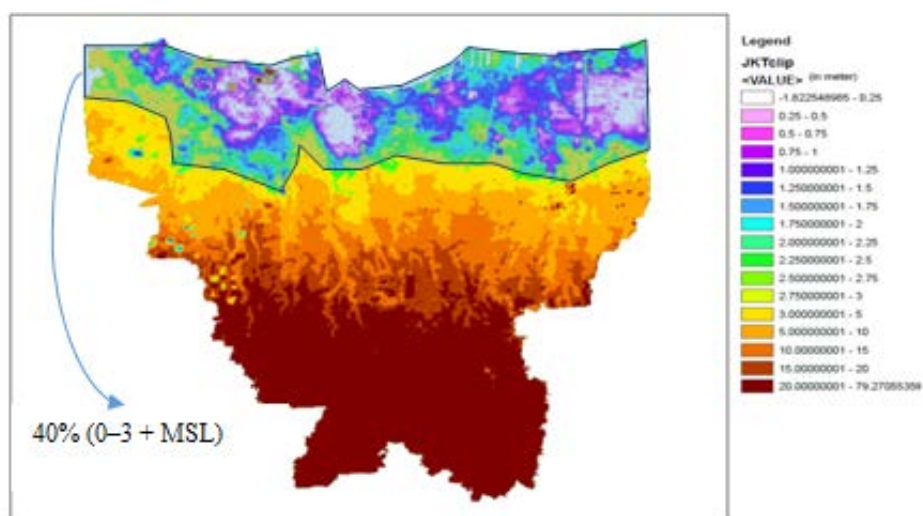


**Figure 2.** Sensitive area for flood in Jakarta. (Winaktoe, 2015).

In a very dense city like Jakarta, new dikes for the polders to separate the hydrological condition cannot be provided easily. Roads as public facility might be the best option to solve it, complicated land acquisition can be avoided by these options. Furthermore, rivers as the natural main drainage passing through the city

can also be used for the outlet of the pump of the polder. This is an opportunity to help the implementation of polder development in Jakarta.

On the other hand, problems in the development of urban polders in Jakarta mainly came from inadequate polder components, lack of operation and maintenance, and space availability for polder expansion. This kind of problems make inundation occurred annually even though polder system has been established.

In some polders, dike does not cover the entire service, which make the polder to be influenced by the other drainage system. Independent hydrological situation is not achieved so that pumps have to deal with excess water from the outside system. Besides, another problem also occurs when the retention basin area is too small to deal with the large service area of the polder. Water in the canal and retention basin will inundate the surrounding area. This type of problem commonly happened in the new polder areas with less availability of the land resources.

Moreover, inadequate operation and maintenance such as the maintenance of canals, water level, retentions basin, and hydraulic structures have decreased the performance of the drainage system. This condition leads to the increasing chance of the system failure. For instance, initial water level in the drainage system remains high during rainy season and as a result, the dynamic storage does not function properly.



**Figure 3.** Water level in drainage canal in the dry season of Rawa Badak Polder.

### 3 SUSTAINABLE URBAN DRAINAGE SYSTEM (SUDS)

Sustainable Urban Drainage System (SUDS) is an alternative solution/tool to reduce surface runoff and to avoid floods in the drainage system. This tool has the benefit to decrease local flood and retain water during high rainfall in the river or drainage canal. Jones and Macdonald (2007) set SUDS as a method to manage the unruly characteristics of storm water inside the urban drainage system rather than forcing it out from the system.

SUDS has many application devices such as retention basins, rain barrels and cisterns, green roofs, swales, wet or dry ponds, wetlands, swales, infiltration trenches, and porous pavements (Mohanasundar Radhakrishnan, 2014).

The hydrological SUDS performance has been tested both in laboratory and the field level. Abbott and Comino and Mateos (2003) measured permeable pavement in the car park that can influence the outflow and cause an average of only 22, 5% of runoff able to leave the system during the storms. Meanwhile, Lee, Hyun, Choi, Yoon, and Geronimo (2012) found that the SUDS application in flood discharge of 50 and 100 year return period can reduce about 7- 15 %.

In this study, Sustainable Urban Drainages SUDS are utilized in order to reduce the amount of runoff water in to the drainage canal by retaining water in the system as long as possible. Application of rain barrel will be considered in the study area. Therefore, the demand for open water can also be reduced.



**Figure 4.** The SUDS application and temporary retention pond.

#### 4 METHODOLOGY

In order to analyze the performance of the selected polder, DUFLOW was chosen for hydraulic mathematical modeling in this study because of its ability to simulate rainfall-runoff process and the hydraulic performance for drainage system with control structure such as pumps, gates, weirs, culverts and siphons. Moreover, the user is enabled to create a network of the water course by using The Networks Editor (STOWA, 2005). DUFLOW computation is using St. Venant equation. The equation is the mathematically translates of laws of conservation of mass and momentum, as in eq. [1] and eq. [2]. The equations are described as follows:

Continuity equation;

$$\frac{\partial H}{\partial t} + \frac{\partial Q}{\partial x} = 0 \quad [1]$$

And Momentum equation;

$$\frac{\partial Q}{\partial t} + gA \frac{\partial H}{\partial t} + \frac{\partial(aQv)}{\partial x} + \frac{gIQIQ}{C^2_{AR}} = \alpha \gamma w^2 \cos^2(\Phi) (\phi - \Phi) \quad [2]$$

where:

t	time (s)
X	distance as measured along the urban drainage axis (m)
H(x, t)	water level with respect to reference level (m)
v(x, t)	mean velocity (averaged over the cross-sectional area) (m/s)
Q(x, t)	discharge at location x and at time t (m <sup>3</sup> /s)
R(x, H)	hydraulic radius of cross-section (m)
a(x, H)	cross-sectional flow width (m)
A(x, H)	cross-sectional flow area (m <sup>2</sup> )
b(x, H)	cross-sectional storage width (m)
B(x, H)	surface width (m)
g	acceleration due to gravity (m/s <sup>2</sup> )
C(x, H)	coefficient of De Chézy (m <sup>1/2</sup> /s)
w (t)	wind velocity (m/s)
Φ (t)	wind direction in degrees (degrees)
Φ(x)	an drainage axis in degrees, measured clockwise from the north (degrees)
γ(x)	wind conversion coefficient (-)
α	correction factor for non-uniformity of the velocity

In this model, the schematization consists of several nodes and sections which is based on the geometrical condition of the selected polder. Pumps and open water storage were inputted in this model. The boundary conditions of this model were design rainfall about 224 mm/day in 25-years return period, pump capacity about 11m<sup>3</sup>/s, and initial condition of the water level in the retention basin about 0.5 m-surface. Pump operation was set to be 16 hours on and off for 8 hours per day according to the existing condition. Total service area of the polder was 570 ha. Schematization in this model can be seen in Figure 5.

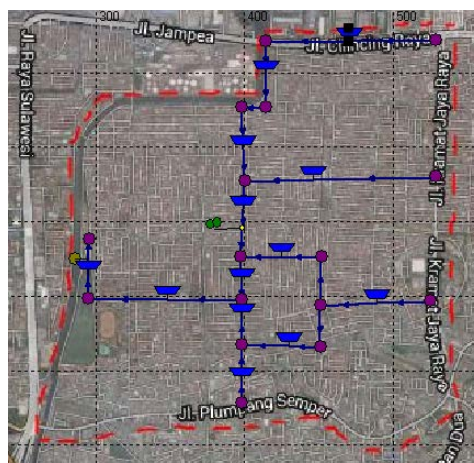


**Figure 5.** The Schematization of urban polder water management model.

(Stovin, 2010) stated that the urban roof as impermeable makes a significant contribution to runoff, Sustainable urban drainage (SUDs) can be used to control and reduce the peak of the discharge (Qin et al, 2013). In this scenario, SUDs was applied as a tool to reduce the demand for the open water storage for polder component expansion. The concept is to retain and release the storm water slowly. The water balance may be written as eq. [3],

$$P-ET-Q=\frac{\Delta S}{\Delta t} \quad [3]$$

where  $\Delta S$  is changing storage over the time step  $\Delta t$  ( $m^3$ ),  $P$  is precipitation (in mm),  $ET$  is evapotranspiration (in mm) and  $Q$  is discharge ( $m^3/s$ ). In this study, the  $\Delta S$  will be represented as storage in SUDs application. Water in the canal and retention basin from the precipitation will be reduced by this storage so that the output discharge will no longer be the same. In the DUFLOW, the effect the storage from SUDs will be modified as setting input of the area.

## 5 CASE STUDY

Rawa Badak Polder is located in the northern of Jakarta. The total service area of this polder was 570 ha with pump capacity about  $11m^3/s$  and open water area / retention basin about 8 ha (1, 4% of total service area). Dikes in this polder do not cover the entire service area, dike is only built to separate the polder from the Java Sea and the Sunter River. Meanwhile, the independent hydrological situation cannot be achieved because dike do not separate the polder from the outside drainage system. Based on the potencies and constraints of urban polder development in Jakarta, Rawa Badak Polder is presented in Table 1.

**Table 1.** Potentials and constraints in Rawa Badak Polder.

1.	Potential	Description
	Topography	0.25 – 1.25 m +MSL; Low land, influenced by tidal,
	Potency of road as dike	Road is available: Plumpang Slemper Road, Kramat Jaya Raya Road
	Potency of river as outlet	River Sunter
2.	Constraint	
	Inadequate polder component	Dike is not provided to separate with the others drainage system, open water area / retention basin is too small compared with the service area (1.4%)
	Operation and maintenance problem	Higher Initial condition of the canals and retention basin, only 0.5 meter from the surface level
	Problem in land availability	Dense residential area,

The existing condition and alternative solutions in this research were conducted in four scenarios;

- A. Model simulation of the polders in existing condition;
- B. Model simulation of the polders with dikes cover entire service area;
- C. Model simulation of the polders with dikes cover entire service area and lower initial water level;
- D. Model simulation of the polders at scenario C and add SUDs application.

## 6 RESULT AND DISCUSSION

By using DUFLOW modeling, four scenarios were conducted to find the best solution for inundation problem in Rawa Badak Polder. Based on the model, the area of inundation in scenario A-B-C is decreasing due to the changing of the water management such as dike surrounding the service area and lower initial water level (1.5 meter-surface). Dike can reduce about 40% of the inundation area. Independent hydrological situation in this polder has proven to be able to reduce the inundation area. Besides that, the lower initial water level brings the dynamic storage effect, thus the retention capacity is increased. Map of Inundation area in Scenarios A-B-C is presented in Table 2 and Figure 6.

**Table 2.** Inundation area at Rawa Badak Polder (Scenario A, B and C).

Scenario	Inundated Area (ha)	Dry Area (ha)
A	529	41
B	272	298
C	368	132

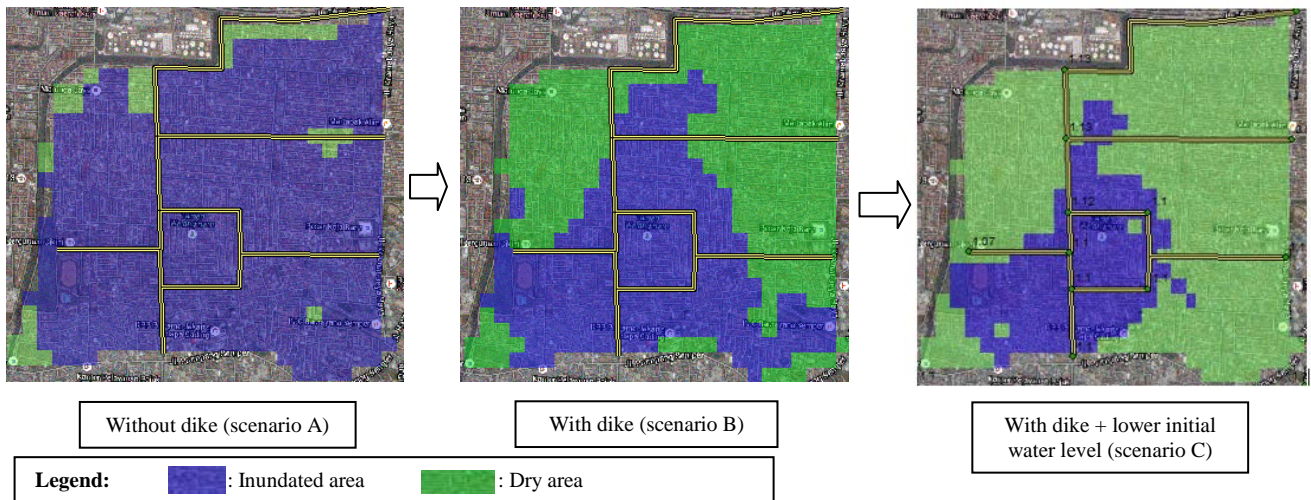


**Figure 6.** Inundation area at Rawa Badak Polder (Scenario A, B and C).

Even though the dike and the initial water level were set to the lower level to overcome the inundation, the inundation still happened. It is because the polder components are not sufficient to deal with the amount of the water in the system. The pump capacity and retention basin area are too small in comparison with the service area of the polder. In the polder system, pump and retention basin have become the important components to deal with inundation problem. By using DUFLOW modeling, the graphic relation between pump capacity and retention basin is made. Two components of Rawa Badak Polder have been plotted by inserting the pump capacity about  $11.3 \text{ m}^3/\text{s}$  and retention basin area about 1.4% from total service area as shown in Figure 7.

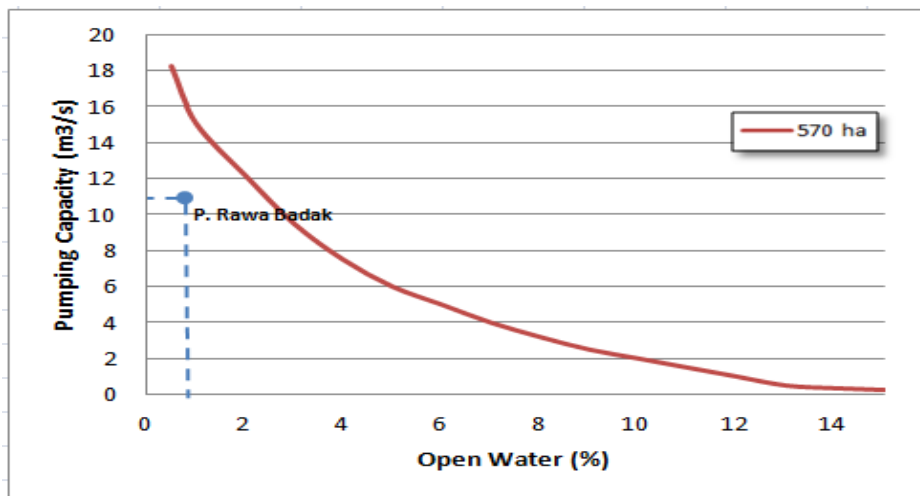
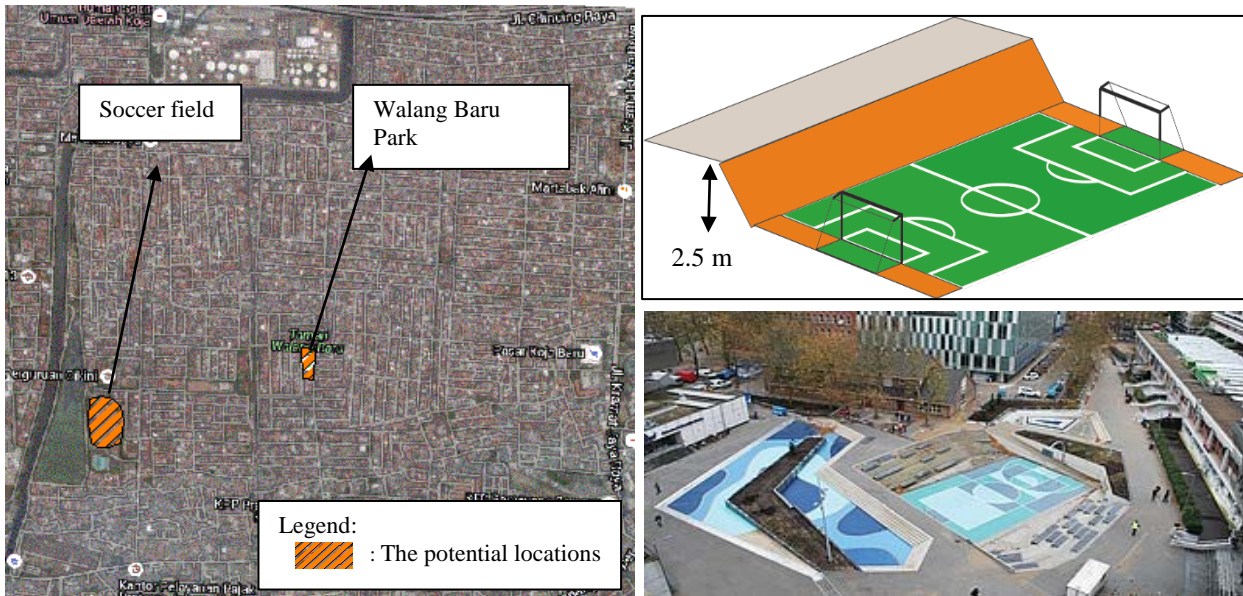


**Figure 7.** Pump capacity vs. open water storage in Rawa Badak Polder.

Based on this relationship between pump capacity and open water storage, Rawa Badak Polder does not meet the minimum criteria of the flood management in the polder. The minimum combination of the pump capacity and retention basin for 570 ha is the curve in the graphic. The value below the curve indicates that the water management system is poor and inundation may occur. This situation can be seen in the result of Scenario C, even though the dike and initial water level were set to the desire level to overcome the inundation, the problem cannot be solved. By using the graph, the solution for inundation in Rawa Badak Polder is to increase the pump capacity up to  $16 \text{ m}^3/\text{s}$  or the open water area up to 2.5% from total service area. In Scenario D, the demand of the open water area has been replaced by using SUDs application. Multipurpose retention basin was conducted in this scenario.

### 6.1 Multipurpose retention basin

The multipurpose retention basin can be implemented in the public area such as park, garden, playground and field. Based on the land use map, the potential locations for this application are at the soccer field completed with the running facilities (3.7 ha) and Walang Baru Park (0.4 ha). The locations and illustration for multipurpose retention basin in Rawa Badak Polder are presented in Figure 8.



Source: (Eurbanlab, 2016)

**Figure 8.** The locations and illustration of multipurpose retention basin in Rawa Badak Polder.

To deal with the demand for the open water storage, soccer field and Walang Baru Park were chosen and modified as multipurpose retention basin. In the DUFLOW, this application is presented an addition water storage, about 4.1 ha was added into the retention basin scheme with the depth of 2.5 m. The results of the simulation shows that inundation does not occur in every observed area. This indicates that the combination between multipurpose retention basin and initial water level are suitable to be implemented in Raw Badak Polder. The result of the SUDs applications is presented in Figure 9.

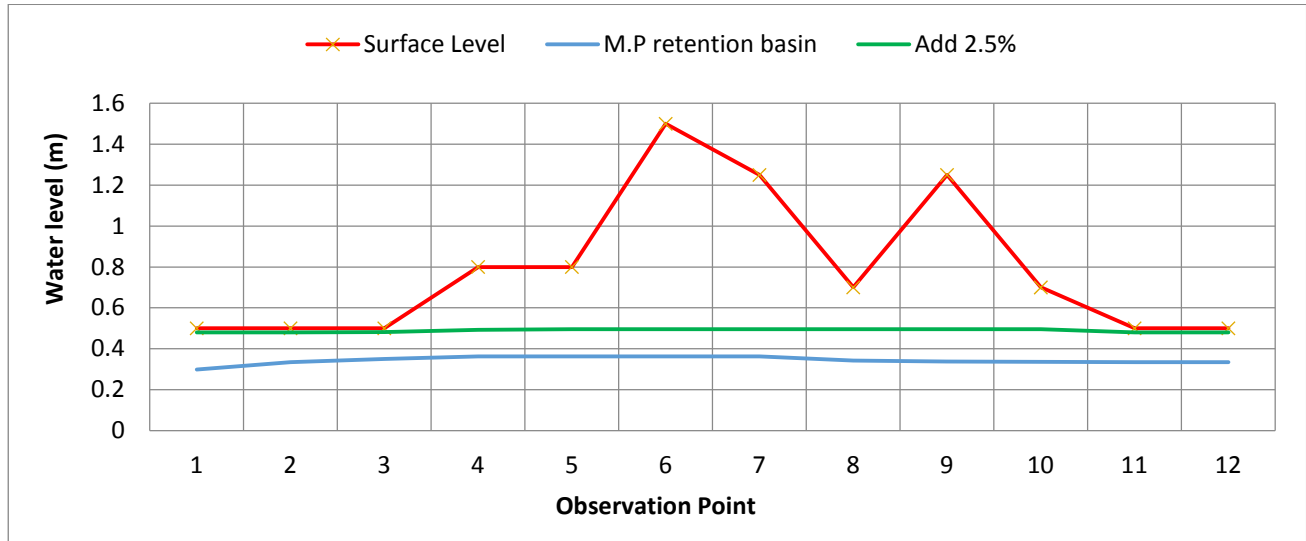


**Figure 9.** Result of the SUDs application in Rawa Badak Polder.

Multipurpose retention basin is successful in reducing demand for the open water storage in dense population such as Rawa Badak Polder. Using the public space, land acquisition can be avoided. This application can also be implemented in other polders in northern Jakarta in order to cope with inundation.

Regarding the ease of the application, this application could be accepted by inhabitants because the location is in the public space. Moreover, without land acquisition, the construction is done faster. The advantage of multipurpose retention basin is that it is easy to maintain because it is an open space area, thus, the maintenance routine can be done manually or mechanically. The side effect of this application could be the increase of the land value in the surrounding areas. Next to that, the economic and environmental aspects need to be considered carefully.

## 7 CONCLUSIONS

According to the analysis of potentials and constraints, model simulations, results and evaluation, several conclusions in this research are presented as follows;

- 1) Urban polder in a very dense city like Jakarta has met with many constraints during the development process such as lack of operation and maintenance, inadequate polder component and unavailability of space for polder component expansion,
- 2) Development of urban polder in Jakarta has been supported by topographical condition, road and river networks. Topography in Jakarta is gradually sinking below the sea level which make the polder system to be considered more seriously. Road networks as public facility can be used as dikes. 13 rivers can be used as main outlet of the polders towards the sea water level.
- 3) In the existing condition, inundation still occurs in Rawa Badak Polder because of the inadequate polder components and the land subsidence. Dike do not cover the entire service area, pump capacity and open water storage were too small in comparison with the total service area.
- 4) Dike utilization in Rawa Badak Polder may reduce 40% of the inundation area. It shows that independent hydrological condition in polder system is absolutely needed.
- 5) Lower initial water level at 1.5 m-surface will reduce the inundation area and bring the dynamic storage effect, thus the retention capacity is increased.
- 6) By using the pump capacity vs. open water area relationship curve, one of the solutions to cope with inundation is to increase the pump capacity up to 16 m<sup>3</sup>/s and increase the open water area up to 2.5%.
- 7) SUDs application can be used as an approach to reduce the demand of the open water storage in Rawa Badak Polder.
- 8) The most appropriate solution to cope with inundation problem is by using dike to cover the entire service area, decreasing the initial water level and adding SUDs application to reduce the demand for open water storage.

## ACKNOWLEDGEMENT

We would like to thank to all people who are involved in this work, especially my fellow on Land and Water Development friends at UNESCO-IHE, Delft, the Netherland for inspiring this work.

## REFERENCES

- Abbott, C. & Comino-Mateos, L. (2003). In-Situ Hydraulic Performance of a Permeable Pavement Sustainable Urban Drainage System. *Water and Environment Journal*, 17(3), 187-190.
- BNPB. (2012). *Inundation Water Level Map in DKI Jakarta*, Jakarta, DKI Jakarta, Indonesia: National Agency for Disaster Management.
- Jones, P. & Macdonald, N. (2007). Making Space for Unruly Water: Sustainable Drainage Systems and the Disciplining of Surface Runoff. *Geoforum*, 38(3), 534-544.
- Lee, J.-M., Hyun, K.-H., Choi, J.-S., Yoon, Y.-J. & Geronimo, F.K.F. (2012). Flood Reduction Analysis on Watershed of LID Design Demonstration District using SWMM5. *Desalination and Water Treatment*, 38(1-3), 255-261.
- Mohanasundar, Radhakrishnan, C.N.X.Q., Assela, P., Phi, H.L., Nguyen H.Q. & Richard, M.A. (2014). *Retrofitting Urban Drainage Capacity to Cope with Change. A Case Study for Nhieu Loc - Thi Nghe Basin change in Ho Chi Minh City*.
- Rochman, D., Rais, J., Abidin, H.Z. & Wedyanto, K. (2004). Land Subsidence of Jakarta Metropolitan area. *3<sup>rd</sup> FIG Regional Conference Jakarta, Indonesia*.
- Stovin, V. (2010). The Potential of Green Roofs to Manage Urban Stormwater. *Water and Environment Journal*, 24(3), 192-199.
- STOWA. (2005). *Duflow Modeling Studio : User's Guide. Version 3.6. Delft, The Netherlands: STOWA*.
- Winaktoe. (2015). *Urban Polder Development Case Study on The Province of Daerah Khusus Ibukota. UNESCO-IHE*.

## EXPLORE THE HYDRODYNAMIC FORCE ON THE SURFACE OF FLOATING STRUCTURE IN FINITE FLOWING WATER

ZHEN CUI<sup>(1)</sup>, ZONG FU FU<sup>(2)</sup>, YUE JUN CHEN<sup>(3)</sup>, SHAN WANG<sup>(4)</sup>, GUANG GANG MA<sup>(5)</sup> & WEN JIANG<sup>(6)</sup>

<sup>(1,2,3,4,5,6)</sup>College of Water Conservancy and Hydropower Engineering, Hohai University, Nanjing, China,  
cuizhen@hhu.edu.cn

### ABSTRACT

Hydrodynamic pressure and shear force on the surface of floating structure are important factors affecting its security and stability during the running process in finite flowing water. In this paper, orthogonal design and CFD simulation are used to explore the effects of different structural parameters and hydraulic factors on the surface force of floating structure. The results show that floating structure scales have a significant effect on the hydrodynamic resistance and shear force. The vertical position of floating structure, discharge per unit width and downstream water level have no significant effects on the hydrodynamic resistance, while these play an important role on shear force. In addition, regression mathematical models describing the relationship between factors and the hydrodynamic resistance and shear force have been set up, respectively. The research methods and results of this paper can provide a reference for designing the stability of the floating structure during its operation.

**Keywords:** Floating structure; CFD; Shear force; Hydrodynamic resistance; Mathematical models.

### 1 INTRODUCTION

Floating structure has been widely used in new types of sluices in plain flood control engineering, tidal power stations, pumping stations, large oil production platforms and so on. Due to the advantages of keeping navigation, producing in factory and installing in field, the floating structure has been widely promoted. The floating structure is often needed to subside and buoy in finite flowing water, the hydrodynamics of floating structure are very complicated. The force affecting the floating structure in flowing water including inertial force, friction and hydrodynamic resistance (Yuan et al., 1993; Yao et al., 1986), the magnitude of force is related to the shape and location of floating structure (Shao et al., 1999; Shen, 1996; Fu et al., 2002; Xu et al., 2009; Xu et al., 1998; Chuan et al., 2008). The hydrodynamic pressure and shear force on the surface of floating structure are important factors that affects its security and stability during its transportation and operation in finite flowing water. Hydrodynamic resistance is the positive pressure acting on the surface of floating structure; it is produced due to the viscosity and gravity of water (Fu et al., 2005). According to the force balance principle, the main factors affecting the floating gate structure in the process of ups and downs were obtained by Fu (2007 and 2014). The main factors include floating structure mass, the height of center of gravity, shape and the free surface of fluid volume inside the structure. The force on the floating gate structure is composed of surface pressure, friction resistance, shear force that comes from the bottom of gate and the force from downstream gate slots; Chen and Dong (1993) analyzed the overall force of the floating tidal barrage and obtained the effect of tidal barrage bottom weight, shape, the position of center of gravity and center of buoyancy on stability by model tests; Chen (2008) tested the force characteristics of caisson when it is sinking in the water. He observed that the longitudinal force of caisson were proportional to the square of water velocity. The mean lateral force is small, however, as the depth increases, it shows a greater growth. Lu (2007) pointed out that the wave pressure acting on the v-shaped bottom-mounted breakwaters is positively correlated to water depth and wavelength. While the torque generated by the surface force is related to the incident wave angle and size of the opening angle of breakwater; Fu and Yan (2007) supported that the pontoon gate is subject to flow resistance and inertia force in the process of propelling. The main influencing factors of the resistance include wave resistance, viscous pressure resistance and frictional resistance; Roth (1999) studied the water resistance of floating gate under the action of viscosity force and surface tension. The pressure distribution and velocity distribution near the gate have been described; He et al. (2008) found that water resistance increases with the increasing ship speed. While under different velocities, the composition of water resistance presents different trends. That is to say, when the ship is at a low speed, the viscous resistance (most component is frictional resistance) plays the predominant role which cannot be ignored.

These studies mainly focus on the overall force of floating structure. They obtained the force acting on floating structure and analyzed the hydrodynamic factors influencing the safety and stability of floating structure. There is some progress in terms of qualitative judgment of the stability of floating structure. However, there remains a need for an efficient method that can obtain the surface force. The sensitivity

analysis of factors influencing the surface force and the specific calculation method for water force may not always be completely successful.

In this paper, a better understanding of mechanics of surface force associated with flows and structure parameters was studied. Based on the Renormalization-group (RNG)  $k$ - $\varepsilon$  Navier-Stokes equations, a two-dimensional numerical flume model was developed on a fixed Cartesian grid system; Fractional Area/Volume Obstacle Representation (FAVOR) was adopted for interface capturing between floating structure and liquid; the free surface was computed by Volume of Fluid (VOF)-type scheme, and the shear force on the surface was solved by Prandtl Mixing Length Model. Furthermore, the orthogonal design was used to explore the effects of different structural parameters and hydraulic factors on the surface force of the floating structure. Also, the sensitivity of various factors was studied, and the numerical method s was also given.

## 2 MATHEMATICAL MODEL

### 2.1 Control equations

For the incompressible viscous fluid in the Cartesian coordinate system, we can obtain the following transient equations by applying the Navier-Stokes equations.

Continuity equation

$$\frac{\partial U_i}{\partial x_i} = 0 \quad [1]$$

Momentum equation

$$\frac{\partial \bar{U}_i}{\partial t} + \bar{U}_j \frac{\partial \bar{U}_i}{\partial x_j} = -\frac{1}{\rho} \frac{\partial \bar{p}}{\partial x_i} + \frac{1}{\rho} \frac{\partial}{\partial x_j} \left( \mu \frac{\partial \bar{U}_i}{\partial x_j} - \overline{\rho u'_i u'_j} \right) + f_i \quad [2]$$

RNG  $k$ - $\varepsilon$  turbulence model was used in the model; the specific equations are listed as follows:

Turbulent energy,  $k$  equation:

$$\frac{\partial (\rho k)}{\partial t} + \frac{\partial (\rho k u_i)}{\partial x_i} = \frac{\partial}{\partial x_j} \left[ \sigma_k (\mu + \mu_t) \frac{\partial k}{\partial x_j} \right] + G_k - \rho \varepsilon \quad [3]$$

Turbulent energy dissipation rate,  $\varepsilon$  equation:

$$\frac{\partial (\rho \varepsilon)}{\partial t} + \frac{\partial (\rho \varepsilon u_i)}{\partial x_i} = \frac{\partial}{\partial x_j} \left[ \sigma_\varepsilon (\mu + \mu_t) \frac{\partial \varepsilon}{\partial x_j} \right] + C_{\varepsilon 1}^* \frac{\varepsilon}{k} G_k - C_{\varepsilon 2} \rho \frac{\varepsilon^2}{k} \quad [4]$$

where the  $\overline{u'_i u'_j}$  is the Reynolds stress, of which  $u_i$  is the component of velocity; the  $\mu_t$  is the eddy viscosity coefficient;  $\rho$  is the density of the fluid;  $\varepsilon$  is the turbulent energy dissipation rate;  $p$  is the micro-fluid pressure,  $f_i$  is the volume force component;  $\mu$  is the turbulent viscosity coefficient.  $k$  is the turbulent energy.

$$\mu_t = \rho C_\mu \frac{k^2}{\varepsilon}, \quad C_\mu = 0.09 \quad [5]$$

$G_k$  is the generation of turbulence kinetic energy.

$$G_k = \mu_t \left( \frac{\partial u_i}{\partial x_j} + \frac{\partial u_j}{\partial x_i} \right) \frac{\partial u_i}{\partial x_j} \quad [6]$$

$\sigma_k, \sigma_\varepsilon$  are the prandtl number of turbulent kinetic energy and dissipation rate, respectively. It is 1.39 both for  $\sigma_k$  and  $\sigma_\varepsilon$ ;

$$C_{\varepsilon 1}^* = C_{\varepsilon 1} - \frac{\eta(1 - \eta/\eta_0)}{1 + \beta\eta^3} \quad [7]$$

$C_{\varepsilon 1}, C_{\varepsilon 2}$  are empirical constants, as 1.42, 1.68 respectively.

### 2.2 Free surface

The Tru-VOF technique is used to track the free surface, the volume fraction  $F(x, y, z)$  is used to achieve the interface motion tracking. In the unit cell,  $F = 0 \sim 1$  indicates that the unit is partially filled with fluid. The complex changes of the free surface in VOF following the description of function:

$$\frac{\partial F}{\partial t} + \frac{1}{V_F} \left\{ \frac{\partial(F A_x u)}{\partial x} + \frac{\partial(F A_y u)}{\partial y} + \frac{\partial(F A_z u)}{\partial z} \right\} = 0 \quad [8]$$

$A_x, A_y, A_z$  represent the flow area fraction in three different directions  $x, y, z$ ;  $V_F$  is the flowable volume fraction; others are the same as above.

The minimum residual method was used to solve the equation, which can solve the complex area and the number of convergence is between 2 and 7. The simple explicit solution method was adopted for the iterative mode, which is not subject to small time step and the calculation result is accurate.

### 2.3 Boundary Conditions

1) Flow field inlet; the distance reaches 5.00m between the upper inlet and the center of floating structure. Flow field inlet boundary condition was water-flow inlet; 2) Flow field outlets; the outlet was set at the downstream and the distance measured from the outlet to the center of the floating structure was 4.00m, and velocity distribution has become uniform in this location. Downstream boundary condition was set to pressure outlet with the appropriate level; 3) Solid wall; the walls of flow flume side and the bottom of the flume were solid wall. No-slip boundary condition was used; 4) Free surface; the top of the flume was set to the free surface, convection velocity and turbulence kinetic energy can be considered as symmetry; 5) Flow monitoring; on the position of upstream and downstream, flux monitor surface was set, which was used to monitor the flux when fluid reaches stable.

## 3 ORTHOGONAL DESIGN AND MODEL VALIDATION

### 3.1 Orthogonal design

The hydrodynamics of floating structure are very complicated; it is easy to overturn in flowing water. The hydrodynamic pressure and shear force on the surface of floating structure are important factors that affects its security and stability by ignoring the inertia force when fixed floating structure in different positions. Shear force and hydrodynamic pressure are mainly related to the floating structure scales, vertical position, and hydraulic parameters. Four key control factors were selected in this study: the floating structure scales  $l$  (floating structure along the flow direction length), the discharge per unit width,  $q$ , the location of floating structure,  $e$  (the vertical distance measured from the bottom of the flume to the bottom of the structure) and downstream water level,  $H'$ , four levels were selected for each factor. Based on the selected experimental factors and levels, orthogonal table L (16) -4-5 was chosen and there was a total of 16 groups of test. In orthogonal table L (16) -4-5, the fifth column is empty, and it is not listed in table 1. The specific calculation design is summarized in table 1.

**Table 1.** Orthogonal factors and level design.

Factors	$l/m$	$q/(m^2/s)$	$e/m$	$H'/m$
1	0.1	0.05	0.02	0.22
2	0.2	0.06	0.05	0.23
3	0.3	0.07	0.08	0.24
4	0.4	0.08	0.11	0.25

### 3.2 Introduction and model validation

The dimensions of the flume were 10.00 m×0.30 m×0.50 m (length×width×height ). The left side of the flume was inlet and the right side of the flume was outlet, floating structure was located in the middle of the flume. The height of the floating structure  $a$  was 0.10m, the width of the floating structures  $B=30.00$  cm (equal to flume width). The simulation region cover the whole experimental flume. The distance from the floating structure to the upstream inlet was 5.00m; the length of downstream was 5.00m. Solid side walls are made with plexiglass, and the equivalent roughness was 0.07mm in simulation which was the same with the physical test. No-slip conditions have been employed at the structure surface and flume walls. The coordinate system was Cartesian. The  $Ox$  axis was parallel to the flow direction, along the flume, the origin being the bottom edge of the flume. The  $Oy$  axis was parallel to the flume width, its origin being the axis of symmetry of the flume. The  $Oz$  axis was vertical, oriented upwards. The origin was located at the bottom of the flume which was under the center of floating structure. Figure 1 is the figure of model solving domain.

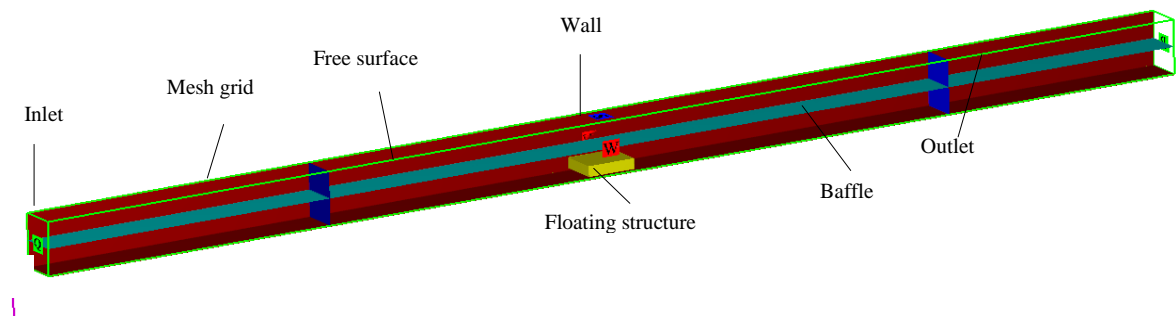


**Figure 1.** Figure of model solving domain.

In the physical model, there is a big error and inconvenience when measuring the shear force. We consider using numerical simulation CFD to obtain the hydrodynamic resistance and shear force. To ensure the accuracy of numerical simulation, the mesh grid size sensitivity analysis was used to examine the accuracy of numerical simulation, and the results were compared with physical test. The accuracy of numerical simulation is within the error range of requirements when the grid scale is 0.01m (Cui et al., 2016). The comparison between the numerical results and measured data reveals that the computational result is capable of obtaining the hydrodynamic features when the grid scale is 0.01m. The comparison between the experimental test and simulation of the hydrodynamic pressure on floating structure surface are listed in table 2. The sketch layout of pressure point can be seen in Figure 2.

At the lower pressure point, the test value is slightly larger than the numerical simulation result. The lower pressure value mainly occurs on the upper surface of the floating structure. By the block of structure, the water appears to be diverted and flows into the downstream area through the upper and lower parts of the structures. The water surface around the floating structure fluctuates greatly and the hydrodynamic pressure changes obviously, which is the reason for the existence of error between the measured values and the simulated values.

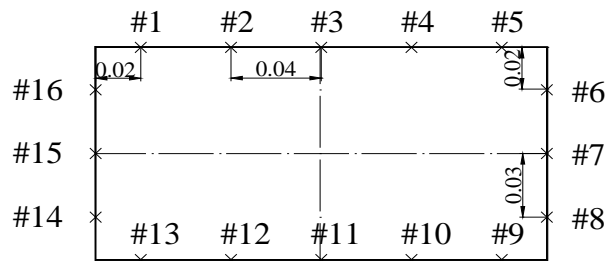


**Figure 2.** Layout diagram of piezometer tube (m).

**Table 2.** Pressure distribution and relative error (pa).

No.	1	2	3	4	5	6	7	8
measured $p$	1738	1740	1744	1759	1760	1960	2254	2548
simulated $p_m$	1685	1690	1695	1699	1702	1925	2219	2513
$(p-p_m)/p\%$	3.03%	-2.85%	-2.82%	3.41%	-3.30%	-1.79%	-1.53%	-1.36%
No.	9	10	11	12	13	14	15	16
measured $p$	2744	2754	2744	2744	2715	2592	2313	1994
Simulated $p_m$	2762	2765	2768	2771	2773	2558	2264	1961
$(p-p_m)/p\%$	0.64%	0.40%	0.87%	0.98%	2.16%	-1.32%	-2.11%	-1.68%

The comparison of the numerical results and measured data reveals that the computational result is capable of obtaining the hydrodynamic features.

## 4 RESULTS AND DISCUSSIONS

### 4.1 Results of orthogonal design

In order to make the result of tests universal, the  $P$  and  $T$  are defined as the force caused by unit width, which means that the force is generated by 1.00m width floating structure. The results of orthogonal design are obtained as shown in Table 3. The magnitude of hydrodynamic resistance  $P$  and shear force  $T$  has a great difference. The different structure parameters and hydraulic factors influence the hydrodynamic resistance,  $P$  and shear force,  $T$ . While the specific influence rules various factors, we are still required to do further analysis and research.

**Table 3.** Orthogonal design and results.

No.	Factors				Index		No.	Factors				Index	
	l/m	q/(m <sup>2</sup> /s)	e/m	H'/m	P/N	T/N		l/m	q/(m <sup>2</sup> /s)	e/m	H'/m	P/N	T/N
1	0.10	0.05	0.02	0.22	100.87	0.10	9	0.30	0.05	0.08	0.25	298.33	0.13
2	0.10	0.06	0.05	0.23	97.20	0.13	10	0.30	0.06	0.11	0.24	289.20	0.27
3	0.10	0.07	0.08	0.24	96.37	0.10	11	0.30	0.07	0.02	0.23	299.73	0.37
4	0.10	0.08	0.11	0.25	88.67	0.17	12	0.30	0.08	0.05	0.22	273.93	0.73
5	0.20	0.05	0.05	0.24	202.77	0.20	13	0.40	0.05	0.11	0.23	379.47	0.33
6	0.20	0.06	0.02	0.25	197.23	0.17	14	0.40	0.06	0.08	0.22	384.83	0.50
7	0.20	0.07	0.11	0.22	171.30	0.30	15	0.40	0.07	0.05	0.25	393.20	0.57
8	0.20	0.08	0.08	0.23	183.47	0.33	16	0.40	0.08	0.02	0.24	400.20	0.57

### 4.2 Range analysis of test factors

The range analysis results of 16 orthogonal design conditions about hydrodynamic resistance and shear force are listed in Table 4.  $S_i$  represents the sum of hydrodynamic resistance and shear force at different levels under four different factors.  $m_i$  is the mean value of the factor at different levels ( $m_i = S_i/4$ ),  $i$  represents the corresponding level number of factors which was taken as 1, 2, 3, 4, respectively. Range value,  $R$  represents the sensitivity of each factor with the different indexes, which is the difference between maximum and minimum under the same factor  $m_i$ . The higher  $R$  indicates this factor has greater impact on the index, that is, the greater sensitivity of the factors on the results. Table 4 shows that, compared with the other three factors, the impact of floating structure scales on the hydrodynamic resistance is most significant and it also has the greatest impact on shear force.

**Table 4.** Range analysis of factors.

Index	P/N				T/N			
	l/m	q/(m <sup>2</sup> /s)	e/m	H'/m	l/m	q/(m <sup>2</sup> /s)	e/m	H'/m
$S_1$	383.11	981.44	998.04	930.93	0.51	0.77	1.20	1.63
$S_2$	754.76	968.47	967.09	959.87	1.00	1.07	1.63	1.16
$S_3$	1161.20	960.60	963.00	988.53	1.49	1.33	1.07	1.13
$S_4$	1557.71	946.27	928.64	977.44	1.97	1.80	1.07	1.04
$m_1$	95.78	245.36	249.51	232.73	0.13	0.19	0.30	0.41
$m_2$	188.69	242.12	241.77	239.97	0.25	0.27	0.41	0.29
$m_3$	290.30	240.15	240.75	247.13	0.37	0.33	0.27	0.28
$m_4$	389.43	236.57	232.16	244.36	0.49	0.45	0.27	0.26
$R$	293.65	8.79	17.35	14.40	0.37	0.26	0.14	0.15
sensibility	$l > e > H' > q$				$l > q > H' > e$			

Figure 3 indicates the contrast results of sensitivity factors of each index. It can be seen that among the factors, the sensitivity of floating structure scales is relatively large on the hydrodynamic pressure and shear force. The vertical positions of floating structures discharge per unit width and downstream water levels have a relatively small influence on the hydrodynamic pressure; however, these three factors have a relatively great influence on shear force.

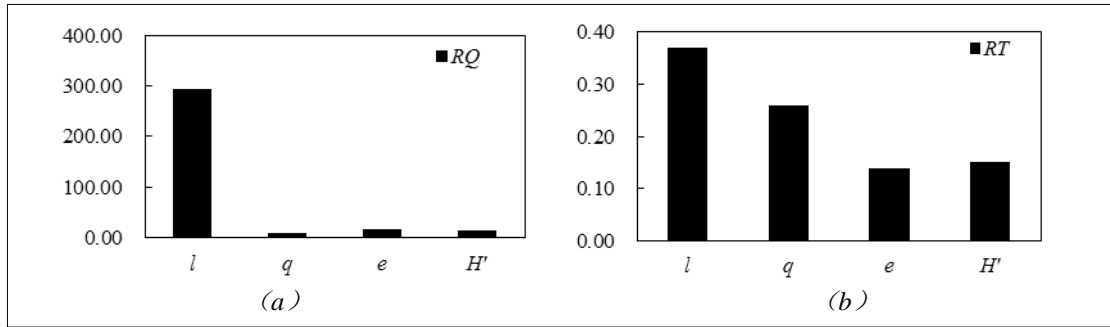


Figure 3. Contrast results of sensitivity factors of each index.

The flow around the floating structure remains in a constant change because of the squeeze and disturbance of floating structure. The movement of water causes the imbalance of water pressure on each side of the floating structure. Figure 4 is the relationship between indexes and design factors. In Figure 4 (a), we can see that with the increasing floating structure scales, hydrodynamic resistance shows a significantly increasing trend under four different levels. Due to the difference in pressure acting on the upper and lower surfaces of floating structure in the flowing water, the pressure difference is produced. With the increasing floating structure scales, the total pressure difference shows an increased trend while the discharge per unit width,  $q$ , the vertical position,  $e$  and downstream water level,  $H'$  have a small impact on hydrodynamic resistance. The data in Figure 4 (a) indicates that the hydrodynamic resistance of floating structure shows a slightly increasing trend as the downstream water level increases, while it reduces slightly with an increasing discharge per unit width and vertical position of the floating structure. In the actual project, the impact of floating structure scales on its overturning should be given priority in the design.

The relationship between mean shear force and factors can be seen in Figure 4 (b). With the floating structure scales increasing, the shear force shows a growth trend, which is the same with the hydrodynamic resistance. According to turbulent boundary layer, the shear stress,  $\tau$  is proportional to the velocity gradient, and the proportional constant is the absolute viscosity of water  $\mu$ ,

$$\tau = \mu \frac{\partial U}{\partial y} \quad [9]$$

The shear force on the surface of floating structure can be expressed as:

$$T = \int \tau dS \quad [10]$$

wherein,  $\tau$  is the shear stress of the floating structure and  $S$  is the surface area of floating structure. The floating structure is positively correlated with the surface area. The shear force also shows a growth trend with an increasing discharge per unit width. However, with the increase of the downstream water level and the vertical position of floating structure, shear force presents a decreasing trend.

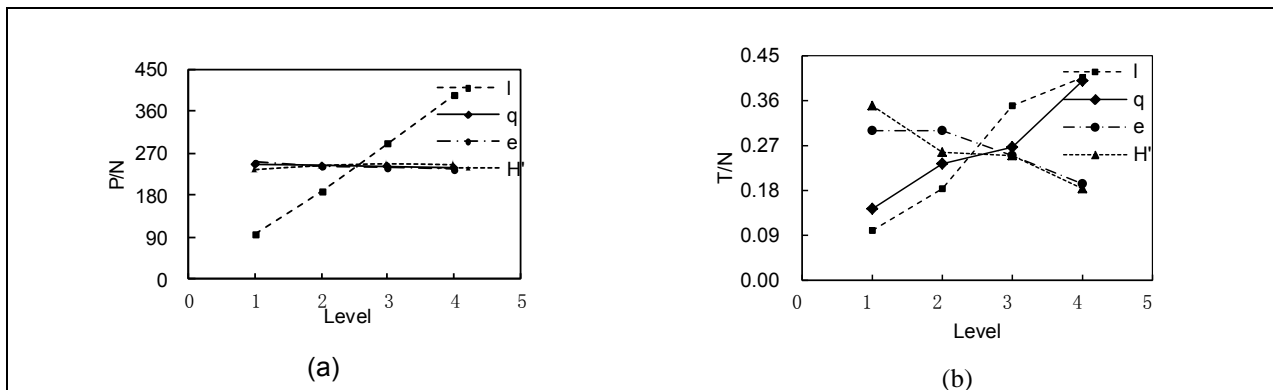


Figure 4. Indexes and design factors.

#### 4.3 Additional experiments

The floating structure is easier to overturn when the force on the surface of floating structure is large. In view of the safety of project, we analyzed the largest combination of various factors, and the factor should be selected by the rule of making the pressure and shear force to reach the maximum level. From Figure 4, the

maximum pressure resistance is obtained when the floating structure length is 0.40 m, the discharge per unit width is 0.05m<sup>2</sup>/s, the vertical position of floating structure is 0.02m and the downstream water level is 0.25m. The emergence of maximum shear force occurred when the floating structure length is 0.40m, the discharge per unit width is 0.08m<sup>2</sup>/s, the vertical position of floating structure is 0.02m and the downstream water level is 0.22m. These above two conditions were simulated. When the maximum hydrodynamic resistance occurs, the  $P$  and  $T$  are 400.73N and 0.23N, respectively; when the maximum shear force occurs, the  $P$  and  $T$  are 398.13N and 0.93N, respectively. The results are the same as the experimental prediction.

#### 4.4 Regression model

It can be seen that the pressure resistance and shear force have a linear function with the floating structure scales, the discharge per unit width, the vertical position of floating structure and the downstream water level, respectively. In order to determine the effect of experimental factors on the hydrodynamic resistance and shear force, the mathematical model between the floating structure force and various factors should be established. The dimensional analysis and multidimensional ordinary least squares linear fitting method were applied in this section to make sure that our results have common generality.

L.Rayleigh was used to establish the physical equation.

$$f(F, q, l, a, e, H', \rho, g) = 0 \quad [11]$$

Take  $\alpha, g, \rho$  as the basic dimension, according to  $\pi$  theorem, it can be obtained:

$$f\left(\frac{F}{\alpha^{\alpha_1} g^{\beta_1} \rho^{\gamma_1}}, \frac{q}{\alpha^{\alpha_2} g^{\beta_2} \rho^{\gamma_2}}, \frac{l}{\alpha^{\alpha_3} g^{\beta_3} \rho^{\gamma_3}}, \frac{e}{\alpha^{\alpha_4} g^{\beta_4} \rho^{\gamma_4}}, \frac{H'}{\alpha^{\alpha_5} g^{\beta_5} \rho^{\gamma_5}}\right) = 0 \quad [12]$$

$$\frac{F}{\alpha^3 g \rho} = f\left(\frac{q}{\sqrt{\alpha^3 g}}, \frac{l}{\alpha}, \frac{e}{\alpha}, \frac{H'}{\alpha}\right) \quad [13]$$

In these experiments, the height of the floating structure  $a$  was constant (0.10m), the relationship between floating structure scales, the discharge per unit width, the vertical position of floating structure, the downstream water level and the force was studied. At normal temperatures,  $\rho$  and  $g$  were constant.

There is a linear relationship between the force acting on the floating structure and four different experimental factors. When we get the quantitative relationship between the force and factors, it will have significance for determining the size of the force acting on the floating structure. The 16 groups of orthogonal experimental design were taken as the data source. The multivariable linear fitting for independent variables related to  $P$  and  $T$  was conducted. Dimensionless independent variables factors ( $l/a, q/\sqrt{\alpha^3 g}, e/a, H'/a$ ) were analyzed with  $P/\alpha^3 g \rho$  and  $T/\alpha^3 g \rho$  in multivariate linear fitting by using least square method, respectively. The following formulas were obtained:

$$\frac{P}{\alpha^3 g \rho} = -7.49 + 10.02 \frac{l}{a} - 2.86 \frac{q}{\sqrt{\alpha^3 g}} - 1.80 \frac{e}{a} + 4.29 \frac{H'}{a} \quad [14]$$

$$\frac{T}{\alpha^3 g \rho} = 0.060 + 0.012 \frac{l}{a} + 0.085 \frac{q}{\sqrt{\alpha^3 g}} - 0.008 \frac{e}{a} - 0.047 \frac{H'}{a} \quad [15]$$

wherein  $P$  is the hydrodynamic resistance, N;  $T$  is the shear force acting on the surface of floating structure, N;  $a$  represent the height of floating structure, m;  $g$  is the acceleration of gravity, 9.81m/s<sup>2</sup>;  $\rho$  is the water density, 1000kg / m<sup>3</sup>;  $q$  is the discharge per unit width, m<sup>2</sup>/s;  $l$  is the length of the floating structure, m;  $e$  is the vertical position of floating structure, m;  $H'$  is the downstream water level, m.

The correlation coefficient  $R$  and  $R^2$  of Eq. [14] were 0.999 and 0.998, respectively, and standard estimated error  $S$  for Eq. [14] was 0.566. The correlation coefficient  $R$  and  $R^2$  of Eq. [15] were 0.943 and 0.889, respectively, and standard estimated error ( $S$ ) was 0.008. The linear relationship of Eq. [14] and Eq. [15] are significant, which means that there is a significant linear relationship between force (water resistance and shear force) and floating structure scales, the discharge per unit width, the vertical position and the downstream water level. It can be obtained by adjusting the four factors to reduce the force acting on the surface of floating structure.

## 5 CONCLUSIONS

The orthogonal design was used to explore the effects of different structural parameters and hydraulic factors on the surface force of the floating structure and the sensitivity of various factors were studied in this paper. The following results were obtained:

All of the factors ( $l, q, e, H'$ ) have an influence on the force; The order of the impact of four experimental factors on the hydrodynamic resistance is:  $l > q > e > H'$  and the hydrodynamic pressure increases with the increase in  $l$  and  $H'$ , while the hydrodynamic pressure decreases with the increase of  $e$  and  $q$ ; The order of the impact of four experimental factors on the shear force is:  $l > q > H' > e$  and shear force on the floating structure surface increases significantly with the increase in  $l$  and  $q$ , while the reduction in  $e$  and  $H'$  results in an increase in the shear force. Regression mathematical models were set up to describe the relationship between factors and the hydrodynamic pressure and shear force. The result predicted by regression mathematical models was shown to be very satisfactory. The research method and the law of the hydrodynamic feature can provide a reference for design and operation of the floating structure; it can also be useful in the design of offshore structures whose columns and caissons are rectangular sections.

## ACKNOWLEDGEMENTS

The authors acknowledge the financial support provided by the National Natural Science Foundation of China (Grant No.51279048), Natural Science Foundation of Jiangsu Province (Grant No. BK2011744) and the Fundamental Research Funds for the Central Universities (2016B40414).

We appreciate the cooperation and efforts of all the authors in producing the Proceedings. This will be a great congress following the tradition of our sponsoring organizations.

## REFERENCES

- Cui, Z., Wang, S. & Fu, Z.F. (2016). The Mesh Scale Analysis of Hydraulic Model Based on FLOW-3D. *Water Resources and Power*, 34(12), 101-105.
- Chen, C. & Zhong, J.C. (2008). A Study on Pressure Property of Floating Caisson in Water Flow During Construction Period. *Railway Standard Design*, 9, 30-32.
- Chen, C.Z. & Dong, C.N. (1993). Simulation Experiment Research of Shanghai Suzhou River Tidal Sluice Floor Sink. *Shuili Xuebao*, 05, 59-67.
- Chuan, T.X. et al. (2008). A Study of Frictional Resistance of Some Coated Surfaces in Water. *The Japan Society of Naval Architects and Ocean Engineers*, 31-37.
- Fu, S.J., Fu, G.G., & Xu, J.X. (2002). Study the Water Resistance of Underwater Travelling Crane. *Ship Engineering*, 03, 27-29.
- Fu, Z.F. & Yan, Z.M. (2007). *Experimental Study on Resistance Characteristics in Pulling Process of Pontoon Gate*. In *Advances in Water Resources and Hydraulic Engineering*. Springer Berlin Heidelberg, 1646-1651.
- Fu, Z.F. & Yan, Z.M. (2005). Stability Analysis on a New Type of Floating Sluice. *Shuili Xuebao*, 36(8), 1014-1018
- Fu, Z.F., Yin, X.J. & Gu, X.F. (2014). Hydraulic Characteristics of Floating Sluices Subsiding and Buoying in Flowing Water. *Advances in Science and Technology of Water Resources*, 5, 24-27.
- Fu, Z.F., Yan, Z.M., Lv, J.C. & Gu, X.F. (2007). Method for Hydraulic Model Test of Large -Scale Floating Sluice. *Advances in Science and Technology of Water Resources*, 27(5), 6-9.
- He, X.H. Wang, J.P., & Cheng, J.H. (2008). Numerical Calculation of the Resistance and Flow Field About Light Boat under Viscous Flows. *Ship Science and Technology*, 30(5), 102-105.
- Roth, A. & HAGER, W.H. (1999). Underflow of Standard Sluice Gate. *Experiments in Fluids*, 27(4), 339-349.
- Shao, S.M., Wang, W.F. & Chen, L. (1999). Influence of Length -Beam Ratio on Resistance for Planning Hulls. *Journal of Shanghai Jiao Tong University*, 03, 130-132.
- Shen, X. (1996). Using the Regression Analysis Method to Estimate the Calm Water Resistance of the Cargo Ship. *Boats and Ships*, 4, 19-21, 57.
- Xu, G.Y., Liu, W.P., & Yang, H.W. (1998). Composition to Water Resistance of Amphibious Vehicle. *Journal of Armored Force Engineering Institute*, 3, 63-67.
- Xu, S.X., Guo, J. & Dong, W. (2009). Study the Floating Resistance on Bridge Side Open Caisson. *Port and Waterway Engineering*, 2, 68-72.
- Yao, J.X., Jin, B.L. & Liu, H.S. (1986). Model Test of Raft Going Through Lock Gates and the Conversion of the Data. *Journal of Nanjing Institute of Forestry*, 2, 58-65.
- Yuan, Y.Z., Huang, X.B. & Fu, Z.F. (1993). Measurement of Boundary Shear Stress and Characteristics of Shear Stress in Aerated Flow. *Journal of Hohai University*, 21(4), 16-20.

## MODELLING THE 1910 FLOOD IN THE BESANCON CENTRE

ANDRÉ PAQUIER<sup>(1)</sup> & ANTOINE CHIAVERINI<sup>(2)</sup>

<sup>(1,2)</sup> Irstea, UR HHLY, Villeurbanne, France  
andre.paquier@irstea.fr; chiaverini.antoine@hotmail.fr

### ABSTRACT

The 1910 flood on the River Doubs is the reference flood for risk analysis. The detailed processes during this reference flood are investigated using several hydrodynamic models. A 2-D model that includes the blocks of buildings and the detailed representation of the flood defense walls demonstrates the influence of these structures on the local flood features, particularly the concentration of the flow in the streets. However, the peak flow elevation can be conveniently calculated even using a 1-D model. The uncertainty due to the failure of the flood defense walls can easily be estimated because, in the case of Besançon, its influence is only for local.

**Keywords:** 2-D shallow water equations; flood modelling; urban flood; flood defense.

### 1 INTRODUCTION

In 1910, high rainfalls hit the whole of Northern France. These latter rainfalls generate the flooding of Paris in the Seine River Basin and up to now, the 1910 flood is the reference flood for Paris. In the town of Besançon on the River Doubs, the 1910 flood was also considered as an important one hazard and remains one of the reference floods. However, there is still a discussion about the causes of the flood that damaged the whole centre of the city because it seems that the water elevation was much higher than expected from the peak flow discharge (Boudou, 2015).

The flood carried out a lot of wood logs (from a paper mill) that were blocked against the piles of the bridges crossing the river inside the town of Besançon (Figure 1). This process was particularly marked upstream the bridge “pont de la République” (Figure 2) because of the arches of the bridge. Then, the head losses between the upstream and downstream sections of the bridge were increased. Another cause of high damages is the failure of the protection system where in this case the town of Besançon was a fortified city with high walls. In the nineteenth century, these walls were thought to be used as flood defenses. All the openings crossing these walls should be closed at flood times. During the 1910 flood, these closures were not as efficient as planned and particularly, upstream from the bridge “Pont Battant”, some panels broke and the flow suddenly invaded the streets of the town centre.

Because floods are still a threat to Besançon, it is still worthwhile understanding the flooding processes during the 1910 flood and estimating the relative influence of the various random events that might occur during flood periods. The historical observations are both the story of what happened and some marks along the river and inside the city that recall the water elevation at peak flow. Then, several scenarios can be set in order to try to reconstitute the flood process throughout the town.

In order to reach the previous objectives, several hydrodynamic models of the River Doubs were built. First one was a 1-D model that cannot define the flooding process inside the town, with some flow paths shorter than the main flow that follows the curve around the city. Thus, it was necessary to build 2-D models. One of these models is built from the same data from that of the 1-D model but uses the possibilities of 2-D shallow water equations. The other one uses another mesh that follows the location of the main streets; thus, this model permits to identify the places that are occupied by buildings. Although water can enter these buildings, there is no important flow crossing them and thus the flow paths inside the town are mainly the streets. With this second mesh, the influence of this latter hypothesis can be estimated.

Then, the paper is organized as follows. A first paragraph describes the software. A second part details the data used and the principles for designing the various models. Finally, the various results are compared with observations.



Figure 1. Old map of Besançon showing the situation of the town around 1910.



Figure 2. Taking out the wood logs from upstream of the bridge “pont de la République”.

## 2 EQUATIONS AND SOFTWARE

The 1-D software called “RubarBE” (El Kadi et al., 2008) solves classical 1-D shallow water equations (Eq. [1] and [2]) using a Godunov type second order explicit numerical scheme.

$$\frac{\partial A}{\partial t} + \frac{\partial Q}{\partial x} = 0 \quad [1]$$

$$\frac{1}{A} \cdot \frac{\partial Q}{\partial t} + \frac{1}{A} \cdot \frac{\partial}{\partial x} \left( \beta \frac{Q^2}{A} \right) + \frac{g}{A} \cdot \frac{\partial l_1}{\partial x} - \frac{g}{A} \cdot l_2 - gS_0 + gS_e = 0 \quad [2]$$

where  $x$  is the distance along the river,  $t$  is time,  $A$  is the wetted area,  $Q$  is the flow discharge,  $\beta$  is the coefficient accounting that the velocities are not uniform inside a cross section,  $g$  is the gravitational acceleration,  $l_1$  is the hydrostatic pressure force term,  $l_2$  is the side pressure force term due to the channel walls contractions and expansions,  $S_0$  is the longitudinal bed slope computed as  $-\partial z_b / \partial x$ , with  $z_b$  as the bed level above a datum, and  $S_e$  is the energy slope computed using the Manning-Strickler equation. In case of compound channel (which is the hypothesis used for Besançon), the variables  $\beta$  and  $S_e$  are calculated using the Debord equations (Nicollet and Uan, 1979) that introduce additional head loss at the interface between main channel and flood plain.

The 2-D software called “Rubar 20” (El Kadi et al., 2009) solves classical 2-D shallow water equations (Eq. [3], [4] and [5]) using a Godunov type second order explicit numerical scheme, similar to the one used for RubarBE (which explains that the two software can easily be coupled (Paquier and Bazin, 2013)).

$$\frac{\partial h}{\partial t} + \frac{\partial(hu)}{\partial x} + \frac{\partial(hv)}{\partial y} = 0 \quad [3]$$

$$\frac{\partial(hu)}{\partial t} + \frac{\partial(hu^2)}{\partial x} + \frac{\partial(huv)}{\partial y} + gh \frac{\partial h}{\partial x} = -gh \frac{\partial z_b}{\partial x} - g \frac{u \sqrt{u^2 + v^2}}{K_s^2 h^{1/3}} + u \frac{\partial}{\partial x} \left( h \frac{\partial u}{\partial x} \right) + u \frac{\partial}{\partial y} \left( h \frac{\partial u}{\partial y} \right) \quad [4]$$

$$\frac{\partial(hv)}{\partial t} + \frac{\partial(huv)}{\partial x} + \frac{\partial(hv^2)}{\partial y} + gh \frac{\partial h}{\partial y} = -gh \frac{\partial z_b}{\partial y} - g \frac{v \sqrt{u^2 + v^2}}{K_s^2 h^{1/3}} + u \frac{\partial}{\partial x} \left( h \frac{\partial v}{\partial x} \right) + u \frac{\partial}{\partial y} \left( h \frac{\partial v}{\partial y} \right) \quad [5]$$

where  $h$  is the water depth,  $u$  and  $v$  are the velocity components along horizontal  $x$  and  $y$ -axis,  $z_b$  is the bottom elevation,  $K_s$  is the Strickler roughness coefficient ( $K_s = 1/n$  with  $n$  the Manning coefficient),  $g$  is the gravitational acceleration and  $\nu$  the diffusion coefficient (set to zero in the Besançon case).

Because of the numerical scheme adapted to strong singularities in the flow, Rubar 20 software can model the flooding flow inside an urban environment (El Kadi et al., 2009). However, one key question is the resulting uncertainty of such modelling (Paquier and Bazin, 2014).

## 3 AVAILABLE DATA AND BUILDING THE MODELS

### 3.1 Available data

All the data used in this study are coming from the local authorities of Besançon (either DDT (department Direction of Territories) or DREAL (Regional Direction of Environment)). They include topographical data with three levels of definition:

- i. 25 cross section profiles of the Doubs main channel set along the ten kilometers of the river that were modelled in the longer models.
- ii. 4800 points located in the flood plain inside the town boundaries. Although there are not regularly spaced, they provide the elevation with accuracy at key points. From one point to another one, the distance is about 30 m.
- iii. A basic D.E.M. (digital elevation model) with a regular spacing of 81 metres in  $x$  and  $y$  directions. Although less accurate than the two previous sets of data, this D.E.M. is useful to complete the ground elevation in some margins of the models.

These topographical data were completed by some scarce data about the hydraulic structures on the river (three weirs and several bridges) and a profile along the top of the walls protecting the city from the river flood. In order to define the location of the urban structure, one can use either the street map of the city or the

limits of the buildings coming from an urban data base. These latter limits were not used directly but the buildings were gathered into blocks (Figure 3).

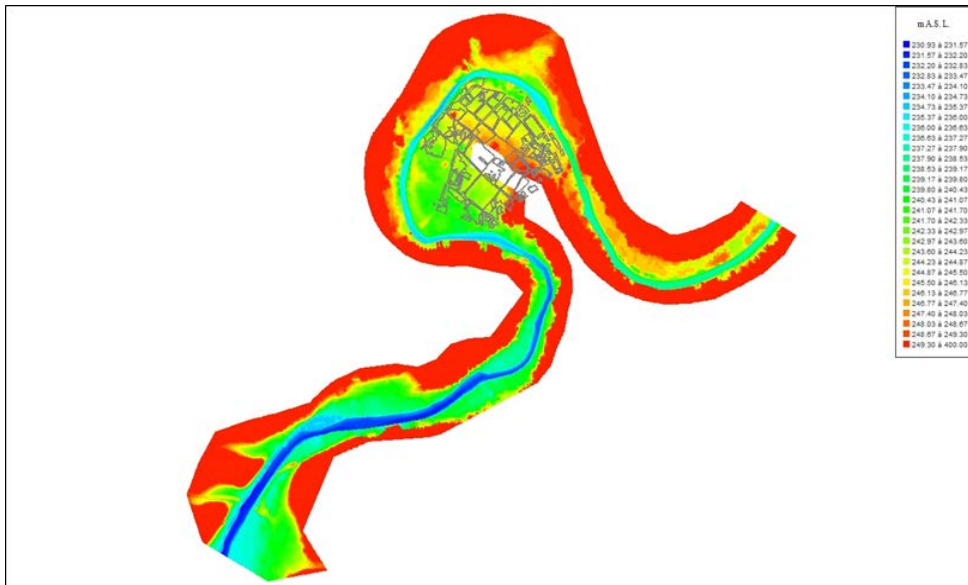


**Figure 3.** Bottom elevation of the study area showing the location of the blocks (grey lines).

The other data were essentially the ones related to the 1910 flood. In fact, they were a synthesis of the observations of peak water depths. One document was the limit of the flooded area in 1910 and the second one were lists of flood marks, either along the river or inside the town centre. The flood marks in the flood plain outside the town centre cannot be used easily because the land use has changed a lot since 1910 while it had not been so much of the case inside the town centre although some localized changes can be noted. In fact, the more important changes concerning the flood processes are the building of new bridges, which creates additional head losses during extreme floods; however, for the present study, all the calculations are performed with the bridges as they were in 1910.

### 3.2 Building the hydrodynamic models

In order to define the topography of the 1-D mesh, cross sections of the main channel were interpolated at 8 meter space step and prolonged as straight as possible in the flood plain. But for the flood plain, the bottom elevation was interpolated from the two other topographical sets. For each cross section, no more than 100 points were kept, which means a space step of about 4 meters each. One of the 2-D models is based on the same topography and even on the same points: the resulting grid made of triangles and mainly quadrilaterals contains 213000 cells. The other 2-D model was based on the blocks of built-up areas and the street map for the flood plain inside the meander of River Doubs and the same grid for the main channel and the right flood plain. As the grid was limited to the town centre, only 39000 cells were generated. On figure 4, one can see that the two grids were completely different except in the main channel (left part of the figures). On the left grid based on the 1-D cross sections, one can note that the location of the streets cannot be distinguished while on the right grid, the streets built with three small cells across the street can be easily seen.

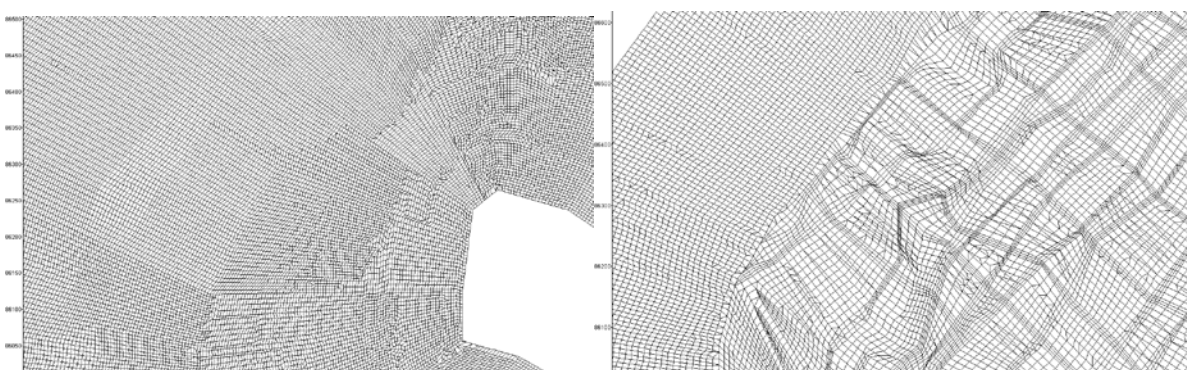


**Figure 4.** Comparison of the grid in the centre of Besançon.

The upstream boundary of all the models is the flow hydrograph of the River Doubs at Besançon during the 1910 flood (Figure 5). This latter hydrograph is coming from a rating curve at the closest gauging station. The peak flow was 1656 m<sup>3</sup>/s and the flood lasts several days with overflowing of more than two days.

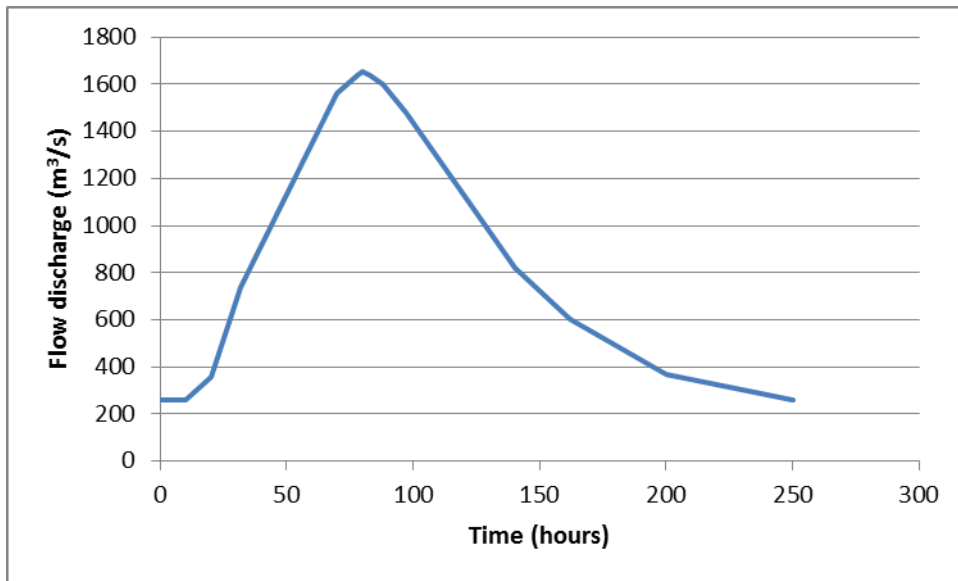


Figure 5. Flow hydrograph of the 1910 flood (estimate used in the models).

The downstream boundary for the 1-D model was set to uniform flow ( $S_0 = S_e$ ). For the 2-D models, a free output was first used but because of the very low slope, this type of condition (or lack of condition) provided to high water elevation; then, the rating curve corresponding to the 1-D uniform flow was preferred.

#### 4 RESULTS OF THE MODELS

##### 4.1 1-D model

The 1-D calculation was performed with a first set of friction (Strickler) coefficients: 15 m<sup>1/3</sup>.s<sup>-1</sup> for the flood plain and 30 m<sup>1/3</sup>.s<sup>-1</sup> for the main channel. The peak water elevation (Figure 6) agrees quite well with the flood marks along the main channel. In the real event, due to the blockage of flow (and wood logs) against the bridges, the head losses seem to be concentrated at these latter structures while the calculation results show head losses to be more distributed along the river although there were also marked effect of the structures at a few locations.

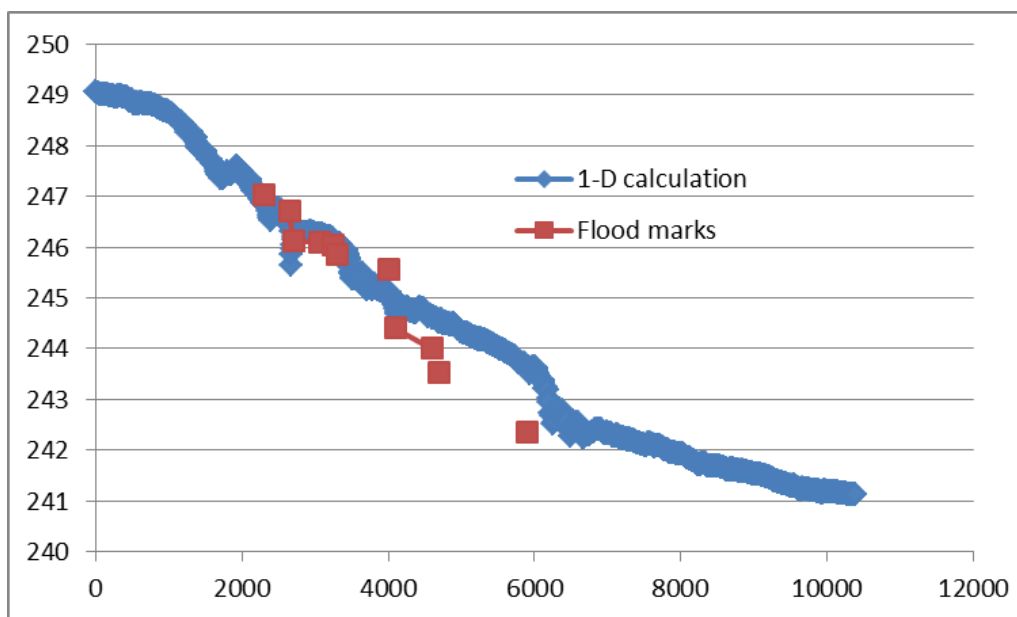
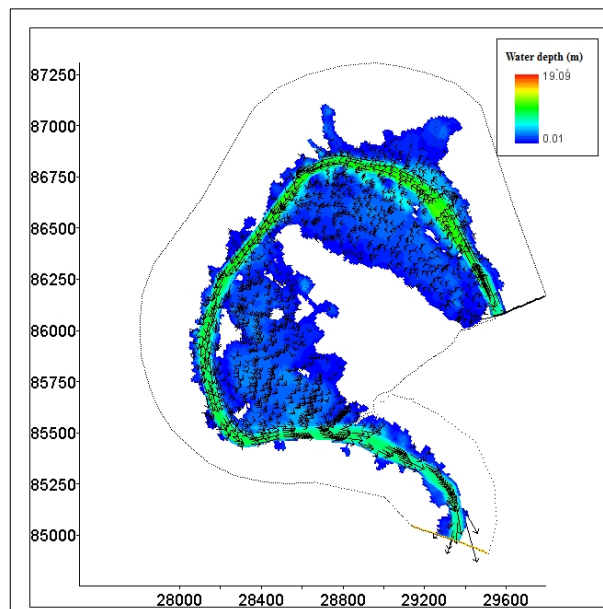


Figure 6. Water elevation along River Doubs.

#### 4.2 2-D models

The 2-D calculations were performed with the same set of friction coefficients as the 1-D model:  $15 \text{ m}^{1/3} \cdot \text{s}^{-1}$  for the flood plain and  $30 \text{ m}^{1/3} \cdot \text{s}^{-1}$  for the main channel. Alternatively, a set of  $25 \text{ m}^{1/3} \cdot \text{s}^{-1}$  and  $40 \text{ m}^{1/3} \cdot \text{s}^{-1}$  was used. The increase of the Strickler coefficients was done in compensating the integration of some details of topography or buildings in the 2-D grid. However, this quite large change of the friction coefficients does not influence the peak water depths a lot because the linear head losses are limited when compared to the effect of the overflow process (head loss at the interface between the main channel and the flood plain) and the flow deviation by hydraulic structures (bridges, weirs, flood defense walls and buildings in case they are represented).

Figures 7 and 8 show the peak water depths for the calculations with the second 2-D grid taking into account the blocks of buildings or not. The flow pattern is globally the same one as well as the extent of the flooded area. However, the blocks of buildings are modifying the velocity pattern inside the meander. Figure 9 shows also higher velocity when an opening in the flood defense wall was added (northeastern part of the figure). This zoom also shows that even if the blocks were not completely closed (openings to inner yards) and then water enters the blocks, the flow remains concentrated in the streets. The first 2-D grid (similar to 1-D) provide results (not shown here) very close to the second 2-D grid without the blocks (Figure 7) although there is a slight influence, mainly linked to the interpolation of the topography.



**Figure 7.** Peak water depths and velocities at peak flow (without blocks of buildings).

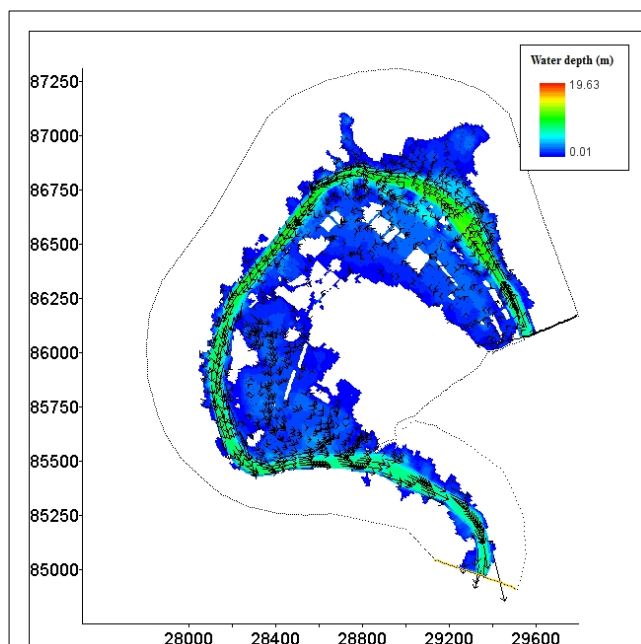


**Figure 8.** Peak water depths and velocities at peak flow (with blocks of buildings).

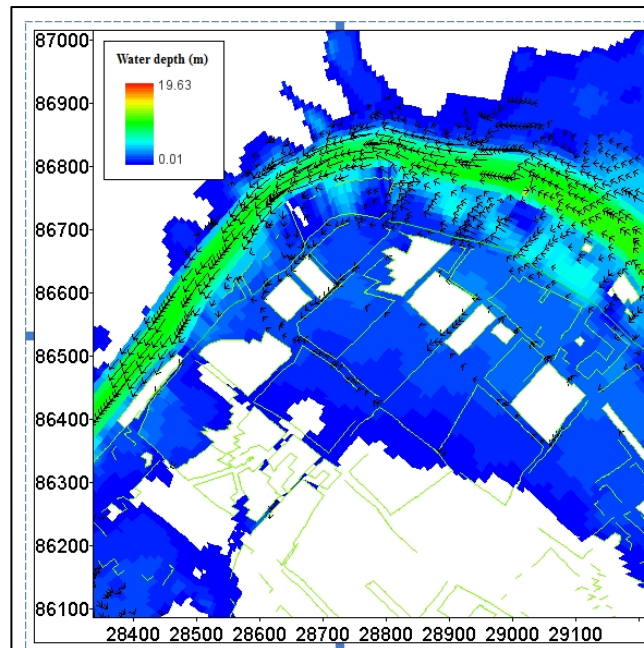


**Figure 9.** Peak water depths and velocities at peak flow: zoom in case of blocks of buildings (walls shown as green lines) and additional opening in the flood defense walls.

## 5 CONCLUSIONS

For the 1910 flood, the water elevation along the River Doubs can be modelled either by a 1-D model or any of the 2-D models, where the quality (or, in other words, the decrease of the uncertainty) is linked with the appropriate calibration of the head losses at the various structures rather than a detailed calibration of friction coefficients. Inside the town centre, the flow pattern is conveniently described only if the blocks of buildings are introduced in the modelling, which permits to concentrate the flow in the streets in some parts of the city as observed in 1910. The openings in the blocks should be carefully described if the local flow pattern is one objective. As observed in 1910, the failure of the flood defense wall influences the local flow pattern as in the modelled example and it generates rather high velocity in one street facing the opening in the wall.

## ACKNOWLEDGEMENTS

The research reported herein is funded by the ANR (National Research Agency of France) grant to project FLOWRES and by Irstea. The authors would like to thank Martin Boudou and Michel Lang that provided data about the 1910 flood.

## REFERENCES

- Boudou, M. (2015). A Multidisciplinary Approach for Characterizing Remarkable Flood Events: Lessons from Nine Events in France (1910-2010), *PhD Thesis*. Université Paul Valéry, Montpellier, France, 463. (In French)
- El Kadi, K., Paquier, A. & Gay, A. (2008). One-Dimensional Numerical Modelling of Dam-Break Waves over Movable Beds: Application to Experimental and Field Cases. *Environmental Fluid Mechanics*, 8, 169-198.
- El Kadi, K., Paquier, A. & Mignot, E. (2009). Modelling Flash Flood Propagation in Urban Areas using A Two-Dimensional Numerical Model. *Natural Hazards*, 50, 433-460.
- Nicollet, G. & Uan, M. (1979). Ecoulements Permanents à Surface Libre en lits Composés. *La Houille Blanche*, 1, 21-30. (in French)
- Paquier, A. & Bazin, P.H. (2013). Coupling 1-D and 2-D Models for Simulating Floods: Definition of The Exchange Terms. *Advances in Hydroinformatics*, Simhydro 2012 - New frontiers of simulation, 11-12.
- Paquier, A. & Bazin, P.H. (2014). Estimating Uncertainties for Urban Floods Modelling. *Houille Blanche-Revue Internationale de l'eau*, 6, 13-18.

## EFFECTS OF VARYING UPSTREAM SIDE SLOPES ON DISCHARGE COEFFICIENT OF RECTANGULAR PROFILE SHORT-CRESTED WEIRS

YUE JUN CHEN<sup>(1)</sup>, ZONG FU FU<sup>(2)</sup>, ZHEN CUI<sup>(3)</sup>, SHAN WANG<sup>(4)</sup>, GUANG GANG MA<sup>(5)</sup>, WEN JIANG<sup>(6)</sup>,  
YAO WANG<sup>(7)</sup> & XUE HAN QIU<sup>(8)</sup>

<sup>(1,2,3,4,5,6)</sup>College of Water Conservancy and Hydropower Engineering, Hohai University, Nanjing, China,  
chen-yuejun@hhu.edu.cn

<sup>(7)</sup>Water Conservancy Bureau of Rizhao, Rizhao, China,  
wangyao98@126.com

<sup>(8)</sup>Shanghai Investigation, Design & Research Institute Co., LTD, Shanghai, China,  
qixuehan@gmail.com

### ABSTRACT

Numerical simulation based on the RNG  $\kappa$ - $\varepsilon$  turbulent model has been used to systemically study the effects of varying upstream side slope coefficient  $S_1$  in the range of 2H:1V to V (vertical) on discharge coefficient of rectangular profile short-crested weirs for free overflow conditions. The results were compared with measurements from physical model experiments, using different total energy head,  $H_0$ . Upstream overflow total energy head,  $H_0$  varying from 8.0 cm to 24.0 cm slightly increased the discharge coefficient, but decreased the influence of degree of upstream side slope on discharge coefficient. For constant  $H_0$ , the rectangular short-crested weir with sloped upstream face had a convex parabola relation between the increasing upstream side slope coefficient and the corresponding discharge coefficient. The discharge coefficient formula of rectangular short-crested weirs including the variable of upstream side slope coefficient,  $S_1$  was derived. This formula not only improved calculation accuracy of discharge coefficient, but also provided references for the structural design of rectangular profile short-crested weir.

**Keywords:** Numerical simulation; Short-crested weir; Upstream side slope coefficient; Free overflow; Discharge coefficient.

### 1 INTRODUCTION

Low weirs as common hydraulic engineering structures have been used to measure discharge in irrigation systems and to increase upstream water level in hydroelectric projects. Flat-topped rectangular profile weirs of finite crest length were classified into long-crested weirs ( $0 < H/\delta \leq 0.1$ ), broad-crested weirs ( $0.1 \leq H/\delta \leq 0.4$ ), short-crested weirs ( $0.4 \leq H/\delta \leq 1.5 \sim 1.9$ ), and sharp-crested weirs ( $1.5 \sim 1.9 \leq H/\delta$ ), depending on the relative length of crest,  $H/\delta$ , where  $H$  was the overflow piezometric head upstream of weir and  $\delta$  was the length of weir crest. However, different weir types had different discharge capacity (Govinda Rao et al., 1963). Under the same inflow condition, the discharge coefficient of short-crested weir is approximately 0.33~0.46, while that of broad-crested weir is 0.32~0.385, so the discharge capacity of short-crested weir is stronger than that of broad-crested weir. In addition, in particular situations, the structural design of rectangular short-crested weirs may provide some flexibility to modify the geometrical configuration to improve the hydraulic characteristics (Inozemtsev, 1969).

The geometrical configuration of weirs can affect the discharge capacity; also the improper geometrical configuration may result in cavitation damage of weir flow structures. Bos (1976) introduced some kinds of typical short-crested weirs, such as triangular profile two-dimensional weir and flat-vee weir, but the rectangular profile weir with varying side slopes as one of the simplest weir types was not mentioned. Actually, the existing of different side slopes of rectangular profile short-crested weir and the variation of total energy head,  $H_0$  over weir crest result in the variation of streamline curvature above the weir crest, which has a significant influence on the head-discharge relationship of weirs. According to the minimum energy assumption of Baxmeteb, regardless of resistance the crest depth,  $h$  of the short-crested weir is rapidly decreasing along the flow direction until the flow leaves the crest. Much research in recent years had focused on the impact factors of discharge capacity of broad-crested weirs in geometry, but little attention has been paid to the effect of geometrical configuration of rectangular short-crested on discharge capacity. In fact, the same weir model can act as a broad-crested weir for low heads ( $H_0/\delta < 0.5$ ), while with an increase of heads ( $H_0/\delta > 0.4$ ), the influence of streamline curvature becomes significant, and acts as a short-crested weir (Bos, 1976). Singer (1964) concluded that the discharge coefficient  $m$  of short-crested weirs and broad-crested weirs was dependent on weir height,  $P$  as well as crest length,  $\delta$ . Also, the discharge coefficient,  $m$  had close relations with the influence factors of the side slope coefficient structurally. Farhoudi et al. (2005) outlined the

discharge capacity of rectangular broad-crested weir with varying upstream side slope angle,  $\alpha$  in the range of  $23^\circ \sim 90^\circ$ . Decreasing the upstream side slope angle increased the discharge coefficient, and the discharge coefficient reached to the maximum value with  $\alpha = 25^\circ$ , which was close to the value of optimum upstream side slope angle of triangular broad-crested weir (Crump & Burkitt., 1952). Compared with trapezoidal broad-crested weir with vertical downstream weir face, Sargison et al. found that trapezoidal broad-crested weir with sloped downstream weir face improves the discharge capacity (2009). Goodarzi et al. (2012) concluded that the flow separation space over the crest indirectly resulted in the effect of upstream side slope on the discharge coefficient of broad-crested weir. Isaacs (Isaacs, 1981), Ranga Raju et al. (1990) recommended that the flow depth over the crest is greater than 5.0 cm in the case of the effect of viscosity and surface tension on the water flowing through weir models.

Recently, many researchers such as Tong et al. (2002; 2011) and Zhang (1982) have carried out much work and made much progress to investigate the flow characteristics of short-crested weir. However, there was no systematical analysis of the effect of varying upstream side slopes on the discharge capacity of short-crested weir. According to the *Hydraulic Calculation Manual*, the discharge coefficient of rectangular short-crested weir with upstream side slope of  $S_1 = 2.0$  is 2.0% larger than that of the rectangular short-crested weir. H.H. Pavlovskiy (SCU, 1980) concluded that the discharge coefficient decreased with the decrement of the upstream side slope. Tong et al. (2002) showed that the discharge coefficient increased firstly, and then decreased with the decrement of the upstream side slope, and the discharge coefficient reached to the maximum at the value of  $S_1$  in range of 2.0 to 3.0, which was very close to the value of broad-crested weir. In addition, for the certain ratio of  $H_0 / \delta$ , the average discharge coefficient of trapezoidal short-crested weir was 2.0% higher than that of rectangular short-crested weir. Zhang et al. (2010) showed that the discharge coefficient decreased with the decrement of the downstream side slope for the trapezoidal short-crested weir with vertical upstream weir face. Almost all of the above conclusions are premised on the identical inflow discharge, whereas this paper is premised on the identical total energy head,  $H_0$  over the crest. The existing discharge coefficient formulae of broad-crested weir included the side slope coefficients (Farhoudi et al., 2005; Sargison et al., 2009), but those formulae of short-crested weir failed to include side slope coefficients (Govinda Rao et al., 1963; Kiselef, 1983; Tong et al., 2002), so it is necessary to systemically study the effect of upstream side slopes on the discharge coefficient of short-crested weir.

Haun et al. (2011) applied Computational Fluid Dynamics (CFD) software Flow-3D to simulate the free flow over the trapezoidal broad-crested weir and to calculate the discharge coefficient, and the results were in good agreement with the experimental data (Sargison et al., 2009). Lee (2015) used the RNG  $\kappa - \varepsilon$  turbulent model to calculate the two flow separation zones for free flow over the rectangular broad-crested weir, which fitted well with those of physical models. In conclusion, the approach of numerical simulation meets the requirement of studying the hydraulic characteristics of weir flow for the free flow condition.

The present paper uses the Flow-3D software to simulate the free flow over the rectangular short-crested weir with varying upstream side slopes, and systematically studies the effect of varying upstream side slope coefficients on the discharge capacity of short-crested weir. Moreover, the discharge coefficient formula including the variables of  $S_1$  is derived by the nonlinear regression method, which provides references for the engineering design of short-crested weir.

## 2 NUMERICAL SIMULATION

### 2.1 Theoretical analysis of the influence factors of discharge coefficient

The common practice to determine discharge coefficient in most discharge measuring structures is based on the method of dimensional analysis. Figure 1 shows the definition sketch of free flow over the short-crested weir. The discharge coefficient of the short-crested weir depends on hydraulic conditions, geometric parameters and fluid properties. Considering these influence factors, one could end up with the following relation:

$$F(Q, H_0, B, \delta, P, S_1, g, \sigma, \rho, \mu) = 0 \quad [1]$$

where  $B$  is the width of weir,  $\delta$  is the length of weir crest;  $P$  is the height of weir;  $S_1$  is upstream side slope coefficients, respectively;  $g$  is gravity acceleration;  $\sigma$  is surface tension of fluid;  $\rho$  is mass density of fluid;  $\mu$  is dynamic viscosity of fluid. The three variables of  $H_0$ ,  $g$  and  $\rho$  are selected as the basic dimensions. Based on Buckingham's  $\Pi$  theorem, the relations between dimensionless numbers could be expressed as follows:

$$\frac{Q}{B\sqrt{2g}H_0^{3/2}} = f\left(\delta/H_0, P/H_0, S_1, H_0\sqrt{2g}/\sqrt{\sigma/\rho}, \sqrt{2g}H_0^{2/3}/\nu\right) \quad [2]$$

The left of the equation represents the discharge coefficient,  $m$ . The first three terms on the right describe the effect of the geometric properties on the discharge capacity, while the last two terms on the right respectively describe the effects of surface tension and viscosity on the discharge capacity. Nevertheless, in view of the effects of surface tension and viscosity being significant only for the water head less than 5.0 cm, the Weber number and Reynolds number are not considered. Hence, the Eq. [2] is simplified as:

$$\frac{Q}{B\sqrt{2gH_0^{3/2}}} = f_1(\delta/H_0, P/H_0, S_1) \quad [3]$$

On the right of Eq. [8], it includes three dimensionless numbers:  $\pi_1 = \delta/H_0$ ,  $\pi_2 = P/H_0$ , and  $\pi_3 = S_1$ , which show the effect of the geometric parameters and hydraulic conditions on the discharge coefficient of short-crested weir.

## 2.2 Numerical model

### 2.2.1 Governing equations

In the three-dimensional numerical simulation, the continuity equation [6] and the Navier-Stokes equation [7] are solved in order to calculate the water flow motion for the turbulent flow.

$$\frac{\partial \rho}{\partial t} + \frac{\partial}{\partial x_i}(\rho u_i) = 0 \quad [4]$$

$$\frac{\partial}{\partial t}(\rho u_i) + \frac{\partial}{\partial x_j}(\rho u_i u_j) = -\frac{\partial p}{\partial x_i} + \frac{\partial}{\partial x_j}(\mu \frac{\partial u_i}{\partial x_j} - \overline{\rho u_i u_j}) + S_i \quad [5]$$

with  $i=1,2,3$ . For accurately computing the free water surface, Flow-3D uses the Volume of Fluid Method (VOF) by Hirt et al. (1981). This is a two-phase approach where fluid and air are modeled in a structured grid of the finite difference algorithm. The method is based on the concept that every cell has a fraction of fluid ( $F$ ), which is 0 when the element is full of air and 1 when the element is totally full of fluid. If the value is between 0 and 1, the element contains the free fluid surface. Therefore, the transport equation [6] of fluid fraction is added.

$$\frac{\partial F}{\partial t} + \frac{\partial (u_i F)}{\partial x_i} = 0 \quad [6]$$

The combination of Eq. [4], Eq. [5] and Eq. [6] is not closed, so the RNG  $\kappa - \varepsilon$  turbulent model (Yakhot and Orszag, 1986) equation [7], [8] are introduced to close the set of equations.

$$\frac{\partial(\rho\kappa)}{\partial t} + \frac{\partial(\rho\kappa u_i)}{\partial x_i} = \frac{\partial}{\partial x_j} \left[ \alpha_\kappa \mu_{eff} \frac{\partial \kappa}{\partial x_j} \right] + G_\kappa + \rho\varepsilon \quad [7]$$

$$\frac{\partial(\rho\varepsilon)}{\partial t} + \frac{\partial(\rho\varepsilon u_i)}{\partial x_i} = \frac{\partial}{\partial x_j} \left[ \alpha_\varepsilon \mu_{eff} \frac{\partial \varepsilon}{\partial x_j} \right] + \frac{C_{1\varepsilon}^* \varepsilon}{\kappa} G_\kappa - C_{2\varepsilon} \rho \frac{\varepsilon^2}{\kappa} \quad [8]$$

where  $\kappa$  is the turbulent kinetic energy, and  $\varepsilon$  is the dissipation rate. This turbulent model is effective to the fully developed turbulence and can better dispose of the flow with a high strain rate and a high curvature. But for the flow close to the wall, or the flow of lower Reynolds number, the wall function method or the low  $\kappa - \varepsilon$  turbulent model should be used.

### 2.2.2 Grid generation

A grid sensitivity analysis, with respect to the computational time, determined that the minimum cell size was 1.0 cm. A roughness sensitivity analysis, with respect to the accuracy of  $H_0$ , was conducted, and the surface roughness was finally set as 0.02 cm. In order to decrease the computation time, an initial fluid level was added. The results were listed in Table 1 and Table 2.

### 2.2.3 Boundary conditions

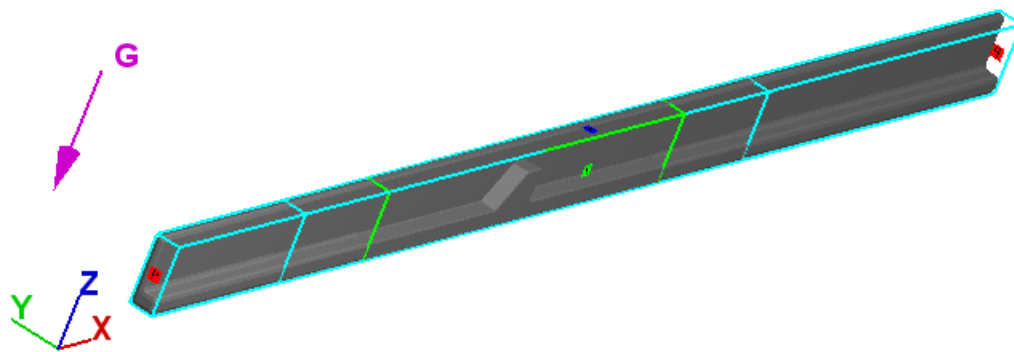
Stagnation pressure boundary conditions are used as the upstream inflow and downstream outflow boundary, and the up- and downstream water levels are set. But for the outlet, the water level should be set as low as possible to ensure that the downstream tail water could not affect the inflow. For the symmetry of weir model, the symmetry boundary condition is set at the symmetrical face and on the top of the flume. No-slip wall boundary conditions are used as the two sides and the bottom of flume. Figure 1 showed the sketch of solving domain of numerical model. This modeling utilizes the explicit viscous solver and implicit pressure solver. The convergence criteria are the same for the explicit viscous algorithm as for the pressure iteration, and could adapt automatically in the range of time-steps. The stability criterion in FLOW-3D leads to time steps varying between 0.004 and 0.006 seconds.

**Table 1** Results of grid sensitivity analysis for  $H_0, Q, m$  and  $t$ .

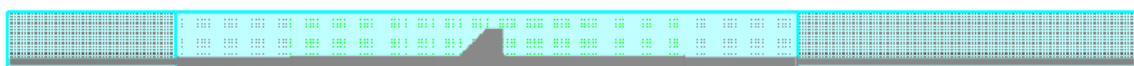
test	Stag. p.(m)	Cell size (cm)	$H_0$ (m)	$Q$ (m <sup>3</sup> /s)	$m$	Comp. time $t$ (sec)
1	0.48	2	0.240	0.069	0.442	70
2	0.48	1	0.239	0.068	0.437	2000
3	0.48	0.5	0.239	0.068	0.436	57600

**Table 2** Results of roughness sensitivity analysis for  $H_0, Q$  and  $m$ .

test	Stag. p.(m)	$k$ (cm)	$H_0$ (m)	$Q$ (m <sup>3</sup> /s)	$m$
1	0.48	0.03	0.239	0.068	0.438
2	0.48	0.02	0.239	0.068	0.437
3	0.48	0.001	0.240	0.068	0.435



(a) Sketch of solving domain of numerical model



(b) Sketch of orthogonal, structured grid

**Figure 1** Sketch of numerical model.

### 2.3 Experimental design scheme of numerical modeling

The trapezoidal short-crested weir model was constructed from three parts in the longitudinal cross-section (Figure 2): the upstream weir face U, the rectangular crest R and the vertical downstream weir face V. Although the ratio of  $\delta/H$  has a decisive effect on the discharge capacity, the ratio of  $P/H$  does not have negligible effect. For low weirs, the ratio of weir height  $P$  to flow depth  $H$  over weir crest was less than 3.0 (Li et al., 2001). Govinda Rao et al. (1963) pointed that the ratio of  $H/\delta$  of the rectangular short-crested weir was in the range  $0.4 \leq H/\delta \leq 1.5 \sim 1.9$ , depending on the particular value of  $H/P$  as shown in Eq.[9]:

$$H/\delta = 1.51 + 0.041H/P \quad [9]$$

with a limitation of  $H/\delta$  in the range of 0.4 to 1.5~1.9. Based on the previous research findings and experimental data, Tong et al. (Tong et al., 2002) concluded that under the condition of  $\delta/H \geq 0.3 \sim 0.5$ , the short-crested weir might convert into the sharp-crested weir for  $P/H \geq 2.0 \sim 2.5$ ; while under the condition of  $\delta/H < 1.5 \sim 2.0$ , the short-crested weir might transform into the broad-crested weir for  $P/H \leq 0.3 \sim 0.5$ . In conclusion, the definition of the short-crested weir is limited to  $0.67 < \delta/H \leq 1.5 \sim 2.0$ , and  $0.5 \leq P/H < 3.0$

According to the above mentioned criteria for defining the short-crested weir, both the weir height,  $P$  and crest length,  $\delta$  are set as constants with the values of 24.0 cm and 16.0 cm respectively. The constant weir width  $B$  is 30.0 cm equal to the flume width. 7 simulated upstream slope coefficients  $S_1$  are 2.0H:1V, 1.5H:1V, 1H:1V, 0.8H:1V, 0.5H:1V, 0.3H:1V and V (vertical) all with effective square edges at the joins. The parameters of experimental design scheme of numerical modeling are listed in Table 3. The total number of weir models is 7, and each weir model was calculated corresponding to 5 total energy heads,  $H_0$  of 8.0 cm, 12.0 cm, 16.0 cm, 20.0 cm, and 24.0 cm over the crest, in each of which the approach velocity  $v_0$  and discharge  $Q$  were obtained. The overflow discharge depends on the discharge coefficient,  $m$ , the crest width,  $B$  and the total energy head,  $H_0$  over the crest, therefore the discharge coefficient,  $m$  could be defined by Eq. [10].

$$Q = mB\sqrt{2g}H_0^{3/2} \quad [10]$$

where the total flow head,  $H_0$  over the crest is given by Eq. [11].

$$H_0 = H + \left[ \frac{Q^2}{2gB^2} (P + H)^2 \right] \quad [11]$$

Based on Eq. [10] and Eq. [11], the discharge coefficient,  $m$  of numerical simulation can be obtained.

**Table 3** The list of experimental design scheme of numerical modeling.

Configuration	No. of Scheme	Upstream side slope coeff. $S_1$	Downstream side slope	Interpretation
VRV	1	0.0	vertical	Only study the effect of the varying $S_1$ on the discharge coefficient of rectangular short-crested weir
	2	0.3		
	3	0.5		
URV	4	0.8		
	5	1.0		
	6	1.5		
	7	2.0		

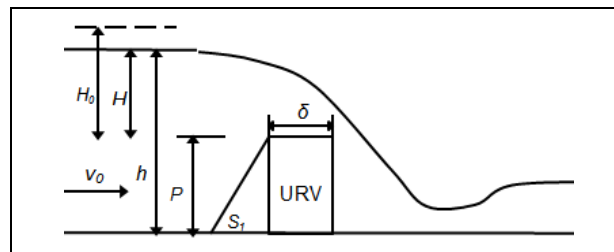


**Figure 2** Geometrical configuration of weir model.

## 2.4 Experimental tests

Tests were conducted in a self-circular, horizontal, rectangular flume, 10.0 m long, 0.3 m wide, and 0.5 m high. The water surface was measured with an accuracy of  $\pm 0.5$  mm using a piezometric tube and the volumetric flow rate with  $\pm 0.01$  L/s using 90° V-notch weir. The tail water level was selected in a way that would not affect the incoming flow. The rectangular short-crested weir model was located at a distance of 4.0 m from the entrance of water basin. The total energy head,  $H_0$  over the crest was 24.0 cm. The contrastive results of numerical simulations and test experiments about the total energy head,  $H_0$  over the crest, overflow discharge,  $Q$  and discharge coefficient,  $m$  were shown in Table 4, with subscripts of phy. and num. representing test experiment and numerical simulation, respectively.

**Table 4** The results of experimental test.

No. of scheme	$S_1$	$H_0$ (cm)	$Q$ (m <sup>3</sup> /s)	$m$	$\frac{H_{0,phy.} - H_{0,num.}}{H_{0,phy.}}$	$\frac{Q_{phy.} - Q_{num.}}{Q_{phy.}}$	$\frac{m_{phy.} - m_{num.}}{m_{phy.}}$
1 <sub>phy.</sub>	0.0	24.1	0.0680	0.433	0.83%	-0.4%	-0.9%
1 <sub>num.</sub>	0.0	23.9	0.0683	0.437			
7 <sub>phy.</sub>	2.0	23.8	0.0670	0.434	0.42%	-0.15%	-0.69%
7 <sub>num.</sub>	2.0	23.7	0.0671	0.437			

All the relative errors were less than 1.0%. In conclusion, the numerical model was able to accurately predict the water surface over the short-crested weir and the directly linked discharge coefficient.

### 3 RESULTS AND ANALYSIS

7 weir models and 35 numerical simulations were conducted to study the effect of varying upstream side slope on discharge capacity of trapezoidal short-crested weir with vertical downstream slope (URV). The discharge coefficients varying with different upstream side slope coefficient,  $S_1$  were shown in Table 5, with the subscript of U representing upstream weir face. Analyzing the data concluded that the discharge coefficient,  $m_U$  had a high logarithm correlation with the relative total energy head,  $\xi = H_0 / (P + \delta)$  over the crest. The results corresponding to different upstream side slope coefficient  $S_1$  were plotted in Figure 3 with  $m_U$  on the Y-axis and  $\ln \xi$  on the X-axis. By assessing, Figure 3 shows that the variation of  $m_U$  with  $\ln \xi$  for varying upstream side slope coefficient,  $S_1$  followed a monotonically increasing linear function as Eq. [12]:

$$m_U = \alpha_U \ln \xi + \beta_U \quad [12]$$

where  $\alpha_U$  and  $\beta_U$  were non-dimensional coefficients determined by the variable of  $S_1$  which could end up with the relation:

$$\alpha_U = -0.0103S_1 + 0.0627 \quad [13]$$

$$\beta_U = -0.0073S_1^2 + 0.0085S_1 + 0.4704 \quad [14]$$

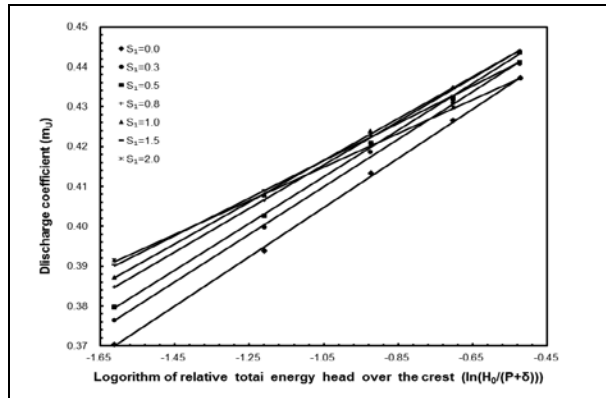
with  $R^2 = 0.994$  and  $R^2 = 0.997$  respectively. The relations were plotted in Figure.4 (a) and Figure.4 (b). In conclusion, the fitting discharge coefficient,  $m_U'$  of trapezoidal short-crested weir with vertical downstream weir face (URV) could be expressed as Eq. [15]:

$$m_U' = [(-1.03S_1 + 6.27) \cdot \ln \xi + (-0.73S_1^2 + 0.85S_1 + 47.04)] \times 10^{-2} \quad [15]$$

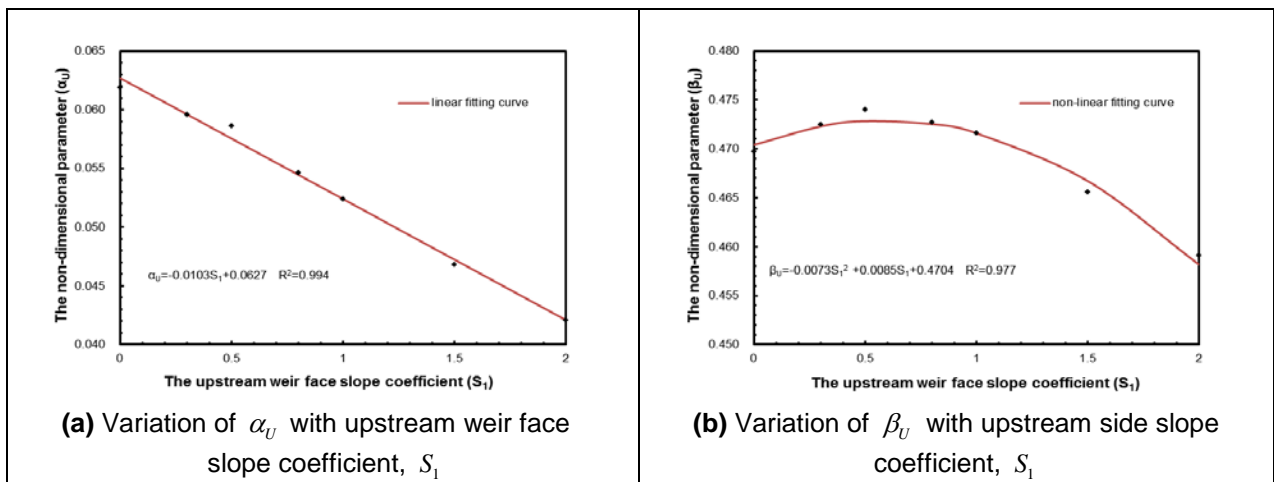
The applicable range of Eq. [15] was  $0.0 \leq S_1 \leq 2.0$ ,  $0.67 \leq \delta / H \leq 2.0$ , and  $1.0 \leq P / H \leq 3.0$ . The deviation from the fitting discharge coefficient,  $m_U'$  by Eq. [15] and the calculated discharge coefficient,  $m_U$  by Eq. [10] was plotted in Figure 5. Compared with  $m_U$ , the relative error of  $m_U'$  was less than 0.28%, hence the fitting results were in good agreement with the simulated results. Analyzing the fitting equation indicated that for some certain  $\ln \xi$ , the discharge coefficient,  $m_U'$  firstly increased until it reached the maximum at the slope coefficient of  $S_1 = 0.5822 - 0.7055 \ln \xi$ , and then decreased with the increasing  $S_1$ . As shown in Figure 3, the effect of degree of upstream side slope coefficients,  $S_1$  on the discharge coefficient,  $m_U$  was decreasing with the increasing total energy head,  $H_0$  over the crest. In view of the law of conservation of energy, the above variation trend concluded that the difference of discharge coefficients among weir models was produced by the frictional head loss of  $h_f$  and local head loss of  $h_j$  in the progress of free outflow. When  $\ln \xi$  is held constant, the gradually slowing upstream slope increased the flow run and reduced the degree of bending of inflow streamline, accordingly  $h_f$  was increasing and  $h_j$  was decreasing, in the progress of which the increment of the former was less than the decrement of the latter, so the discharge coefficient continued to increase until  $S_1 = 0.5822 - 0.7055 \ln \xi$ . When the upstream slope continued to slow down, the increment of  $h_f$  exceeded the decrement of  $h_j$ , so the discharge coefficient was gradually decreasing. With the increasing total energy head of  $H_0$  over the crest the difference of the total head loss of  $h_w$  where  $h_w = h_f + h_j$  was gradually decreasing, so the effect of the difference among upstream slope coefficients,  $S_1$  on the discharge coefficient,  $m_U$  was gradually decreasing.

Table 5. The discharge coefficient  $m_U$  of different upstream side slope coefficients  $S_1$

$H_0$ (cm)	discharge coefficient $m_U$						
	$S_1 = 0.0$	$S_1 = 0.3$	$S_1 = 0.5$	$S_1 = 0.8$	$S_1 = 1.0$	$S_1 = 1.5$	$S_1 = 2.0$
8.0	0.370	0.376	0.380	0.385	0.387	0.390	0.391
12.0	0.394	0.400	0.403	0.406	0.408	0.409	0.408
16.0	0.413	0.419	0.421	0.423	0.424	0.423	0.420
20.0	0.426	0.431	0.432	0.435	0.435	0.433	0.430
24.0	0.437	0.441	0.444	0.444	0.444	0.441	0.437



**Figure 3** Variation of discharge coefficient,  $m_u$  with  $\ln(H_0/(P+\delta))$  for the upstream slope coefficient,  $S_1$  ranging from 0.0 to 2.0.



**Figure 4** Variation of non-dimensional parameters with upstream side slope coefficient,  $S_1$ .

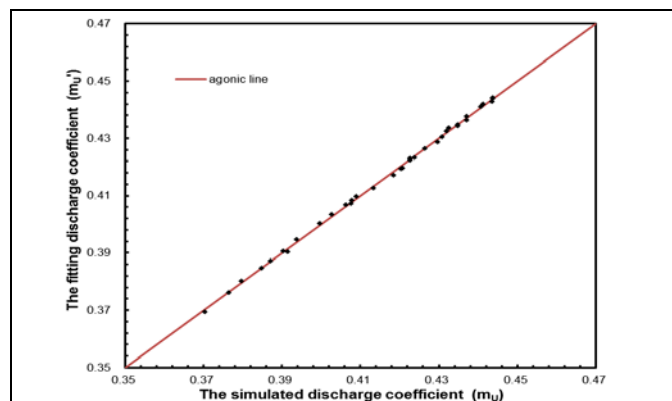


**Figure 5** Deviation from the fitting discharge coefficient,  $m_u'$  and simulated discharge coefficient,  $m_u$ .

#### 4 CONCLUSIONS

According to numerical models tested by physical model experiments, this paper systemically studies the effect of varying upstream side slope coefficients on the discharge coefficient of rectangular profile short-crested weir for free flow conditions. By analyzing the data carefully, many characteristics include the following:

- i. For the certain configuration of short-crested weir, the discharge coefficient,  $m$  is slightly increasing with the increasing total energy head,  $H_0$  over the crest.
- ii. For the certain  $\ln \xi$ , the discharge coefficient,  $m$  of short-crested weir firstly increases, and then decreases with the increasing upstream side slope coefficient,  $S_1$ .

- iii. With the increasing total energy head,  $H_0$  over the crest, the effect of degree of upstream side slope coefficients,  $S_1$  on the discharge coefficient,  $m_U$  is decreasing.
- iv. The present research work provides references for the further study on the trapezoidal short-crested weir, including the optimization of configuration and the discharge capacity for submerged outflow condition.

## ACKNOWLEDGMENTS

The authors acknowledge the technical assistance of Qingsheng Chen, Professor of Hydraulics and River Dynamics, for his help and encouragement in the work. The first author is grateful for the financial support of Zongfu Fu, Assistant Professor of Hydraulics and River Dynamics (Hohai University).

## REFERENCES

- Bos, M.G. (1976). *Discharge Measurement Structures*. Third revised edition, International Institute for Land Reclamation and Improvement/ILRI, Wageningen, The Netherlands, 1-27.
- Crump, E.S. & Burkitt, F.H. (1952). A New Method of Gauging Stream Flow with Little Afflux by Means of a Submerged Weir of Triangular Profile. *Proceedings of the Institution of Civil Engineers: Bridge Engineering*, 1(2), 223-242.
- Goodarzi, E., Farhoudi, J. & Shokri, N. (2012). Flow Characteristics of Rectangular Broad-Crested Weirs with Sloped Upstream Face. *Journal of Hydrology and Hydromechanics*, 60(2), 87-100.
- Govinda Rao, N.S. & Muralidhar, D. (1963). Discharge Characteristics of Weirs of Finite-Crest Width. *La Houille Blanche*, (5), 537-545.
- Haun, S., Olsen, N.R.B. & Feurich, R. (2011). Numerical Modeling of Flow over Trapezoidal Broad-Crested Weir. *Engineering Applications of Computational Fluid Mechanics*, 5(3), 397-405.
- Hirt, C.W. & Nichols, B.D. (1981). Volume of Fluid (VOF) Method for the Dynamics of Free Boundaries. *Journal of Computational Physics*, 39(1), 201-225.
- Inozemtsev, Y. P. (1969). Cavitation Destruction of Concrete and Protective Facings under Natural Conditions. *Hydrotechnical Construction*, 3(1), 35-42.
- Isaacs, L.T. (1981). *Effects of Laminar Boundary Layer on a Model Broad-Crested Weir*, (No. CE38) Department of Civil Engineering at the University of Queensland, 1-20.
- Fathoudi, J. & H, S.A. (2005). Slope Effect on Discharge Efficiency in Rectangular Broad Crested Weir with Sloped Upstream Face. *International Journal of Civil Engineering*, 3(1), 58-65.
- Kiselef. (1983). *Hydraulics*. Beijing: China Water and Power Press. (In Chinese).
- Lee, N.J. (2015). Numerical Modeling of Free Surface Flow over a Broad-Crested Rectangular Weir. *Journal of Korea Water Resources Association*, 48(4), 281-290. (In Korean).
- Li, J. X. & Zhao, Z.X. (2001). *Hydraulics*. Nanjing: Hohai University Press. (In Chinese).
- Ranga Raju, K. G., Srivastava, R. & Porey, P. D. (1990). Scale Effects in Modelling Flow over Broad-Crested Weirs. *Irrigation and Power*, 47, 101-106.
- Sargison, J.E. & Percy, A. (2009). Hydraulics of Broad-Crested Weirs with Varying Side Slopes. *Journal of Irrigation and Drainage Engineering-ASCE*, 135(1), 115-118.
- SCU. (1980). *Hydraulics*. Beijing: People's Education Press. (In Chinese).
- Singer, J. (1964). Square-Edged Broad-Crested Weir as a Flow Measurement Device. *Water and Water Engineering*, 28(820), 229-235.
- Tong, H.H., Ai, K.M. & Ding, X.Q. (2002). Discharge Capacity of Broken-Line Practical Weir. *Journal of Yangtze River Scientific Research Institute*, 19(2), 19-22. (In Chinese)
- Tong, H.H., Li, M.C. & Ding, X. Q. (2011). Relation between Low Weir Shape and Discharge Capacity. *Journal of Yangtze River Scientific Research Institute*, (04), 25-28. (In Chinese)
- Yakhot, V. & Orszag, S.A. (1986). Renormalization Group Analysis of Turbulence. I. Basic theory. *Journal of Scientific Computing*, 1(1), 3-51.
- Zhang, J., Zhai, X.T., Miao, R.Z. & Hou, C. (2010). Experiment on Discharge Coefficient of Broken-Line Practical Weir. *Journal of Shandong Agricultural University (Natural Science)*, 41(03), 469-473.
- Zhang, S.F. (1982). Calculation on Overflow Capacity of Low Weirs. *Journal of Hydraulic Engineering* (11), 53-57. (In Chinese)

## URBAN POLDER DEVELOPMENT RELATED TO FLOOD PROTECTION IN KOTA LAMA, SEMARANG AS PROPOSED UNESCO HERITAGE

FAJAR BASKORO WICAKSONO<sup>(1)</sup>, FRANSISCUS XAVERIUS SURYADI<sup>(2)</sup> & ARIE SETIADI MOERWANTO<sup>(3)</sup>

<sup>(1)</sup> Directorate General of Water Resources, Ministry of Public Works and Housing Republic of Indonesia;  
bwicaksono@gmail.com

<sup>(2)</sup> Department of Water Science and Engineering, UNESCO-IHE Institute for Water Education, Delft, the Netherlands;  
f.suryadi@unesco-ihe.org

<sup>(3)</sup> Research and Development Agency, Ministry of Public Works and Housing Republic of Indonesia;  
ariemoerwanto@yahoo.com

### ABSTRACT

Kota Lama Semarang which is located 1.5 km from the sea shore of Java Island, Indonesia has been part of the UNESCO heritage site tentative list because it has been maintaining the continuity of 105 European-style colonial buildings. Even though Kota Lama (26 ha) is in the list and a new drainage scheme is already applied, the flood events still occurred. The new drainage scheme for Central Semarang drainage system has been developed in 2012, all the outlets of Semarang and Baru River that are connected to the sea have been closed. However, Kota Lama drainage system is still connected to Banger River through Banger sub drainage system which the tidal fluctuation still influences Kota Lama. Kota Lama drainage canals are connected to Tawang Retention Basin with the area of about 1 ha and the capacity of 20,000 m<sup>3</sup>. Survey and mathematical model simulation showed that the occurrence of high rainfall intensity, sediment and solid waste in drainage system, lack of capacity of working pump during flood and tidal fluctuation through Banger sub drainage system will affect the inundation problem in Kota Lama. Water level in Semarang and Baru River are also crucial for determination operations of drainage system in Kota Lama. Gravity driven polder system is the most appropriate possible solution to solve the flood problems in Kota Lama due to the constraint of land availability for open water storage. A new micro drainage scheme and some of hydraulic structures are needed to be applied and constructed due to implementation of the polder. The inside area of polder is designed with the existing pump capacity of 0.45 m<sup>3</sup>/s. The height of the ring dike is 1.0 m by considering the highest water level outside of the polder with 1000 years return period of rainfall, land subsidence and high tides.

**Keywords:** Urban Flood; Polder System; Polder components; Mathematical Model.

### 1 INTRODUCTION

According to Suryadi (1996), lowland is the land which is affected by fluctuating surface water level (e.g. tides and floods). Jha et. al (2012) explained that flood is the most often occurred as natural disaster and no exception for urban or rural areas. Demographic growth of cities, towns and villages is one of the characteristic of urbanization, especially in developing countries.

UNESCO (2015) stated that Semarang was the one of the important cities in the colonial era around 17<sup>th</sup> century because this port city became part of the trade route in central part of Java Island. UNESCO also noted that Kota Lama is the best preserved colonial city because this area can describe about the important historical phases of human civilization (economic, political and social aspects) in the South East Asia and the World. Based on Regional Regulation of Semarang City No. 8/2003 regarding Spatial and Environment Planning of Kota Lama, the Kota Lama Regional Plan consists of the Kota Lama area and the influenced area. The boundary for influenced area is the boundary outside the boundary for Kota Lama until the boundary for Kota Lama Regional Plan, see Figure 1.

Kota Lama is located in the northern part of Java Island which is well known as the lowland areas with distance to the sea shore is only about 1.5 km. Kota Lama has developed Tawang retention basin at the northern part of the area, but unfortunately this was not followed by a polder development which should be completed with other polder components, so that the retention basin is not appropriate with the planned capacity. This situation causes the flood to happen still in the area. The current condition has been affected by urbanization and the development. Land subsidence and those aspects become the considerations in determining the area and type of polder which are appropriate for Kota Lama.

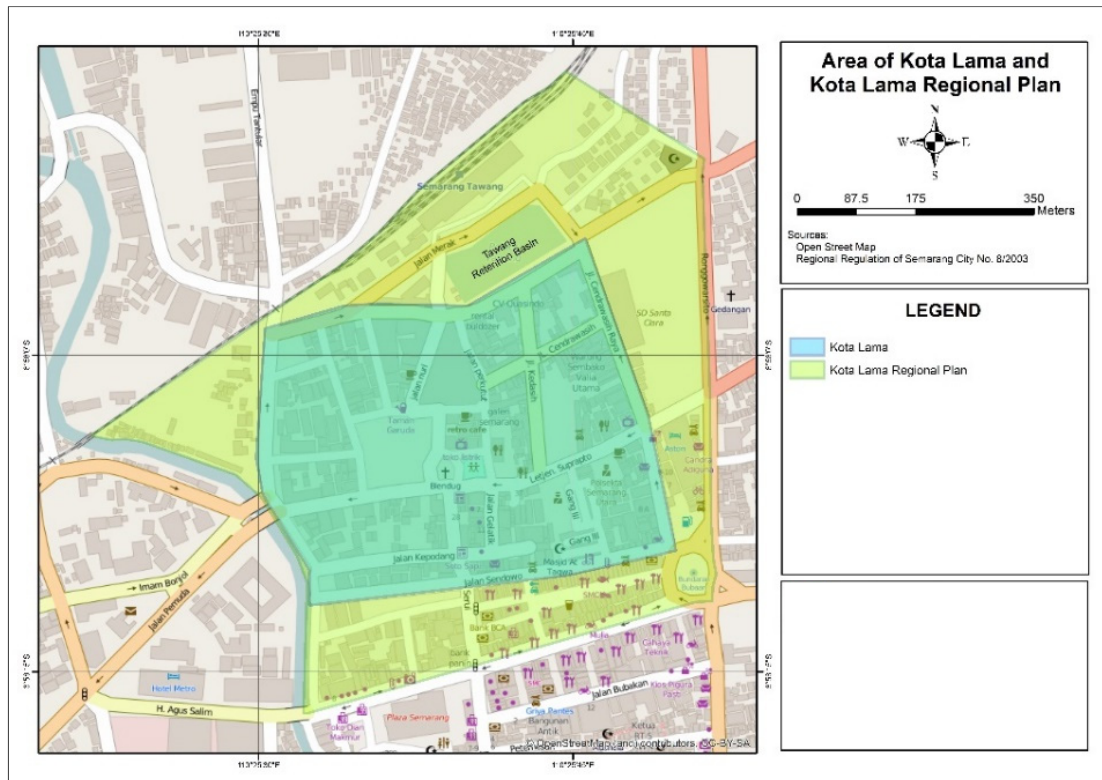


Figure 1. Area of Kota Lama Regional Plan (Regional Regulation of Semarang City No. 8/2003).

## 2 METHODOLOGY

### 2.1. Topography and land subsidence

Kota Lama is lying on 0.2 to 0.3 m+MSL. At that altitude, Kota Lama is vulnerable to tidal flooding because the highest tides (HHWS) can reach up to 0.5 m+MSL. Geological Agency, Ministry of Energy and Mineral Resources and Germany Federal Institute for Geosciences and Natural Resources in 2008 have researched that the land subsidence occurred in Semarang, especially in the Northern part. The latest study was conducted by Bandung Institute Technology from 2009 to 2012. An observation point for land subsidence measurement from the study was located in Kota Lama. It shows that the land subsidence has a tendency to increase in time. If there is no measure in 50 years, the land subsidence might occur about 2.7 m. This analysis can also be proven by survey photos which is presented in Figure 2.



Figure 2. Land Subsidence in Kota Lama.

### 2.2. Drainage system

Ministry of Public Works and Housing through Drainage and Sanitation Working Unit (Satker PPLP) constructed a pumping station, retention basin and trash rack at the end of Semarang River by using a loan from JICA. Thus, Kota Lama does not connect to tidal fluctuation any more from Semarang River because all the outlets of Semarang River that are connected to the sea have been closed. Then, the outlet of Baru River is blocked by the local government because the sedimentation from this river was disturbing the daily operation of Tanjung Mas Port. However, there is an outlet (Baru River Pump Station) from Kota Lama sub drainage system in Baru River, so the flow from Kota Lama is diverted to Kali Semarang through Baru River. In the other side, National road on the north of Kota Lama has also been raised by 1 m to prevent tide of the sea comes through the mainland. This new system started to operate in the middle of 2014. The sketch of location can be seen in Figure 3.

Banger Polder is already planned and located on the east side of Kota Lama (Figure 4), but this polder system has not been fully developed. Therefore, Kota Lama drainage system is still connected to Banger River through Banger sub drainage system. The tidal fluctuation still happens in Banger system and might influence Kota Lama as well.

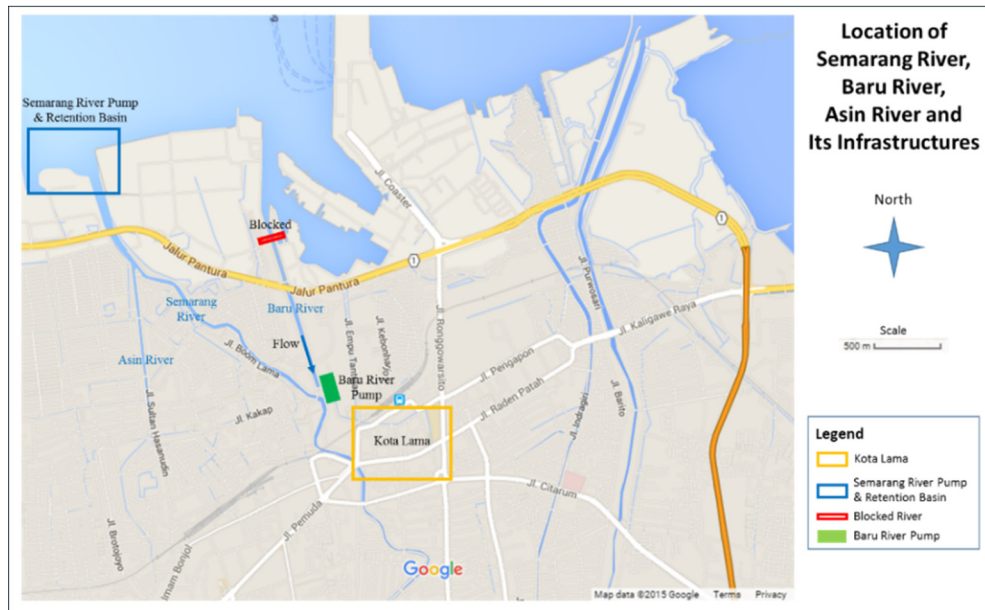


Figure 3. Sketch location of Semarang River, Baru River, Asin River and Its Infrastructures.

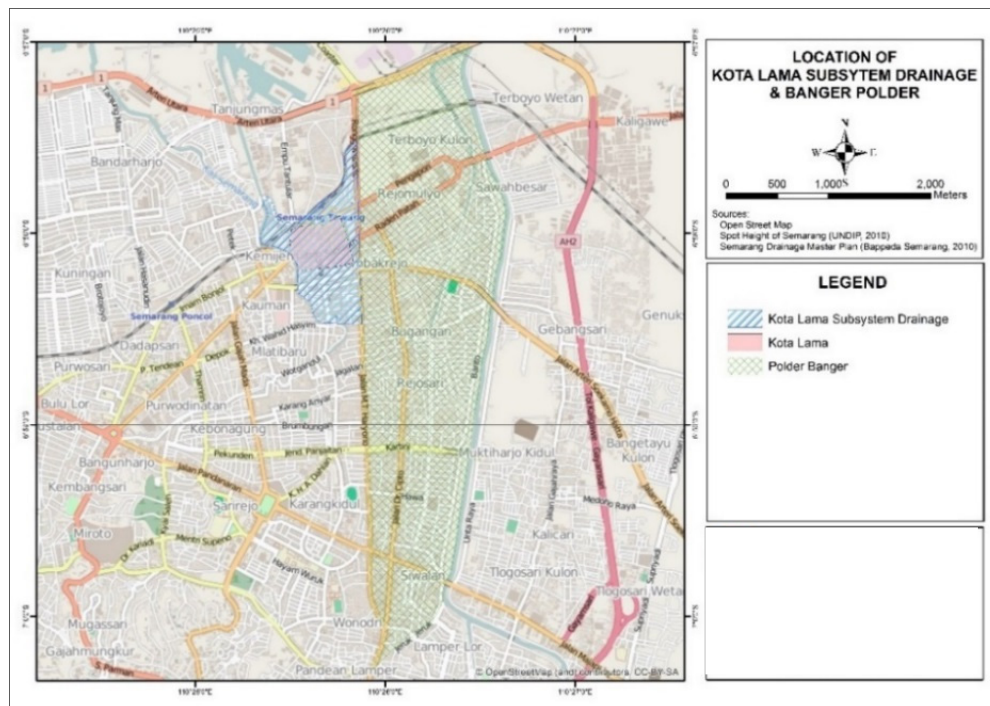
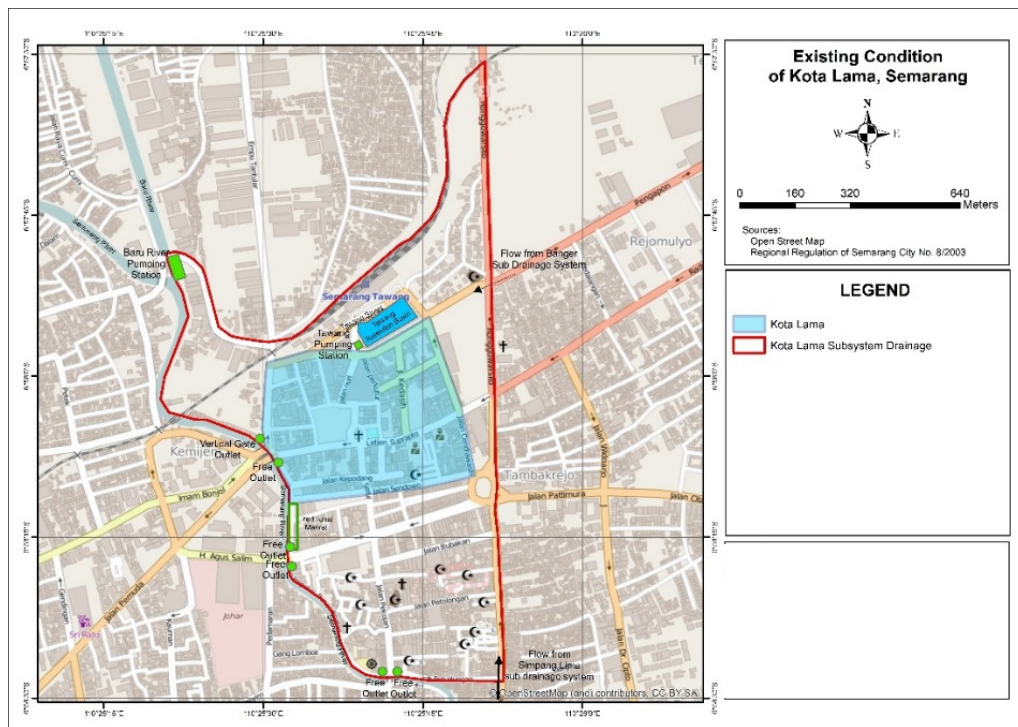


Figure 4. Location of Kota Lama and Banger Polder.

From micro drainage system point of view, all drainage canals are connected to Tawang Retention Basin, except drainage canal at Mpu Tantular Street. Main drainage at Merak Street is very important to Kota Lama because most of the flow from Kota Lama is going through this drainage canal. Banger drainage is connected with drainage canal along Merak Street and Simpang Lima drainage is connected from the beginning of drainage canal at MT. Haryono Street. The outlet of the drainage system is Baru River Pump Station which is located in Baru River. The sketch of existing condition of Kota Lama is presented in Figure 5. Tawang Retention Basin is about 1 ha with a capacity of 20,000 m<sup>3</sup>. There are 4 vertical gates of 1.5 m width for inlet and 2 vertical gates of 1.5 m width for outlet and also a pump of 450 l/s which is used for pumping the water from retention basin to secondary canal on Merak Street.



**Figure 5.** Sketch of Existing Condition of Kota Lama, Semarang.

Baru River Pump consists of 6 units of submersible pump with a capacity of 400 l/s for each unit, 1 unit axial pump of 100 l/s and also equipped with 2 units of vertical gate with 1.5 m for each gate. There is no water level measurement at the pump station. Based on the interview with the pump operator, only 3 pumps were started when water reached the upper black marked (marked of high water level) in the canal or about 50 cm below the surface and stop when water reached the lower black marked about 80 cm below the surface. Vertical gate near Berok Bridge consisted of 2 units of vertical gate, which is a new structure. There is no water level measurement and operation rules at the gate. The solid waste and sedimentation are accumulated in the canals. To prove this, some measurements were done by using the simple gauge into the drainage canal, average sediment thickness in the drainage canal is about 34.2% of canal capacity.

### 2.3. Polder system

Polder development forms its own hydrological unit and controlled water levels by a certain height. Polder area is separated with the surrounding area by dikes that surrounds it. Water management in a polder can be done by gravity or pump. Water can be drained to the outside water body by gravity when the water level outside the polder is lower than the water level inside the polder. According to Witteveen+Bos (2009), cited by the Ministry of Public Works and Housing (2009), Polder components which is presented in Figure 6. compose of:

- Open water storage (drainage canals and retention ponds);
- Pumping station or other hydraulic control structures (sluice gate, flap gates, etc.);
- Ring dike.

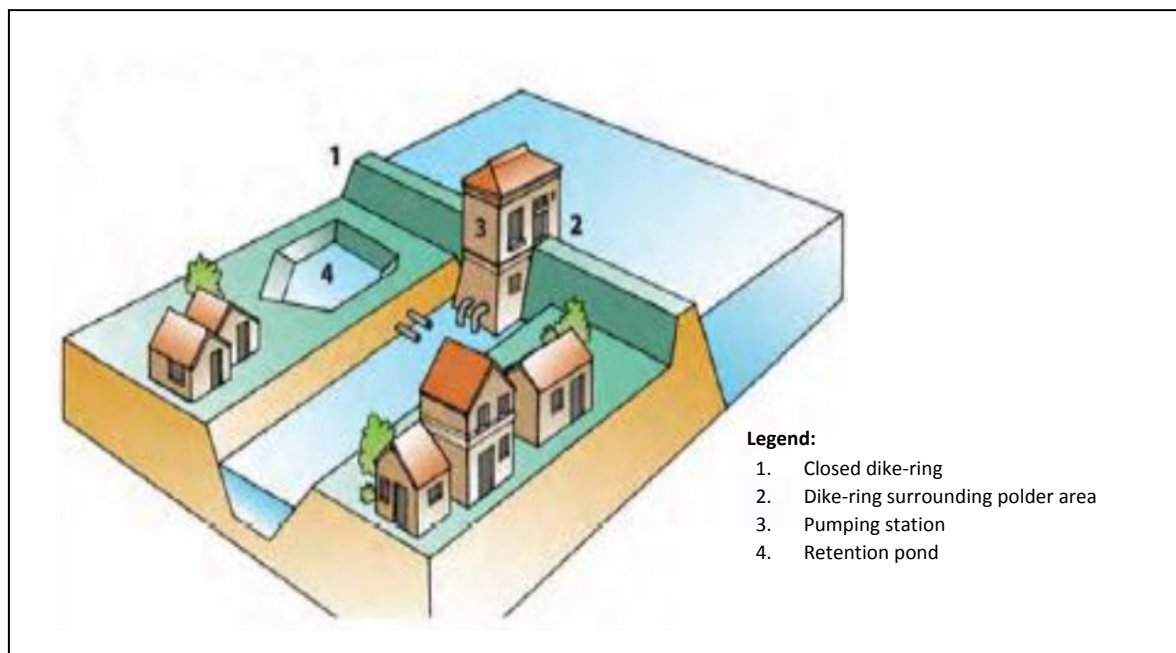


**Figure 6.** Polder Components (Witteveen+Bos, 2009).

#### 2.4. Unsteady flow

In this study, DUFLOW software was used, which apply the unsteady flow method. Unsteady flow is defined as the flow condition that changes at any point of fluid and at any time. Principle of continuity and mass equations are needed to formulate the unsteady flow which are known as the St. Venant Equation. Unsteady flow can also be assumed as one dimensional calculation which can make simplification as perpendicular flow velocity can be neglected, average shear stress of channel wall can be applied to all cross sections and Manning or Chezy equation can be used for evaluating shear stress of canal's bottom. The equations with lateral inflow effects are calculated with continuity equation and momentum equation. At DUFLOW, the implicit four point Preismann scheme is usually used to discretize in space and time. Defining a section  $\Delta x_i$  from node  $x_i$  to node  $x_{i+1}$  and a time interval  $\Delta t$  from time  $t = t^n$  to time  $t = t^{n+1}$ , those expressions approximate the derivatives at the point of references ( $x_{i+1/2}, t^{n+\theta}$ ). The factor controlling numerical dumping ( $\theta$ ) influences the precision and stability of calculation, because lesser  $\theta$  is more precise but less stable for the calculation and vice versa.

### 3 RESULTS & DISCUSSIONS

#### 3.1 Simulation of existing condition

Duflow software was used as the modelling. All the canals materials in Kota Lama drainage system were set to 1:1 for the side slope, canal's material which is affected by sediment is assumed change from concrete (unpolished) in every sides to canal with concrete, wild plants in the cracking spots and sand in the bottom of the canals. Rainfall intensity was assigned based on the 3 hours hyetograph of 166 mm/day which was 25 years return period. Evaporation was set constant for 3.8 mm/day or the same month of the highest rainfall. HHWS and LLWS of Semarang was on +0.5 m+MSL and -0.5 m+MSL with semidiurnal type of tides. The schematization of the system can be seen in Figure 7. The simulation result shows that flood in Kota Lama is affected by the rainfall and tidal fluctuation from Banger system which can be seen in Figure 8. The inundation area was simulated with ArcGIS. It shows that 30% of Kota Lama is inundated more than 0.2 m. 51% of Kota Lama are inundated from 0.1 m to 0.2 m. It is unfortunate that only 11% of this heritage site is not inundated. Figure 9 shows inundated area of Kota Lama.

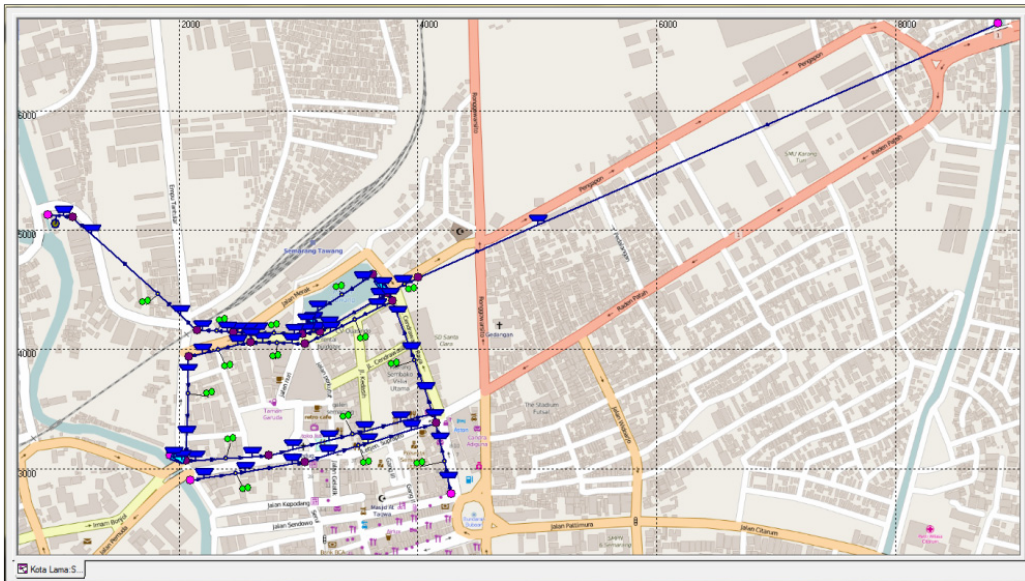


**Figure 7.** System Schematization of Kota Lama Subsystem Drainage.

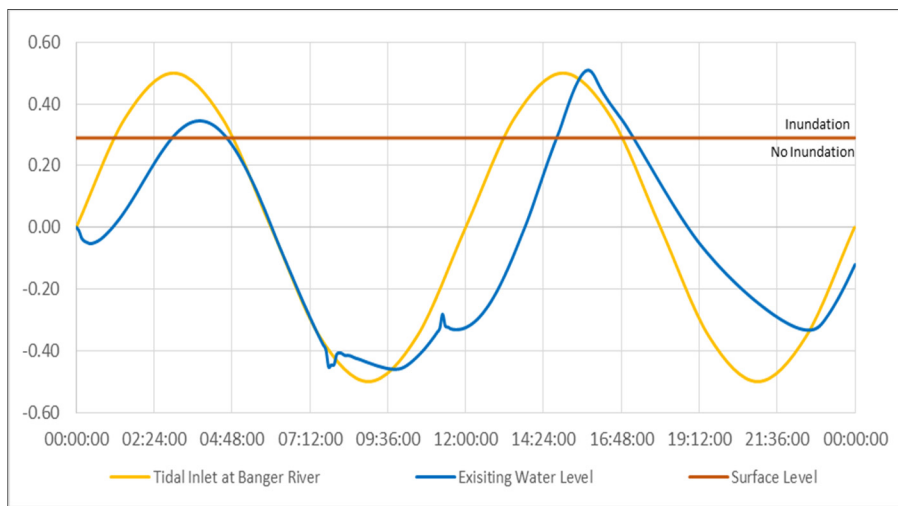


**Figure 8.** Rainfall and Tidal Fluctuation Effects at Merak Street for Existing Condition.

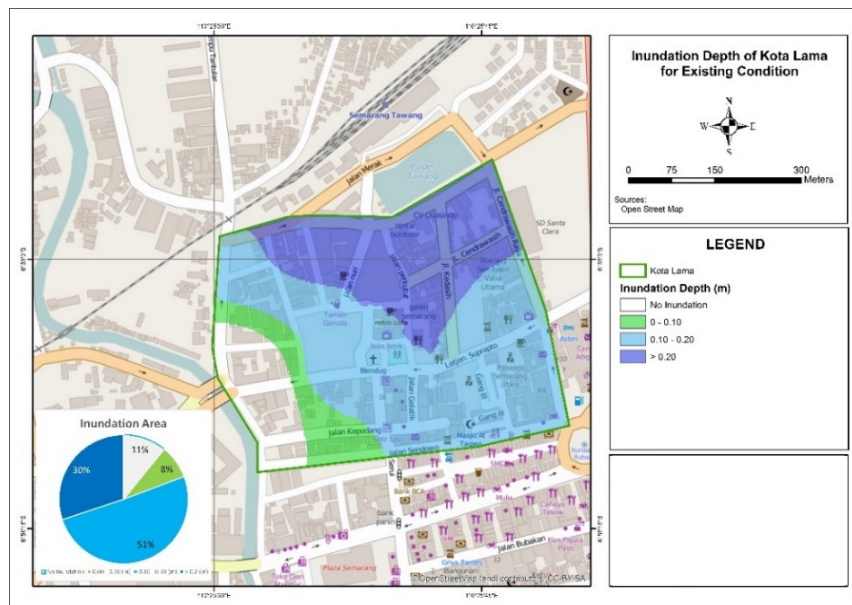


**Figure 9** Simulation Result of Inundated Area for Kota Lama.

### 3.2. Polder area

This scenario aims to provide advice and analysis when the fully developed polder system is to be applied in Kota Lama. Proposed area of Kota Lama Polder is 26 ha. Boundary map of proposed Kota Lama Polder is presented in Figure 10. Gravity driven polder was chosen due to the limitation of land availability to implement different types of polders. This type of polder has minimum construction cost but requires high energy, if it compares to belt canal or separate polder system. Changes in drainage scheme needs to be done because there is main drainage canal (Merak Street drainage) which is passing through Kota Lama.

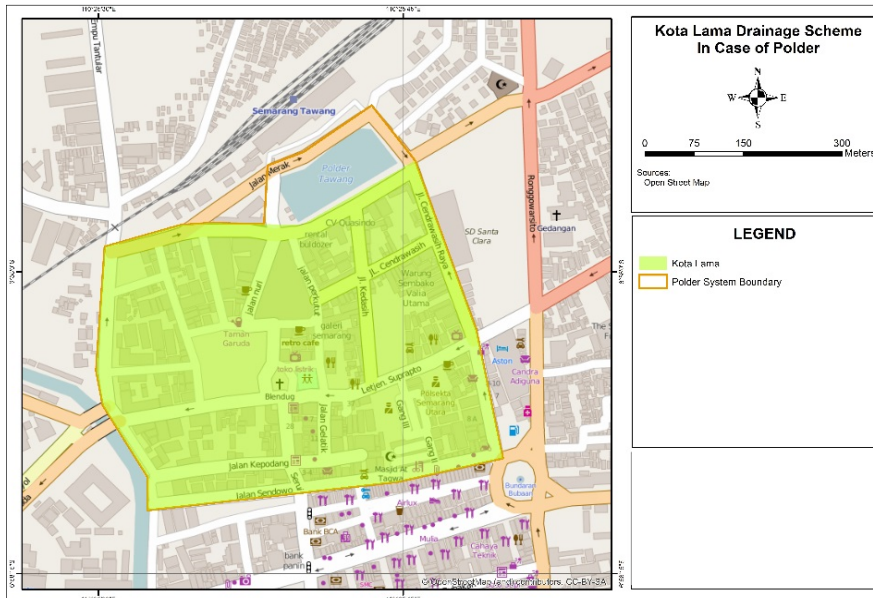


Figure 10. Boundary Map of Kota Lama Polder.

### 3.3. Pumping capacity

The pump is expected to be able to overcome the tidal fluctuation and 25 years (for existing condition) and 50 years return period rainfall (suggested by Ministry of Public Work and Housing, 2009). The simulation was done for several rainfall return period which are 10, 25, 50, 100, 200 and 1000 years. The inundation starts to occur when the rainfall is more than 100 years return period rainfall or more precisely the pump can cope with rainfall of 208 mm/day. If the canal must have a freeboard of 0.2 m below the surface as required, the results show that the existing pump can serve up to 25 years rainfall return period or 175 mm/day accurately. Water depth curve for inside Kota Lama Polder is presented in Figure 11.

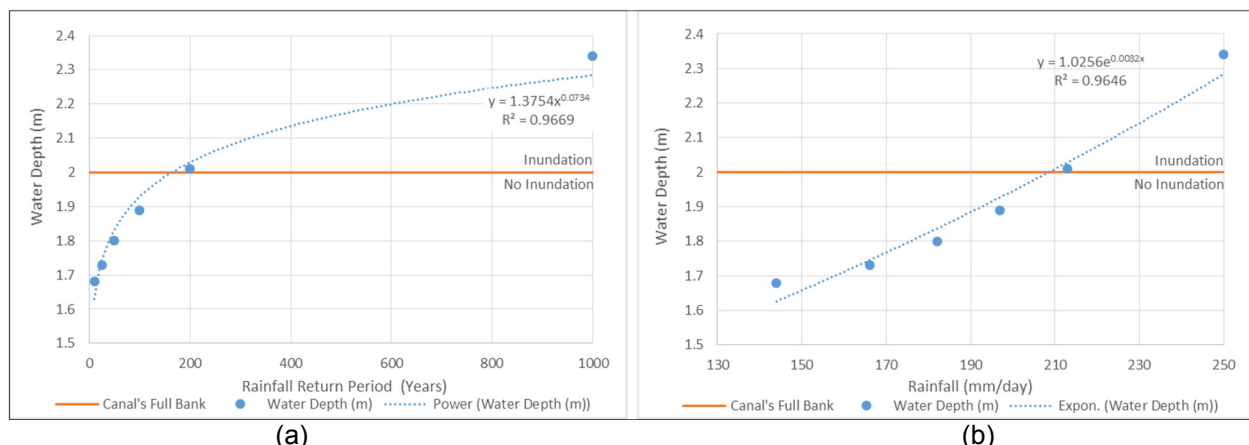
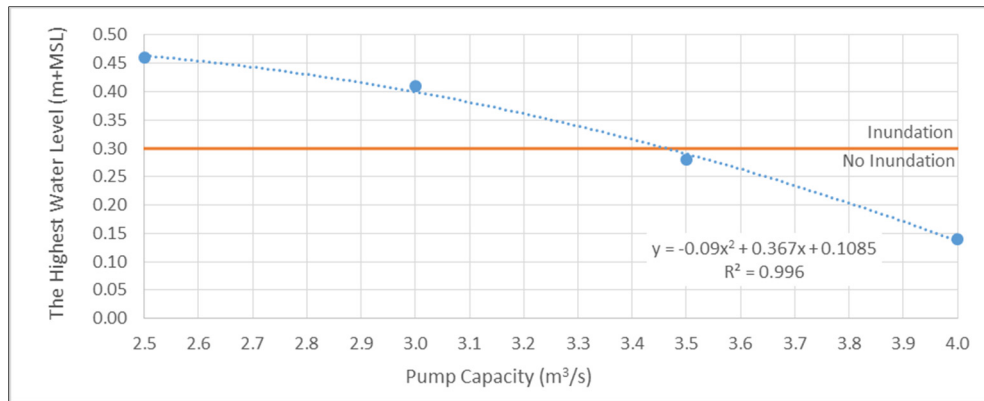


Figure 11. Water Depth Curve for Inside of Kota Lama Polder with Existing Pump, (a) Return Period Rainfall & (b) Rainfall.

The existing pump capacity at Kali Baru Pump Station (Outside Kota Lama Polder) cannot overcome even for the rainfall of 10 years return period, so the bigger capacity of the pump is needed. According to Figure 12, the results of pump selection simulation show that the pump capacity of 3.5 m<sup>3</sup>/s can cope with the 50 years return period rainfall or up to 189 mm/day accurately.



**Figure 12.** Pump Selection for Outside of Kota Lama Polder.

### 3.4 Hydraulic structure components

The proposed situation of Kota Lama can be seen in Figure 13. Resume of proposed control structures and pumps for Kota Lama Polder and its surrounding, among others:

- Inside Kota Lama Polder
  - a) Tawang pump station (existing, 0.45 m³/s of pumping capacity),
  - b) vertical gates for inlet and outlet at Retention Basin (existing, four vertical gates of 1.5 m for inlet and two vertical gates of 1.5 m for outlet),
  - c) vertical gate at first outlet of Semarang River (existing, two vertical gates of 1 m for each gate),
  - d) flap gate at second outlet of Semarang River (proposed, width of 0.6 m),
  - e) flap gate at western part of Merak Street drainage (proposed, width of 3.5 m),
  - f) flap gate at eastern part of Merak Street drainage (proposed, width of 3.5 m),
  - g) flap gate at the western connection of Kota Lama and main drainage (proposed, width of 2 m)
  - h) enlargement of the western canal connection (proposed, dimension of 2.6 m²)
- Outside Kota Lama Polder
  - a) Baru River pump station for Kota Lama sub drainage system (proposed, 3.5 m³/s of pumping capacity and two vertical gates of 1.5 m for each gate),
  - b) connection canal from Merak Street drainage to Tawang Street drainage (proposed, dimension of 4.8 m²)



**Figure 13.** Proposed Kota Lama Polder Drainage Scheme.

### 3.5 Dike height

Ministry of Public Works and Housing (2009) recommended that the design of dike height is 1000 years return period rainfall at the outside of polder area which is 0.13 m with the proposed pump capacity. Considering the occurrence of land subsidence with the “do nothing” scenario in 15 years, the estimated land subsidence is 0.8 m. Therefore, it is recommended that the dike height is 1.0 m. Polder’s ring dike suggested by elevating the road, so it does not diminish the aesthetic values of colonial buildings. This is possible because the average width of the road as the boundary is 12 m.

### 3.6 Polder system simulation

The simulation was done by using the rainfall of 25 years return period. The proposed drainage scheme of Kota Lama Polder was created by the previous description. The canals were in clean condition. The start and stop interval for Tawang pump and Baru River pump were changed to 0.3 m as starting surface level for start and 0.50 m at stopping surface level.

Water level inside and outside of Kota Lama Polder was increased after 14:00 because of the addition of inflow from rainfall. Outside the polder has higher water level due to its larger service area and tidal fluctuation effects. The highest water level in Kota Lama occurred at 20:40 of +0.02 m+MSL or 0.27 m-surface level. Then, for the highest water level outside the polder was +0.26 m+MSL or 0.04 m-surface level. It is proved that the polder system can keep Kota Lama from inundation. The water level inside and outside Kota Lama can be seen in Figure 14.

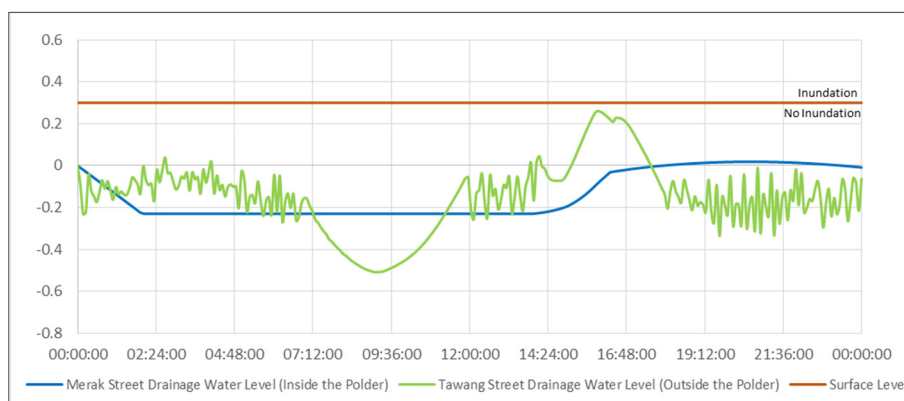


**Figure 14.** Water Level Condition on Merak Street and Tawang Street after Implementation of Polder System.

#### 4 CONCLUSIONS

The main causes of flood problem in Kota Lama is the occurrence of sediment and waste in drainage canal, high rainfall intensity, lack of capacity of working pump during flood and tidal fluctuation due to its connection with Banger sub drainage system. Water level in Semarang and Baru River are also crucial for determination operations of drainage system in Kota Lama.

Kota Lama Polder is a gravity driven polder which can serve 26 ha of Kota Lama Semarang UNESCO heritage site. The inside area of polder is designed with the existing pump capacity of 0.45 m<sup>3</sup>/s. The polder is installed with 4 flap gates to restrict the water outside entering the polder. Tawang retention basin is used within the polder system. The height of ring dike is 1.0 m by considering the highest water level outside the polder of 1000 years rainfall, 15 years the occurrence of land subsidence and tidal fluctuation effects. Capacity of Baru River pump should also be increased to 3.5 m<sup>3</sup>/s to protect the outside area of the polder.

#### REFERENCES

- Jha, K.A., Bloch, R. & Lamond, J. (2012). *Cities and Flooding: A Guide to Integrated Urban Flood Risk Management for the 21<sup>st</sup> Century*. Washington, D.C.: The World Bank.
- Ministry of Public Works and Housing. (2009). *Prosedur and Instruksi Kerja Validasi Data Hidrologi*. Jakarta: Directorate General of Water Resources.
- Ministry of Public Works and Housing. (2009). *Urban Polder Drainage: General Aspects*. Bandung: Water Resources Research Development Centre.
- Ministry of Public Works and Housing. (2009). *Urban Polder Drainage: Institutional Aspects*. Bandung: Water Resources Research Development Centre.
- Ministry of Public Works and Housing. (2009). *Urban Polder Drainage: Technical Aspects*. Bandung: Water Resources Research Development Centre.
- Ministry of Public Works and Housing. (2009). *Urban Polder Drainage: Case Study Banger Polder Semarang*. Bandung: Water Resources Research Development Centre.
- Suryadi, F.X. (1996). Soil and Water Management Strategies for Tidal Lowlands in Indonesia. *PhD Thesis*. Delft University of Technology – IHE Delft. Rotterdam: A.A. Balkema.
- UNESCO. (2015). *Semarang Old Town*. Jakarta: Indonesia National Commission for UNESCO.
- Witteveen+Bos. (2009). Conceptual design report, Development pilot polder Semarang and guidelines polder development. Deventer, the Netherlands.

# FLOOD SIMULATION AND RISK ANALYSIS BASED ON SEMANTIC 3D CITY MODELS COUPLED WITH HYDRONUMERIC MODELS (FLORICIMO)

TORSTEN HEYER<sup>(1)</sup>, HELLEN HAMMOUDI<sup>(2)</sup>, ROBERTO TATIS MUVDI<sup>(3)</sup>, STEFAN TROMETER<sup>(4)</sup>, ARNE  
SCHILLING<sup>(5)</sup> & JUERGEN STAMM<sup>(6)</sup>

<sup>(1,2,3,6)</sup> Institute for Hydraulic Engineering and Technical Hydromechanics, TU Dresden, Germany,  
torsten.heyer@tu-dresden.de

<sup>(4)</sup> CADFEM GmbH, Grafing b. Munich, Germany,  
strometer@cadfem.de

<sup>(5)</sup> virtualcitySYSTEMS GmbH, Berlin, Germany,  
aschilling@virtualcitysystems.de

## ABSTRACT

Research project FloRiCiMo aims to couple semantic digital city models with hydronumeric models for the simulation of river floods in urban areas. Despite containing large volumes of data that can be used in the simulation of physical processes (terrain elevation; flow obstacles like houses, bridges or culverts etc.) and for risk analysis (damage potential evaluation), digital city models have mainly been used for visualization purposes so far. In order to allow for city-model-based flood simulations, this research project addresses issues such as the semi-automated fixing of geometric imperfections, web-based queries for user-defined data extraction, and data transformation for the generation hydronumeric models. 2D (floodplain scale) and 3D (local scale) numerical simulations are then performed based on the data extracted from the city model, and results are imported back and post-processed in the digital city model for visualization purposes. Linking semantic 3D city models with hydrodynamic modules offers numerous advantages in the management of river floods in urban areas, including centralized data management, enhanced communication and easy inspection of simulation results, to name but a few. This paper presents the basic idea, methodical concepts and the results of the first phase of the project.

**Keywords:** semantic digital city models; risk analysis; hydronumerics; urban floods.

## 1 INTRODUCTION

Numerous extraordinary flood events that occurred in Middle Europe during the last twenty years seem to prove the IPCC's climate change predictions of an increased occurrence of extreme hydrologic events in terms of frequency and intensity. For instance, the return periods of Elbe river floods at gauge Dresden (Germany) were 100 to 200 years in 2002 and 50 to 100 years in 2013, with another major flood event in 2006. The European floods in 2002, with an overall damage of approximately 15 billion EUR (only 9 billion EUR in Germany), were probably the main drivers for the preparation and implementation of the "directive on the assessment and management of flood risks" ("EU Floods Directive") by the European Union in November 2007. This legislation required all member states to develop flood risk management plans for endangered regions until the end of 2015. Moreover, these plans have to be revised every six years for all relevant regions. Since flood risk analysis, being an essential component within flood risk management, usually incorporates the need for hydronumeric computations, the great efforts required in this field become obvious. This holds particularly true for flood risk assessment in urban areas, where the damage potential is high and flood relevant structures and conditions (over- and underground) are usually very complex and might change rapidly with the city's development.

In conclusion, hydronumeric models for urban areas need to be updated regularly, according to the EU Floods Directive at least every six years. In practice, however, the reasonable interval for model updating is much shorter, depending e.g. on the speed and extent of urban development. From a broader perspective, possible inundation processes are just one of the many aspects that need to be considered in development plans for urban regions. Other issues, such as population and transport development or alternative emergency scenarios (e.g. bomb alert) are of equal importance to gain a holistic interlinked view to future urban developments. In this regard, semantic 3D city models are important tools nowadays that are used increasingly in urban planning around the world. These models are based on the international standard CityGML, a database solution that allows for various object queries in opposition to simple 3D visualizations of buildings. Until now, such models exist for larger cities or cities of greater importance, e.g. historic sites. Usually, virtual city models are of high complexity and contain large volumes of data that is also relevant for the simulation of physical processes (terrain elevation; obstacles like houses, bridges or culverts etc.) and for risk analysis (damage potential evaluation). From this, the idea arose to generate hydronumeric models for urban areas based on the semantic 3D city models. Likewise, the results of hydronumeric simulations can be

visualized and post-processed in a virtual city model. The strategy of interlinking semantic 3D city models with hydrodynamic modules offers numerous advantages, such as central data management, increased result acceptance in the public or easy inspection of simulation results to name but a few.

## 2 GENERAL CONCEPT

Project FloRiCiMo builds on valuable experience and know-how that was gathered by two of the involved partners in a previous research project called "DETORBA" (Trometer & Mensinger, 2014). This project pursued the objective of simulating the blast pressure wave propagation using virtual city data in order to analyze the risk and the impact of aerial bombs from World War II that might be exploding in urban environments. Based on the technologies developed in DETORBA, other urban simulation applications in the field in the field of acoustics, air pollution and mobility are currently under development. In this context, FloRiCiMo focuses on the simulation of surface flows induced by river floods in urban environments.

The main objective of the first phase of FloRiCiMo was to develop and test a methodological framework for flood simulations based on semantic virtual city models. In order to couple the city models with hydronumeric solvers, a semi-automated workflow in combination with the required interface tools and transformation techniques was established, taking into account the requirements of surface flow simulation models (data, parameters, geometric resolution etc.). Firstly, the workflow contemplates the inclusion of flood-relevant data (e.g. bathymetry) into a virtual city model and the setup of an online portal used for the selection of target areas, user-defined queries and data transfer and conversion between the city model and the hydronumeric models. Two types of hydrodynamic simulations will be possible:

- fast 2D simulations for large regions (floodplain scale), with a higher degree of simplification regarding flow velocities (depth-averaged velocities), pressures (hydrostatic), and building representation (level of detail 0 = holes or 1 = blocks), and
- detailed 3D simulations for selected objects (local scale) or small areas (slow, with high computational effort, buildings represented in level of detail 2 or higher)

Although both simulation techniques can be employed independently, they can be linked by using the results of the 2D computation (large scale) as hydraulic boundary conditions for the local-scale 3D simulations. Based on the required level of detail, computational efficiency and flexibility (e.g., regarding the representation of bridges, weirs, etc. through different empirical formulae) for the 2D floodplain-scale simulations, a raster-based finite volume 2D solver was implemented in this project. 3D hydronumeric simulations were conducted by using ANSYS-CFX. Auxiliary tools provided by ANSYS were used for the optimization of model setup and simulation. The results of the 2D as well as the 3D simulations can be transferred, visualized and analyzed in the virtual city model. In order to establish and test the new modeling strategy, the German cities of Dresden (Federal State of Saxony) and Magdeburg (Saxony-Anhalt) were chosen. Both cities are located along the Elbe River and suffered from the extreme flood events of 2002 and 2013. The first project phase focused on the city model of Dresden only.

## 3 3D CITY MODELS AND DEVELOPMENT OF ONLINE PORTAL

Virtual 3D city and landscape models are often used for visualizing urban environments. Applications that benefit from having 3D representations of buildings, bridges, and other man-made objects include urban planning, public relation activities, navigation, underground developments, line-of-sight analyses, and 3D measuring. These applications require an accurate visual representation of objects often involving texture mapping and visual effects such as Phong rendering, shadow mapping, and ambient occlusion.

The capabilities that huge data sets can be made available online has been brought to the attention of a wider audience with the introduction of WebGL and related internet technologies, which enables customers to access complex 3D city models using standard internet browsers. 3D assets can now be embedded into web portals in the same way as videos. The technologies for streaming 3D city models are currently being standardized in order to increase the interoperability between vendor implementations (Schilling et al. 2016).

Many city municipalities and regional administrations are currently including 3D city models into their geospatial data infrastructure. In this context, the OGC CityGML standard (Open Geospatial Consortium, 2012) has been adopted by many authorities for storing and managing their 3D geo data sets (Kolbe, 2009; Gröger et al., 2012). Although Geographic Information Systems (GIS) and Spatial Data Infrastructures (SDI) are well suited for applications that focus on the geometric and visual representation of objects, numerical simulation scenarios have rarely been associated with geographic information science. Attempts of coupling GIS with numerical simulations were made by Kashiyama et al. (2008) and Tymkow et al. (2016). A major benefit of automatic workflows that make 3D city models available to simulation frameworks is that urban data is managed and updated by the municipal authorities and can be made available for simulation tasks on demand without the need of redundant data creation or processing.

With special regard to flood simulation, the required formats and interfaces for accessing the relevant spatial data depend on the type of the hydronumeric simulation. Solvers of 2D runoff models can operate on raster data sets encoding elevation values on a regular grid. Accurate Digital Elevation Models (DEM) are usually available at land surveying offices. Bathymetric data on riverbeds and lakes must be acquired

separately and merged with the DEM. Spatial subsets can be extracted e. g. as GeoTIFFs from GIS. 3D solvers such as ANSYS-CFX require physically correct volumetric models, for which CityGML can be used as data management backend. As semantic information model covers a wide range of urban object types, CityGML is not limited to a specific application. The availability not only of a building module, but also a bridge module, a relief and land use module and a water module describing underwater features allows to model complete city landscapes accurately. However, a series of transformation steps must be performed in order to make 3D city models available to numerical solvers (Piepereit et al. 2016).

For the project FloRiCiMo, we imported a complete CityGML building data set that we received from the land surveying office of the city of Dresden into a 3DCityDB database. This database maps the entire CityGML structure as object relational schema and enables extracting spatial subsets as well as specific Level of Detail (LoDs). Buildings are available up to LoD 2, which represents objects as simple outer hull. Bridges are even available as LoD 3, which allows to model piers and the deck accurately, which is important e. g. for simulating backwater effects correctly (see Figure 1).



**Figure 1.** Sections of the semantic 3D city model of Dresden, visualized in the online portal.

From this database, spatial subsets along the river Elbe were extracted including the available man-made objects as well as the elevation model representing the terrain and the riverbed (bathymetry) as CityGML. However, CityGML formats cannot be used directly in the simulation software. Therefore, the following steps were performed:

- Conversion into a CAD boundary representation model. This step maps the CityGML geometry classes into a topological half edge data structure used in CAD. ISO 10303 (STEP) was used as a reference for defining geometry classes and topological relationships. ISO 10303 files can be imported into CAE software such as ANSYS and for setting up 3D simulation models.
- Creating watertight models. In order to create meshes and finite element representations from 3D city models, each object must be represented as a collection of solid geometries. Buildings could be transformed into solids easily because LoD 2 specifies that buildings must not have interior surfaces and are built up of only wall, roof, and ground surfaces. However, the terrain model and land use areas are represented as surfaces. These surface parcels must be transformed into solids by an extrusion operation (Figure 3).
- Healing and removing inconsistencies in the model. The requirements of the mesh creation process regarding the model quality are quite high. For example, the allowed geometrical tolerance values for planar polygons is higher than that for graphics systems, because CAE software was primarily developed for designing mechanical parts, not for larger urban models. The 3D GIS data creation processes are often operating with higher tolerance values. The resulting inconsistencies must be corrected by local geometry modifications. More details can be found in Piepereit et al. (2016).



**Figure 2.** Online map of flood scenario (2D) in Dresden including buildings and bridges with detailed geometries.

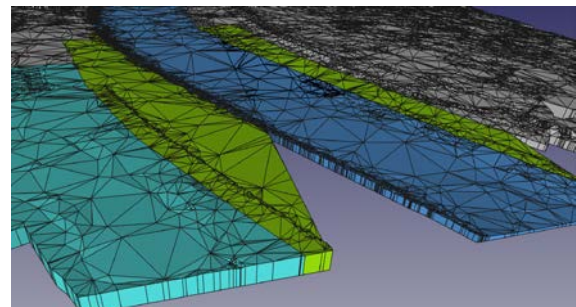


**Figure 3.** Solid modeling of elevation and bathymetry surfaces.

#### 4 FLOODPLAIN-SCALE 2D SIMULATION

Given their computational cost and required level of detail, 3D HN simulations are restricted to specific buildings and/or small sections of the full river floodplain (inundation area). Thus, as a starting point, the implementation of HN simulations based on semantic city models requires less computationally demanding alternatives that are able to model the inundation process at the scale of the entire floodplain more efficiently. At the same time, this guarantees the validity of the boundary conditions used in the 3D computations by anchoring the models at the available river gauging stations.

The simulation domains involved in this task are of the order  $10^2 - 10^4 \text{ km}^2$ , which is an appropriate scale for 2D shallow water models considering the relative magnitude of horizontal and vertical water motion, computational costs and the required accuracy of the results (Lane & Fergusson 2005). At the same time, shallow water models are able to represent hydraulically relevant urban structures such as buildings, dykes, floodwalls and, through empirical formulae, bridges, weirs and overpasses.

The development of the 2D solution in FloRiCiMo was achieved in two steps. First, several tests were conducted with existing shallow water models in order to derive criteria for the implementation of an ad-hoc 2D HN shallow water solver. This exploratory study showed that, although shallow water models based on an irregular mesh can provide a more detailed description of river and urban geometry, mesh quality considerations can increase manual processing times considerably. In contrast, models based on a regular Cartesian mesh allow simulations to be run directly on floodplain-scale geometric and hydraulic roughness data (Falter et al. 2015; Hunter 2008) with very little manual processing. The loss of geometric detail resulting from the use of a regular grid can be compensated when high-resolution data (e.g.,  $<10 \text{ m} \times 10 \text{ m}$  grids) are available.

In the second step, the 2D HN solver was implemented in C++ using the DIFFPACK library (Langtangen 2013). The numerical scheme selected was the well-balanced, 1<sup>st</sup>-order, shock-capturing finite volume scheme with wetting-and-drying proposed by Liang and Borthwick (2009). This scheme, which is based on the HLLC approximate Riemann solver proposed by Toro (2001), solves the conservation form of the inviscid shallow water equations. In vector form, these can be written as:

$$\frac{\partial \mathbf{u}}{\partial t} + \frac{\partial \mathbf{f}}{\partial x} + \frac{\partial \mathbf{g}}{\partial y} = \mathbf{s} \quad [1]$$

The vector quantities  $\mathbf{u}$ ,  $\mathbf{f}$ ,  $\mathbf{g}$  and  $\mathbf{s}$  are as follows:

$$\mathbf{u} = \begin{bmatrix} \eta \\ uh \\ v_h \end{bmatrix}, \mathbf{f} = \begin{bmatrix} uh \\ u^2h + \frac{1}{2}g(\eta^2 - 2\eta z_{bed}) \\ uvh \end{bmatrix}, \mathbf{g} = \begin{bmatrix} vh \\ uvh \\ v^2h + \frac{1}{2}g(\eta^2 - 2\eta z_{bed}) \end{bmatrix}, \mathbf{s} = \begin{bmatrix} 0 \\ -g\eta \frac{\partial z_{bed}}{\partial x} - \frac{\tau_{bed,x}}{\rho} \\ -g\eta \frac{\partial z_{bed}}{\partial y} - \frac{\tau_{bed,y}}{\rho} \end{bmatrix} \quad [2]$$

where  $x$  and  $y$  are the two Cartesian directions on a horizontal plane,  $t$  = time,  $\eta$  = water level,  $u$  =  $x$ -velocity component,  $v$  =  $y$ -velocity component,  $h$  = water depth,  $z_{bed}$  = bed elevation,  $g$  = gravity ( $9.81 \text{ m/s}^2$ ),  $\tau_{bed}$  = bed friction and  $\rho$  = water density ( $1000 \text{ kg/m}^3$ ).

The finite-volume form of the equation system is

$$\mathbf{u}_{i,j}^{t+1} = \mathbf{u}_{i,j}^t - \frac{\Delta t}{\Delta x} (\mathbf{f}_{E,i,j}^t - \mathbf{f}_{W,i,j}^t) - \frac{\Delta t}{\Delta y} (\mathbf{g}_{N,i,j}^t - \mathbf{g}_{S,i,j}^t) + \Delta t \mathbf{s}_{i,j}^t \quad [3]$$

where  $\mathbf{u}$ ,  $\mathbf{f}$ ,  $\mathbf{g}$  and  $\mathbf{s}$  are defined as in equation [2], subscripts  $i$  and  $j$  refer to the horizontal and vertical directions, superscripts  $t$  and  $t+1$  indicate time steps  $t$  and  $t+1$ ,  $\Delta x$ ,  $\Delta y$ ,  $\Delta t$  indicate the step size in  $x$ ,  $y$  and  $t$ , and subscripts  $E$ ,  $W$ ,  $N$  and  $S$  refer to the east, west, north and south faces of computational cell  $i, j$ .

The implementation of this numerical scheme was validated against an existing calibrated 2D shallow water model for the city of Dresden (Germany) based on an irregular grid. Preliminary simulations show satisfactory agreement between the water levels of the two models along the main channel during an extreme Elbe river flood ( $Q = 6255 \text{ m}^3/\text{s}$ ) (figure 4). These results suggest that the loss in geometric detail caused by the use of a regular grid did not affect the quality of the model. However, local inaccuracies may arise due to the exclusion of sub-grid geometric details such as floodwalls or gaps between buildings in the digital elevation model.

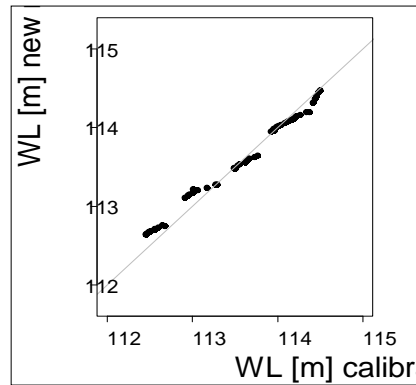


**Figure 4.** Comparison between the water levels (WL [m]) of the calibrated and newly implemented shallow water models. The grey line corresponds to the perfect agreement line. Root-mean-square-error = 0.11 m.

## 5 LOCAL SCALE 3D SIMULATION

### 5.1 3D flood simulation: Simplified city model

In order to investigate the computational effort and time as well as the definition of appropriate model parameters and boundary conditions, 3D simulations were carried out first on a simplified city model using ANSYS CFX. The simplified city model represents a small urban area containing buildings (LoD 1), a river, a bridge and a flood wall (Figure 5, left). Steady state simulations were conducted for three different scenarios. Furthermore, a scenario with a partially breached flood wall was investigated by means of an unsteady simulation. The four scenarios defined were:

- Scenario 1: mean discharge conditions (in-channel flow)
- Scenario 2: flood conditions with water level below the floodwall crest
- Scenario 3: flood conditions with water level at floodwall crest
- Scenario 4: floodwall failure scenario (unsteady, initial conditions from scenario 3)

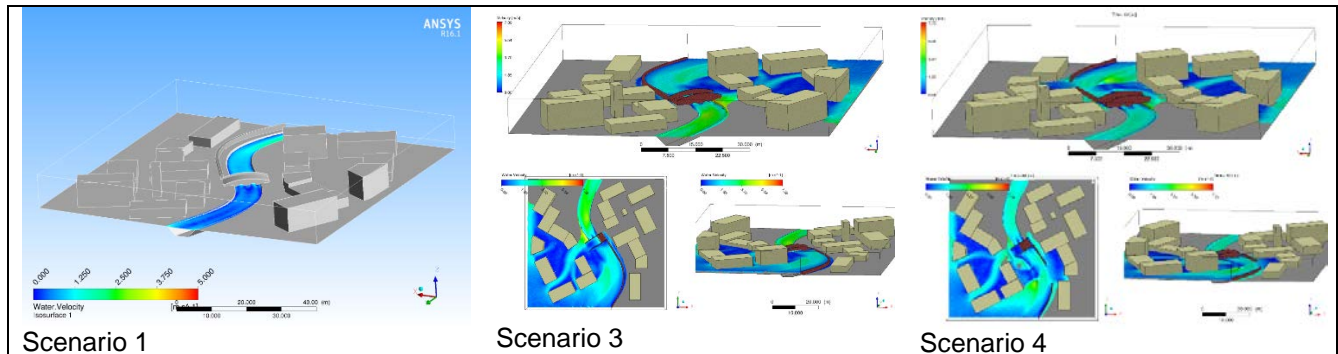


**Figure 5.** Flow velocity distribution in a simple city model for different scenarios.

The edge lengths of the computational grid ranged from 30 to 80 cm. The hydraulic boundary conditions were defined with respect to measured data in natural rivers of similar size. The roughness characteristic was set to 400 mm in the river bed and 6 mm for all other surfaces. As a result of preliminary tests, the k- $\omega$ -model was used for the simulations since the computational speed was the highest and flow patterns were reasonable. All 3D simulations were carried out at the Center for Information Services and High Performance Computing (ZIH) of the TU Dresden, using about 10 to 20 cores at the time.

### 5.2 3D simulation model: test case Dresden

In order to test the developed methodology and to show the 3D simulation capabilities, a test area near the Augustus Bridge in the historic city center of Dresden was selected. The investigation area was specified by means of the online city model platform (see Figure 6) and then transferred to the ANSYS simulation framework.



**Figure 6.** Investigation area near the Augustus Bridge in the historic city center of Dresden.

In order to set up a 3D simulation, the digital elevation model, the bathymetry and city model objects (buildings) in LoD 2 were extracted and converted. The resulting geometric model (Figure 7, left) met the quality requirements without any additional manual adjustments. In contrast, the integration of the detailed bridge (Figure 7, right), which was originally not included in the city model, was challenging. The original 3D CAD data for the Augustus Bridge contained a number of geometric inconsistencies, such as disconnected planes, which created gaps and holes in the model. These have no effect on model visualization but need to be fixed for a numerical flood simulation. Thus, a semi-automatic procedure was developed to create geometrically sound structures.

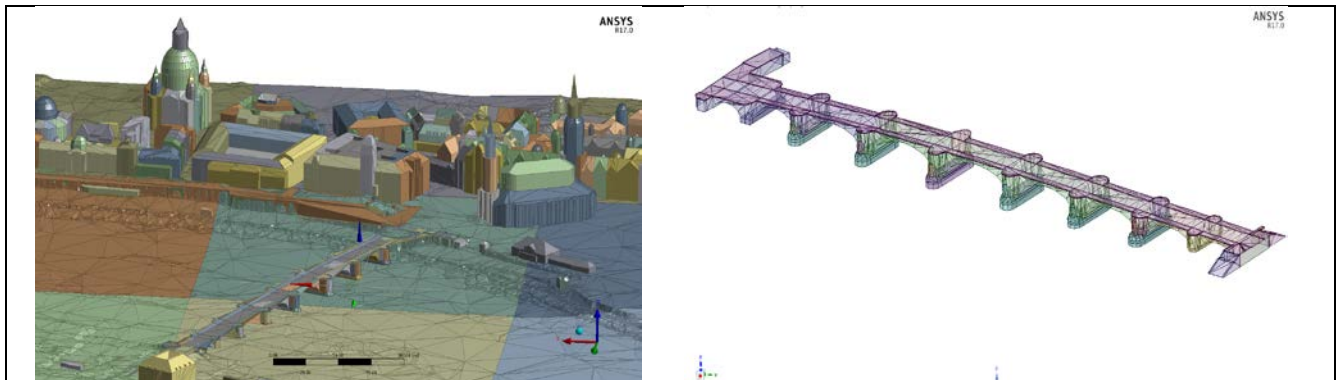


**Figure 7.** Geometric representation of the old town of Dresden (left) and the model of the Augustus Bridge (right) that had to be included separately.

After an initial manual cleaning of large inconsistencies, the CAD model was converted into a faceted geometry, which allows the application of a set of repair functions that are available in the Space Claim Direct Modeler1 of ANSYS. In order to derive a solid body definition for the bridge model, a shrinkwrap algorithm was applied subsequently (Figure 8, left). Based on this, a 3D negative water volume body could be created (Figure 8, right).

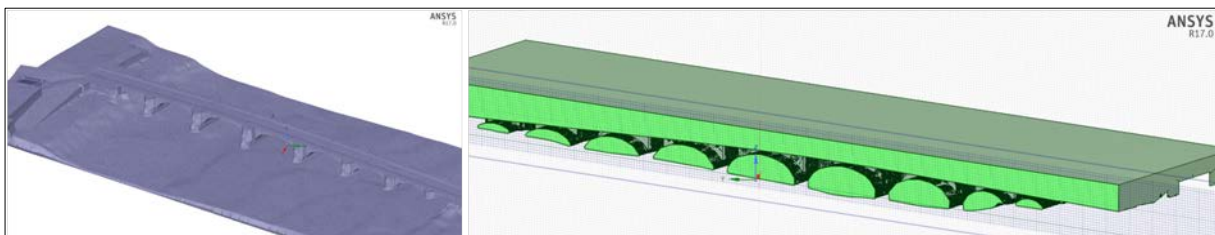


**Figure 8.** Detailed and cleaned 3D geometric model (left) as basis for the negative water volume body (cross-section) required for 3D simulations.

The grid of the fluid domain was generated using ANSYS meshing. A high quality unstructured tetrahedral mesh with a maximum cell size ranging from 20 to 80 cm was created using global and local sizing parameters. The final grid has about 5 million tetrahedral cells. For steady state simulations, water levels and discharges were defined as hydraulic boundary conditions. Parameter values were defined according to available measurements during the Elbe flood in 2013 at gauge Dresden. The walls of buildings and other surfaces were defined as free slip walls, while the roughness of the river bed was set to 400 mm. All simulations were carried out using the k- $\omega$ -turbulence model. For validation purposes, the results obtained by ANSYS CFX were compared with real data and photos gathered during the flood event in 2013. It can be concluded that the 3D simulation represented the natural conditions to a satisfactory extent (Figure 9).

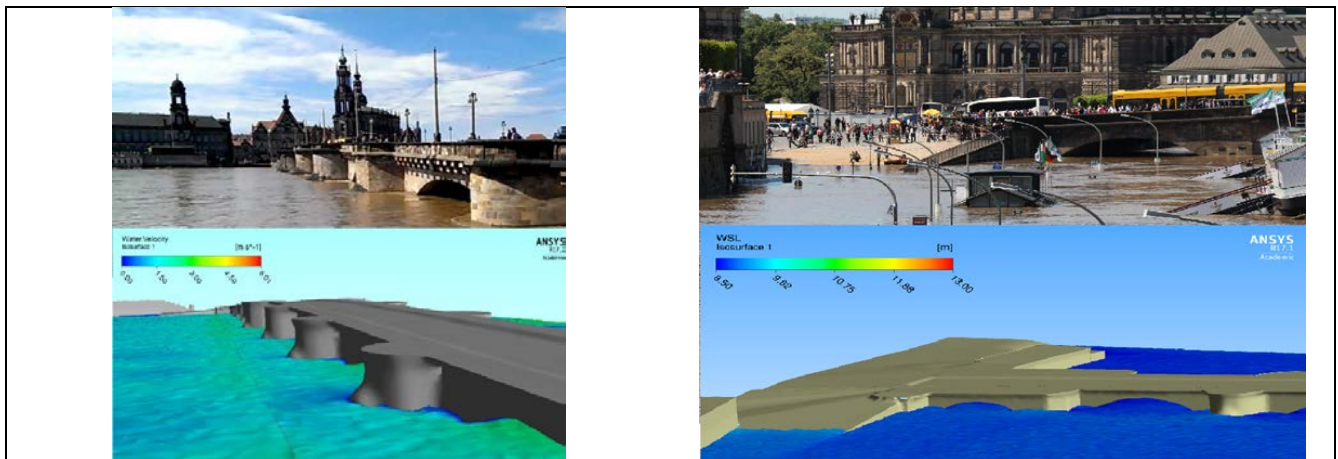


**Figure 9.** Result images of the 3D simulation compared to photos taken during the flood 2013 in Dresden.

Figures 10 and 11 illustrate the advantage of 3D simulation of mapping the velocity (left) and the pressure distribution on bridge piers (right) in all directions of space.

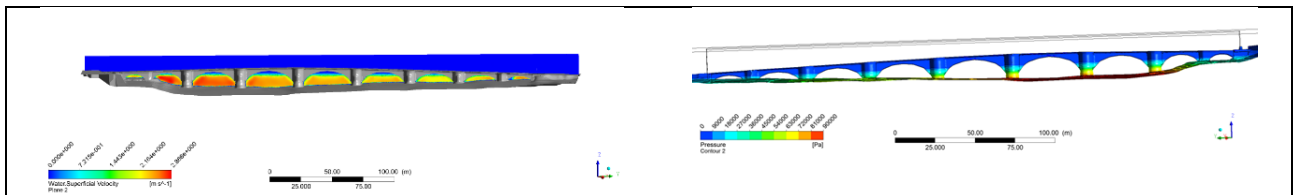


**Figure 10.** Flow velocity distribution through bridge openings for flood scenario 2013.

**Figure 11.** Pressure distribution at bridge piers for flood scenario 2013.

## 6 CONCLUSIONS

The combination of semantic 3D city models with 2D and 3D hydronumeric simulations proposed in project FloRiCiMo is in line with the ongoing trend towards urban digitalization and smart city applications. The feasibility of the proposed modeling framework could be proven in phase 1 of the project. Given that further enhancements of the modeling strategy can be expected in phase 2 of the project (in planning), this methodology will become a valuable tool in modern flood risk management in the future. In their current state, many existing virtual city models do not yet meet the requirements for numerical simulations and need to be further enhanced.

Virtual city models have a large application potential in risk analysis for other physical processes, given that enormous amounts of information relevant for hazard and damage assessments can be implemented and administered. Regarding flood damage evaluation, information regarding the hydraulic vulnerability and resistance of buildings can be analyzed in a more detailed and integrated way, for instance by implementing LoD buildings (Figure 12) or by linking building information models (bim) to the virtual city models.

Since the simulation results, such as flow velocities, depths or intensities, can be visualized more realistically (Figure 13), this approach might also bridge the gap between standard hydronumeric and physical models with respect to raising or maintaining the public flood risk awareness, e.g. by means of augmented reality applications.

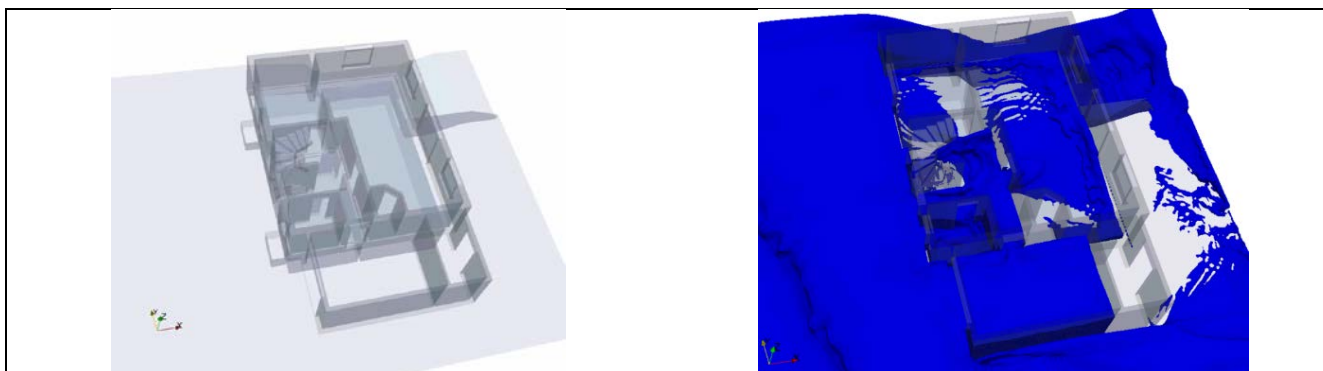


**Figure 12.** Geometric model and simulation of flooding of a residential house in LoD 3 using ANSYS-CFX.



**Figure 13.** Photorealistic rendering of flood simulation results displayed in a 3D city model.

## ACKNOWLEDGEMENTS

Project FloRiCiMo was funded by the Deutsche Bundesstiftung Umwelt (German Federal Environmental Foundation, DBU). The DBU is one of Europe's largest foundations and promotes innovative and exemplary environmental projects. We thank the DBU for supporting phase 1 of the project (July 2015 – March 2017) and hope that the support continues in phase 2 (planned for 2017/18). Furthermore, we thank the environmental and the land surveying offices of the federal state capitals Dresden (Saxony) and Magdeburg (Saxony-Anhalt) for supporting the project with data and ideas, e.g. to identify issues and research goals with focus on practical relevance (applicability of the method, data maintenance costs etc.).

## REFERENCES

- Falter, D., Schröter, K., Nguyen, V. D., Vorogushyn, S., Kreibich, H., Hundecha, Y., Apel, B. & Merz, B. (2015). Spatially Coherent Flood Risk Assessment Based on Long-Term Continuous Simulation with a Coupled Model Chain. *Journal of Hydrology*, 524, 182–193.
- Gröger, G., Kolbe, T. H., Nagel, C. & Häfele, K. H. (2012). OGC City Geography Markup Language (CityGML) Encoding Standard, Version 2.0.0, 12-019. *Open Geospatial Consortium*.
- Hunter, N. M., Bates, P. D., Neelz, S., Pender, G., Villanueva, I., Wright, N. G., Liang D., Falconer R. A., Lin B., Waller S., Crossley A. & Mason D. C. (2008). Benchmarking 2D Hydraulic Models for Urban Flooding. In: *Proceedings of the Institution of Civil Engineers, Water Management*, Thomas Telford (ICE publishing), 16(1), 13-30.
- Kashiyama K., Takada T. & Miyachi H. (2008). Large Scale Finite Element Modeling, Simulation and Visualization for Wind Flows in Urban Area Using Virtual Reality. In: *Tsinghua Science and Technology*, 13(1), 84-89.
- Kolbe T. H. (2009). *Representing and Exchanging 3D City Models with Citygml*. In: 3D geo-information sciences, Springer Berlin Heidelberg, 15–31.
- Lane, S. & Ferguson, R. (2005). *Modelling Reach-Scale Fluvial Flows*. Computational Fluid Dynamics: Applications in Environmental Hydraulics, John Wiley & Sons, 217-269.
- Langtangen, H.P. (2013). *Computational Partial Differential Equations: Numerical Methods and Diffpack Programming (Vol. 2)*. Springer Science & Business Media, 1-685.
- Liang, Q. & Borthwick, A. (2009). Adaptive Quadtree Simulation of Shallow Flows with Wet–Dry Fronts over Complex Topography. *Computers & Fluids*, 38, 221–234.
- Pieperit R., Schilling A., Alam N., Wewetzer M., Pries M. & Coors V. (2016). Towards Automatic Processing of Virtual City Models for Simulations. In: *ISPRS Annals of Photogrammetry, Remote Sensing and Spatial Information Sciences*, 4(2), 39-45.
- Schilling A., Bolling J. & Nagel C. (2016). Using glTF for Streaming Citygml 3D City Models. In: *Proceedings of the 21st International Conference on Web3D Technology*, ACM New York, 109-116.
- Toro, E (2001). *Shock-Capturing Methods for Free-Surface Shallow Flows*. John Wiley, 1-309.

- Trometer, S. & Mensinger, M. (2014). DETORBA – Detonationsszenarien im urbanen Umfeld – Neue Möglichkeiten mit GIS-basierten Stadtmodellen. In: *Proceedings BMBF-Innovationsforum "Zivile Sicherheit"*.
- Tymkow P., Karpina M. & Borkows A. (2016). 3D GIS for Flood Modelling in River Valleys. In: *The International Archives of the Photogrammetry, Remote Sensing and Spatial Information Sciences*, 175-178.

## URBAN FLOOD MODELLING – PROCESS OR REGRESSION?

JAMES E BALL<sup>(1)</sup>

<sup>(1)</sup> School of Civil and Environmental Engineering, University of Technology Sydney, Broadway, Australia  
james.ball@uts.edu.au

### ABSTRACT

Design flood estimation remains a problem for many professionals involved in the management of urban catchments. Advice is required regarding design flood characteristics for many design problems including the design of culverts and bridges necessary for cross drainage of transport routes, the design of the pipes and channels comprising urban drainage systems, the design of flood mitigation levees and other flood mitigation structures, design of retarding basin spillways, and many environmental flow problems. This advice is complicated further by the increasing the requirement to consider the impact of changing climatic states on design floods. The data desired for these design problems must be interpreted from a statistical viewpoint which contrasts to the deterministic viewpoint necessary to assess catchment response to a historical event. When data is not available for the site or system of interest, a common approach with development of the desired data for these design problems is utilized from catchment modelling systems. The aim of these catchment modelling systems is to predict the data that would have been recorded if a stream gauge were present for the event arising when the boundary conditions are simulated. Presented herein is a discussion of the design of flood problem for urban catchments under both current and future climate states.

**Keywords:** Hydroinformatics; urban; flood; modelling.

### 1 INTRODUCTION

Design flood estimation remains a problem for many engineers concerned with management of urban catchments. Advice is required regarding design flood characteristics for the design of culverts and bridges necessary for cross drainage of transport routes, for design of the pipes and channels comprising urban drainage systems, the design of flood mitigation levees and other flood mitigation structures, design of retarding basin spillways, and many other environmental flow situations. The flood characteristic of most importance depends on the nature of the design problem which is under consideration but, typically, is one of the following:

- Flood flow rate;
- Flood level;
- Flood rate of rise;
- Flood volume; or
- System performance.

While all of these flood characteristics have been noted as being of interest to flood designers, the dominant characteristic of concern has been the flood flow rate. This historical focus of the design flood problem is shown by Robinson (1987) who, in discussing selection of design floods, notes "*Hydrologic structures are required to perform in a predictable manner over a wide range of discharges. In Australia this can vary from zero to very large flows*". Current developments for management of urban water systems inclusive of WSUD, SUDS, LID and their many variants require consideration of flood volumes and flood levels in addition to this historical focus. Hence, for urban environments, these flood characteristics can be inserted into the statement of Robinson (1987) in lieu of flows without loss of generality and without changing the range of potential values.

In discussing the type of flood characteristic that is being considered for a design problem, it is worth noting that the desired flood characteristic(s) to be used for the design must be interpreted from a statistical viewpoint. This contrasts with analysis of the flood characteristics from a historical event where a deterministic viewpoint is appropriate. The need for the statistical interpretation of a design flood characteristic arises from the need to consider both the hazard arising from the magnitude of the design flood characteristic and the likelihood of that hazard occurring or being exceeded. In other words, there is a need to consider the relationship between the magnitude and the exceedance probability of a design flood characteristic. An example of this relationship is shown in Figure 1. From a design flood perspective, therefore, it is the analysis of data leading to the relationship shown in Figure 1 that is fundamental to the estimation of the quantile for the desired flood characteristic.

As discussed by Ball et al. (2011), alternative approaches for estimation of the design flood quantile are shown in Figure 2. As shown in that figure, there are two alternative situations when design flood characteristics are required and they are:

- Sufficient and suitable historical information is available; and

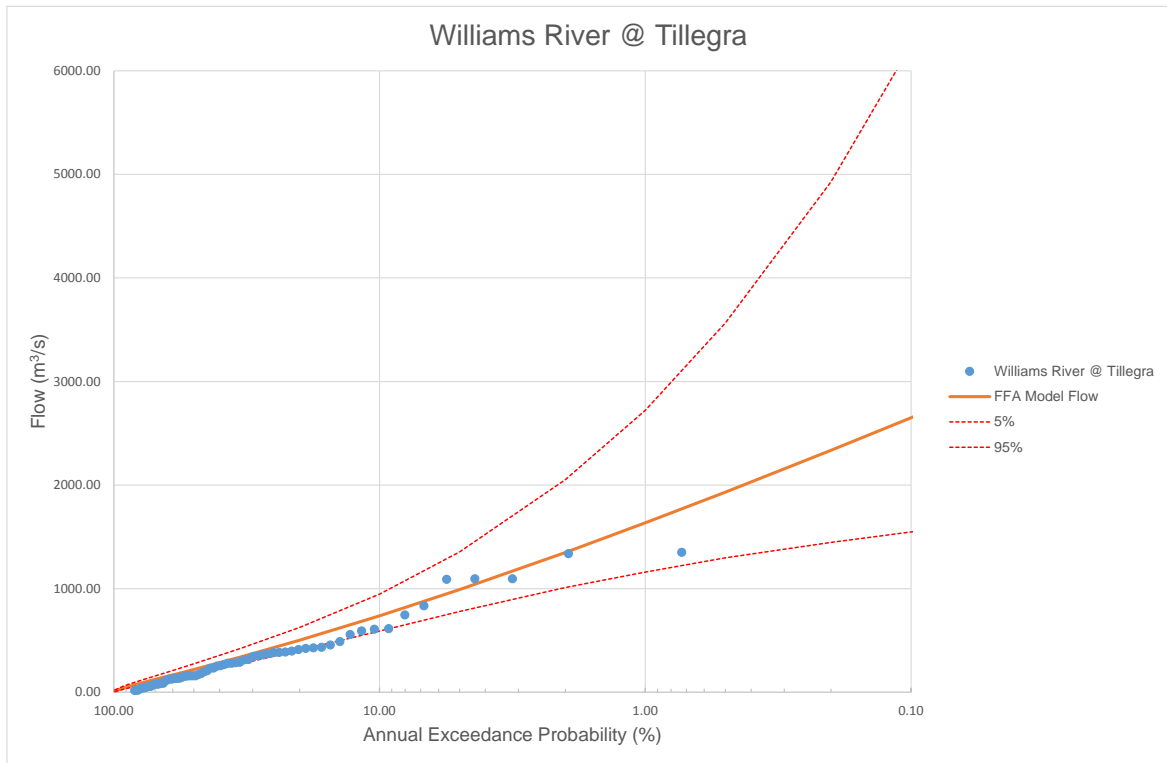


**Figure 1.** Relationship between flood magnitude and flood probability.

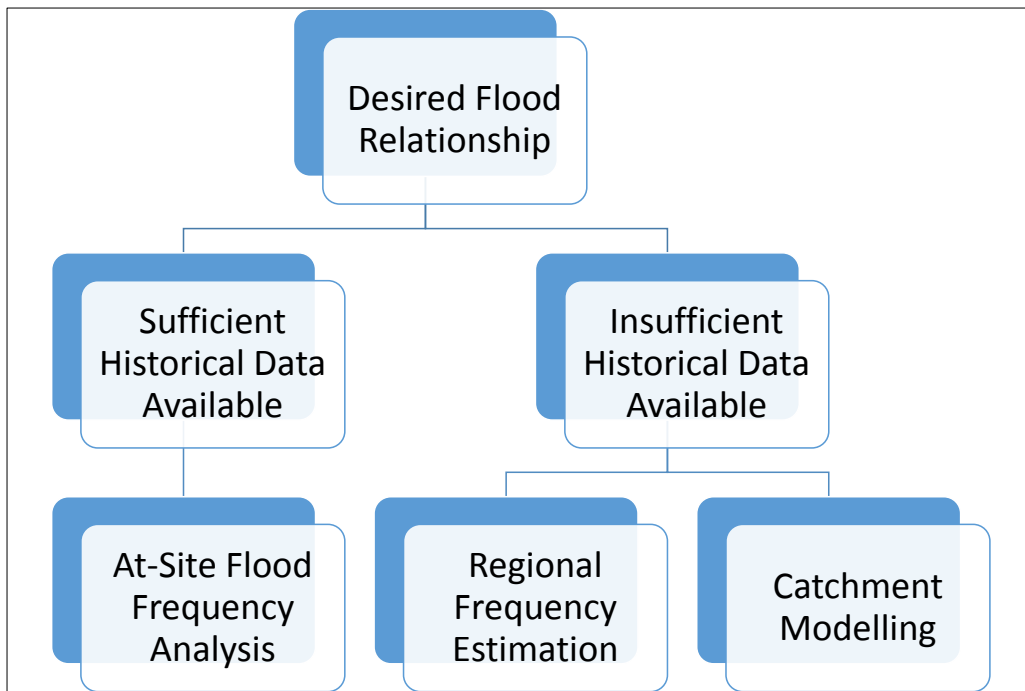


**Figure 2.** Alternative Design Flood Approaches.

- Sufficient and suitable historical information is not available.

When historical information is not available, a common approach is to use catchment modelling. In general, the philosophical basis of catchment modelling is the generation of data that would have been recorded by a streamflow gauging station if a streamflow gauging station were present at the location of the predictions. This is consistent with a deterministic interpretation of catchment modelling. Characteristics of the

catchment and rainfall used for generation of the data maybe the historical or the potential future characteristics of either the rainfall or catchment or both the rainfall and catchment.

When used with this philosophical underpinning, the catchment modelling system consists of a number of models. These models include those representing processes influencing the generation and propagation of floods. An example, of these process models is the routing model used to represent the propagation of flow through the catchment storage. In addition to these models of catchment processes, the system includes those models needed for representation of, for example, the rainfall characteristics in space and time across the catchment. When considered in this manner, it is convenient to categorise the models in the system into conceptual components; Ball (1992) presents a detailed discussion of this categorisation. These conceptual components are:

- Generation - This component is concerned primarily with the estimation of the input data such as the spatial and temporal characteristics of the rainfall, and the parameters necessary for operation of the catchment modelling system;
- Collection - This component of the system is concerned primarily with the accurate prediction of the flow at a point where the flow enters the drainage network, i.e. the hydrologic component of the system;
- Transport - This component of the system is concerned primarily with the routing of flows through the drainage system, i.e. the hydraulic component of the system; and
- Disposal - This component of the system is concerned with models describing how the flow is discharged into the receiving waters.

Due to the number of alternative problems encountered where design flood information is needed, different approaches for the application of catchment modelling systems for design flood estimation have been developed and these approaches range from single storm burst analyses to multi-storm burst analyses. Included in the multi-storm burst approaches are continuous simulation and Monte-Carlo approaches; both of these approaches have the aim of including variability in the factors influencing flood generation and propagation.

Application of a catchment modelling system with a single burst approach is usually associated with the assumption that the statistical properties of the rainfall are transferred to the predicted flows. This assumption is referred to in Australian Rainfall and Runoff (ARR) (Ball et al., 2016) as AEP Neutrality.

A question that needs to be addressed, however, is what combination of catchment and rainfall factors (excluding the IFD statistics) is necessary to achieve the desired AEP Neutrality. In many cases, the techniques used to ensure AEP neutrality are based on parameter calibration aimed at ensuring AEP Neutrality. As these calibration approaches are focused on parameter values that ensure the transformation of statistical characteristics rather than parameter values that ensure the relevant process is replicated, there is a need to investigate whether these calibration approaches are consistent with the philosophical basis of the catchment model. Furthermore, there is an argument that adoption of the AEP Neutral calibration approach results in a complex regression model.

Use of Monte-Carlo and Continuous Simulation approaches do not require the need for AEP Neutrality as the predicted flood characteristics are analysed to develop the necessary statistical parameters. Nonetheless, there is a need to ensure that the full range of parameter values used to describe the rainfall and catchment characteristics are sampled in the simulations. Furthermore, there is a need to ensure that the correlations between the parameter values used to describe meteorological and catchment conditions is maintained.

Discussed herein will be an analysis of the suitability of the AEP Neutral calibration by addressing the relationship between the rainfall statistics and the resultant flood statistics at an urban stream gauging station over a 50 year period.

## 2 CATCHMENT MODELLING

As shown in Figure 2, catchment modelling techniques was one of the approaches used for estimating the desired relationship between flood magnitude (quantile) and probability. Conceptually, the aim of catchment modelling was to generate data that would have been recorded if catchment monitoring had been in place for the event, or sequence of events, being considered. Hence, the generated data should have the same characteristics as the historical data that could have been monitored at the site or sites of interest. Furthermore, data generated using catchment modelling techniques should be analysed using the same techniques as applied to the historical data obtained from catchment monitoring.

Situations where catchment modelling maybe needed include:

- Events of a suitable magnitude have not been recorded and there is a need to extrapolate from recorded events to more extreme flood events;
- Data has not been monitored at the point of interest and there is a need to generate data at a point remote from the monitoring points; and
- Changed management options for a catchment are being considered and there is a need to predict the impacts of the proposed changes on the design flood characteristics prior to implementation of the proposed catchment management strategy.

Alternative techniques for generation of the desired data can be categorised as:

- Single burst (either the design peak burst of an event or the design total event) technique;
- Monte-Carlo technique (see, for example, Weinmann et al., 2002); or
- Continuous simulation technique (Wagener and Wheeler, 2006).

Historically, applications of techniques considering a single burst have been the more popular. The alternative approaches, however, are gaining in popularity as computing capacity increases.

Where the single burst technique had been implemented with an assumption that the frequency of the rainfall is transformed to the frequency of the resultant flood characteristic, it can be argued that the method as applied was a RFFE technique where the catchment model is a complex regression relationship. This question becomes more relevant when implementation of the approach requires values of the parameters to be selected on the basis that the transformation of rainfall frequency to flood frequency was ensured. An example of this approach (commonly referred to as AEP neutrality) was provided by Hill et al. (1998) who developed a method of estimating loss model parameters that are likely to result in the frequency of the rainfall being transferred to the frequency of the design flood flow. Implicit in the adoption of this approach is the assumption that AEP neutral parameter values were available from studies analogous to Hill et al. (1998).

It is possible to use a single burst approach without the assumption of AEP neutrality. In these circumstances, the catchment model was being used to analyse the catchment response to a design rainfall event. In these situations, the probability of the resultant flood characteristics is unknown.

When either of the other two alternative techniques, namely a Monte Carlo or a Continuous Simulation technique, were applied for generation of the data, it was necessary to undertake a statistical analysis of the generated data to develop an estimate of the design flood quantile. This statistical analysis was required as the aim of either technique in the generation of data that could have been recorded if a gauge was present and the catchment conditions reflected in the model parameters occurred. Hence, application of a catchment simulation approach using these techniques reflected a different conceptual basis to that necessary for a single burst approach with AEP neutrality. These different conceptual bases are shown schematically in Figure 3.

Application of a catchment simulation approach for design flood estimation requires calibration and validation of the modelling system parameters and structure prior to use for estimation of the design flood characteristics. During this calibration phase, the primary aim is the selection of parameter values that ensure the modelling system adequately replicates the catchment response; in other words, the primary aim is determination of generic values for the many parameters in the modelling system.

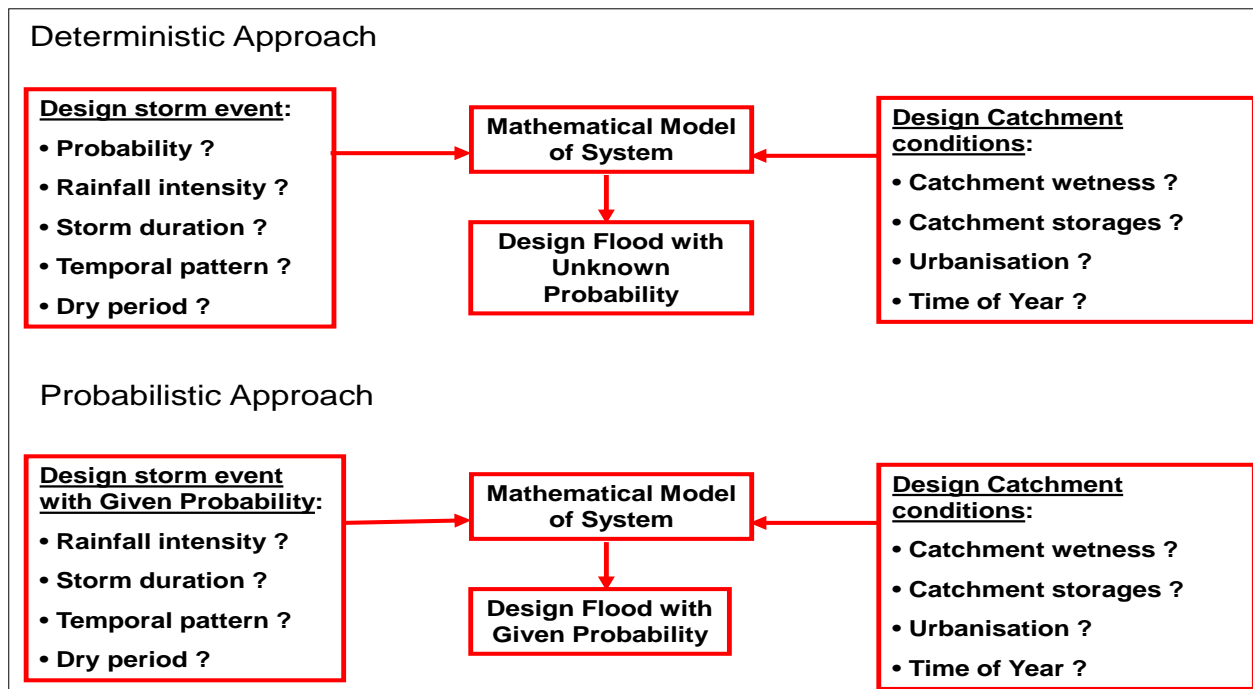
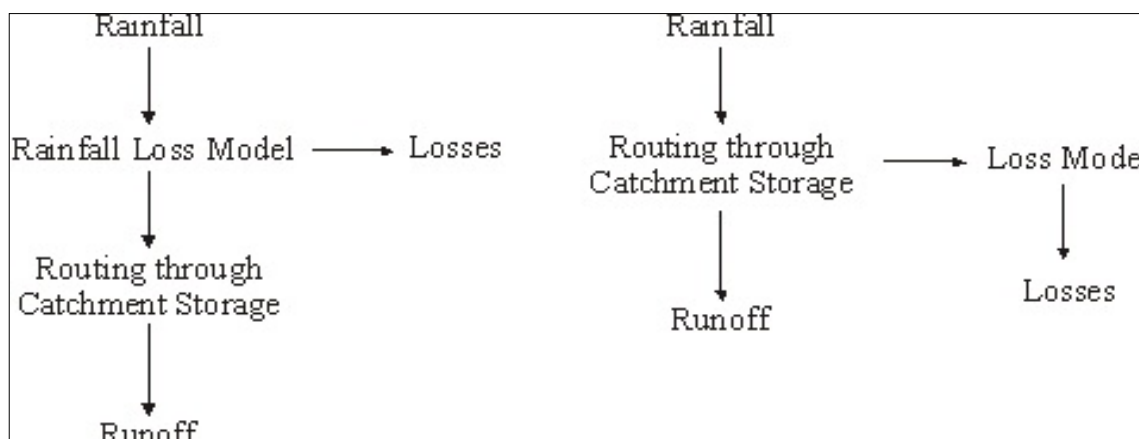


Figure 3. Alternative Conceptual Bases for Catchment Modelling.

Fundamental to a discussion of calibration and validation was the concept that all predictions obtained from systems of models for prediction of catchment response to either individual storm events or sequences of storm events will contain residuals, or differences between the predicted and recorded values. While these residuals arise from multiple sources during the modelling process, following Kuczera et al. (2006), the sources can be categorised as:

- Process errors;
- Model Errors comprising;
  - Structural errors;
  - Parameter errors; and
- Data errors.

Process errors arise from the difference between the conceptual process incorporated in the modelling system and the actual process within the catchment; in other words, the process errors arise from the need for representation of physical processes in a mathematical formulation. The magnitudes of these errors were influenced directly by the degree of simplification within the modelling system. For example, use of one-dimensional and two-dimensional river models result in differing simplifications and different errors. It was worth noting, however, that additional complexity in the process model may not result in a reduction in residuals due to the increased number of parameters necessary for definition of the more complex model.



**Figure 4.** Alternative Loss of Conceptual Models.

Structural errors are the result of the manner in which the various process models were combined to provide the catchment modelling system. In many situations, alternative structures are available. For example, shown in Figure 4 are the two alternative conceptual loss model structures presented by Ball et al. (2011) for incorporation of rainfall losses in a catchment modelling system. Consideration of this example, it illustrates the linkage between conceptualisation of processes in the catchment modelling system and the existence of structural errors. Hence, the distinction between a process model and a structural error was diffused and, in many cases, difficult to quantify. This difficulty was shown also through consideration of Umakhanthan and Ball (2005) who investigated the influence of the model used to estimate the spatial and temporal distribution of rainfall across the catchment.

The third form of errors are the parameter errors. For discussion of parameter errors, there are two alternative cases that need consideration. The first of these cases is where sufficient monitored data is available for estimation of the parameter values using data from the catchment. The second case occurs where there is insufficient data available for estimation of parameter values using data from the catchment and hence estimation of parameter values is based on regional relationships and other inference models. An example of the use of inference models for estimation of parameter values was presented by Choi and Ball (2002a) who investigated the use of land-use classifications for prediction of the imperviousness of subcatchments.

In both cases, parameter errors arise from differences between the true value of the parameter and that used in the simulation. Residuals arising from errors of this type have been the focus of significant historical research with a significant volume of this research focussed on the problem of obtaining optimal or near optimal values for the modelling system parameters. Arising from this research has been the concept of equifinality (Beven and Binley, 1992) which can be paraphrased as there are multiple sets of parameter values that will result in similar system performance.

The concept of equifinality becomes increasingly relevant as the catchment modelling system becomes more distributed. As urban catchments especially heterogenous, the issue of equifinality is very important for modelling of urban catchments. This is illustrated in Figure 5 where the Sum of Squared Error (SSE) for alternative values for the conceptual width of a single subcatchment are shown; 10,000 alternative combinations of parameter values were considered. As shown in this figure, similar values of the SSE can be obtained over a wide range of values. Consideration of this figure also illustrates the need to consider sets of parameter values rather than the value of a single parameter. The same value of the conceptual width parameter can result in different values of the SSE; these multiple SSE values were the result of alternative values for the other parameters.

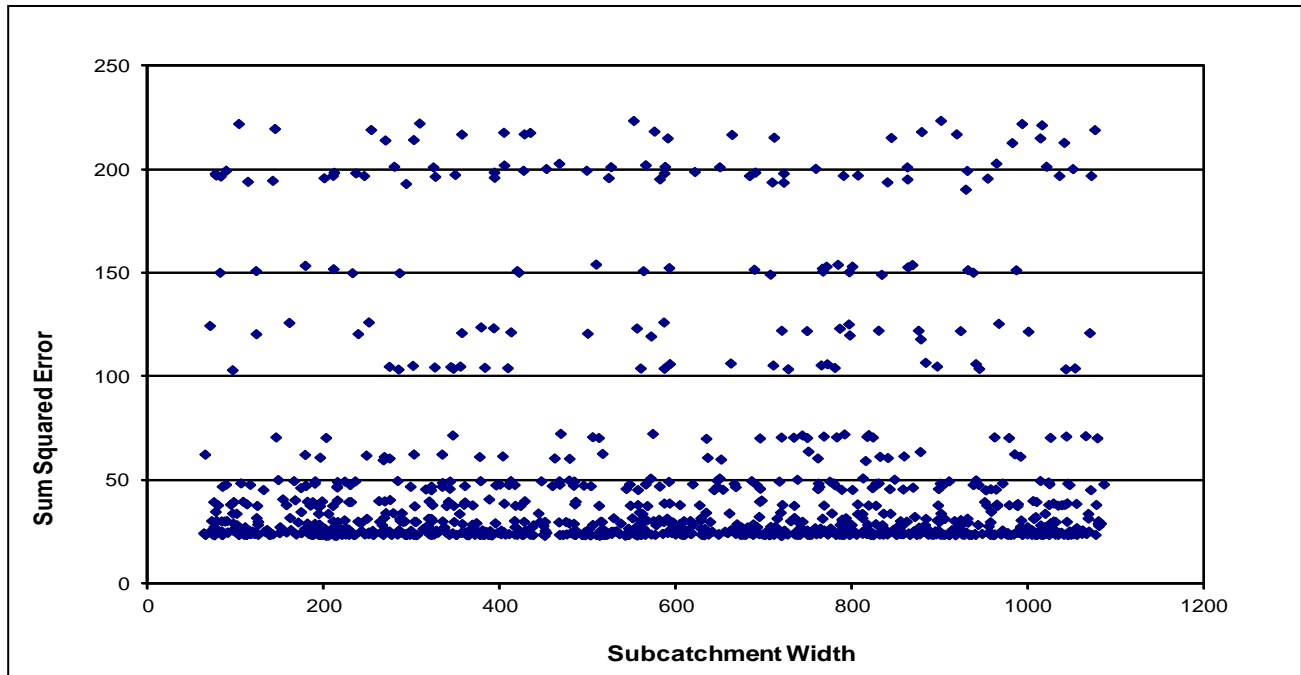


**Figure 5.** Conceptual Width of Subcatchment 103.

The last form of error is the data errors. While there are many types of data errors, the characteristic of these errors are that they represent the difference between the true value of the monitored data and the value recorded in the database. An example of errors of this type are those errors arising from the need to extrapolate the rating table for a gauging station above the highest gauging to enable transformation of the recorded level to an equivalent flow. Note that, in addition to the extrapolation error, a measurement error associated with the recording of the level also occurs; these measurement errors are discussed by Ball et al. (2016).

As previously discussed, the focus of the calibration and validation of a catchment modelling system for generation of data necessary for design flood estimation was minimisation of the residual. While the parameter error generally is the major concern, the alternative forms of error cannot be neglected. The need for this was discussed by Choi and Ball (2002b) who showed that minimising the prediction residual can result in degraded predictions for alternative events. In other words, the parameter values that minimise the prediction residual include corrections for the non-parameter errors that occurred during the event.

All of the above discussion regarding calibration and validation of catchment modelling systems has been aimed at ensuring that a historical event had been predicted to a suitable degree of accuracy. In other words, calibration and validation was based on a deterministic interpretation of catchment modelling. As a result, the probability of the rainfall input to the catchment modelling system cannot be guaranteed to be the same; in other words, AEP neutrality was not ensured.

Design flood estimation using traditional catchment modelling approaches (i.e. single burst rainfalls), however, is based on prediction of a flood characteristic for a given probability; this requires AEP neutrality.

### 3 STUDY CATCHMENT

The Powells Creek catchment, sometimes referred to as the Strathfield catchment, is an 841.5ha catchment situated 10km west of Sydney's central business district. The location of this catchment is shown in Figure 6. The catchment lies within the Sydney suburbs of Homebush West, North Strathfield, Rookwood and Strathfield, and is administered by the local government areas of Strathfield, Canada Bay and Auburn. Land uses within the catchment are outlined in Table 1. In general, the catchment is classified as low-lying, with gently slopes between 4% and 5.5%. The maximum elevation is 40m AHD and the minimum elevation is governed by the tidal regime of the Parramatta River. The drainage network comprises a closed piped system that opens out to a lined channel and then into the Parramatta River. The main open channel was established in 1892 and the closed pipe system was established in the 1920's. Historically, flooding has occurred upstream of the lined channel when the runoff capacity has exceeded the capacity of the closed pipe drainage system.

The School of Civil Engineering, University of New South Wales, has been collecting hydrologic data on Powells Creek catchment since 1958. Hence, for the period of record, the catchment has been urbanised. A stage gauging station and pluviometer are located at the open channel section of the Main Strathfield Channel adjacent to Railway Crescent. Rating curves are available for conversion of the recorded gauge level to an equivalent flow rate. In addition, another pluviometer was installed at Santa Sabina College, which is also

located within the catchment boundary. Using the data recorded at the stream gauging station, an At-Site Flood Frequency Analysis was undertaken with the results shown in Figure 7; for this At-Site Flood Frequency Analysis, an Annual Maxima Series (AMS) was analysed using the approach recommended in ARR (Ball et al., 2016).

In addition, the 263 largest events were extracted from the database. These events were those where the peak flow was greater than  $5\text{m}^3/\text{s}$ . It is worth noting that all of these events had a peak flow greater than the rank 40 event in the AMS. Rainfall data for these events were extracted from the database also. Following review of the extracted data, 175 of the 263 recorded flood events were considered suitable for further analysis. In other words, 33% of the events were excluded due to uncertainty about the reliability of the data.

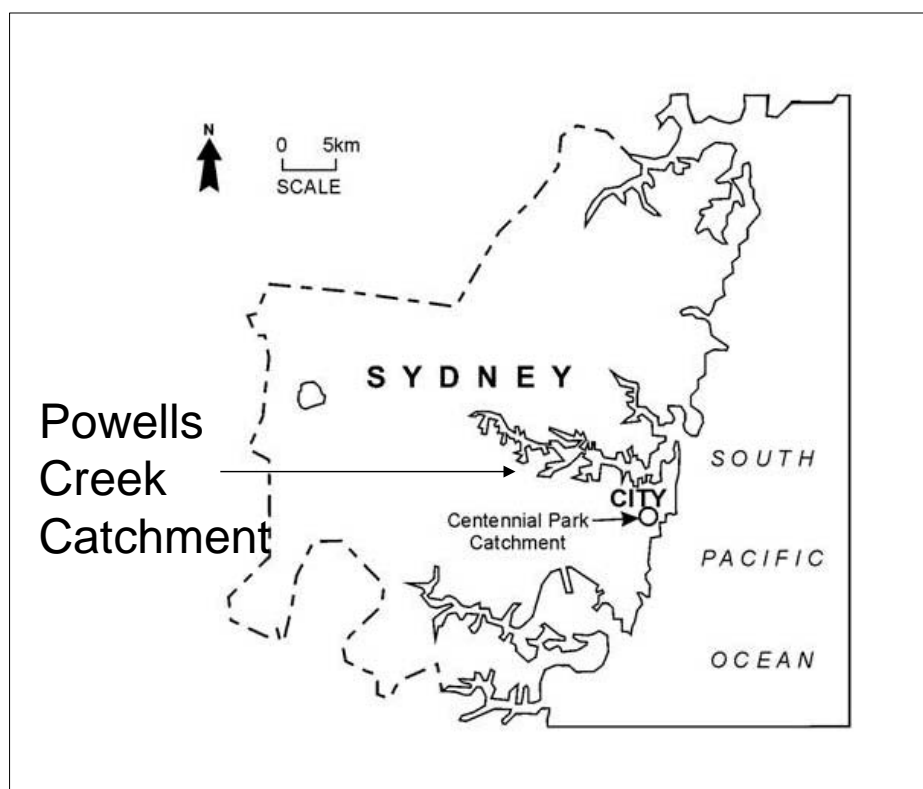


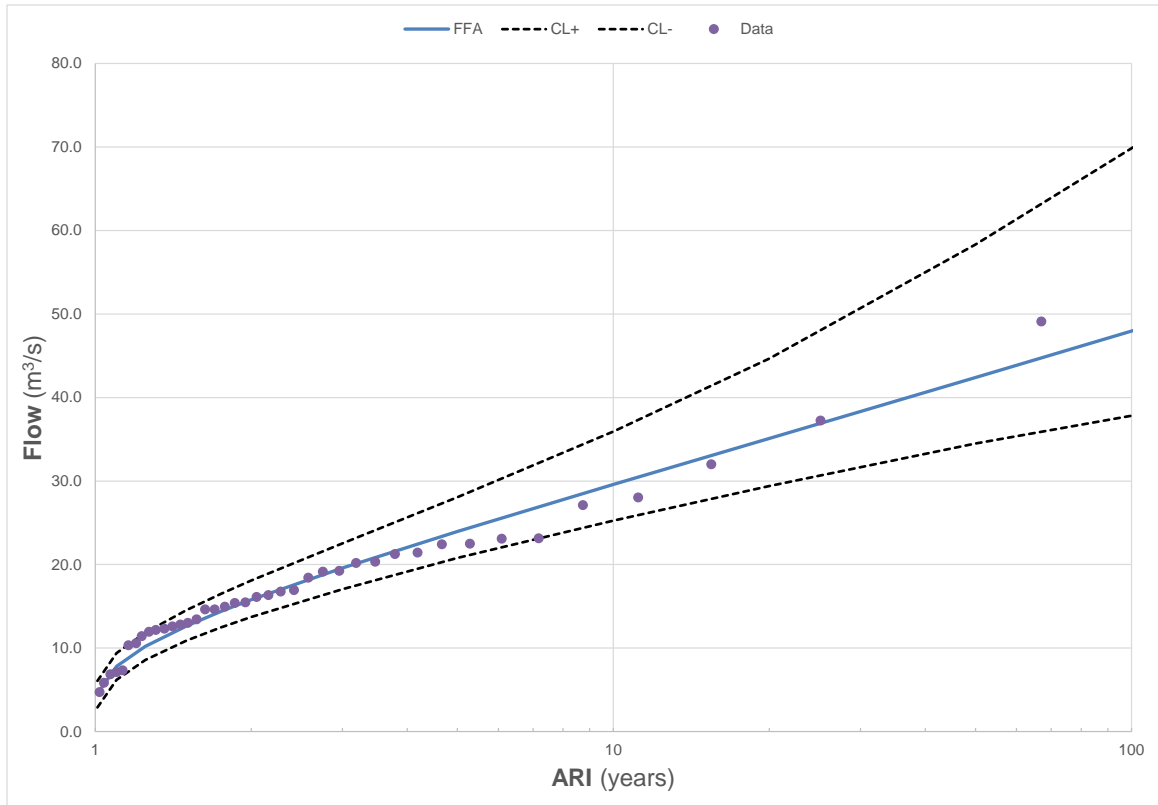
Figure 6. Location of powells creek catchment.

Table 1. Land uses in the powells creek catchment.

Land Use	Area (ha)	Proportion (%)
Residential	504.71	60.0
Industrial	40.45	4.8
Business/Commercial	27.10	3.2
Open Space	61.13	7.3
Special Use	208.12	24.7
<i>Total</i>	841.5	100.

#### 4 DATA ANALYSIS

For each of the 175 flood events, the maximum 60 minute rainfall intensity at one of the two rain gauges within the catchment was determined. Shown in Figure 8 are these rainfall intensities plotted against the peak discharge of the flood event. Also shown in this figure is the design for 1 hour rainfall intensities plotted against the equivalent peak discharge as determined from the at-site flood frequency analysis.



**Figure 7.** Powells Creek Flood Frequency.

Consideration of the data plotted in Figure 8 suggests that, while the rainfall is an important factor in the magnitude of the resultant flood, there are other factors that significantly influence the resultant flood magnitude. One factor that has been suggested in the past is the antecedent moisture. Osthus (2016) investigated the correlation between antecedent rainfall and rainfall intensity. As part of this study, the antecedent moisture for the 175 events of largest flood events with data was determined for 6, 12, 24, 48 and 144 hours prior to occurrence of the flood event. For each duration, the antecedent moisture was divided into categories based on the rainfall depth. Shown in Figure 9 is the number of occurrences in each of the categories considered for the 24 hours prior to commencement of the storm event.

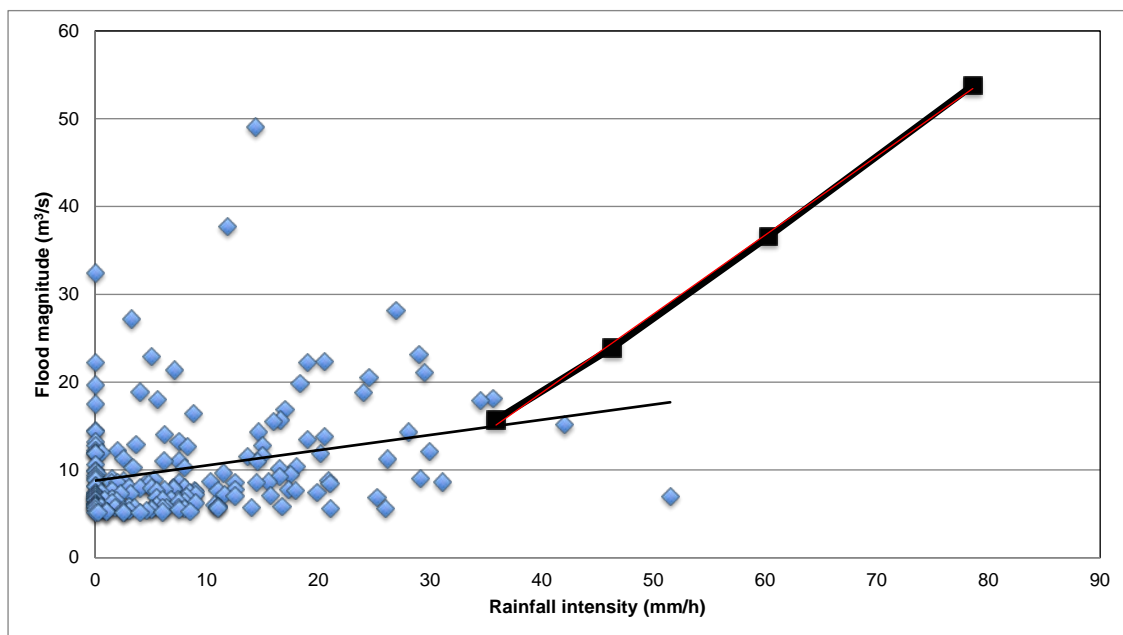


**Figure 8.** Rainfall Intensity against Flood Peak.

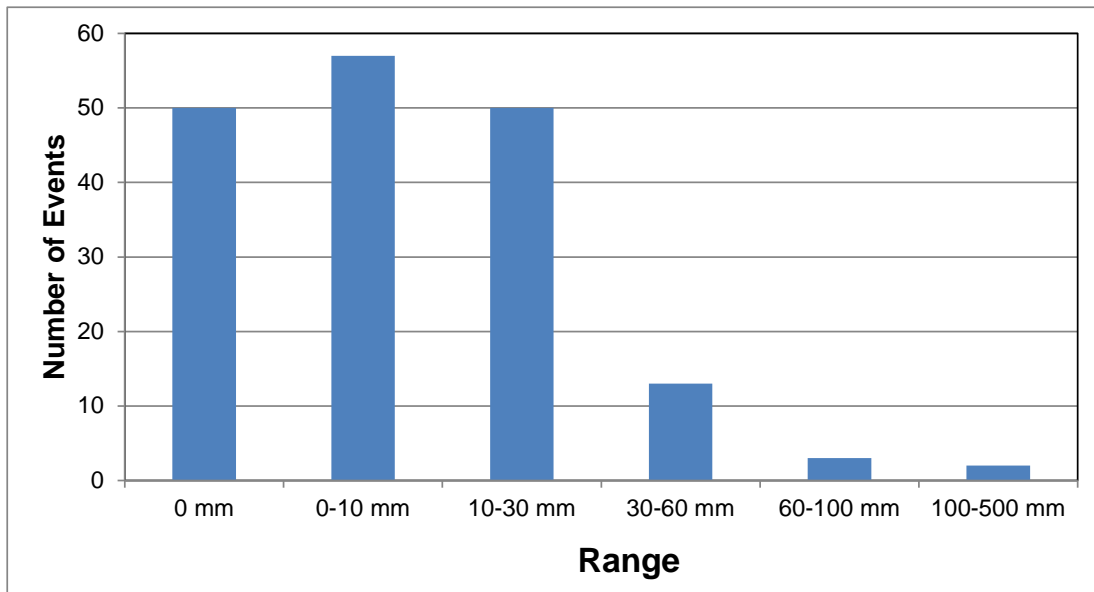


**Figure 9.** 24 Hour Antecedent Moisture.

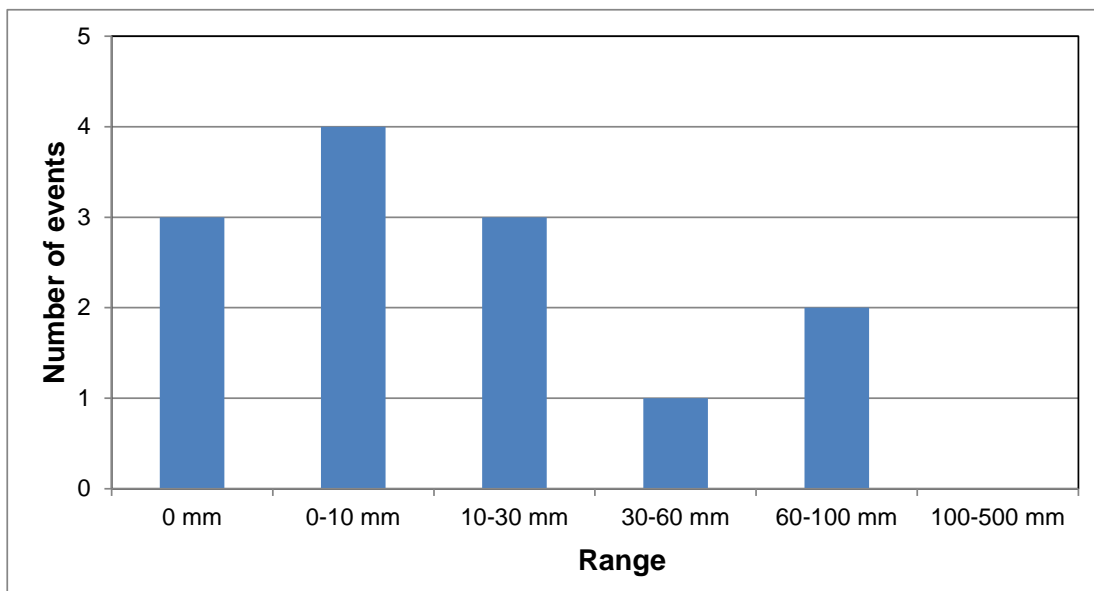


**Figure 10.** 24 Hour Antecedent Moisture for Flood Events above 20m<sup>3</sup>/s.

Inclusion of the flood peak as a co-variate modified the results shown in Figure 9 but did not alter the generic characteristics of the distribution. This outcome is shown in Figure 10 where only events resulting in peak flood flows greater than 20m<sup>3</sup>/s (approximately a 3 year ARI event) were considered. In both Figures 9 and 10, the majority of flood events occurred with less than 30mm of precipitation in the 24 hours prior to the event. Additionally, for those flood events with a peak greater than 20m<sup>3</sup>/s, it is worth noting that the number of flood events with greater than 30mm of antecedent moisture decreased; in other words, a wet catchment is not a requirement for a large flood event.

## 5 CONCLUSIONS

An analysis of historical flood events for the Powells Creek catchment in Sydney, Australia has shown:

- The largest flood events are not the result of the highest rainfalls and, hence, other factors influence the catchment response;
- The antecedent rainfall is not related to the rainfall intensity with the majority of flood events occurring when less than 30mm of rainfall has occurred in the previous 24 hours; and
- High antecedent rainfall (considered to be greater than 30mm) does not ensure occurrence of larger flood events.

Consideration of these outcomes suggests when catchment modelling is applied for estimation of a design flood characteristic that translation of the frequency from the rainfall to the flood event is not ensured

unless the model parameters are selected to ensure the frequency translation. Conceptually, this approach is analogous to a regression model.

A consequence of this outcome, is the application of catchment modelling for design flood estimation when the catchment conditions are changing; examples of changing catchment conditions are:

- Runoff storage facilities are being added within the catchment; and
- Land use of an area within the catchment is changing; particularly from rural to urban, but also from residential to industrial.

## REFERENCES

- Ball, J.E. (1992). Review of Numerical Models for Prediction of Catchment Water Quantity and Quality. *Research Report No. 180*, Water Research Laboratory, Dept. of Water Engineering, School of Civil Engineering, The University of New South Wales, Sydney, Australia, ISBN 0/85824/419/5, 38.
- Ball, J.E., Babister, K.M. & Retallick, M. (2011). Revisiting the Design Flood Problem, *Proceedings 34<sup>th</sup> IAHR World Congress*, Brisbane, Australia, 31-38, ISBN 978-0-85825-868-6.
- Ball, J.E., Babister, M., Nathan, R., Weeks, W., Weinmann, E., Retallick, M. & Testoni, I. (2016). *Australian Rainfall and Runoff: A Guide to Flood Estimation – 4<sup>th</sup> Edition*, Commonwealth of Australia, Canberra, Australia, ISBN 9781925297072.
- Ball, J.E., Kerr, A., Rocha, G.C. & Islam, A. (2016). A Review of Stream Gauge Records for Design Flood Estimation, *Proceedings 37th Hydrology and Water Resources Symposium*, Queenstown, NZ.
- Beven, K., & Binley, A. (1992). The Future of Distributed Models: Model Calibration and Uncertainty Prediction. *Hydrological Processes*, 6(3), 279-298.
- Choi, K.S. & Ball, J.E. (2002a). Parameter Estimation for Urban Runoff Modelling. *Urban Water*, 4(1),31-41.
- Choi, K.S. & Ball, J.E. (2002b). A Generic Calibration Approach: Monitoring the Calibration, *Proc. 2002 Hydrology and Water Resources Symposium*, Melbourne, Australia, I.E., Aust.
- Hill, P.I., Mein, R.G. & Siriwardena, L. (1998). *How Much Rainfall Becomes Runoff? - Loss Modelling for Flood Estimation*, Industry Report 98/5, Cooperative Research Centre for Catchment Hydrology, Department of Civil Engineering, Monash University, Clayton, Australia, ISSN 1039-7361
- Kuczera, G., Kavetski, D., Franks, S. & Thyer, M. (2006). Towards a Bayesian Total Error Analysis of Conceptual Rainfall-Runoff Models: Characterising Model Error using Storm-Dependent Parameters. *Journal of Hydrology*, 331(1-2), 161-177.
- Osthus, V. (2016). *An Investigation on Correlation Between Antecedent Moisture Conditions and Flood Magnitude in Powell's Creek Catchment - Sydney, Australia*, Unpublished Master of Engineering Report, School of Civil and Environmental Engineering, University of Technology Sydney, Australia.
- Robinson, D.K. (1987). *Australian Rainfall and Runoff: A Guide to Flood Estimation*. 3rd Edition, The Institution of Engineers Australia, Barton, ACT, Chapter C12.
- Umakhanthan, K. & Ball, J.E. (2005). Rainfall Models for Catchment Simulation. *Australian Journal of Water Resources*, 9(1), 55-67.
- Wagener, T. & Wheater, H.S. (2006). Parameter Estimation and Regionalisation for Continuous Rainfall-Runoff Models Including Uncertainty. *Journal of Hydrology*, 320(1-2), 132-154.
- Weinmann, P.E., Rahman, A., Hoang, T.M.T., Laurenson, E.M. & Nathan, R.J. (2002). Monte Carlo Simulation of Flood Frequency Curves from Rainfall - The Way Ahead. *Australian Journal of Water Resources*, 6(1), 71-79.

## DECENTRALIZED APPROACH FOR OPTIMAL EFFICIENCY OF MULTIPLE DETENTION RESERVOIRS IN URBAN AREA

THI THUY NGO<sup>(1)</sup>, DO GUEN YOO<sup>(2)</sup> & JOONG HOON KIM<sup>(3)</sup>

<sup>(1,3)</sup> Dept. of Civil, Environmental and Architectural Engineering, Korea University, Seoul, South Korea  
tide4586@gmail.com (T.T.N); jaykim@korea.ac.kr (J.H.K)

<sup>(2)</sup> Software Center & K-water Research Institute, Korea Water Resources Corporation, Daejeon, South Korea  
dgyoo411@kwater.or.kr

### ABSTRACT

Urbanization with the decrease of pervious area combining with climate change impacts has caused more flooding in the urban area. To dispose of flooded water, detention basins have been considered as one of the most effective measures. Recently, applying meta-heuristic algorithms to optimize layout and design of the detention system is well documented in literature focusing on flood reduction for the whole watershed. In fact, the urban area is flooded at many sites in extreme storm events and the overall optimizing approach may not satisfy for all inundation places. In this paper, a decentralized approach is proposed to analyze flood damages in the urban area. A controlled node network is proposed to comprehensively represent the effects of detention reservoir system. Instead of minimizing the total flooded volume, present study searches the optimal design of detention reservoir system to minimize flood peak at multiple locations. The proposed approach is verified by comparison with another optimization approach and current system design. The new detention design outperforms in terms of flooding mitigation and construction cost as well.

**Keywords:** Multiple detention reservoirs; urban drainage network; optimization; decentralized based.

### 1 INTRODUCTION

Nowadays, detention basins have been considered as one of the most important engineered means to dispose flooded water under rapid urbanization context. The detention basins can be located upstream, midstream or in the outlet of the drainage system. The detention reservoirs in upstream or midstream are constructed to mitigate flooding situation in the regional scale. These detention ponds temporarily capture storm water for slow release when the peak period passes. This slow drainage of a detention may influence the downstream and exacerbate flooding. Thus, a system of detention is needed to be considered as a solution for flood control (Travis and Mays, 2008).

Recently, meta-heuristic algorithms have been widely applied for optimizing layout and design of the detention system. The dynamic programming method was utilized to obtain optimal detention facilities such as storage size, location, and outlet structures (Bennett and Mays, 1985; Behera et al., 1999; Travis and Mays, 2008). The mathematical and probabilistic perspectives were also considered to solve the optimization problems (Papa and Adams, 1997; Behera et al., 1999). More recently, the linear programming and binary linear integer programming methods were applied to optimize the size of stormwater control measures, while satisfying water quality thresholds (Loaiciga et al., 2015).

The research into detention reservoir network has solved with optimizing size and location to maximize flood reduction and minimize construction cost. To carry out the flood reduction purpose, studies tend to maximize the reduction of the total flooded volume (Yazdi and Neyshabouri, 2012), flood peak at the outlet (Yeh and Labadie, 1997) or critical node (Tao et al., 2014). In fact, the urban area is flooded at many sites in extreme storm events and the centralization-based optimization approach that focuses on overall downstream flood reduction may not satisfy for all inundation places. Under this circumstance, the more powerful measurement is proposed in this study. The overall flooding situation is decentralized into regional areas. The objective function of optimization problem is then to maximize regional flood reduction of the whole detention system. The comparison between decentralization and centralization approaches is also given to verify the effectiveness of the proposed method in different flood events.

### 2 METHODOLOGY

#### 2.1 Case study

The urban drainage network in Hanoi - the capital of Vietnam was selected as a case study. The study area called To Lich drainage system is a combined system constructed since early of the 20<sup>th</sup> century. The citadel area occupying around 77.5 km<sup>2</sup> is surrounded by the Red River, To Lich River and Nhue River. The

system includes more than 30km open channel, conduit system, and Yen So headworks (Figure 1) according to the master plan of Hanoi (Decision No.108, 1998).

In the watershed, only 16 reservoirs out of 70 natural and artificial ponds are controlled for flood regulation purpose, under Hanoi Sewerage and Drainage Limited Company (HSDC). However, most of these ponds are maintained at high elevation (around 4.5-5.0m) for fishing and tourism purposes as well (JICA, 1995). Their effectiveness in flood control is thus limited. Since the existing detentions are mostly natural in the crowded resident area, enlarging their size seems an impossible task. The optimal operation and/or inlet-outlet structures are those factors this study is interested in. In this study, the side weir inlet of the detentions is considered as the decision variables for the optimization problem.

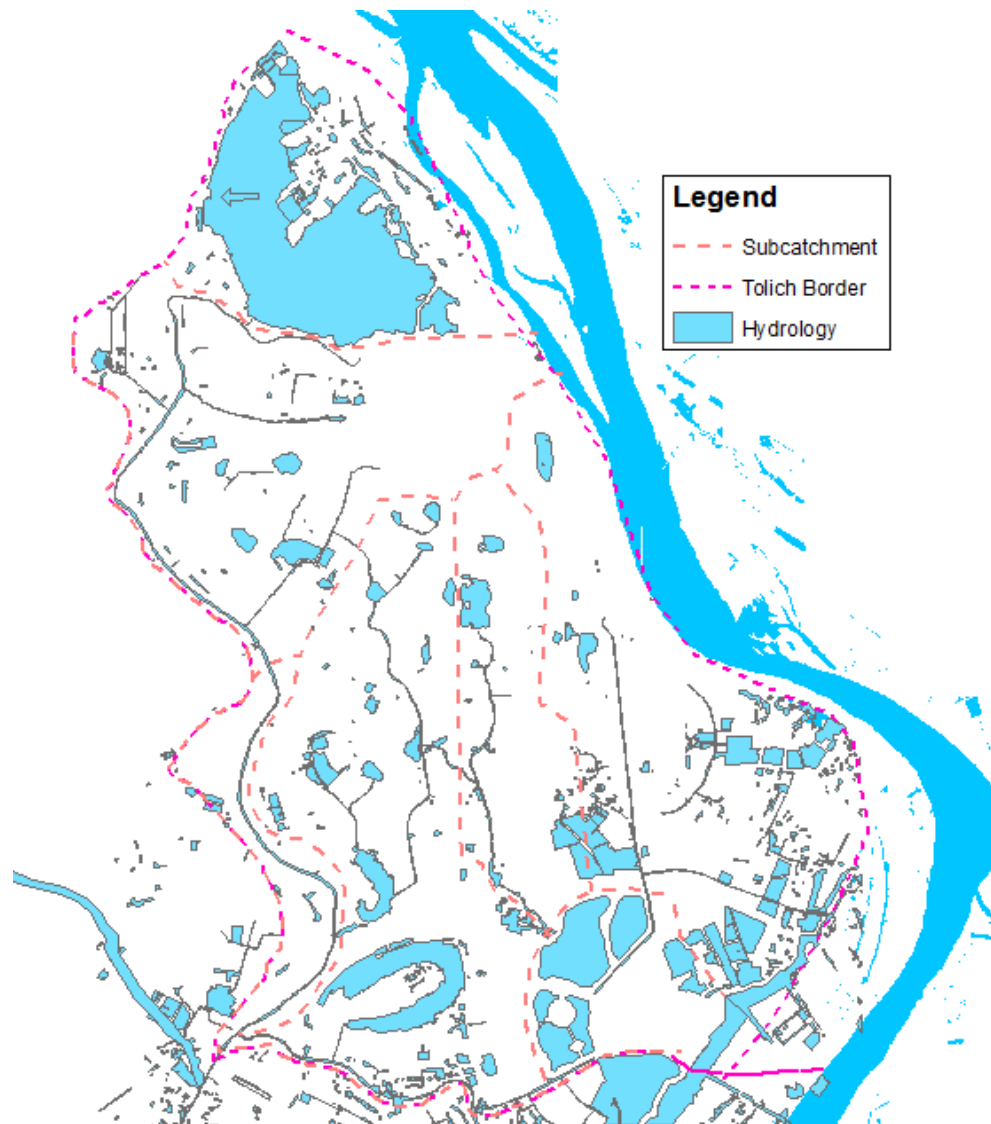


**Figure 1.** Layout of the To Lich drainage system (JICA, 1995).

## 2.2 Decentralized-based approach to determine control node system

The decentralization approach was utilized to partially zone the whole detention system into typical regions. The regional influences of detention ponds were assessed instead of the overall impact to the downstream outlet. The detention regions should be independent in terms of flooding situation. The regions could be based on the sub-watershed division. Each region was controlled by a critical node that presented the overall impact of detentions within the region. The control nodes should be representative of the flooding features of corresponding regions. The less number of control nodes was preferred to make the system simpler. Therefore, the determination of detention region became control node selection. The control node system was selected by principles as follow.

- The control node was downstream of all detention ponds in the region.
- The control node could detect the change of detention pond. That means the change in detention pond facilities would impact on the control node flow.
- The most sensitive control node was preferred to detect detention change.

- The most vulnerable downstream node was preferred.
- The number of control nodes should be minimized.

Based on the decentralized approach, the eight control nodes corresponding to eight detention regions were determined. The detailed characteristics of these regions are shown in Table 1.

**Table 1. Regional detention network and control nodes system.**

Region	Detention ponds			Control nodes	
	ID	Name	Max depth (m)	Name	Max depth (m)
I	HT	Ho Tay	6.20	Node 4	2.82
	TB	Truc Bach	6.20		
II	TL	Thu Le	5.00	Node6	3.79
	GV	Giang Vo	4.50		
III	NK	Ngoc Khanh	4.80	Node 12	3.76
	TC	Thanh Cong	5.00		
	DD	Dong Da	5.10		
IV	DC	Dinh Cong	5.00	Node 18	4.40
	LD	Linh Dam	5.00		
V	ND	Nam Dong	3.95	Node 48	2.83
	TQ	Thien Quang	5.20		
VI	BM	Bay Mau	5.10	Node 61	2.29
	TN	Thanh Nhan	4.60		
VIII	HVT	Hoang Van Thu	4.90	Node 64	2.30

### 2.3 Optimization problem formulation

Suppose that the  $M$  detentions are placed in the case study and partially zoned into  $N$  regions. The study aims to maximize the detention efficiency in flood reduction. To verify the proposed decentralized approach, two single objective functions were generated.

The first single objective function based on the centralization approach in which the flood reduction was assessed by the minimum total flooded volume in the whole watershed (Eq. [1]). The second one was the decentralization-based objective function representing the regional effectiveness of detention system. The efficiency of each detention region presents in the reduction flood peak level at control node (Ngo et al., 2016a). For a detention system, it is the systematic peak level reduction. Due to the difference in node depth and level, the relative peak water level was used. The importance of detentions was also handled by using weighted factors. The non-dimensional objective function is presented in Eq. [2].

$$\text{Minimize } F_1 = V_{WS}^{flood} \quad [1]$$

$$\text{OR Minimize } F_2 = \sum_{i=1}^N \left\{ \left( \frac{H_i^{\max}}{H_i^0} + \sum_{j=1}^{M_i} \frac{H_j^{flood}}{H_j^0} \times p_j \right) \times w_i \right\} \quad [2]$$

Subject to:

$$w_i = \frac{\sum_{k=1}^{N_i} V_{DB}^k}{V_{all}} \quad (i=1,2,\dots,N) \quad [3]$$

$$H_j^{flood} = \frac{V_j^{flood}}{A_j} \quad (j=1,2,\dots,M_i) \quad [4]$$

where  $M$  is the number of detention reservoirs in the whole watershed;  $N$  and  $M_i$  are numbers of regions and detention reservoirs in each region, respectively;  $H_i^{\max}$  is peak water level at control node  $i^{\text{th}}$  during flood event;  $H_i^0$  is maximum depth at control node  $i^{\text{th}}$ ;  $H_j^{flood}$  is flooded depth at detention reservoir  $j^{\text{th}}$ ;  $V_j^{flood}$  and  $A_j$  are flooded volume and maximum surface area of detention reservoir  $j^{\text{th}}$ , respectively;  $H_j^0$  is maximum depth of detention reservoir  $j^{\text{th}}$ ;  $p_j$  is the penalty coefficient;  $w_i$  is the weighted factor for each region;  $V_{DB}^k$  is the

total volume of detention reservoir  $k^{th}$  in the region  $i^{th}$ ;  $V_{all}$  is the total volume of all detention reservoirs in the whole watershed;  $V_{WS}^{flood}$  is the total flooded volume in the whole watershed.

### 3 APPLICATION AND RESULTS

In this study, coupling method of the optimization algorithm and a flood routing simulation model was applied to solve the two single objective functions in Eq. [1] and Eq. [2], alternately. The extraordinary particle swarm optimization (EPSO) (Ngo et al., 2016b) was interfaced with Storm Water Management Model (SWMM) to tackle the above objective functions. The decision variables were side-weir crest heights of detention reservoirs in the whole watershed. The fourteen detention reservoirs and eight regions (Table 1) were taken into account to simulate the To Lich drainage system. The severe flood in late October 2008 corresponding to 100-year return period was considered as a critical event to solve optimization problem. The optimal detention facilities were then modeled for the normal flood with lower return period to perform the effectiveness of the decentralized approach. The comparison of the centralized (F1) and decentralized (F2) approaches and the present facilities are illustrated in Tables 2 and 3.

**Table 2.** Comparison of the two approaches in terms of peak water level at control nodes and flooding situation.

Criteria	Flood in 2008 (100yrs)			Flood in 2001 (20yrs)			
	Present	F1	F2	Present	F1	F2	
Peak water level at control nodes (m)	Node4	2.23	2.27	2.26	1.54	2.00	1.54
	Node6	3.45	3.49	3.48	2.74	2.90	2.74
	Node12	3.48	3.51	3.53	2.77	2.87	2.77
	Node18	3.84	3.91	3.84	2.95	3.00	2.95
	Node48	2.83	2.83	2.83	2.83	2.83	2.83
	Node61	1.82	1.80	1.83	1.19	1.19	1.19
	Node68	2.79	2.79	2.80	2.10	2.09	2.12
Node64	1.43	1.44	1.44	1.05	1.00	0.94	
Flooding at nodes	Volume ( $10^3 m^3$ )	3695	3219	3295	753	753	776
Flooding at detention reservoirs	Volume ( $10^3 m^3$ )	304	154	122	0	0	0

**Table 3.** Comparison of the two approaches with present facilities in terms of pond utilization (%).

Region	ID	Flood in 2008 (100yrs)			Flood in 2001 (20yrs)		
		Present	F1	F2	Present	F1	F2
I	HT	95.8	93.4	93.4	90.3	90.3	89.4
	TB	95.8	93.5	93.5	90.3	90.3	94.6
II	TL	100.0	100.0	100.0	84.8	84.9	87.8
	NK	98.4	99.7	100.0	82.7	82.7	83.9
III	GV	97.5	98.6	98.9	81.3	81.2	82.2
	TC	92.0	93.2	93.6	77.8	77.8	79.0
	DD	100.0	100.0	100.0	88.4	88.3	89.3
IV	DC	96.2	93.7	93.8	79.0	79.5	97.2
	LD	91.8	91.3	93.0	74.2	74.1	75.2
V	ND	94.7	94.7	94.4	88.6	90.2	90.1
VI	TQ	100.0	100.0	100.0	93.8	97.9	93.8
	BM	83.1	83.2	96.7	73.1	73.3	73.0
VII	TN	93.0	95.4	93.8	85.9	88.5	88.2
VIII	HVT	85.3	85.4	84.6	79.2	76.9	78.1

The total flooded volume in the whole watershed and detention reservoirs was dramatically reduced in the optimal designs obtained from both decentralized and overall approaches in severe flood event (2008), while it was increased in the moderate events (2001) (Table 2). The peak water level at control nodes in 100-year return period was slightly changed when the optimal designs were applied. In the lower design rainfall scenarios (20-year return period), the peak water levels at several nodes obtained from minimizing F2 (decentralization) were similar to present design, while the centralized approach gave the higher water level. The number of flooded node in optimal designs was also smaller than current facilities.

Table 3 illustrates the comparison of detention utilization in the optimal designs as well as in the present scenario in different storms. During extreme flood event (2008), the TL, NK, DD and TQ detention ponds used all the available storage for storm water capturing. Even though this situation could not be improved in optimal scenarios, the flooding situation in adjacent areas is eliminated. In TC, LD and BM detentions, the percentage of pond storage used in storm increased that presented a more effective operation of these detentions. In other detentions which were mostly in full operation in present scenarios, the optimal utilizing percentage slightly decreased, in particular in the optimal solution obtained by F2. In storm 2001, the optimal scenarios showed outperformance in detention utilization. In most of detention ponds, the new facilities increased the

percentage of using storage, while maintaining the possible water levels especially in the TB, TL and DC ponds. The optimal design obtained from decentralized approach (F2) surpasses that of centralized approach (F1) as well as the present facilities.

When considering the cost of weir construction, or in other words, total construction area (the length is the same for all weirs), the decentralization optimizer also shows outperformance than the centralized one in different rainfall events (Table 4).

**Table 4.** The optimal design obtained by the two approaches in different flood event.

Region	ID	Width (m)	Optimal design in flood 2008			Optimal design in flood 2001		
			Present	F1	F2	Present	F1	F2
I	HT	6	2.7	4.5	0.9	2.7	2.6	2.9
	TB	6	5.0	5.0	5.0	5.0	0.5	5.0
II	TL	6	0	4.8	0.4	0	0.2	0.1
	NK	6	0	2.0	0.6	0	2.6	0.4
III	GV	6	0	1.8	0.2	0	5.0	2.0
	TC	6	0	0.3	1.2	0	4.3	3.0
	DD	6	0	5.0	1.0	0	1.2	1.1
IV	DC	10	0	1.1	1.1	0	2.6	0.9
	LD	10	0	4.0	3.8	0	2.2	1.1
V	ND	6	0	2.3	0.9	0	5.0	0.7
VI	TQ	6	0	1.5	3.8	0	0.3	0.3
	BM	10	0	1.3	3.1	0	0.5	2.3
VII	TN	6	0	0.3	0.9	0	2.7	0.6
VIII	HVT	6	0	0.3	2.6	0	4.1	1.6
Construction area (m <sup>2</sup> )			46.2	230.8	185	46.2	205.6	149.2

In general, the F2 surpasses F1 in terms of flooding reduction and construction cost as well. With the same solver technique (EPSO), the decentralization approach works better than the centralization one in cutting off flooded volume for extreme flooding. The former model also improves reservoirs' efficiency in moderate flood events than the latter. Therefore, this approach is suggested to be applied to solve further optimization problems of the reservoir system.

#### 4 CONCLUSION

This study proposes a new approach to present flood reduction objective of the optimization detention problem. The decentralized approach performs its advantages in terms of regional and overall flooding situations. The verification in detention storage utilization also presents the efficiency of the proposed approach compared to the overall approach. The optimization model based on decentralization also produces the optimal detention designs with lower cost than the centralization one.

#### ACKNOWLEDGMENTS

This research is supported by a grant (13AWMP-B066744-01) from the Advanced Water Management Research Program funded by the Ministry of Land, Infrastructure, and Transport of the Korean government.

#### REFERENCES

- Behera, P.K., Papa, F. & Adams, B.J. (1999). Optimization of Regional Storm-Water Management Systems. *Journal of Water Resources Planning Management -ASCE*, 125(2), 107–114.
- Bennett, M.S. & Mays, L.W. (1985). Optimal Design of Detention and Drainage Channel Systems. *Journal of Water Resources Planning Management -ASCE*, 111(1), 99–112.
- Decision No. 108/1998/QD-TTg, (1998). Prime Minister of Vietnam.
- Japan International Cooperation Agency, (JICA). (1995). *The Study on Urban Drainage and Waste Water Disposal System in Hanoi City*, Final report: Main report.
- Loaiciga, H.A., Sadeghi, K.M., Shivers, S. & Kharaghani, S. (2015). Stormwater Control Measures: Optimization Method for Sizing and Selection. *Journal of Water Resources Planning Management-ASCE*, 10, 1061.
- Ngo, T.T., Yoo, D.G., Lee, Y.S. & Kim, J.H. (2016a). Optimization of Upstream Detention Reservoir Facilities for Downstream Flood Mitigation in Urban Areas. *Water*, 8, 290.
- Ngo, T.T., Sadollah, A. & Kim, J.H. (2016b). A Cooperative Particle Swarm Optimizer with Stochastic Movements for Computationally Expensive Numerical Optimization Problems. *Journal of Computational Science*, 13, 68-82.
- Papa, F. & Adams, B.J. (1997). Application of Derived Probability and Dynamic Programming Techniques to Planning Regional Stormwater Management Systems. *Water Science Technology*, 36(5), 227–234.
- Tao, T., Wang, J., Xin, K. & Li, S. (2014). Multi-Objective Optimal Layout of Distributed Storm-Water Detention. *International Journal of Environmental Science Technology*, 11, 1473–1480.

- Travis, Q.B. & Mays, L.W. (2008). Optimizing Retention Basin Networks. *Journal of Water Resources Planning Management-ASCE*, 134, 432–439.
- Yazdi, J. & Neyshabouri, S.A.A. (2012). Optimal Design of Flood-Control Multi-Reservoir System on a Watershed Scale. *Natural Hazards*, 63, 629-646.
- Yeh, C.H. & Labadie, J.W. (1997). Multi Objective Watershed-Level Planning of Storm Water Detention Systems. *Journal of Water Resources Planning Management-ASCE*, 123(6), 336–343.

## RESEARCH ON THE IMPACT OF BOUSSINESQ COEFFICIENT FOR NUMERICAL SCHEMES TO MODEL DAM-BREAK FLOODS

FAN YANG<sup>(1,2)</sup>, DONGFANG LIANG<sup>(1,2)</sup>

<sup>(1)</sup> State Key Laboratory of Ocean Engineering, Shanghai Jiao Tong University, Shanghai, China, d.liang@sjtu.edu.cn

<sup>(2)</sup> Department of Engineering, University of Cambridge, Cambridge, UK, fy250@cam.ac.uk

### ABSTRACT

The Alternating Direction Implicit (ADI) model has been proved to be incapable of modelling trans-critical flows, but it is still widely used in commercial flood routing software. This study examines one of the widely-adopted numerical treatments that enables the use of ADI scheme in simulating rapid dam-break flows: modifying the Boussinesq coefficient which quantifies the non-uniformity of the velocity distribution over the depth. The treatment partly mitigates the inherent instability of the ADI computations for trans-critical flows. The test cases include instantaneous 1-D and 2D dam-break floods on a frictionless flat bed, with the results by a shock-capturing TVD-MacCormack model used as references. Systematic parametric studies were carried out in this study to assess the influence of the Boussinesq coefficient on the computational results of both ADI and TVD models. The results suggest that with the increase of the Boussinesq coefficient, the amplitudes of the spurious oscillation can be reduced. Meanwhile, the value of the Boussinesq coefficient also influences the propagation speed of the dam-break wave. These results are useful for evaluating the accuracy of the ADI models for simulating rapid dam-break flows. Finally, the paper describes the application of the 2-D ADI model to the floods in an urban area. The results reveal that the increase of the Boussinesq coefficient can significantly reduce the amplitude of the numerical oscillation inherent to the ADI model and the coefficient also influences the extent of the flooding.

**Keywords:** Alternating Direction Implicit (ADI); dam break; floods; artificial viscosity; Boussinesq coefficient.

### 1 INTRODUCTION

The main functions of dams include hydro power generation, irrigation, flood control as well as industrial and domestic water supply. However, dams also post a threat to the properties and lives of surrounding residents. An increasing number of dam-break catastrophe have happened in the last few decades due to both natural and anthropic factors, such as the aging of the infrastructures, military confrontations, earthquake as well as extreme climate change. Therefore, it is of considerable importance to pay attention to the safety of dams, and it is necessary to establish an efficient and stable mathematical model to simulate the evolution process of dam-break flood.

Normally, Shallow water equations (SWEs) are widely used for solving these dam-break problems (Morris 2000), and they are derived from the depth integration of the three-dimensional incompressible Navier–Stokes equations under the assumptions of hydrostatic pressure distribution and negligible vertical velocity (Cunge et al. 1980). In recent decades, researchers have developed robust and practical numerical models to solve SWEs. Alternating direction implicit (ADI) scheme is one of the traditional methods which are widely used to solve these equations as its stability domain is relatively large, and the balance between computational cost and accuracy is attractive (Leendertse JJ et al. 1971). This scheme was proposed firstly by Peaceman et al. (1955), after which Leendertse modified this model by combining it with the alternating grid. Then it is used to calculate the two-dimensional flow for the first time. However, it has been theoretically and practically proved by (Liang et al. 2006) that it is unable to predict trans-critical and supercritical flows because of the existence of shocks or bores in flows. Two approaches are suitable for resolving these discontinuities in the solution of the hyperbolic SWEs, including shock-fitting and shock-capturing. Shock-capturing methods are preferable as the methods utilize a universal solution strategy over the whole domain without treating shocks separately. However, the higher computational cost is one of the major reasons that prevent these methods from being widely used in practical studies (Chen et al. 1980). Therefore, a rather simple TVD-MacCormack model has been developed by Liang et al. (2006), which has been tested to be highly efficient and accurate in computation.

In fact, the ADI scheme is still widely used in commercial computing software as the benefits of the TVD-MacCormack method are yet to be widely proven. There are two widely-adopted numerical treatments available for enabling the use of ADI scheme in simulating rapid dam-break flows. One is to introduce large artificial diffusion, and the other is to modify the Boussinesq coefficient which quantifies the non-uniformity of the velocity distribution over the depth. These treatments partly mitigate the inherent instability of the ADI model when solving trans-critical flows. This paper aims at researching the impact of the computing

parameters when the numerical method is used to simulate the dam-break problems. The test cases consider instantaneous 1-D and 2D dam-break floods on a friction-less and flat bed, with the solutions by the TVD-MacCormack model and experimental data from Fraccarollo et al. (1995) used as references. Finally, the paper describes the application of a 2-D ADI and TVD models to the flood flows in a densely urbanised area.

## 2 SHALLOW WATER EQUATIONS

Navier-Stokes equations and the three-dimensional Reynolds averaged continuity can be integrated over the water column when the assumption of the hydrostatic pressure distribution and the kinematic boundary condition of the free surface are utilized. The resulting depth-integrated equations are referred to as the shallow water equations. When neglecting the Coriolis, viscous and wind forces, the standard SWEs can be simplified in the following form:

$$\frac{\partial \eta}{\partial t} + \frac{\partial q_x}{\partial x} + \frac{\partial q_y}{\partial y} = 0 \quad [1]$$

$$\frac{\partial q_x}{\partial t} + \frac{\partial(\beta q_x^2 / H)}{\partial x} + \frac{\partial(\beta q_x q_y / H)}{\partial y} = -gH \frac{\partial \eta}{\partial x} - \frac{g q_x \sqrt{q_x^2 + q_y^2}}{H^2 C^2} + \nu \left[ 2 \frac{\partial^2 q_x}{\partial x^2} + \frac{\partial^2 q_x}{\partial y^2} + \frac{\partial^2 q_y}{\partial x \partial y} \right] \quad [2]$$

$$\frac{\partial q_y}{\partial t} + \frac{\partial(\beta q_y^2 / H)}{\partial y} + \frac{\partial(\beta q_x q_y / H)}{\partial x} = -gH \frac{\partial \eta}{\partial y} - \frac{g q_y \sqrt{q_x^2 + q_y^2}}{H^2 C^2} + \nu \left[ \frac{\partial^2 q_y}{\partial x^2} + 2 \frac{\partial^2 q_y}{\partial y^2} + \frac{\partial^2 q_x}{\partial x \partial y} \right] \quad [3]$$

where  $t$  is time;  $\eta$  represents the water surface elevation above the still water datum;  $q_x$  and  $q_y$  are the volumetric discharge per unit width in the  $x$  and  $y$  directions respectively;  $H (= h + g)$  is the total water column depth, in which  $h$  is the depth below the still water datum;  $g$  is the gravitational acceleration;  $C$  represents the Chezy roughness coefficient which is determined from the Manning formula in this study;  $\beta$  is the correction factor for the non-uniform vertical velocity profile; Eqs. [1-3] are non-conservative formulas of SWEs. As a set of hyperbolic equations, SWEs allow discontinuity in their solutions. In order to maintain the correct motion of the shock during numerical prediction, the conservative form of SWEs should be deployed to ensure mass and momentum conservation after numerical discretization (Liang et al. 2006). Therefore, Eqs. [1-3] are rearranged into the following conservative forms:

$$\frac{\partial X}{\partial t} + \frac{\partial F}{\partial x} + \frac{\partial G}{\partial y} = S + T \quad [4]$$

where

$$X = \begin{bmatrix} H \\ q_x \\ q_y \end{bmatrix}, F = \begin{bmatrix} q_x \\ \frac{\beta q_x^2}{H} + \frac{gH^2}{2} \\ \frac{\beta q_x q_y}{H} \end{bmatrix}, G = \begin{bmatrix} q_y \\ \frac{\beta q_x q_y}{H} \\ \frac{\beta q_y^2}{H} + \frac{gH^2}{2} \end{bmatrix} \quad [5]$$

$$S = \begin{bmatrix} 0 \\ gH \frac{\partial Z_b}{\partial x} - \frac{g q_x \sqrt{q_x^2 + q_y^2}}{H^2 C^2} \\ 0 \end{bmatrix}, T = \begin{bmatrix} 0 \\ 0 \\ gH \frac{\partial Z_b}{\partial x} - \frac{g q_y \sqrt{q_x^2 + q_y^2}}{H^2 C^2} \end{bmatrix}$$

## 3 NUMERICAL METHODS

### 3.1 Alternating Direction Implicit scheme

In the ADI scheme, each time step is divided into two time steps when the shallow water equations are discretized. More specifically, in the first half of the time step, the  $x$  direction is solved by using the implicit scheme, while the explicit scheme is used to solve the  $y$  direction; on the contrary, the second half time step is solved by using the implicit scheme in  $y$  direction, while the explicit scheme is used to solve the  $x$  direction. By using the implicit alternating operation steps, the growth of the computation error can be offset. The detailed numerical schemes for the ADI model used in this paper can be found in Falconer et al. (1986).

### 3.2 TVD-MacCormack scheme

Based on the operator-splitting technique, the solution of the two-dimensional SWEs can be decomposed into the solution of two sets of 1-D equations in each time step, as shown in Eq. [6]. The explicit discretization of the Eq. [6] can be written into the Eq. [7] by using a uniform rectangular grid system.  $L_x$ ,  $L_y$  are the finite-difference operators. The subscript and superscript of  $x$  represent the spatial and temporal grid levels respectively. The finite difference solution to Eq. [4] can be approximated by Eq. [8].

$$\frac{\partial X}{\partial t} + \frac{\partial F}{\partial x} = S, \quad \frac{\partial X}{\partial t} + \frac{\partial G}{\partial y} = T \quad [6]$$

$$X_{i,j}^{n+1} = L_x X_{i,j}^n, \quad X_{i,j}^{n+1} = L_y X_{i,j}^n \quad [7]$$

$$X_{i,j}^{n+2} = L_x L_y L_y L_x X_{i,j}^n \quad [8]$$

The discretization scheme for Eq. [6] in the  $x$  direction is given by the following steps.

$$X_i^p = X_i^n - (F_i^n - F_{i-1}^n) \cdot \Delta t / \Delta x + S^n \cdot \Delta t \quad [9]$$

$$X_i^c = X_i^n - (F_{i+1}^p - F_i^p) \cdot \Delta t / \Delta x + S^p \cdot \Delta t \quad [10]$$

$$X_i^{n+1} = (X_i^p + X_i^c) / 2 + [G(r_i^+) + G(r_{i+1}^-)] \cdot \Delta X_{i+1/2}^n - [G(r_{i-1}^+) + G(r_i^-)] \cdot \Delta X_{i-1/2}^n \quad [11]$$

where the superscripts  $p$  and  $c$  denote the predictor and corrector steps respectively,  $\Delta x$  and  $\Delta t$  are the spatial and time steps.

$$\Delta X_{i+1/2}^n = X_{i+1}^n - X_i^n \quad [12]$$

$$\Delta X_{i-1/2}^n = X_i^n - X_{i-1}^n \quad [13]$$

$$r_i^+ = \frac{\langle \Delta X_{i-1/2}^n, \Delta X_{i+1/2}^n \rangle}{\langle \Delta X_{i+1/2}^n, \Delta X_{i+1/2}^n \rangle} \quad [14]$$

$$r_i^- = \frac{\langle \Delta X_{i-1/2}^n, \Delta X_{i+1/2}^n \rangle}{\langle \Delta X_{i+1/2}^n, \Delta X_{i+1/2}^n \rangle} \quad [15]$$

The point brackets in the numerator and denominator of Eqs. [14-15] denote the scalar product of the two vectors within the point brackets. The function  $G(x)$  is defined by Eq. [16].

$$G(x) = 0.5 \times C \times [1 - \varphi(x)] \quad [16]$$

where the flux limiter function and the variable  $C$  are given by Eq.[17] and Eq.[18] respectively.

$$\varphi(x) = \max(0, \min(2x, 1)) \quad [17]$$

$$C = \begin{cases} Cr \times (1 - Cr), & Cr \leq 0.5 \\ 0.25, & Cr > 0.5 \end{cases} \quad [18]$$

$$Cr = \frac{(|q_x/H| + \sqrt{gh})\Delta\Delta}{\Delta x} \quad [19]$$

By adding an extra term after the corrector step, the TVD-MacCormack scheme enhances the standard MacCormack scheme. In this way, the numerical oscillations are removed theoretically near the sharp-gradient regions and the numerical solution therefore is equipped with the TVD property. The whole scheme has second-order accuracy in both time and space by using the predictor–corrector two-stage scheme.

#### 4 IDEALISED DAM-BREAK PROBLEM

##### 4.1 One-dimensional case

Figure 1 depicts a profile perpendicular to the dam, in which  $h_1$  and  $h_0$  represent the water depths at the upstream headwater and downstream tail-water respectively. The dam was located at  $x = 500\text{m}$  with the initial upstream water depth being 10 m and the downstream water depth being 2 m. The time step was 0.1 s and the grid spacing was 10 m, unless specified. This situation is considered as a one-dimensional problem because the dam is assumed to collapse together. Conversely, if the dam is only partially ineffective, it needs to be considered as a two-dimensional problem, which is discussed in the next section.

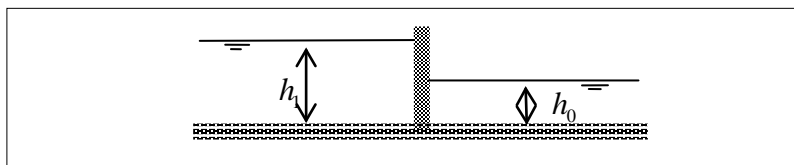


Figure 1. Dam-break problem illustration

Figure 2 shows the water surface elevation at 18s after the dam failure, which are given by the two models with a series of  $\beta$ . Solid lines represent solutions of TVD-MacCormack scheme while dash lines represent solutions of ADI scheme. In general, the significant difference between the solutions of the two numerical schemes is the occurrence of spurious oscillation in the discontinuous region appearing in the solutions of ADI model. It is worth noting that when the value of  $\beta$  is relatively large, as shown in Figure 2, the oscillation is significantly inhibited. This can be interpreted as a decrease in the height of the interface, so that the amplitude of the oscillation is also relatively reduced.

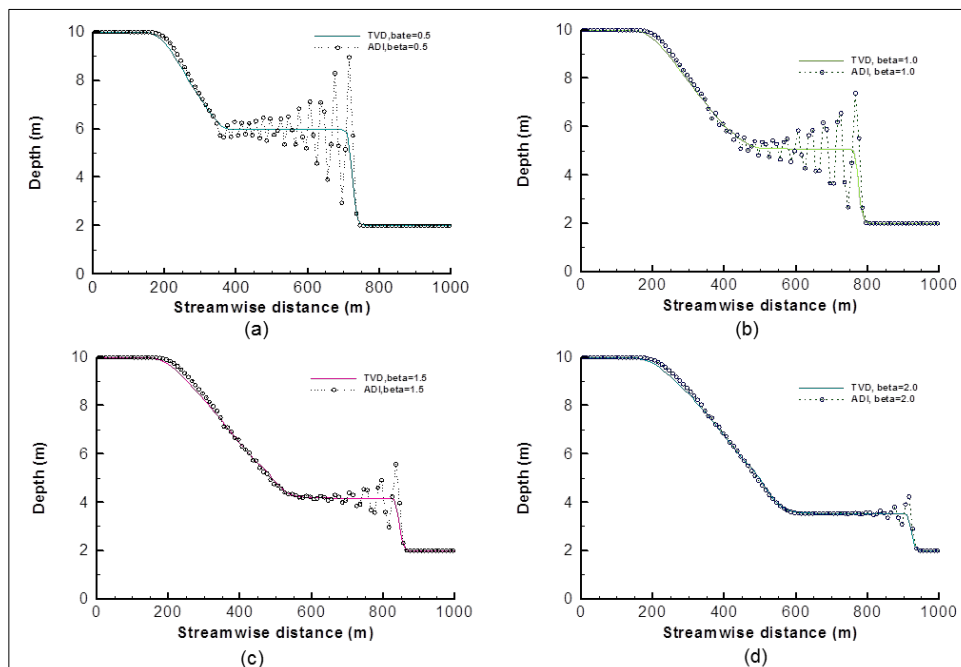


Figure 2. The Comparison between ADI model and TVD-MacCormack model:  
 (a)  $\beta = 0.5$ ; (b)  $\beta = 1.0$ ; (c)  $\beta = 1.5$ ; and (d)  $\beta = 2.0$ .

In addition to the position where the oscillation exists, the solutions of ADI scheme in Figure 2 almost coincide with the solutions of TVD scheme. Also, the similarity between the two is that the height of interface predicted by the two scheme decreases as the  $\beta$  value increases. Figure 3 and Figure 4 demonstrate the trend of the  $\beta$  impact by using the TVD-MacCormack model, in which the colorful lines illustrate the predicted results with different Boussinesq coefficients. It can be seen that lower interface and larger velocity are predicted by a larger  $\beta$ , which indicates the flood wave travels more quickly.

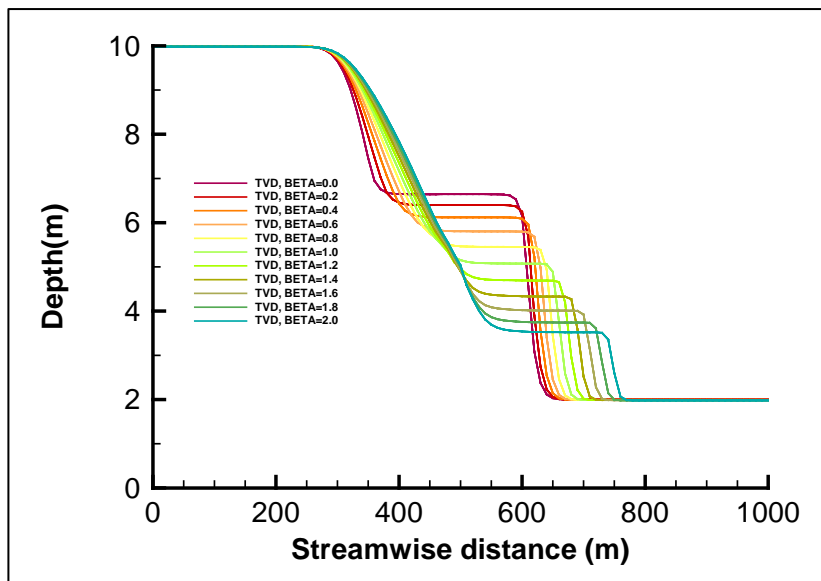


Figure 3. Water depth at 18s predicted by the TVD-MacCormack model

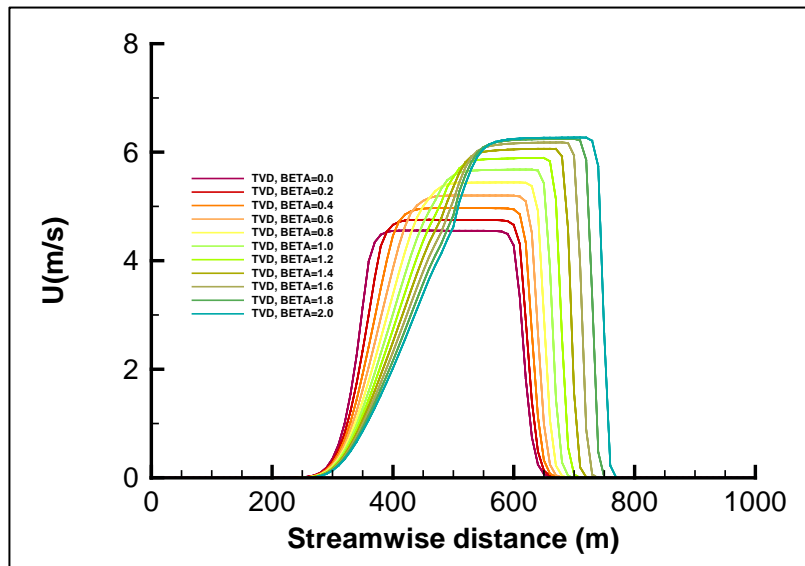
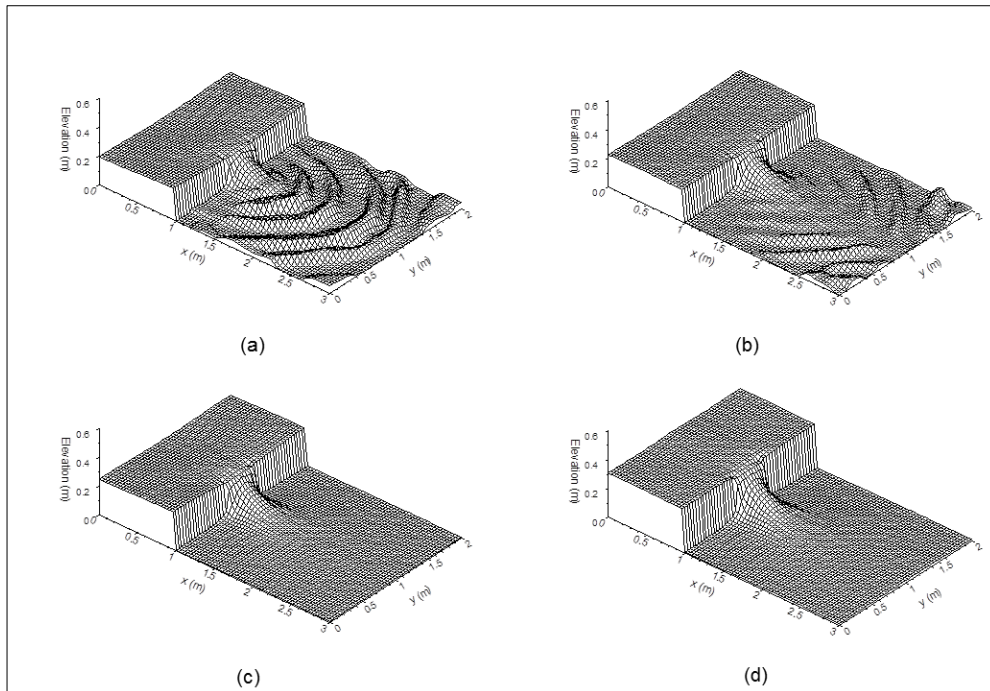


Figure 4. Velocity at 18s predicted by the TVD-MacCormack model

#### 4.2 Two-dimensional case

The test case considered in this part is an instantaneous two-dimensional dam-break flood on a frictionless and flat bed. As shown in Figure 4, the dam located at  $x = 1\text{m}$  divided the whole domain ( $3\text{m} \times 2\text{m}$ ) into two parts. The water was still in the left reservoir at the beginning, at a depth of  $0.64\text{m}$ , while the flood plain on the right was dry. The critical water depth for the wetting/drying was set to be  $0.000001\text{mm}$ , which has been found small enough so that the results are independent of this value. The boundary condition was an open flooded zone boundary, and thus, a zero gradient condition was specified at all boundaries. In the present simulations, the spatial step was set to be  $0.04\text{m}$  and time step was set to be  $0.0001\text{s}$ . A same symmetrical dam-break experiment was performed Fraccarollo et al. (1995). Their experimental data is used in this section as references.

Figure 5 shows four snapshots of the water surface elevation with different value of  $\beta$  at  $5\text{s}$  after dam failure. The stability of the calculation increases with a larger  $\beta$  setting. In the downstream region, the number of the waves grows as the  $\beta$  value increases, with the height of these wave decreases. In the upstream region, the water depth decreases with the drop of  $\beta$ , indicating a higher propagation velocity of the wave. Figure 6 compares the predicted and measured water depth with the change of time at four locations. The fluctuations are obvious in the Figure6 (a) as the point is located at the dam breach where flows change rapidly. It can be seen that a higher  $\beta$  prevents the oscillation, which encourages the smoothness of water surface depth variations. In addition, the predicted depth of water surface in the upstream shows an upward trend with the growth of Boussinesq coefficient.



**Figure 5.** Snapshot of the water surface elevations for the 2-D dam-break simulation at 5s: (a)  $\beta = 0.6$ ; (b)  $\beta = 0.8$ ; (c)  $\beta = 1.0$ ; and (d)  $\beta = 2$ .

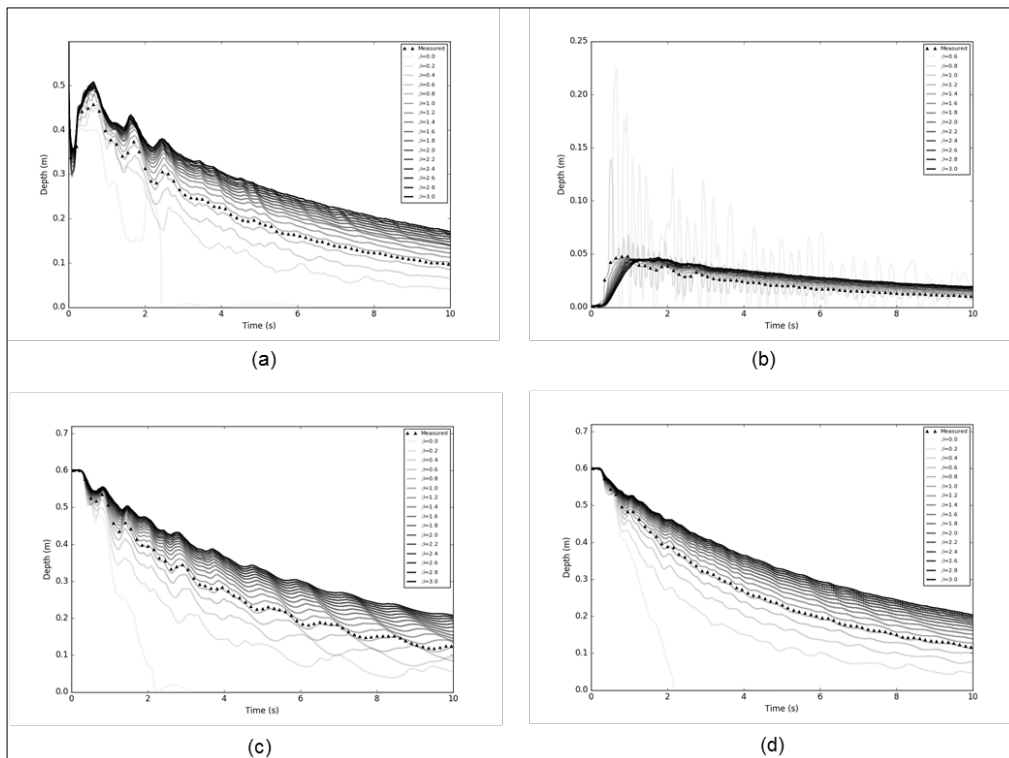


**Figure 6.** Water depth variations at four locations with a series of  $\beta$  value for the 2-D dam-break simulation: (a)  $(x = 1\text{m}, y = 1\text{m})$ ; (b)  $(x = 1.8\text{m}, y = 1.44\text{m})$ ; (c)  $(x = 0.2\text{m}, y = 1\text{m})$ ; (d)  $(x = 0.48\text{m}, y = 0.4\text{m})$ .

## 5 ACTUAL URBAN FLOODING

The dam-break case considered here is based on a real flood that occurred in the city of Glasgow, Scotland, UK on 30 July 2002. A two-dimensional ADI model was applied to simulate the flood event in the  $1.0\text{km} \times 0.4\text{km}$  urban catchment. A single set of friction coefficients was used, with the Manning coefficient of roads and vegetation being 0.015 and 0.05 respectively. Flooding at this site was caused by a 1m wide stream that enters near the north-east corner. The detailed information, data availability about the area as well as the treatment of the boundary conditions for this case can be found in Villanueva et al (2008). In order to

demonstrate the changes of water level clearly, four reference points were selected, representing the vicinity of the breach, the main channel, the main tributaries and the downstream region, respectively. The exact location of the reference point is shown in Figure 7.

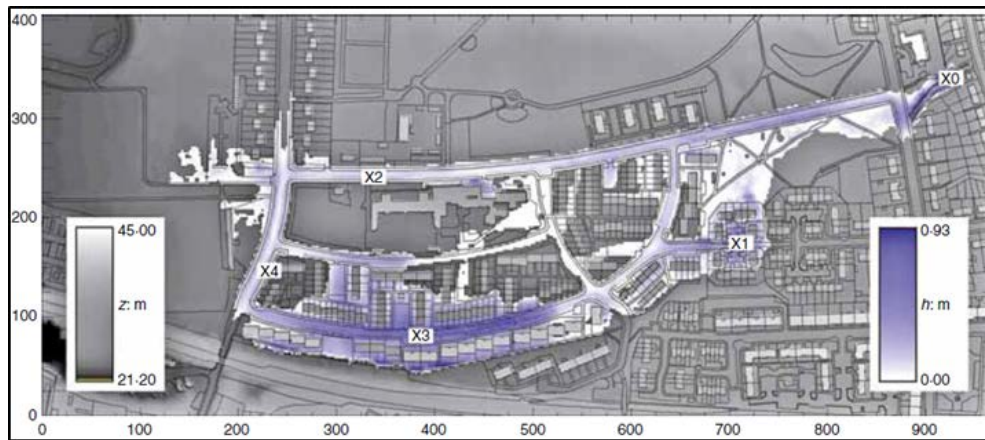


Figure 7. Map of the study site and the locations of point X1-X4

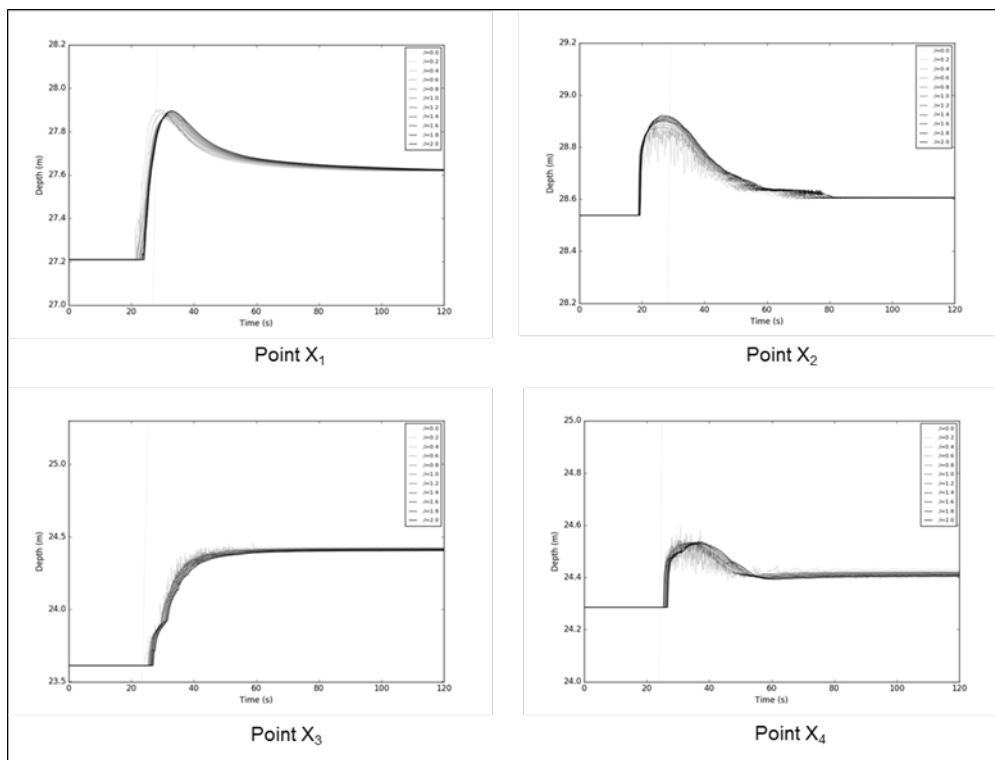


Figure 8. Variations of water depths predicted by 2-D ADI model with the value of  $\beta$  ranging from 0.0 to 2.0

The predictions of water depth at the four points over the whole flooding process are shown in Figure 8. In this case, darker grey line represents a larger Boussinesq coefficient value. Similarly, spurious oscillations are obvious when the  $\beta$  is close to zero, especially for the point  $X_2$  and point  $X_4$  where shallow, high-velocity and convergent flows exist. On the contrary, the water-depth variation curves with larger  $\beta$  are relatively smooth, indicating that large  $\beta$  set mitigate the inherent instability of the ADI model when simulating transcritical and super-critical flows. In addition, the arriving time of dam-break flood and maximum submerging depth are also influenced by the change of  $\beta$ , but the deviations are all less than 4% at the four points when the value of  $\beta$  ranging from 0.0 to 2.0.

## 6 CONCLUSIONS

In this paper, the influence of the Boussinesq coefficient on the computational results of both ADI and TVD-MacCormack models is assessed through stimulating ideal 1-D and 2-D dam-break floods over a frictionless and flat bed. The comparison between the solutions of the two models suggests that the amplitudes of the spurious oscillation can be reduced with the increase of the Boussinesq coefficient, which means that using a large  $\beta$  value makes contributions to mitigate the inherent instability of the ADI model in

simulating rapid dam-break flows. In addition, adding the value of the Boussinesq coefficient increases the propagation speed of the dam-break wave in the one-dimensional case. Finally, the simulation of dam-break floods on a complex urban terrain is studied and the impact of the coefficient on the solution of a 2-D ADI model is further analyzed. The results confirm the finding that the increase of the Boussinesq coefficient can significantly reduce the amplitude of the numerical oscillation inherent to the ADI model. These results are useful for evaluating the accuracy of the ADI models when simulating rapid dam-break problems and provide references for users of ADI and TVD-MacCormack scheme based computing software.

#### ACKNOWLEDGMENTS

We are grateful to the financial support by the National Natural Science Foundation of China (Grant No. 51479111).

#### REFERENCES

- Chen, C. L., & Armbruster, J. T. (1980). Dam-break wave model: formulation and verification. *Journal of Hydraulic Engineering*, 106(5), 747-767.
- Cunge, J. A., Holly, F. M., & Verwey, A. (1980). *Practical aspects of computational river hydraulics*. Pitman Advanced Publishing Program (Boston, MA, USA), Book.
- Falconer, R. A. (1986). A two-dimensional mathematical model study of the nitrate levels in an inland natural basin. International Conference on Water Quality Model, Inland Natural Environment. Bournemouth, UK, 325-344.
- Fraccarollo, L., & Toro, E. F. (1995). Experimental and numerical assessment of the shallow water model for two-dimensional dam-break type problems. *Journal of hydraulic research*, 33(6), 843-864.
- Leendertse, J. J., & Gritton, E. C. (1971). *A Water-Quality Simulation Model for Well Mixed Estuaries and Coastal Seas: Computation Procedures*. New York Rand Institute Report R-708-NYC.
- Liang D, Falconer RA and Lin B. (2006). Comparison between TVD-MacCormack and ADI-type solvers of the shallow water equations. *Advances in water resources*, Vol. 29(12), 1833-1845.
- Liang, D., Lin, B., & Falconer, R. A. (2007). Simulation of rapidly varying flow using an efficient TVD-MacCormack scheme. *International journal for numerical methods in fluids*, 53(5), 811-826.
- Morris, M. W. (2000). *Concerted Action on Dambreak Modelling-CADAM*. HR Wallingford Limited Report SR571.
- Peaceman, D. W., & Rachford, Jr, H. H. (1955). The numerical solution of parabolic and elliptic differential equations. *Journal of the Society for Industrial and Applied Mathematics*, 3(1), 28-41.
- Villanueva, I., Pender, G., Lin, B., Mason, D. C., Falconer, R. A., Neelz, S., & Wright, N. G. (2008). Benchmarking 2D Hydraulic Models for Urban Flooding. *Proceedings of the ICE-Water Management*, 161, 13-30.

## COMMUNITY PERCEPTION OF SUSTAINABLE URBAN DRAINAGE SYSTEM: A CASE STUDY OF NHIEU LOC – THI NGHE BASIN, HO CHI MINH CITY, VIETNAM

LAN HOANG MY NGUYEN<sup>(1)</sup>, PHU LE VO<sup>(2)</sup> & TRUNG VAN LE<sup>(3)</sup>

<sup>(1,2,3)</sup> Faculty of Environment and Resources, Ho Chi Minh City University of Technology, VNU-HCM, Ho Chi Minh City, Viet Nam  
e-mail: mylannh@hcmussh.edu.vn

### ABSTRACT

In recent years, Ho Chi Minh City has suffered extreme inundation from heavy rainfall events as the results of rapid urban development. The City government has implemented plenty of hard engineering options such as building flood gates and upgrading sewer systems, but the problem persists and it gets worse. Sustainable Urban Drainage System – SUDS, introduced in the 1990s and commonly applied in many developed countries, is one of the sustainable approaches in urban flood management. SUDS with the philosophy of stimulating ways that Nature behaves under extreme contexts, specifically by modeling and replicating at a particular site is one of the most sustainable approaches to controlling and minimizing the impacts of flooding in urban development along with the ability to achieve multiple benefits on environmental and social aspects. The purpose of this paper is, firstly, to overview the SUDS implementation and benefits. Then, through a social survey, the community perception of some SUDS techniques will be examined and analyzed. It has been observed that most of the respondents have no idea about SUDS techniques but impressed by its ability to mitigate urban flood. The residents are willing to apply these SUDS techniques, including rainwater harvesting, green roof, pervious open space, pervious pavement, and pervious parking lot, mostly due to flooding reduction instead of environment enhancement or landscape improvement.

**Keywords:** Sustainable urban drainage system; urban flood management; community perception; Ho Chi Minh city; social benefits.

### 1 INTRODUCTION

Natural water cycle in the urban area is affected strongly by impervious surface, a particular characteristic of urban growth. It results in decrease of the volume of evapotranspiration as well as infiltration but affects inversely as well when the increase in surface run-off occurs. Many cities and urban areas have drainage system which is out-of-date and often overwhelmed after heavy and intensive rain events. The conventional drainage system has usually been designed to collect and transport water run-off from surface areas as quickly as possible via sewer networks and water treatment facilities to nearby receiving water bodies (Zhou, 2014) but not to improve environment quality or provide green spaces.

Sustainable Urban Drainage System – SUDS, introduced in the 1990s and commonly applied in developed countries, is one of the most sustainable approaches to deal with urban flooding. The philosophy of SUDS is to replicate as closely as possible the nature drainages from a site before development. SUDS is designed to minimize the impacts from the development on the quantity and quality of the runoff, to maximize amenity and biodiversity opportunities (Woods-Ballard et al., 2007). These objectives should all have equal standing. The amenity arm of the SUDS triangle is however arguably the most important from a social and a sustainability perspective, including safety, aesthetic, recreation, etc. As Everett and Lamond (2016) argued, people will need not only need to understand SUDS' direct functions but also need to notice and appreciate their more indirect benefits, such as adding green infrastructure. They have to also comprehend how they might contribute to amenity as well. If they do not feel SUDS elements contribute to their lives, they might be less willing to adapt their behavior to facilitate longer-term functioning, or to pay for their wider rollout and maintenance.

The purpose of this paper is, firstly, to overview the SUDS implementation and benefits. Then, through a social survey and interview, the community perception of some SUDS techniques will be collected and evaluated by statistical analysis.

### 2 EXAMPLE OF SUDS IN PRACTICE

It is very difficult to establish SUDS solutions in urbanized city, generally, due to lack of available spaces for making new drainage system (Sharma, 2008), even though SUDS and its philosophy have been the best alternative for reducing storm-water run-off so as to overcome flooding situation in worldwide urban areas. Some SUDS implementations will be described briefly in this section.

In Islington, the UK, every urban surface must be considered as a rainfall collector, allowing water to pass through to a drainage layer below or flow to a soakage area so that volumes do not accumulate to cause

problems downstream (Islington Council, 2010). SUDS elements could be applied at any places as long as they met proposed criteria and followed a design process, including three steps as follows conceptual drainage design, outline drainage proposal and detailed drainage design. They could be schools, car parks, existing house estates, high-ways, and streets or anywhere else and yet they should still follow the guidelines. Due to limited green and open spaces, green roof was well established as a technique to collect, clean and attenuate flows from roof surfaces with an agreed 40% to 60% reduction in run-off co-efficient dependent on the roof construction, in particular the substrate depth. The integration of roads and SUDS has been a challenge because of difficulties in collection of run-off from linear trafficked surfaces and the perceived conflicts between SUDS design requirements and road management practices. Pervious pavement applied along the streets should satisfy some requirements, such as to drain completely surface run-off within 24 – 48 hours after rainfall event, not to impact on structure of adjacent road and other traffic features, to create attractive landscape, and to be cost-benefit solution in terms of operation and maintenance.

Another site for SUDS implementation in the UK is Lamb Drove, Cambourne. Unlike Islington, Lamb Drove is a new development residential area with 35 affordable homes on a one-hectare site where flooding in river valleys and urban watercourse is a major concern. Besides environmental benefits, the estimated cost savings due to SUDS are approximately £11,000 for County and £30/year/household. Because of the gentle-slope terrain with clay ground, rainwater collecting at source has been preferred to pervious pavement or other infiltration techniques. The lesson learnt from this study is that SUDS should be implemented and integrated from the beginning of the design phase as part of a holistic approach to sustainable development and perceived concern of stakeholders was one of the important factors to realize sustainable urban drainage systems.

From the review study of BOOGAAR (2015), a 40-meter-long grass swale was installed to capture sediment in an urban catchment with frequent, short-duration, and high-density rainfall events. This grass swale could remove between 50 % and 70 % of the total suspended solid within the first 10 m of length. Beyond 10 m, only a further approximately 20% reduction could be expected, regardless of the total length. Thus, the installation of excessively long swale for sedimentation may not be the most cost effective solution. Whereas, swale-trench systems were widely used in a developed area with low permeable soil, high ground water table, and limited drainage capacity of the small existing creek. However, BOOGAARD (2015) concluded that using treatment train approach achieved more efficiencies than single SUDS devices. For example, gross pollution traps could be used as the first treatment step to remove larger sediment particles followed by permeable pavements which removed smaller ones and nutrient to meet the water quality standard.

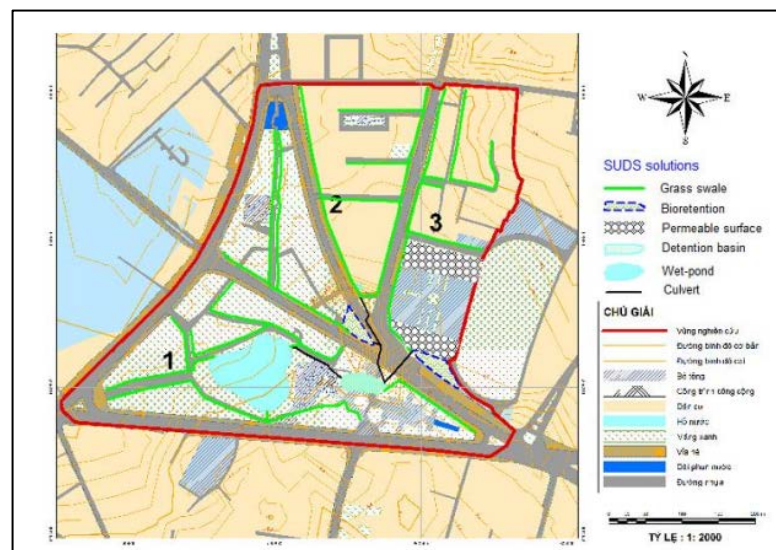


**Figure 1.** Assessing and choosing SUDS techniques in Hoang Van Thu park, Ho Chi Minh City (Duong Van Truc, 2015).

According to Duong Van Truc (2015), retrofitting SUDS in Ho Chi Minh City is to apply suitable SUDS techniques into current or re-developing urban areas to mitigate the impacts of development, overload of current urban drainage as well as climate change adaptation. In this study, Hoang Van Thu park was selected to apply some SUDS techniques, for example grass swale, bio-retention, detention basin, pervious pavement, and wet-pond. After retrofitted, a water quantity of 4,717 m<sup>3</sup> was kept temporarily and then discharged all after a period of about 24 to 36 hours, leading to flood peak reduction. Moreover, retrofitting SUDS could treat 80% of load of non-point pollution sources to keep water quality cleaner and create more green spaces, which is

approximately 10.7% of the catchment area, and amenity for the community, as well. Similarly, retention pond has been introduced to overcome flooding problems in Can Tho city (Quan et al., 2014). Consistent with the social consensus in the research area in Can Tho city, the retention pond makes the beautiful landscape, makes the weather equable, reduces inundation, and assists the drainage of residential area (100.0%, 100.0%, 76.0% and 94.0%, respectively).

### 3 CASE STUDY AREA

Ho Chi Minh City is located at the downstream section of the Dong Nai and Sai Gon rivers in the South of Vietnam. Sixty percent of the city land is less than 2 meters above the sea level. Low-land elevations combined with the increasing urban density, loss of blue and green spaces and steady land subsidence makes the city extremely vulnerable to water-logging and floods. Besides, tides, high river discharges, excessive rainfall, combinations of all the above 3 are considered as the objective reasons to cause flooding in Ho Chi Minh City (Moens and Phuoc, 2013). Based on the topographical conditions, the master plan of the drainage system in Ho Chi Minh City divides into 6 areas, one of which contains Nhieu Loc – Thi Nghe basin.

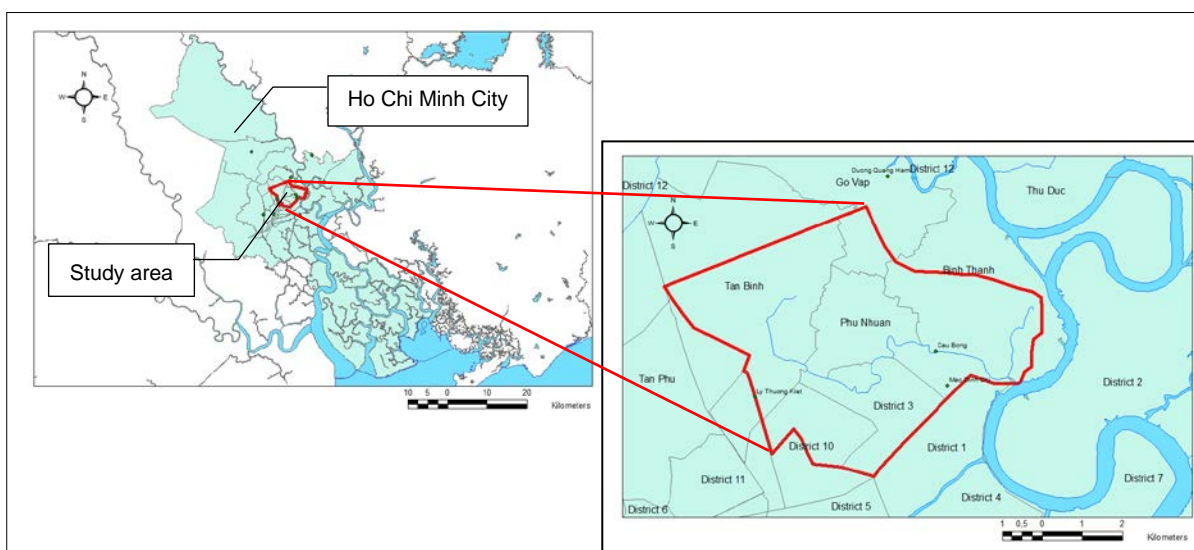


**Figure 2.** Location of Nhieu Loc – Thi Nghe basin in Ho Chi Minh City.

Nhieu Loc – Thi Nghe is located in the center drainage system of the city with the area of 33.2 km<sup>2</sup> and comprises of 7 districts: 1, 3, 10, Phu Nhuan, Tan Binh, Binh Thanh and Go Vap. As reported in Loc et al. (2014) the population of the basin is about 1.2 million people and the density is 290 people per hectare. Land use is mixed, with 49.3% being residential and the remaining representing commercial, public and industrial uses. Elevation within the basin is variable, with the north and northwest sections being up to 8 m above sea level, while the southern part of the basin averages only 1.3 m above sea level. Flooding happens in the rainy season, from August to November and concentrates in the North area. Thus, the research area will be divided into 3 sites for survey:

1. Site 1: The Northwest area which has potential to realize some infiltration techniques, such as pervious pavement and pervious surfaces.
2. Site 2: The East area which has the most serious flooded points.
3. Site 3: The Center area which has the most density of impervious surfaces.

### 4 METHODS

A questionnaire was used to understand and estimate the residents' perception of several SUDS techniques. The research questions were:

1. How are they aware of the flooding situation and implemented solutions in this area?
2. What do they know about the SUDS techniques?
3. How do they accept the SUDS techniques and SUDS benefits?

In the beginning, six SUDS techniques selected for the survey were rainwater harvesting, green roof, pervious open space, pervious pavement, pervious parking lot and detention pond. The first two techniques are applied in private places and the rest is in public areas.

Rainwater harvesting can be designed to maximize rainwater capture and reduce runoff during extreme events. Besides, the harvesting of rainwater refers to the collection of water from surfaces on which rain falls, and subsequently storing this water for later use (Vo et al., 2012). Green roofs are the systems which cover a building's roof with vegetation and designed to intercept, retain precipitation, reduce runoff volume, and

attenuate peak flows. Generally, pervious surfaces allow rainwater to infiltrate through the surface into an underlying storage layer, where water is stored before infiltration to the ground, reuse or release into surface water (Woods-Ballard et al., 2007). In this survey, three types of permeable surfaces include pervious pavement, pervious open space, and pervious parking lot, which are different in scale, operation and maintenance requirements as well as place to apply. Detention pond is the storage facility that provides flow control through attenuation of storm-water runoff. It also facilitates some settling of particulate pollutions so as to improve the quality of water environment.

There was one picture per SUDS technique added to the questionnaire for good illustration. A pilot survey was conducted using face-to-face interview in November 2016 to identify and refine the unclear or misunderstood questions. After the pilot survey, detention pond was omitted because the participants had no sufficient information to answer the questions. The finalized questions comprised 12 questions divided into three parts. The first section was to assess the respondents' awareness of their flooding situation and efforts to reduce inundation. The second was used to identify their willingness to accept SUDS techniques and preference for SUDS benefits. The last part was to provide demographic information. A total of 200 questionnaires were distributed randomly in three research sites with the ratio of 60, 60 and 80 for site 1, site 2 and site 3, respectively. The Excel software was employed to analyze the data. After cleaning data, a total of 191 questionnaires (95.5%) were used for final analysis.

The 5 Likert scale was used to quantify the respondents' answer. Regarding to willingness to accept, 1 represents for Strongly disagree and 5 represents for Strongly agree. While from 1 to 5 denotes Lowest to Highest in ranking the priority of SUDS benefits. In this survey, SUDS benefits consist of flood reduction, environmental enhancement and landscape improvement.

## 5 RESULTS AND DISCUSSION

Most of the respondents are female (59.2%) and above 50 years old (50.9%). Women in the survey spend most of their time to take care of their houses. Thus, they showed their anxiety for the techniques that would be installed at their private places and have difficulties in either operation or maintenance. The majority of the respondents stated that their household income was below USD 500 per month (56.7%). From the analysis, the residents would be willing to get involved in SUDS retrofit if they had the financial support from the city or local government and high agreement from the community.

**Table 1.** Respondents' demographic information.

Information	REPOSE RATE (%)
<b>GENDER</b>	
MALE	40.8
FEMALE	59.2
<b>AGE</b>	
≤ 30	10.5
31 – 50	38.6
≥ 50	50.9
<b>INCOME (USD/MONTH/HOUSEHOLD)</b>	
≤ 500	56.7
500 – 1000	29.8
≥ 1000	13.5

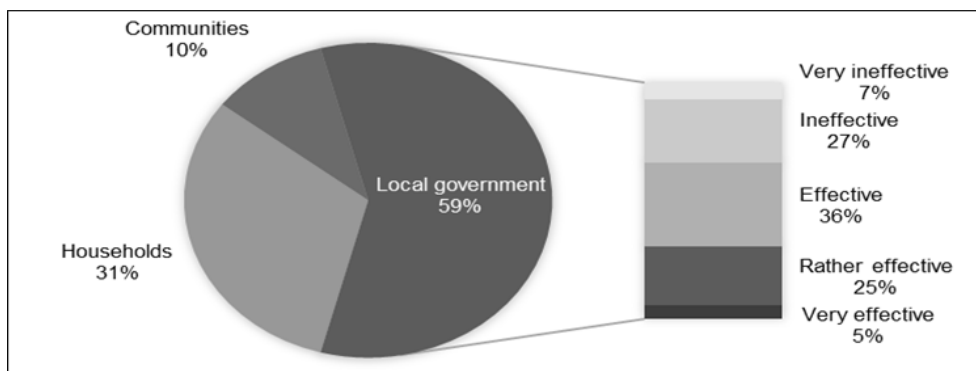


**Figure 3.** Residents' assessment of flooding reduction solutions from the local government.

All the respondents easily stated the reasons why flooding happened at their home places. These reasons include heavy rain, tide, the combination of rain and tide and inefficient urban drainage system. Among these reasons, heavy rain is the most important for flooding in Nhieu Loc – Thi Nghe basin. When being asked about the flood frequency, 76.6% of interviewees said that flooding rarely and occasionally happened in the research area, which is the result of stakeholders' efforts. Over the last fifteen years, the city government has implemented numerous infrastructure projects to reduce urban flood risk based on a plan developed by Japan International Cooperation Agency – JICA, resulting 6.000 kilometers of canals and pipes to improve the discharge capacity of the storm-water system and 172 kilometers of dikes and river barriers for tidal control. Of 56 responses, 68% stated that local government's solutions were much more effective in flood reduction (Figure 2). Moreover, the households chose some appropriate methods to adapt to flood risk, such as contributing their resources (in cash or service) to government or community's solutions, using hard materials to prevent water getting into their houses and raising the floor. Although they were satisfied with the effectiveness of all the methods to overcome the flooding, they desired to have a better approach for flooding reduction so as to make a better living condition.

Initially, a great majority of the respondents (92%) had no idea what the concept of sustainable urban drainage system is about. After being explained, most of them were impressed by these techniques' capacity to drain in a sustainable way, though they had used to apply such techniques, for example, rainwater harvesting and green roofs. However, the number of respondents who did not agree to implement these techniques at their living places is over 50% for five methods, especially 92% and 83% said "No" to rainwater harvesting and green roofs, respectively. The reasons not to accept includes lack of financial capacity, cost-benefit inefficiency, difficulties in operation and maintenance, lack of spaces and inappropriate housing structure (Figure 3). Those who were unwilling to install SUDS for private properties are 1.2 to 2 times as much as for public areas. It has been also found that pervious pavement was the most preferred SUDS technique in Nhieu Loc – Thi Nghe basin, followed by pervious parking lot, pervious open space, rainwater harvesting, and green roof, which is equivalent to the finding in Loc et al. (2014).

For rainwater harvesting, most of the respondents said that they didn't have enough space to install the storage tank or other facilities to collect rainwater from their rooftop because they lived in one of the most densely built-up areas in Ho Chi Minh City. Further, there's no need for them to collect or reuse rainwater since utilization of rainwater has been ignored for a long time by the urban dwellers and the water supply can satisfy the residential demands, which is similar to the observation in the study of Vo et al. (2012).

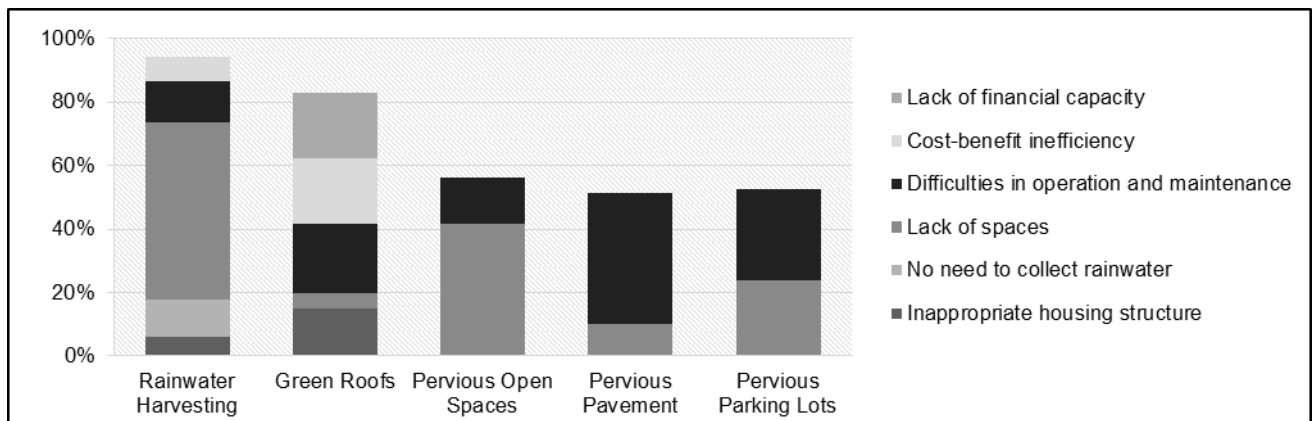


Figure 4. Reasons for not accepting SUDS techniques in Nhieu Loc – Thi Nghe basin.

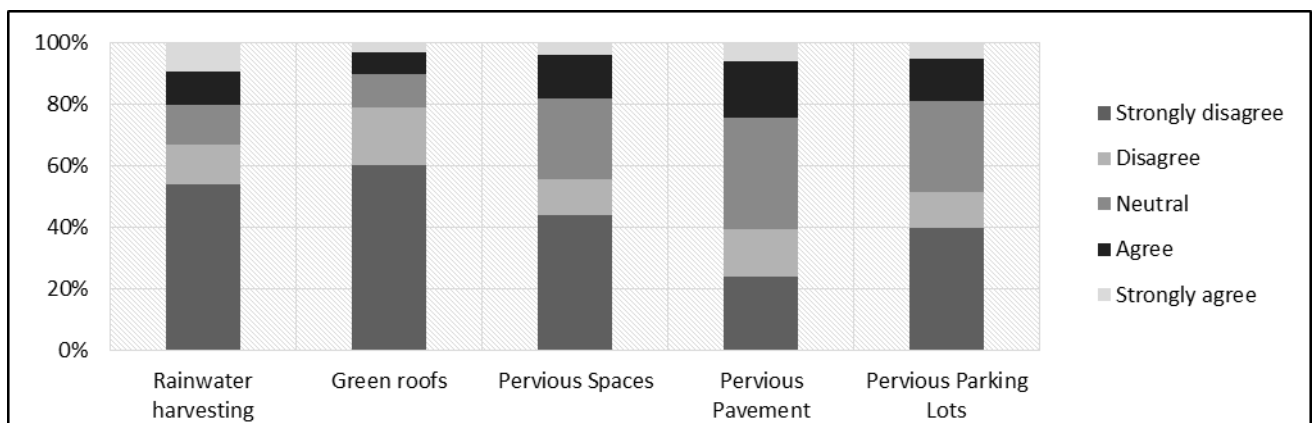


Figure 5. Willingness to accept SUDS techniques in Nhieu Loc – Thi Nghe basin.

Although green roofs in which green devices are installed around or on the top of building can change the aesthetics of homes and surroundings (Everett and Lamond, 2016) and have a positive impact on residents in high density areas (Bastien et al., 2011), this SUDS techniques had the largest number (60%) of “strongly disagreeing” answer (Figure 4). The reason of lack of spaces is not significant for such method, which is different from rainwater harvesting. The most important point is the limitations in investment, installation, operation and maintenance when applying green roof.

The respondents were then asked to rank the SUDS benefits, including flood reduction, environment enhancement, and landscape improvement. As shown in Figure 6, the largest number of respondents (44.5%) rated “flood reduction” as the highest priority, which is double and triple those choosing “environment enhancement” and “landscape improvement”. Moreover, there is little difference in priority order of SUDS benefits between groups of respondents’ age and income (Table 2). All the respondents ranked “landscape improvement” as the lowest priority. Whereas “environment enhancement” had the highest rank for those in under 30 age group and “flooding reduction” was the first choice for the rest of respondents. The highest-income group prioritized their preferences: landscape improvement first, environment enhancement, and flooding reduction. For the lowest-income, the amenity arm of SUDS techniques was the first preference and the last one was the quality objective. But the middle-income group made a converse order.

These findings indicate that flooding is still a big problem in Ho Chi Minh City in general and Nhieu Loc – Thi Nghe basin in particular, the community focuses on the quantity objective more than the quality or amenity when considering flooding control methods. As mentioned above, the finding that nearly all of the respondents are not aware of the objective to provide additional creational area and beautify the city leads “landscape improvement” to the lowest priority. Thus, the city government needs to organize some community-based activities to improve the awareness of SUDS concept and benefits, especially the amenity aspect. Good knowledge will lead to positive behavior toward further sustainable approaches in flooding control.

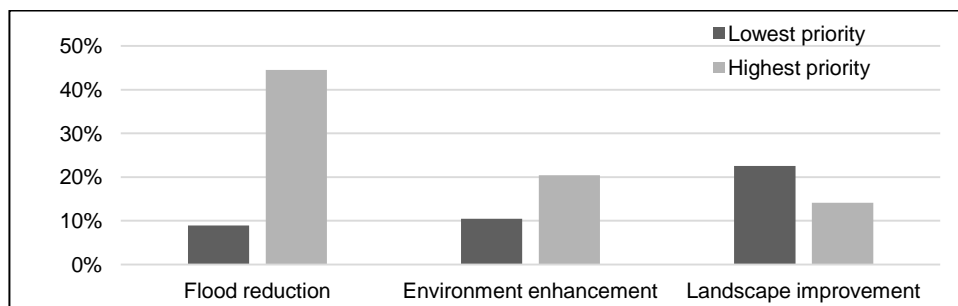


Figure 6. Ranking of SUDS benefits.

Table 2. Average score of SUDS benefits based on group of respondents’ age and income.

	AGE (YEARS OLD)			INCOME (USD/MONTH/HOUSEHOLD)		
	≤ 30	30 – 50	≥ 50	≤ 500	500 – 1000	≥ 1000
FLOOD REDUCTION	3.83	3.72	3.97	3.93	3.46	<b>2.81</b>
ENVIRONMENT ENHANCEMENT	4	3.58	3.43	3.67	3.75	<b>3.16</b>
LANDSCAPE IMPROVEMENT	2.78	3.08	2.94	3.96	3.43	<b>3.26</b>

## 6 CONCLUSIONS

This study reveals the residents’ willingness to accept SUDS techniques and awareness of SUDS benefits in Nhieu Loc – Thi Nghe basin, Ho Chi Minh City. Although their understanding of SUDS is not strong, they are willing to get involved in SUDS retrofit so as to control and mitigate the state of flooding. The SUDS elements that was asked can be applied for both private properties and public places, in which the one in public spaces are more favored than the other. In general, the respondents rated pervious pavement as the first accepted, followed by pervious parking lot, pervious open spaces, rainwater harvesting, and green roof. The perception of SUDS benefits is examined based on the priority order of the objective of flooding control method. While the youngest group ranks environment enhancement as the highest priority, the rest of respondents prioritize flooding reduction. Regarding the respondents’ income, landscape improvement is placed at the top rank by the highest and lowest income groups but becomes the last one in middle group’s opinion.

## REFERENCES

Bastien, N., Arthur, S. & McLoughlin, M. (2011). Public Perception of SuDS Ponds–Valuing Amenity. *12th International Conference on Urban Drainage*.

- BOOGAARD, F.C. (2015). *Stormwater Characteristics and New Testing Methods for Certain Sustainable Urban Drainage Systems in The Netherlands*, Technische Universiteit Delft.
- Duong Van Truc. (2015). *Retrofitting Suds: A Case Study for Hoang Van Thu Park Area, Hochiminh City*, Green designs for Integrated Urban Water Cycle Management – Solutions for Secondary Cities in Global South to Cope with Climate Change. Can Tho.
- Everett, G. & Lamond, J. (2016). SuDS and Human Behaviour: Co-Developing Solutions to Encourage Sustainable Behaviour. *FLOODrisk 2016 - 3rd European Conference on Flood Risk Management*.
- Islington Council. (2010). *Promoting Sustainable Drainage Systems*, Design guidance for Islington: Islington, UK.
- Loc, H.H., Gupta, A.D., Duyen, P.M. & Rajbhandary, J. (2014). Social Aspects of the Application of SUDS for the Case of Nhieu Loc Thi Nghe Basin, Ho Chi Minh City, *2nd International Conference on Green Technology and Sustainable Development*. Ho Chi Minh City, Vietnam.
- Moens, E. & Phuoc, N.V. (2013). Ho Chi Minh City Moving towards the Sea with Climate Change Adaptation. *Ho Chi Minh City Climate Adaptation Strategy Project*, 1, 126.
- Quan, N.H., Phi, H.L., Tran, P.G., Pathirana, A., Tadhakrishnan, M. & Quang, C.N.X. (2014). Urban Retention Basin in a Developing City: From Theoretical Effectiveness to Practical Feasibility, *13th International Conference on Urban Drainage*. Malaysia.
- Sharma, D. (2008). Sustainable Drainage System (SuDs) for Stormwater Management: A Technological and Policy Intervention to Combat Diffuse Pollution, *11th International Conference on Urban Drainage*. Edinburgh, Scotland, UK.
- Vo, P.L., Tinh, V.T.T., Tu, P.H.C., Dung, H.P.T., Dien, N.V. & Huyen, T.T.B. (2012). Rainwater Harvesting as an Adaptation to Climate Change: An Implication for Ho Chi Minh City, *2nd International Engineering Symposium - IES 2012* (8). Japan.
- Woods-Ballard, B., Kellagher, R., Martin, P., Jefferies, C., Bray, R. & Shaffer, P. (2007). *The DUDS Manual*, 697, Ciria London.
- Zhou, Q. (2014). A Review of Sustainable Urban Drainage Systems Considering The Climate Change and Urbanization Impacts. *Water*, 6(4), 976-992.

## AN OPEN-SOURCE MODELLING AND DATA SYSTEM FOR NEAR REAL-TIME FLOOD FORECASTING

QIUHUA LIANG<sup>(1)</sup>, YUN XING<sup>(2)</sup>, XIAODONG MING<sup>(3)</sup>, XILIN XIA<sup>(4)</sup>, HUILI CHEN<sup>(5)</sup>, XUE TONG<sup>(6)</sup>, GANG WANG<sup>(7)</sup> & HAIBO YANG<sup>(8)</sup>

<sup>(1,2,7,8)</sup>Key Laboratory of Coastal Disaster and Defence (Hohai University), Ministry of Education, Nanjing, China, Qiuhua.Liang@ncl.ac.uk

<sup>(1,3,4)</sup>School of Civil Engineering and Geosciences, Newcastle University, Newcastle upon Tyne, UK,

<sup>(5)</sup>State Key Joint Laboratory of Environmental Simulation and Pollution Control, Peking University, China,

<sup>(6)</sup>School of Water Conservancy and Environment, Zhenzhou University, Zhenzhou, China.

### ABSTRACT

Accurate real-time urban flood inundation forecasting has long been a technologically challenging task due to the complex urban environment and lack of high-resolution data and high-performance hydrodynamic models to accurately predict the highly transient flood hydrodynamics. In recent years, there has been a rapid development in data acquisition and high-performance computing technologies. Data from different sources are now widely available to support different aspects of urban flood modelling. A number of computationally efficient hydrodynamic models have been reported to support full-scale urban/catchment flood modelling at high resolutions. This paper develops and tests a (near) real-time flood forecasting system based on a GPU (i.e., graphics processing unit) accelerated high-performance hydrodynamic inundation model and supported by data from open sources. The flood forecasting systems were tested in the Chinese city of Fuzhou for a recent severe urban flood event caused by Typhoon Meranti using a freely available 30m digital elevation model (DEM) data. The results show that the predicted inundation map, together with street photos and other information from the crowd sources (e.g. social media), may effectively indicate the inundation extent and flood depth of the city in (near) real time, potentially providing useful information for the public to improve preparedness and hence reduce flood impacts.

**Keywords:** Flood forecasting; intense rainfall; crowd-sourced data; remote sensing; high-performance computing.

### 1 INTRODUCTION

It is generally accepted that climate change will increase the recurrence of extreme weather events such as storms and intense rainfall (IPCC, 2014). Flood risk is therefore expected to increase significantly throughout the world. This is evidenced by the outburst of multiple urban flood events in the recent years in different parts of the world, which has led to huge economic and human losses. In China, intense rainfall induced urban flooding has become a wide-spreading issue affecting socio-economic development at national scale. While it is impossible to prevent these damaging natural hazards from happening, it is important to manage the hazard risk, mitigate the impact and improve the resilience of our cities to these devastating events. An effective way to improve flood resilience and reduce loss is to implement and operate a reliable flood forecasting and warning system to enhance the preparedness of the public and relevant government agencies.

Due to the temporally transient and spatially varying nature of the intense rainfall induced flood events, accurate real-time forecasting has long been a technologically challenging task. However, the recent advancements in high-performance computing and data-acquisition (particularly the new 'big' data from different sources) technologies have offered an exceptional and timely opportunity to revolutionize the required flood simulation and forecasting technologies to the next step. As a core component of a flood forecasting system, flood inundation models have undergone a long way of development in the last two decades. A number of hydrological and hydraulic models have been developed and widely applied for assessing urban flood inundations, for example the SWMM model (Gironás et al., 2010) and Infoworks CS model (e.g., Koudelak and West, 2007). For urban flood modelling, application of high-resolution models is essential in order to capture the complex topographic features in the urban environment, which will inevitably lead to unrealistic long simulation times using the traditional desktop PC stations based on central processing units (CPUs). The computational practice has welcomed a step-change, with heterogeneous processors featured with general-purpose graphics processing units (GPUs) and network-based cloud computing that recently became available for scientific computation. High-performance flood modelling tools based on these new computing technologies (e.g. Glenis et al., 2013; Liang and Smith, 2015) have proved to be particularly effective in permitting hydrodynamic flood simulations over a large domain at ground-breaking resolutions.

Concerning the access to high-resolution data to support different aspects of urban flooding modelling, in addition to the high-resolution data and imageries obtained by the more traditional remote sensing and earth observation technologies to describe earth surface including snapshots of natural events, the wide availability of different types of sensors and data harvested from social networks has simultaneously produced vast quantities of real-time data that are available for monitoring different aspects of the natural and built environments and activities therein. In many cases, certain crowd-sourced data, e.g. the data from social networks, may update faster than the data from traditional media, providing ‘near’ real-time information about the hazardous events and their impacts (Guan and Chen, 2014). Crowd-sourcing is therefore being more and more recognised as a valuable means to acquire information for flood management and response. With an effective tool to collect, process and disseminate them, these data from different online social networks can potentially provide a vast amount of real-time information describing the development and impact of a natural hazardous event (Smith et al., 2015), which may be directly used to assess flood risk, support flood modelling and create useful information for (near) real-time flood forecasting.

Taking advantages of the aforementioned latest technological developments, this paper initiates the effort to develop and test a real-time urban flood forecasting system supported by open-source data, including GDEM (i.e. Global Digital Elevation Model), land use information, rainfall forecasts or real-time records, satellite images, and crowd-sourced photos, video clips and messages.

## 2 REAL-TIME FLOOD FORECASTING SYSTEM SUPPORTED BY OPEN-SOURCED DATA

The presented flood forecasting system consists of a simulation engine that predicts flood inundation in complex urban environments with real-time rainfall inputs, a model pre-processing environment that collates data and process data for setting up the flood model, and a visualisation component that post-processes and visualises, in real time, the simulation results on street maps (e.g. Google maps or Google Earth). If necessary, the flood maps may be also incorporated with near real-time crowd-sourced data streams to provide extra information for flood forecasting. The crowd-sourced ‘observations’ may be also used to verify simulation results.

### 2.1 Flood simulation Engine

The urban flood modelling engine for the proposed flood forecasting system is based on numerical solution to the 2D shallow water equations (SWEs), which is given in the matrix form as follows

$$\frac{\partial \mathbf{q}}{\partial t} + \frac{\partial \mathbf{f}}{\partial x} + \frac{\partial \mathbf{g}}{\partial y} = \mathbf{R} + \mathbf{S}_b + \mathbf{S}_f \quad [1]$$

where  $t$  is time,  $x$  and  $y$  are the Cartesian coordinates,  $\mathbf{q}$  is the vector containing the conserved flow variables,  $\mathbf{f}$  and  $\mathbf{g}$  are the flux vector terms in the two Cartesian directions,  $\mathbf{R}$ ,  $\mathbf{S}_b$  and  $\mathbf{S}_f$  are the source terms representing the effects of rainfall, bed slope and friction. The vector terms are respectively given by

$$\mathbf{q} = [h, uh, vh]^T, \mathbf{f} = \left[ uh, u^2h + \frac{1}{2}gh^2, uvh \right]^T, \mathbf{g} = \left[ vh, uvh, v^2h + \frac{1}{2}gh^2 \right]^T, \quad [2]$$

$$\mathbf{R} = [R, 0, 0]^T, \mathbf{S}_b = \left[ 0, -gh \frac{\partial b}{\partial x}, -gh \frac{\partial b}{\partial y} \right]^T, \mathbf{S}_f = \left[ 0, -\frac{\tau_{bx}}{\rho}, -\frac{\tau_{by}}{\rho} \right]^T$$

where  $u$  and  $v$  are the two depth-averaged velocity components,  $h = \eta - b$  is the total water depth,  $\eta$  and  $b$  respectively represent the water surface elevation and bed elevation above datum,  $g$  is the acceleration due to gravity,  $\mathbf{R}$  is the rainfall rate,  $\rho$  is the water density, and  $\tau_{bx}$  and  $\tau_{by}$  are the friction stresses which may be estimated using the Manning equation

$$\tau_{bx} = \rho C_f u \sqrt{u^2 + v^2}, \tau_{by} = \rho C_f v \sqrt{u^2 + v^2} \quad [3]$$

where  $C_f$  is the roughness coefficient. Denoting  $n$  as the Manning coefficient,  $C_f = gn^2/h^{1/3}$ .

In this work, the above SWEs were numerically solved using a uniform grid based first-order finite volume Godunov-type scheme incorporated with an HLLC (Harten–Lax–van Leer contact wave) approximate Riemann solver. Particularly designed for an efficient and accurate modelling rainfall-induced overland flows and the resulting flooding, the numerical scheme is featured with a new well-balanced surface reconstruction method (SRM) for correct calculation of bed slopes and a more stable fully implicit discretisation approach for friction source terms (Xia et al., 2017; Liang et al., 2017). The resulting flood inundation model was implemented for GPU parallel computation using the CUDA programming framework. On a single GPU, the

model may be computationally up to 70 times more efficient than its counterpart running on a traditional single CPU core (Smith, 2013), providing a viable tool for real-time urban flood modelling at high resolutions.

## 2.2 Data collecting and pre-processing

In order to develop an effective platform for (near) real-time flood forecasting, essential data are needed, which include rainfall observations/predictions, DEMs and other geographic information. Nowadays, certain common internet platforms, such as Geographic Information Resources Service (<http://www.webmap.cn/>) and Geospatial Data Cloud (<http://www.gscloud.cn/>) in China, can provide resources of geographic information, including the DEMs to represent the topography of the simulation areas and land use data detailing land use types (e.g. road, building, grassland, river system, etc.). SRTM (i.e., Shuttle Radar Topography Mission) and ASTER GDEM (i.e., Advanced Spaceborne Thermal Emission and Reflection Radiometer Global Digital Elevation Model) are also freely available at the 30-meter resolution. Real-time meteorological and hydrological data, e.g., rainfall, river flows and tidal levels, may be available for downloading from governmental information platform (e.g., <http://xxfb.hydroinfo.gov.cn/>). Although the quality of these open-source datasets varies, it may still be used to drive flood forecasting models and provide useful information for the public to react to the events. This will be explored in the current work.

After the geospatial data (i.e., DEMs, land use data) and meteorological and hydrological data (e.g., rainfall and river flows) are collated, they need to be pre-processed for model set up. A model pre-processing environment consisting of a number of scripts was developed for this purpose. Taking the rainfall data as an example, a Python-based middleware was developed to construct Thiessen polygons and convert the point coordinates of rainfall stations to cover the whole simulation area. The middleware also automatically convert the format of the continuously received rainfall data to drive the flood model.

Recently, crowd-sourcing has become a popular and effective means to harvest useful information for hazard management (e.g., Guan and Chen, 2014; Allaire, 2016). Equipped with the increasingly available powerful mobile devices, citizens have become the reporters via micro-blogging sites. Recognising the potential of social media for effective flood preparation (Allaire, 2016), more and more researchers and government organisations proposed and reported effective methodologies and tools to collect and filter geo-referenced posts (e.g. texts, photos and videos) from social media to understand, forecast and prepare for natural hazard events (Smith et al., 2015; Fohringer et al., 2015; Coz et al., 2016). In China, instead of Twitter, people resort to local social media, e.g. Weibo and Weixin, to share photos, videos and messages with the public. Weibo is equipped with quick and easy searching engine systems to enable data/information collection for a specific event, e.g. flooding. In this work, we use the imbedded social media searching engine systems to search and receive messages (filtered through keywords) for specific flood events. The received information will then be sorted according to time and spatial locations. While analysing and visualising them in real-time together with the model outputs, these crowd-sourced data may provide useful information for understanding and predicting the hazardous event, and validating modelling tools.

## 2.3 Real-time visualisation

In order to provide useful information to the public to enhance flood preparedness, it is important to carefully design the means to effectively visualise and disseminate the model results and collected crowd-sourced data so that they can be well received and understood by the general public (Connors et al., 2012). Recently, a number of attempts have been reported to use open-source platforms mostly through applications of volunteered geographical information, such as Crowdmap/Ushahidi platform (Hirata et al., 2015) and OpenStreetMap (Mooney and Corcoran, 2014), to visualise and share crowd-sourced flood data and reports.

In this work, the real-time flood model results were outputted as raster files, which may be visualised as flood maps on any GIS (Geographic Information System) software. To facilitate quick and easy-to-understand visualisation of model results, a Python-based middleware was developed to convert the raster files into KML (Keyhole Markup Language) files for direct display on Google Earth, Maps and Mobile Apps, or any other geospatial software implementing with KML encoding. This effectively provides an automatic and dynamic visualisation system that updates the flood simulation results on Google Earth or Maps in real-time. To provide further information, the geo-referenced crowd-sourced photos and text descriptions as received may be also marked and visualised on the Maps at the same time.

## 3 APPLICATION TO TYPHOON MERANTI INDUCED URBAN FLOOD EVENT IN FUZHOU

As the capital city, Fuzhou is the political, financial, cultural and transportation centre of Fujian Province in China. Fuzhou is also a coastal city located in the Min River estuary, surrounded by mountains on three sides and opened to the sea at the east. The city also has the well-developed river systems in the downtown. Due to its special geographic features, Fuzhou has been frequently threatened by multi-source flood hazards originated from both the mountainous catchments and the coast. Following more frequent weather extremes (e.g. typhoons) and more intensive urbanisation that has substantially increased the pressure on the existing drainage systems, Fuzhou has experienced more frequent and severe urban flood events in the recent years.

In mid-September 2016, Typhoon Meranti landed in Fujian Province and brought in record-breaking rainfall that caused severe flooding in Xiamen, Fuzhou and the surrounding cities and towns. While Fujian was still in the aftermath of Typhoon Meranti, another super typhoon (Typhoon Megi) formed and devastated the province again on 27th September. The successive Typhoon events have resulted in tremendous economic loss. According to the government statistics, Typhoon Meranti and the subsequent floods have caused RMB 16.9 billion of economic loss and affected over 1.8 million people in Fujian Province alone. Figure 1 shows the hourly rainfall collected at one of gauge stations in Fuzhou. From 02:00 to 04:00 on 15th September, the hourly peak reached 70.1mm and the three-hour accumulation rainfall was recorded as 170.3mm. The intense rainfall produced runoff well exceeded the capacity of the city drainage systems and subsequently led to severe urban flooding, as shown in Figure 2.

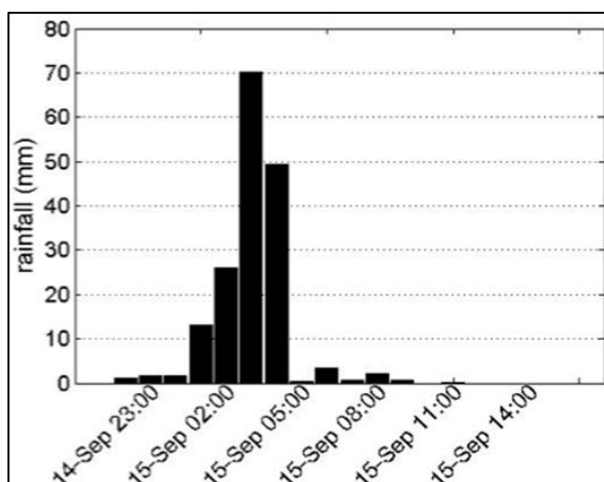


Figure 1. Time series of hourly rainfall for the Fuzhou gauge station.



Figure 2. Photos showing the Typhoon Meranti induced urban flooding in Fuzhou (the names of the blogger are marked on the photos).

### 3.1 Data and model set up

The city of Fuzhou is separated into two parts by the Min River and the old town in the Northern bank of the river usually suffers more during a flood event due to the dense population and urban buildings as well as deteriorated drainage systems. The proposed flood forecasting system was set up and tested for the northern part of the city, which covers 267km<sup>2</sup> of area including the surrounding mountains. The computational domain reproduced from a 30m open-source DEM is illustrated in Figure 3. The land use data (including roads, buildings, grasslands, river systems, etc.) are used to help specify relevant model parameters, e.g. coefficients for the Green Ampt infiltration model component, Manning coefficient and spatially varying drainage capacity coefficient. Rainfall records, river flows and tidal levels were downloaded from the government's open information platforms, which were then used to specify the model boundary conditions and drive the inundation modelling. Photos and text descriptions were retrieved from social media as extra sources of information about inundation depth and extent.

Although the rainfall peak only lasted for three hours (as shown in Figure1), the simulation was run for 18 hours from 21:00 on 14th to 15:00 on 15th September to consider the entire process of the event. Following the warning Typhoon Meranti issued by the local meteorological departments on 13th September, active discussion about the event has started and propagated through the social media. Then, in the early morning of 15th, with the emerging floods across the city, photos and text messages about the event has started to exponentially grow and flood different social media. This has provided huge amount of photos, videos and text

messages that describes the event to be collected. In addition to provide data (spatially varying water depth and flood extent) for model validation, the crowd-sourced information, on its own, can be used to understand the evolution of the event and the behaviour of people. In the present flood forecasting framework, the photos from the social media and the public collected and visualised are part of the forecasts in the envelope.

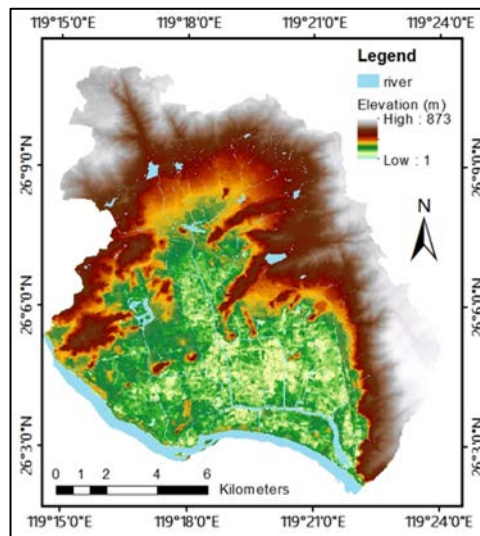


**Figure 3.** The simulated area reproduced from the 30m DEM

### 3.2 Results and discussion

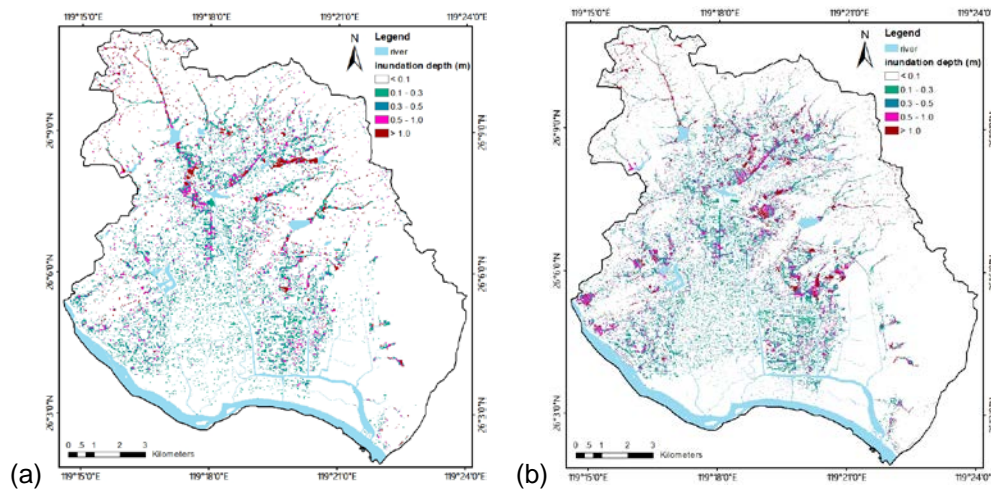
The flood forecasting system was tested on the 30m open-source DEM, as shown in Figure 3. In order to compare and verify the model results, simulation was also carried on a 10m DEM, which should better represent the complex topographic features in the urban areas and theoretically produce more reliable predictions. Figures 4 and 5 show the maximum flood inundation maps predicted respectively on the DEMs of 30m and 10m resolutions. The maps only plot those areas with a flood depth greater than 0.1m. Inundation depth of less than 0.1m is considered to have no obvious effect on pedestrians according to the urban flood classification for Chinese cities (Jian et al., 2007). From the overall flood maps for the whole computational domain and the zoom-in maps concentrated on the city centre, it can be seen that certain level of discrepancy exists on the flood maps and the higher resolution simulation appears to predict more flooded areas, particularly in the surrounding mountain areas. The reason may be due to the less accurate representation of smaller river courses by the coarse resolution DEM. Some rivers/channels/spillways inside the computational domain are very narrow, especially spillways. Most of the spillways are less than 30m wide, some are even less than 7m wide (e.g. the spillway in the Dengyun Reservoir). These spillways convey substantial amount of discharge from the reservoirs during a flood event, which provides an important source contributing to the downstream inundation. Using a 30m DEM, most of the spillways will not be represented and therefore different inundation extent would be expected for certain downstream areas.

Figure 5 presents a zoom-in maximum flood map focusing on the central business district (CBD) of Fuzhou. This is a low-lying area that has frequently suffered from severe urban flooding. A key reason is that this region is close to the Jinan River that drains a large catchment in the northern mountainous areas. Jinan River has been intensively engineered and become disconnected from its originally floodplains, leading to substantially reduced flood storage capacity upstream. Overbank flow and flooding to the primary roads and surrounding developed areas most likely happen every time when there is an intense rainfall event. Following the intense rainfall brought in by the Super Typhoon Longwang in 2005, the inundation depth of this area was up to 1.9m. Later in 2006, the flood depth caused by Typhoon Bilis was measured to be up to 1m. Most recently in 2016, several typhoon events, including Typhoon Meranti as considered herein, affected Fuzhou and the average inundation depth in this area has been reported to be approximately 0.5-1.0m. Due to the less accurate representation of the urban topographic features and the course of Jinan River using the 30m DEM, the corresponding flood map presents certain level of difference from the 10m prediction, particularly in those small-scale structures. But from a macro-scale, the inundation maps predicted by the two DEMs appear to be consistent, which indicates that the prediction produced on the open-source 30m DEM may identify the key flooded areas for Fuzhou.

Figure 6 shows the time sequence of flood maps of the central business district reproduced by the two simulations, in comparison with the photos taken at the same area. From the rainfall record as shown in Figure 1, heavy rainfall started from 02:00 on 15th September. Subsequently, obvious inundation starts one hour later at 03:00. As presented in Figure 8, flood extent and depth increased gradually from 03:00 to 09:00,

which was also captured by the photos. The key flooded areas were captured by both of the simulations, confirming the reliability of the coarse 30m simulation in capturing the key flood extent and dynamics.

Point-based inundation depths extracted from the images and text messages collected from social media were used to further verify the prediction obtained from the 30m simulation. Ten of these points where obvious inundation occurred were selected as examples and their locations are shown in Figure 7. Due to the highly uncertain nature of the crowd-sourced information, the exact locations of the water depths as extracted may not be easily identified. For example, the exact location of the reference point in the photo where water depth is estimated may be different from the geo-referenced location of the photo. Therefore, when comparing the simulated water depth with these 'observations', a circular buffer area of 120m diameter centred at considered 'observation' point is used, i.e. the predicted water depth in the cells within this buffer area is considered and compared with the 'observed' depth using different statistical approaches. Table 1 compares the maximum water depths inside the buffer areas with the 'observations' in the ten points as selected. Considering the high uncertainty associated with the crowd-sourced 'observed' data, the comparison may be considered as satisfactory and the model correctly predicts those areas being flooded during the event.



**Figure 4.** Maximum flood inundation maps produced on: (a) 30m resolution DEM; (b) 10m resolution DEM.

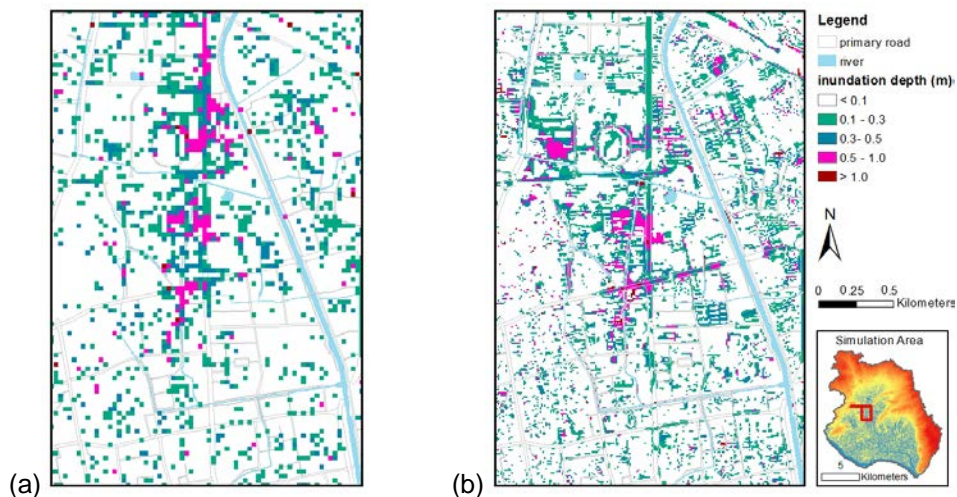


**Figure 5.** Maximum flood inundation maps focused on the central business district of the city: (a) 30m resolution DEM; (b) 10m resolution DEM.

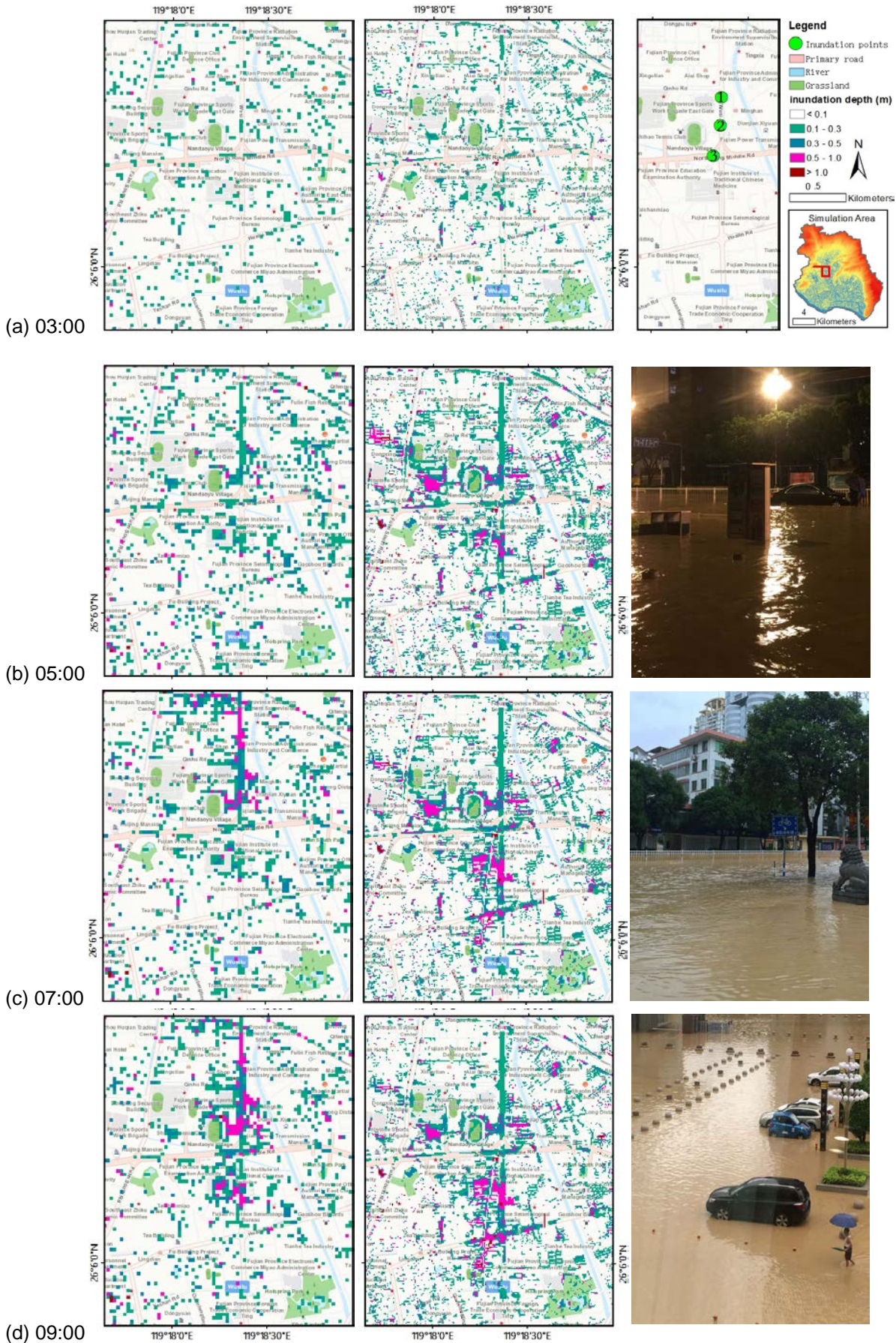


**Figure 6.** Time sequence of the flood maps of the central business district in Fuzhou on 15th September. Column 1: predicted at 30m resolution; Column 2: predicted at 10m resolution; Column 3: photos from online social networks showing part of the flooded area (Photo source: MoJi—a weather APP in China).

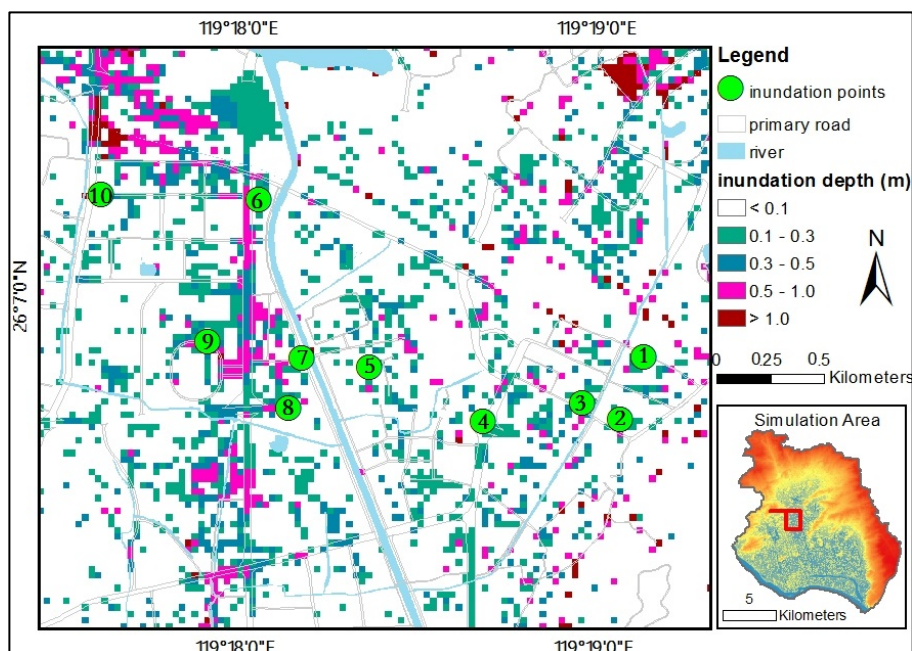


**Figure 7.** Locations of the selected sample inundation points used to verify the simulation results.

**Table 1.** Comparing simulated maximum depth and crowd-sourced ‘observed’ depth at ten sample points.

Points	Simulation maximum depth (m)	Actual data (m)
1	0.52	0.30
2	0.35	0.30
3	0.53	0.30
4	0.17	0.30
5	0.19	0.30
6	0.77	0.30
7	0.53	0.30
8	0.32	0.30
9	0.64	0.30
10	0.46	0.30

The images and videos collected from social media may provide additional sources of information for mitigating flood risk and facilitating decision-making. When they are properly visualised, it will also provide an effective way to communicate flood risk with the public. When presenting our forecasted flood maps on web, the locations where these images and videos are available are also automatically marked on the map. The users can click on a marker and view directly the image or video taken at the marked location to have a better understanding of what happens at the scene. Figure 8 presents part of a predicted flood map with the crowd-sourced photos being incorporated. Furthermore, by referencing to certain objects in the photos (e.g. rails, vehicle wheels and pedestrians), we can quickly estimate the water depth at the scene and verify the simulation results. For example, the last photo in Figure 8 shows that the water depth is close to the thigh of an adult, which is about 0.8m.

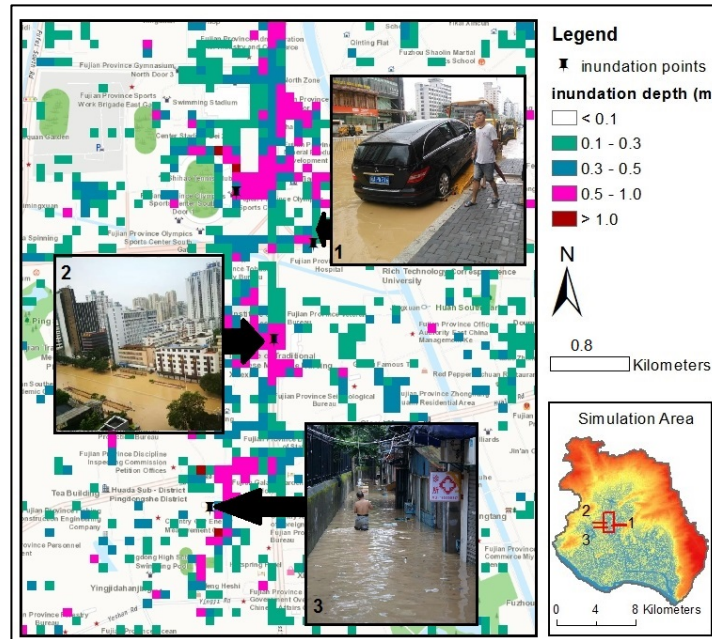


**Figure 8.** Simulated flood map incorporated with photos collected from online social media (Photo sources: Photos 1&3 from <http://www.fjsen.com/>, Photo 2 from <http://www.chinanews.com/>).

The model may also present the time histories of selected flow variables, e.g. water depth and velocities, at selected locations. Figure 9 shows the time histories of water depth at the three locations as marked in Figure 8. The time histories provide detailed flood information and clearly depict the evolution of the flood event, e.g. how the inundation depth increases and decreases during the event, at certain locations. For the flood risk managers, they may use the information to identify hotspots for special measures. For the general public, they may want to know the detailed flood information near to their homes, working places or other locations of interests.

To support real-time flood forecasting, the computational efficiency of the flood simulation tool is one of the most important factors to be considered. Being implemented for parallel computing on GPUs, the flood simulation engine presented in this work is computationally highly efficient and can be used to perform real-time high-resolution flood simulations over a city scale involving millions of the computational nodes. The simulations presented in this work were run on a NVIDIA Tesla K80 GPU. The respective runtimes for the two simulations are presented in Table 2. Both simulations can be completed much faster than real-time. At 30m resolution, on average every one hour of the actual event can be predicted/reproduced in 6 seconds. At 10m resolution, the simulation can predict one hour of the actual event in 5 minutes.

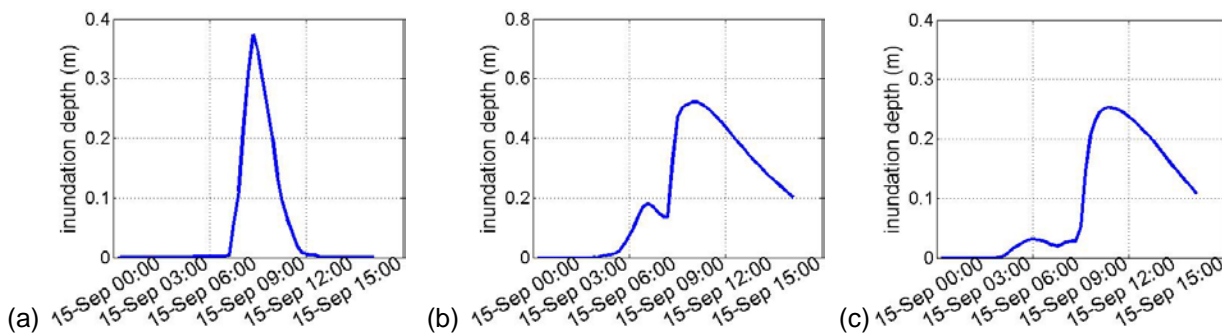


**Figure 9.** Time histories of water depth for the three points as marked in Fig. 8.

**Table 2.** The runtimes of the simulations at different spatial resolutions (hh : mm : ss)

Resolution	Area (Km <sup>2</sup> )	Cells	Runtime on Tesla K80	Duration of event
30m	267	297,632	00:01:54	19:00:00
10m	267	2,676,984	01:30:00	19:00:00

#### 4 CONCLUSIONS

In this work, we presented an integrated flood forecasting system including pre-processing, inundation modelling and post-processing components. The forecasting system may be driven by data from different sources and may potentially use open-sourced data (including those from crowd-sourcing) to provide flood forecasts for the general public. As the core component of the forecasting system, the flood modelling engine is based on a GPU-accelerated high-performance hydrodynamic model solving the fully two-dimensional shallow water equations using a finite volume Godunov-type scheme. Therefore, the resulting forecasting system may be used to provide real-time forecasts for highly dynamic flash floods induced by intense rainfall in the complex urban environments. The presented flood forecasting system was tested in Fuzhou, China to reproduce 'in real time', the severe urban flood event caused by Typhoon Meranti, demonstrating its potential for wider applications.

#### ACKNOWLEDGEMENTS

This work was partly funded by the UK NERC SINATRA and TENDERLY projects (Grant No. NE/K008781/1), the National Natural Science Foundation of China (NSFC) standard research award (Ref. 51379074).

#### REFERENCES

- Allaire, M.C. (2016). Disaster Loss and Social Media: Can Online Information Increase Flood Resilience?. *Water Resources Research*, 52(9), 7408–7423.
- Connors, J.P. & Kelly, S.L.M. (2012). Citizen Science in the Age of Neogeography: Utilizing Volunteered Geographic Information for Environmental Monitoring. *Annals of the Association of American Geographers*, 102(6), 1267-1289.
- Coz, J.L., Patalano, A., et al. (2016). Crowd-Sourced Data for Flood Hydrology: Feedback from Recent Citizen Science Projects in Argentina, France and New Zealand. *Journal of Hydrology*, 541, 766-777.
- Fohringer, J., Dransch, D., Kreibich, H. & Schröter, K. (2015). Social Media as an Information Source for Rapid Flood Inundation Mapping. *Natural Hazards & Earth System Sciences*, 15(12), 2725-2738.
- Gironás, J., Roesner, L.A., Rossman, L.A. & Davis, J. (2010). A New Applications Manual for the Storm Water Management Model (SWMM). *Environmental Modelling & Software*, 25(6), 813-814.
- Glenis, V., McGough, A.S., Kutija, V., Kilsby, C. & Woodman, S. (2013). Flood Modelling for Cities Using Cloud Computing. *Journal of Cloud Computing: Advances, Systems and Applications*, 2(1), 7.
- Guan, X., & Chen, C. (2014). Using Social Media Data to Understand and Assess Disasters. *Natural Hazards*, 74(2), 837-850.
- Hirata, E., Giannotti, M.A., Larocca, A.P.C. & Quintanilha, J.A. (2015). Flooding and Inundation Collaborative Mapping – Use of the Crowdmapp/Ushahidi Platform in the City of Sao Paulo, Brazil. *Journal of Flood Risk Management*.
- IPCC (2014). *Climate Change 2014: Impacts, Adaptation, and Vulnerability*. Cambridge University Press.
- Jian, L.I., Yin, J.M., et al. (2007). Numerical Simulation of Storm Sewer Discharge in Nanchang Urban Region. *Journal of Nanjing Institute of Meteorology*, 30(4), 450-456.
- Koudelak, P. & West, S. (2007). Sewerage Network Modelling in Latvia, Use of Infoworks CS and Storm Water Management Model 5 in Liepaja City. *Water & Environment Journal*, 22(2), 81-87.
- Liang, Q., & Smith, L.S. (2015). A High-Performance Integrated Hydrodynamic Modelling System for Urban Flood Simulations. *Journal of Hydroinformatics*, 17(4), 518-533.
- Liang, Q., Smith, L.S. & Xia, X. (2017). New Prospects for Computational Hydraulics by Leveraging High-Performance Heterogeneous Computing Techniques. *Journal of Hydrodynamics*, 28(6), 977-985.
- Mooney, P. & Corcoran, P. (2014). Has Openstreetmap a Role in Digital Earth Applications?. *International Journal of Digital Earth*, 7(7), 534-553.
- Smith, L.S. & Liang, Q. (2013). Towards a Generalised GPU/CPU Shallow-Flow Modelling Tool. *Computers & Fluids*, 88(12), 334-343.
- Smith, L.S., Liang, Q. & Quinn, P.F. (2015). Towards a Hydrodynamic Modelling Framework Appropriate for Applications in Urban Flood Assessment and Mitigation Using Heterogeneous Computing. *Urban Water Journal*, 12(1), 67-78.
- Smith, L., Liang, Q., James, P. & Lin, W. (2015). Assessing the utility of social media as a data source for flood risk management using a real-time modelling framework. *Journal of Flood Risk Management*.
- Xia, X., Liang, Q., Ming, X. & Hou, J. (2016). An efficient and stable hydrodynamic model with novel source term discretisation schemes for overland flow and flood simulations. *Water Resources Research*, 53.

## INFLUENCE OF URBAN PATTERNS ON FLOODING

MARTIN BRUWIER<sup>(1)</sup>, AHMED MUSTAFA<sup>(2,)</sup>, DANIEL G. ALIAGA<sup>(3)</sup>, SÉBASTIEN ERPICUM<sup>(4)</sup>, PIERRE ARCHAMBEAU<sup>(5)</sup>, GEN NISHIDA<sup>(6)</sup>, XIAO WEI ZHANG<sup>(7)</sup>, MICHEL PIROTTON<sup>(8)</sup>, JACQUES TELLER<sup>(9)</sup> & BENJAMIN DEWALS<sup>(10)</sup>

<sup>(1,4,5,8,10)</sup>Hydraulics in Environmental and Civil Engineering (HECE), University of Liege (ULG), Belgium  
martinbruwier@ulg.ac.be

<sup>(2,9)</sup>Local Environment Management and Analysis (LEMA), University of Liege (ULG), Belgium  
<sup>(2,3,6,7)</sup>Computer Science Department, Purdue University, USA

### ABSTRACT

The goal of this paper is to identify the respective influence of different characteristics of urban patterns on urban flooding. A set of 2,290 alternate urban patterns is generated randomly using an urban generator tool providing the geometry of buildings and their relative location to the ground, over a square area of 1 km<sup>2</sup>. Steady 2-D hydraulic computations are performed for these 2,290 different urban patterns with identical hydraulic boundary conditions. The computational time is reduced by using an anisotropic porosity model. This model uses relatively coarse computational cells; but preserves information from the detailed topographic data through the use of porosity parameters. Based on the computed maps of water depths for the 2,290 urban patterns, a sensitivity analysis based on a multiple linear regression is performed to outline the most influential urban characteristics.

**Keywords:** Urbanization; porosity model; urban inundation modeling; urban planning.

### 1 INTRODUCTION

The geometric characteristics of urban patterns (e.g. street width, orientation or curvature) have a strong influence on flow properties during urban flooding. They influence the discharge partition between the streets as well as the flow depths and velocities, both within the considered urban area as well as upstream and downstream. In this paper, a systematic analysis is performed to determine the influence of various characteristic of urban patterns on urban flooding.

The study considers 10 parameters controlling the urban pattern: average street length, street orientation, street curvature, major and secondary street widths, parks coverage, maximum parcel area and three different building's setbacks. By varying the values of the different urban parameters, a set of 2,290 synthetic urban networks are generated.

The high number of urban networks generated by the urban generator tool makes the computation challenging using classical hydraulic models. Subgrid models enable improvements of the computational efficiency by enabling a coarsening of the computational grid, while preserving the essence of the detailed topographic information available at a fine scale. Anisotropic porosity models are one kind of subgrid models for which fine scale information are maintained at the coarse scale by including porosity parameters in the governing equations (Sanders et al., 2008). Storage porosities reproduce the available storage volume within the cells and conveyance porosities consider the effects of buildings on the fluxes evaluated along the edges. An additional drag loss term is used to consider the resistance of obstacles to the flow. This allows an increase of the grid spacing by roughly one order of magnitude, while preserving a similar level of accuracy as with a fine mesh (Schubert and Sanders, 2012; Kim et al., 2014; Kim et al., 2015).

In this paper, the relationship between characteristics of urban patterns and flooding is explored through a multiple linear regression. The results of the sensitivity analysis are exemplified by comparing the inundation water depths resulting from different combinations of urban characteristics.

The findings of this study contribute to a better understanding of the interactions between complex urban systems and flooding to guide more flood-proof urban developments.

### 2 METHOD

This study followed the methodology presented in Figure 1 for which three different tools had been developed:

- An urban generator tool generated 2,290 synthetic urban networks over a 1 km<sup>2</sup> area through the selection of the values of 10 parameters controlling the building geometries and locations (section 2.1).
- A porosity-based hydraulic model computed the flow characteristics for the 2,290 urban networks with identical hydraulic boundary conditions (section 2.2). Indicators of the flooding intensity were determined from the computed maps of water depths.

- A sensitivity analysis based on a multiple linear regression was performed to highlight the specific influence of the different urban characteristics on the inundation indicators (section 2.3.2).

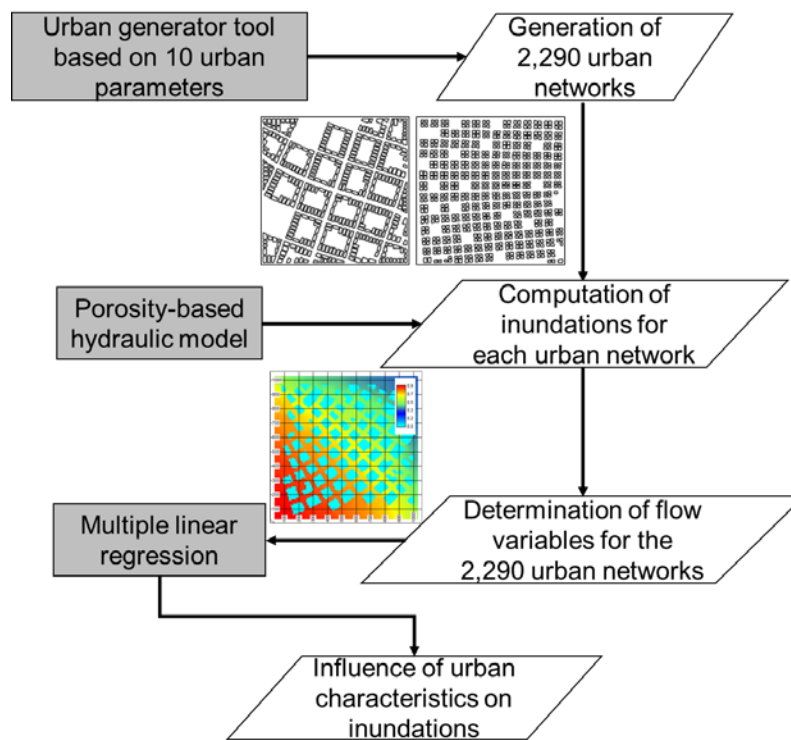


**Figure 1.** Methodology for the determination of the influence of urban patterns on urban flooding.

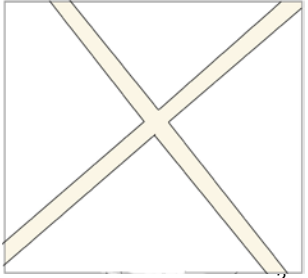
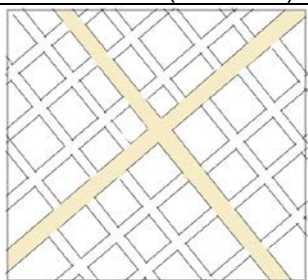
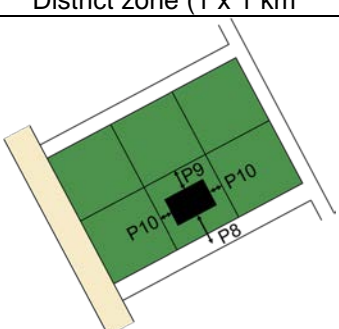
### 2.1 Urban generator tool

The urban generator tool is based on a procedural modeling (Parish and Müller, 2001) which automatically generates urban networks given a set of rules and parameter values (Prusinkiewicz and Lindenmayer, 1990). The outputs of the urban generator consist of locations and shapes of streets and buildings. While this approach was originally proposed by Parish and Müller (2001), the tensor field using the approach of Chen et al. (2008) was adapted in this study for street generation, as it supports more variations in the street networks. The urban generator is based on 10 input parameters (Table 1) and follows the five-step process sketched in Figure 2.

The 2,290 urban networks were generated based on input parameters selected randomly in the range between the minimum and maximum values reported in Table 1. Once the input parameters are fixed, the urban generator produces a single urban network without including any random seeds. The ranges of variation of the input parameters are representative of real-world information obtained from cadastral data for a building area of about 500 km<sup>2</sup> in Wallonia (Belgium).

**Table 1.** Input parameters and building coverage for the urban generator engine.

ID	Parameter	Minimum value ( $P_{min}$ )	Maximum value ( $P_{max}$ )
P1	Average street length	40 m	400 m
P2	Street orientation	0°	180°
P3	Street curvature	0 rad.	0.42 rad.
P4	Major street width	16 m	33 m
P5	Minor street width	8 m	16 m
P6	Park coverage	5%	40%
P7	Maximum parcel area	300 m <sup>2</sup>	1,100 m <sup>2</sup>
P8	Building front setback	0 m	5 m
P9	Building rear setback	0 m	5 m
P10	Building side setback	0 m	5 m
BC	Building coverage	0%	42.8%

Step	Description	Input parameters	Illustration
1	Definition of grid points with a spatial resolution of 1 m		
2	Definition of the shape of two orthogonal major streets	P1 to P4	 District zone (1 x 1 km <sup>2</sup> )
3	Tracing of the local streets based on the tensor field	P1 and P5	 District zone (1 x 1 km <sup>2</sup> )
4	Definition of parks and parcels	P6 and P7	 District zone (1 x 1 km <sup>2</sup> )
5	Construction of buildings in the parcels	P8 to P10	 Parcel zone

**Figure 2.** Flow chart of the urban generator tool.

## 2.2 Flow computations

### 2.2.1 Hydraulic conditions

The 2,290 urban networks were placed over a slopeless urban zone of 1 x 1 km<sup>2</sup>, where buildings were considered sufficiently high for not being overtopped by the flooding. The left and bottom sides of the urban zones were the upstream sides, while the right and top sides were the downstream ones. At the upstream sides, a steady discharge of 200 m<sup>3</sup>/s and uniformly distributed was prescribed as a boundary condition. At the downstream sides, free flow conditions were assumed. The Manning roughness coefficient of the bottom was  $n = 0.04 \text{ sm}^{-1/3}$  over the entire domain. Flow characteristics were computed on a Cartesian grid of 10 m x 10 m.

### 2.2.2 Anisotropic porosity model

Hydraulic computations were performed with the hydraulic model WOLF 2-D, which has been extensively used for studies of inundations in urban areas (Ernst et al., 2010; Beckers et al., 2013; Bruwier et al., 2015; Detrembleur et al., 2015). WOLF 2-D solves the fully two-dimensional shallow-water equations on Cartesian grids based on a conservative finite volume scheme with a flux vector splitting technique (Epicum et al., 2010). An anisotropic porosity model has been included in the existing WOLF 2-D which has been validated over multiple test cases (e.g. Arrault et al., 2016).

The integral form of the governing equations of anisotropic porosity models (Sanders et al., 2008) is discretized with a finite volume scheme for a cell  $j$  and its  $K$  edges  $k$  as in Eq. [1].

$$\frac{\partial \langle \mathbf{U} \rangle_j}{\partial t} + \frac{1}{\Omega_j} \sum_{k=1}^K [\mathbf{F}]_k \partial \Omega_k = \langle \mathbf{S} \rangle_j \quad [1]$$

where,

$$\langle \mathbf{U} \rangle = \phi \begin{bmatrix} \langle h \rangle \\ \langle uh \rangle \\ \langle vh \rangle \end{bmatrix},$$

$$[\mathbf{F}] = \psi \begin{bmatrix} [uh] & [vh] \\ [u^2h] + \frac{g}{2}([h]^2 - h_{\eta_0,x}^2) & [uvh] \\ [uvh] & [v^2h] + \frac{g}{2}([h]^2 - h_{\eta_0,y}^2) \end{bmatrix}, \quad [2]$$

$$\langle \mathbf{S} \rangle = -\phi \begin{bmatrix} 0 \\ (c_D^f + c_{D,x}^b) \langle uV \rangle \\ (c_D^f + c_{D,y}^b) \langle vV \rangle \end{bmatrix}.$$

where  $t$  is the time,  $\Omega$  the total area of the cell,  $\partial \Omega$  the total length of the edge,  $h$  the water depth,  $u$  and  $v$  the  $x$ - and  $y$ - velocity components,  $V = \sqrt{u^2 + v^2}$ ,  $g$  the gravitational acceleration,  $c_D^f$  the roughness coefficient and  $c_D^b$  the drag coefficient estimated consistently with the simplified method proposed by Schubert et al. (2012). The term  $h_{\eta_0}^2$  corresponds to the water depth computed for a piecewise stationary water level  $\eta_0$ . The notations  $\langle \rangle_j$  and  $[ ]_k$  refer respectively to flow variables at the cells and for their reconstruction to the edges.

The divergence formulation of the bed slope (Valiani and Begnudelli, 2006) term is used in Eq. [2] in which the stationary water level  $\eta_0$  of a cell is determined as a linear combination of the water levels at its edges minimizing the error in the energy balance (Bruwier et al., 2016).

The storage porosity  $\phi_j$  and the conveyance porosity  $\psi_k$  are respectively defined by Eq. [3] and [4]:

$$\phi_j = \frac{\Omega_{f,j}}{\Omega_j}, \quad [3]$$

$$\psi_k = \frac{\partial \Omega_{f,k}}{\partial \Omega_k}. \quad [4]$$

where  $\Omega_{f,j}$  and  $\partial \Omega_{f,k}$  represent respectively the cell area and the edge length, available for water.

The stability condition of the scheme is given in Eq. [5] considering the porosity parameters (Sanders et al., 2008). The criterion writes, with  $c = V + \sqrt{gh}$  the wave celerity:

$$\Delta t \leq CFL \min \left( \frac{1}{c} \frac{\phi \Omega}{\max(\psi \partial \Omega)} \right), \quad [5]$$

Since low storage porosities can reduce dramatically the computational time, cells with a storage porosity lower than a threshold  $\phi_{\min}$  are removed from the computation domain.

Based on a comparison between results computed at the coarse scale with the anisotropic porosity model using a drag coefficient of  $c_D^b = 3$  and a threshold porosity  $\phi_{\min} = 0.1$  and results computed at the fine scale, for three arbitrary urban networks, average errors on water depths at the upstream sides are estimated around few millimeters ( $<1$  cm).

### 2.3 Determination of the influence of urban characteristics on inundation characteristics

In this paper, the intensity of a flooding was assessed through inundation indicators computed as quantiles of computed water depths  $h_{Q\%}$  either over the whole inundated area or along the upstream sides of the domain. The influence of 11 characteristics of urban patterns was evaluated on these inundation indicators: the 10 urban parameters (P1 to P10) used as inputs for the urban generator tool and the building coverage (BC) representing the part of building areas over the total urban zone.

Using  $x_i$  with  $i = 1, \dots, 11$  and  $y$  to represent respectively the 11 urban characteristics and the inundation indicator, two non-dimensional forms of the variables  $x_i$  and  $y$  are defined: a normalized form and a standardized form.

The normalization forms of the variables  $\bar{x}_i$  and  $\hat{y}$  are computed with Eq. (6) based on the minimum ( $x_{\min}$  and  $y_{\min}$ ) and maximum ( $x_{\max}$  and  $y_{\max}$ ) values over the 2,290 computed urban networks:

$$\bar{x}_i = \frac{x_i - x_{i,\min}}{(x_{i,\max} - x_{i,\min})} \quad \text{and} \quad \hat{y} = \frac{y - y_{\min}}{(y_{\max} - y_{\min})}, \quad [6]$$

This normalization enables comparing the relative variations of variables within their own ranges of values.

The standardized forms of the variables  $\bar{x}_i$  and  $\bar{y}$  are rewritten based on the mean ( $x_{i,\text{mean}}$  and  $y_{\text{mean}}$ ) and standard deviation ( $x_{i,\text{std}}$  and  $y_{\text{std}}$ ) values over the 2,290 computed urban networks:

$$\bar{x}_i = \frac{x_i - x_{i,\text{mean}}}{x_{i,\text{std}}} \quad \text{and} \quad \bar{y} = \frac{y - y_{\text{mean}}}{y_{\text{std}}}, \quad [7]$$

The standardization is used for the multiple linear regression presented hereafter.

The matrix notations  $\mathbf{X}$  and  $\mathbf{Y}$  are defined with  $\bar{x}_i^n$  and  $\bar{y}^n$  the values of  $\bar{x}_i$  and  $\bar{y}$  corresponding to the  $n^{\text{th}}$  computed urban network:

$$\mathbf{X} = \begin{bmatrix} -1 & -1 & \dots & -1 \\ x_1 & x_2 & \dots & x_{11} \\ -2 & -2 & \dots & -2 \\ x_1 & x_2 & \dots & x_{11} \\ \vdots & \vdots & \ddots & \vdots \\ -2,290 & -2,290 & \dots & -2,290 \\ x_1 & x_2 & \dots & x_{11} \end{bmatrix} \quad \text{and} \quad \mathbf{Y} = \begin{bmatrix} -1 \\ y \\ -2 \\ y \\ \vdots \\ -2,290 \\ y \end{bmatrix}. \quad [8]$$

A multiple linear regression is used to determine the least squares linear parameters  $\mathbf{A} = [a_1, a_2, \dots, a_{11}]^T$  which represent the sensitivity of the inundation indicator with respect to each urban characteristic.

$$\mathbf{A} = (\mathbf{X}^T \mathbf{X})^{-1} \mathbf{X}^T \mathbf{Y}. \quad [9]$$

## 3 RESULTS AND DISCUSSION

The sensitivity parameters  $a_i$  were computed from Eq. (8) for inundation indicators between  $h_{85\%}$  and  $h_{95\%}$  over all the inundated area and between  $h_{50\%}$  and  $h_{95\%}$  along the upstream sides of the domain, with a constant quantile step of 5%. Figure 4 compares the minimum and maximum values of the computed values of  $a_i$  depending on the domain over which quantiles values are determined. This shows that sensitivity parameters are weakly influenced by the chosen inundation indicator.

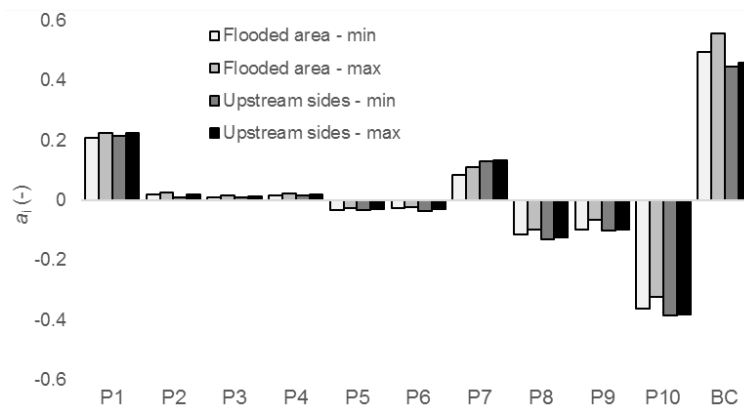


**Figure 4.** Minimum (- min) and maximum (- max) values of the linear parameters  $a_i$  depending on the domain over which quantiles are determined for the 11 urban characteristics.

In the following of the paper, the  $h_{90\%}$  value computed along the upstream sides was used to discuss the influence of urban characteristics on inundation water depths (Table 2). The correlation coefficient associated to the multiple linear regression was equal to  $R = 0.92$ .

The building coverage (BC) was the urban characteristic having the highest influence on inundation water depths ( $a_{11} = 0.457$ ). This strong influence suggests to fixing the building coverage to constant values in future studies to highlight more clearly the influence of other urban patterns on flooding.

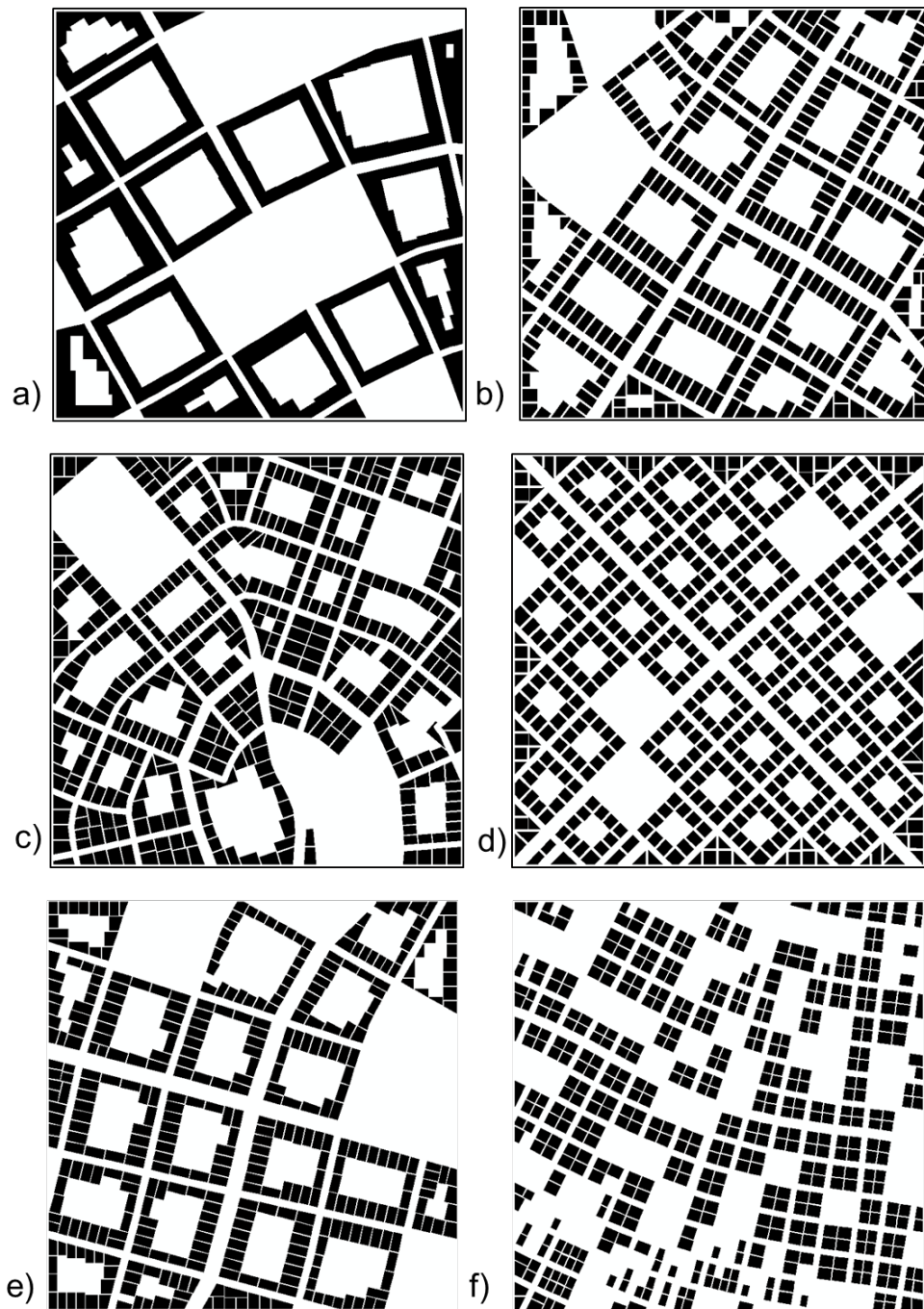
The building side setback (P10), which represented the distance between two adjacent buildings, was the urban characteristic with the second highest influence on inundation characteristics ( $a_{10} = -0.385$ ). The negative value indicates that inundation characteristics tend to be more severe if the value of P10 decreases, as a reduction of the conveyance capacity between buildings. This was exemplified by comparing the  $h_{90\%}$  values for the two urban networks represented in Figures 5a and 5b, for which the main differences were the building setback parameters. The inundation water depths were well higher for the urban network with a setback side value equaled to 0 (Figure 5b). Parameter P10 had about three times as much influence as the other building setbacks (P8 and P9). Indeed, the inundation indicator in Figure 5d was lower than in Figure 5c because the distances between adjacent buildings (P10) are higher, even if the building setbacks P8 and P9 decreased.

The third highest sensitivity parameter value was related to the average street length (P1). The inundation water depths increased with a rise in this urban characteristic. Comparing the urban networks of Figure 5e and Figure 5f, large groups made of multiple buildings increased for high values of P1. Since the void area enclosed in these groups of buildings hardly contributes to the conveyance of the flow, inundation water depths increased with an augmentation of the value of P1.

Urban inundation water depths were weakly influenced by the values of the street orientation (P2) and street curvature (P3), which did not affect the conveyance ability of the urban network. The validity of this finding should be tested for more dynamic flow conditions (i.e. higher flow velocity). Here the maximum value of the Froude number in the urban area did not exceed 0.4. More surprising were the low sensitivity parameters values obtained for streets widths (P4 and P5) and park coverage (P6). This is certainly related to the absence of constraints on the value of the building coverage in the urban generator tool, leading to a mix of the effects of parameters P4 to P6 with the high influence of the building coverage value (BC). Therefore, the building coverage will be set to constant values in future analysis.

**Table 2.** Sensitivity parameters computed for  $h_{90\%}$  along the upstream sides with  $a_{\max} = a_{11}$ .

	P1	P2	P3	P4	P5	P6	P7	P8	P9	P10	BC
$a_i$	0.127	0.010	0.011	0.018	-0.032	-0.031	0.133	-0.125	-0.102	-0.385	0.457
$\frac{a_i}{a_{\max}}$	47%	2%	3%	4%	-7%	-7%	29%	-27%	-22%	-84%	100%



	P1	P2	P3	P4	P5	P6	P7	P8	P9	P10	BC	$h_{90\%}$
a)	0.57	0.28	0.63	0.38	0.58	0.65	0.74	<b>0.00</b>	<b>0.00</b>	<b>0.00</b>	0.74	0.73
b)	0.50	0.95	0.72	0.47	0.55	0.14	0.86	<b>0.32</b>	<b>0.57</b>	<b>0.64</b>	0.75	0.33
c)	0.32	0.09	0.93	0.23	0.10	0.14	1.00	<b>0.36</b>	<b>0.39</b>	<b>0.46</b>	0.88	0.49
d)	0.29	0.24	0.02	0.59	0.23	0.10	0.90	<b>0.22</b>	<b>0.25</b>	<b>0.71</b>	0.89	0.37
e)	<b>0.48</b>	0.52	0.55	0.85	0.38	0.57	0.75	0.48	0.34	0.41	0.71	0.45
f)	<b>0.09</b>	0.90	0.10	0.19	0.25	0.66	0.49	0.26	0.61	0.44	0.71	0.28

**Figure 5.** Normalized values of the urban characteristics  $\hat{x}_i$  and inundation indicator  $\hat{y}$  for different computed urban networks.

Over the 2,290 computed urban networks, the three urban configurations leading to the highest flow depths are represented in Figure 6. These urban networks correspond to building setbacks equal to 0 for which enclosed areas free for water are surrounded by buildings, limiting hence the available space to convey the flow. The urban network with the highest inundation indicator (Figure 6a) was characterized by a very high average street length (P1 = 1.00), as for Figure 6c (P1 = 0.81). The second highest inundation indicator was computed for an urban network combining high values of average street length P1, average parcel areas P7 and building coverage BC.

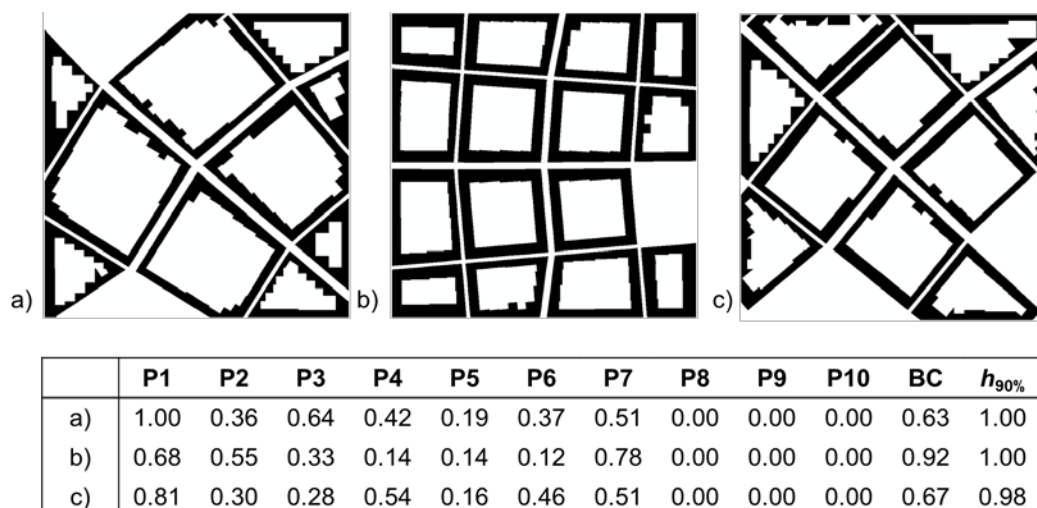


**Figure 6.** Normalized values of the urban characteristics  $\hat{x}_i$  and inundation indicator  $\hat{y}$  for the three urban networks leading to the highest values of the inundation indicator.

#### 4 CONCLUSIONS

The aim of this paper is to present a methodology to evaluate the sensitivity of urban flooding to different urban characteristics. By varying the values of 10 urban pattern parameters, 2,290 urban networks are generated by an urban generator model. Using identical hydraulic conditions, inundations characteristics are computed for each urban network with a shallow-water model with porosity which enables to reduce the computational cost by using a coarse grid, while preserving the detailed topographic data to some extent through porosity parameters. A sensitivity analysis is performed based on a multiple linear regression to highlight the influence of several urban characteristics on the urban inundation water depths.

The preliminary results show that the building coverage is the urban characteristic with the highest influence on inundation water depths. This strong influence suggests to fixing the building coverage to a constant value in future studies to highlight more clearly the influence of other urban patterns on flooding. Additionally, the values of the sensitivity parameters suggest that average street length and building side setback have a higher impact on inundation water depths than other urban characteristics.

#### ACKNOWLEDGEMENTS

The research is funded through the ARC grant for Concerted Research Actions, financed by the Wallonia-Brussels Federation.

#### REFERENCES

- Arrault, A., Finaud-Guyot, P., Archambeau, P., Bruwier, M., Ercicum, S., Piroton, M. & Dewals, B. (2016). Hydrodynamics of Long-Duration Urban Floods: Experiments and Numerical Modelling. *Natural Hazards and Earth System Sciences*, 16, 1413–1429.
- Beckers, A., Dewals, B., Ercicum, S., Dujardin, S., Detrembleur, S., Teller, J., Piroton, M. & Archambeau, P. (2013). Contribution of Land Use Changes to Future Flood Damage along the River Meuse in the Walloon Region. *Natural Hazards and Earth System Sciences*, 13, 2301–2318.
- Bruwier, M., Archambeau, P., Ercicum, S., Piroton, M. & Dewals, B. (2016). *Discretization of the Divergence Formulation of the Bed Slope Term in the Shallow-Water Equations and Consequences in Terms of Energy Balance*. *Applied Mathematical Modelling*, 40, 7532–7544.
- Bruwier, M., Ercicum, S., Piroton, M., Archambeau, P. & Dewals, B.J. (2015). Assessing the Operation Rules of a Reservoir System based on a Detailed Modelling Chain. *Natural Hazards and Earth System Sciences* 15, 365–379.
- Chen, G., Esch, G., Wonka, P., Müller, P. & Zhang, E. (2008). Interactive Procedural Street Modeling. *ACM Transactions on Graphics*, 27(3), Article 103, 1-10.

- Detrembleur, S., Stilmant, F., Dewals, B., Erpicum, S., Archambeau, P. & Pirotton, M. (2015). Impacts of Climate Change on Future Flood Damage on the River Meuse, with a Distributed Uncertainty Analysis. *Natural Hazards*, 77, 1533–1549.
- Ernst, J., Dewals, B.J., Detrembleur, S., Archambeau, P., Erpicum, S. & Pirotton, M. (2010). Micro-Scale Flood Risk Analysis based on detailed 2D Hydraulic Modelling and High Resolution Geographic Data. *Natural Hazards*, 55, 181–209.
- Erpicum, S., Dewals, B.J., Archambeau, P. & Pirotton, M. (2010). Dam Break Flow Computation based on an Efficient Flux Vector Splitting. *Journal of Computational and Applied Mathematics*, 234, 2143–2151.
- Kim, B., Sanders, B.F., Famiglietti, J.S. & Guinot, V. (2015). Urban Flood Modeling with Porous Shallow-Water Equations: A case Study of Model Errors in the Presence of Anisotropic Porosity. *Journal of Hydrology*, 523, 680–692.
- Kim, B., Sanders, B.F., Schubert, J.E. & Famiglietti, J.S. (2014). *Mesh Type Tradeoffs in 2D Hydrodynamic Modeling of Flooding with a Godunov-based Flow Solver*. *Advances in Water Resources*, 68, 42–61.
- Parish, Y.I.H. & Müller, P. (2001). Procedural Modeling of Cities. *Proceedings of the 28th Annual Conference on Computer Graphics and Interactive Techniques, SIGGRAPH '01*.
- Prusinkiewicz, P. & Lindenmayer, A. (1990). *Modeling of Cellular Layers. The Algorithmic Beauty of Plants*. Springer, 145–174.
- Sanders, B.F., Schubert, J.E. & Gallegos, H.A. (2008). Integral Formulation of Shallow-Water Equations with Anisotropic Porosity for Urban Flood Modeling. *Journal of Hydrology*, 362, 19–38.
- Schubert, J.E. & Sanders, B.F. (2012). *Building Treatments for Urban Flood Inundation Models and Implications for Predictive Skill and Modeling Efficiency*. *Advances in Water Resources*, 41, 49–64.
- Valiani, A. & Begnudelli, L. (2006). Divergence Form for Bed Slope Source Term in Shallow Water Equations. *Journal of Hydraulic Engineering*, 132, 652–665.

## APPROPRIATE INTERVENTIONS TO METRO CEBU'S FLOODING PROBLEMS

DANILO T. JAQUE<sup>(1)</sup>, ANDRE-PAUL AMPONG<sup>(2)</sup>, JOAN ARCE-JAQUE<sup>(3)</sup> & PRIMITIVO CAL<sup>(4)</sup>

<sup>(1,2,3)</sup> Hydronet Consultants Inc. Cebu City, Philippines

hydronetconsult@yahoo.com; apc.ampong@gmail.com; joanjaque@yahoo.com

<sup>(4)</sup> UP Planning and Development Research Foundation, Inc., Quezon City, Philippines  
primcal@yahoo.com

### ABSTRACT

Flooding in Metro Cebu has affected many urban services such as transport system resulting in high economic losses for many business establishments. Undersized and clogged drainage system results in flooding not only in low lying areas of the catchment but also in several elevated sections of the city. Despite the many conducted drainage master planning studies in the past and the corresponding investments poured on drainage programs, the number of flooding incidents both in frequency and severity has increased overwhelmingly over the last 10 years. This paper provides technical description and analysis of proposed engineering and non-engineering intervention to address the flooding within the Subangdaku catchment. Various technical solutions are analyzed based on technical effectiveness, financial requirements, and socio-economic consideration as well as do-ability of identified flood intervention programs. It is found that implementation of previous drainage flood control projects do not follow coherent engineering intervention program resulting in a piece-meal solution that simply transfers the same problem to another. It is also recognized by the stakeholders that appropriate and effective solution to the flooding problems hinges mainly on sound technical engineering and sustained through non-structural measures implemented in a proper sequence. In order to realize the appropriate flood control program in Metro Cebu, full support of the local government is required which demands political will to address many obstacles. Support from the private sectors such as the Metro Cebu Development and Coordinating Board (MCDCB) also serves as a strong catalyst in the implementation of a sustainable program to address flooding.

**Keywords:** Flood control and management; inter-agency collaboration; drainage master planning; structural and non-structural measures.

### 1 INTRODUCTION

Metro Cebu is the center of trade, industry, tourism and education in the Central Visayas, situated at the heart of the Philippines. Its pace of growth and development has been consistent and its rate of urbanization, rapid. Recently however, a major concern that requires immediate attention is the perennial flooding of the metropolitan area during heavy rains.

In 1983, a drainage study or master plan was completed for Metro Cebu composed of four adjoining Cities of Talisay, Cebu, and Mandaue, and the municipality of Consolacion. The comprehensive drainage study was conducted by Norconsult, a Norwegian consulting company in association with PhilNor, a Filipino consulting company under a foreign loan agreement. In this study, 18 flood prone areas in the 4-mentioned locality of Metro Cebu were identified. In 1995, another study was conducted by JICA (Jica, 1995) to address the flooding woes. Because none of the recommendations in the 1983 and 1995 studies and no guidelines for regulating run-off were implemented, flooding in Metro Cebu increased. A more detailed study was conducted for Cebu City by Genson-TCGI (2005), but its implementation was stalled due to budget constraints. Today, the flooding problem has reached a critical and alarming level resulting in loss and damage to property damage (cars, appliances), loss of man-hours due to the disruption of the mobility of residents, and increased fuel-consumption caused by heavy traffic during heavy rains.



Photo 1. Flooding situation in Metro Cebu.

A recent study is implemented using an integrated-watershed approach to rationalize the problem and to look closely on the issues pertaining to the non-implementation of the flood control and drainage programs. Through the collaborative efforts of private sectors and local government units, appropriate solutions are currently on its first level of implementation, and supported by concerned agencies. The program adopts an integrated watershed-based analysis that explores both structural and non-structural measures. Challenges and lessons learned are documented and presented to the stakeholder in seeking collaborative solution to long term flooding woes.

## 2 DATA COLLECTION AND ANALYSIS OF CATCHMENT

Pertinent information related to flooding within the catchment of Metro Cebu includes the rainfall intensity, catchment characteristics such as area, catchment slope, vegetative cover, extent of urbanization and programs adopted by the local government units in addressing the localized flooding. Cities that share the boundary within the catchment have incorporated some level of flood management through construction of cisterns. However, the effectiveness could not be measured due to lack of monitoring. In addition, drainage systems were also inventoried and showed that more than 40% of the drainage system are clogged and silted. As a result, capacity has reduced substantially resulting in surcharge in many drainage sections. The study focuses on one of the urban catchments known as Subangdaku within the Cities of Cebu and Mandaue.

### 2.1 Description of Subangdaku Catchment

Subangdaku catchment is situated at the center of Metro Cebu (Figure 1) and covers the cities of Cebu and Mandaue. It has a total catchment area of 17.20 km<sup>2</sup> and its highest point of elevation is at 353 meters above mean sea level. Its peak flow at 25-year return period is estimated at 293m<sup>3</sup>/s. The main river of the catchment is the Subangdaku River with a tributary creek named Hipodromo Creek. The river empties itself into the Mactan Channel as shown.

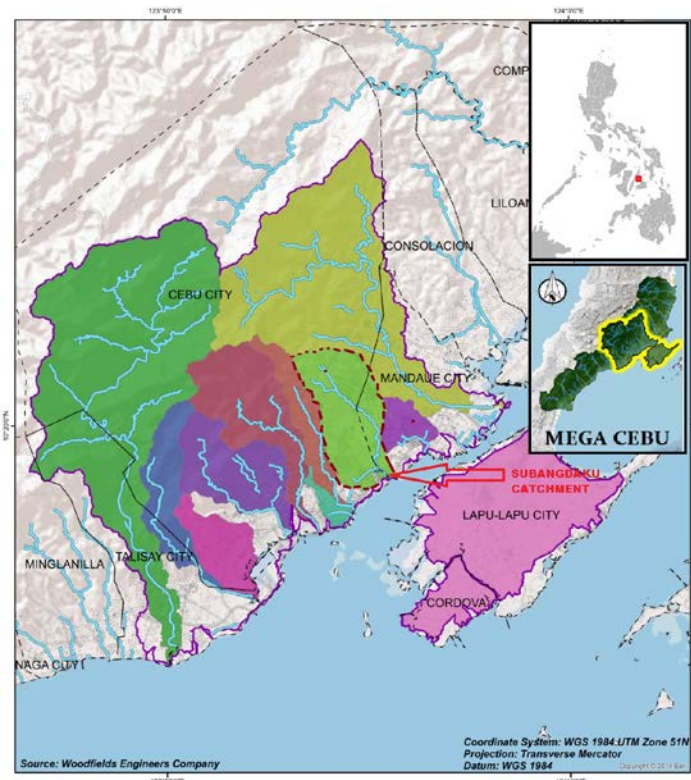


Figure 1. Project location showing the Subangdaku catchment

### 2.2 Rainfall Intensity-Frequency Duration

The rainfall in the area is characterized by heavy burst and short normally extending to 30 minutes to 2 hours. The rainfall intensity frequency and duration data was obtained from Philippine Atmospheric Geophysical Astronomical Services Administration (PAGASA) with more than 30 years of record in the nearest synoptic station in Mactan island which is 6 kilometers from the catchment. The Department of Public Works and Highways (DPWH) requires that drainage and flood control infrastructure shall be designed based on 50 years return period for rivers with less than 40 km<sup>2</sup> catchment size, while the drainage mains are designed based on 15 years return period. Hence, the rainfall depth (mm) for various durations is as follows.

**Table 1.** Rainfall intensity frequency duration in Mactan Island.

Return period/Duration	Rainfall in millimeters				
	30 mins	1 hour	1.5 hours	2.0 hours	3.0 hours
15 years	62.7	85.5	101.2	115.9	134.6
50 years	77.9	107.2	125.5	147.2	172.6

**2.3 Land use and topography**

Within the Metropolitan Cebu, 71% of its land area is categorized as urban. The upland portion consisting of around 25.66 % of the Metro Cebu is classified as protected areas; which is further classified as forest reserves and national parks. Within the Subangdaku catchment, around 76% are considered developed and built-up areas with remaining of 24% undeveloped and mountainous grasslands, with average slopes of 35%.

**2.4 Soil and geology**

The geology in Metro Cebu is generally karstic limestone formation. Caverns and underground solution channels are common features in the area. This type of geologic formation extends up to approximately 2 kilometers upstream. The soil has high capacity to absorb rainfall and replenish the groundwater table. However, due to rapid development and absence of policy on stormwater management, the increasing volumes of surface runoff water render the nearby creeks and channels inadequate.

Given the above rainfall and catchment characteristics, coupled with the encroachment of structures along the waterways, flooding is inevitable. Hence, analysis on various intervention programs is done using multifaceted criteria for guidance to the local planners and implementing agencies.

**3 ANALYSIS OF INTERVENTIONS PROGRAM**

Determination and agreement to support appropriate program to address flooding is quite a challenge when interests of some stakeholders are affected and when political will is put to the test. These challenges are discussed in the subsequent sections.

From the engineering perspective, three (3) basic interrelated structural intervention programs were identified to address the flooding. These were river improvement, diversion channels and construction of drainage mains, and construction of detention basins. In addition, these structural programs must be supported non-structural program by means of legislation to manage stormwater at source.

A conceptual plan for the Subangdaku river shows a wide range of intervention which includes: river improvement, construction of drainage mains, construction of detention basin/lagoon, and diversion channels.

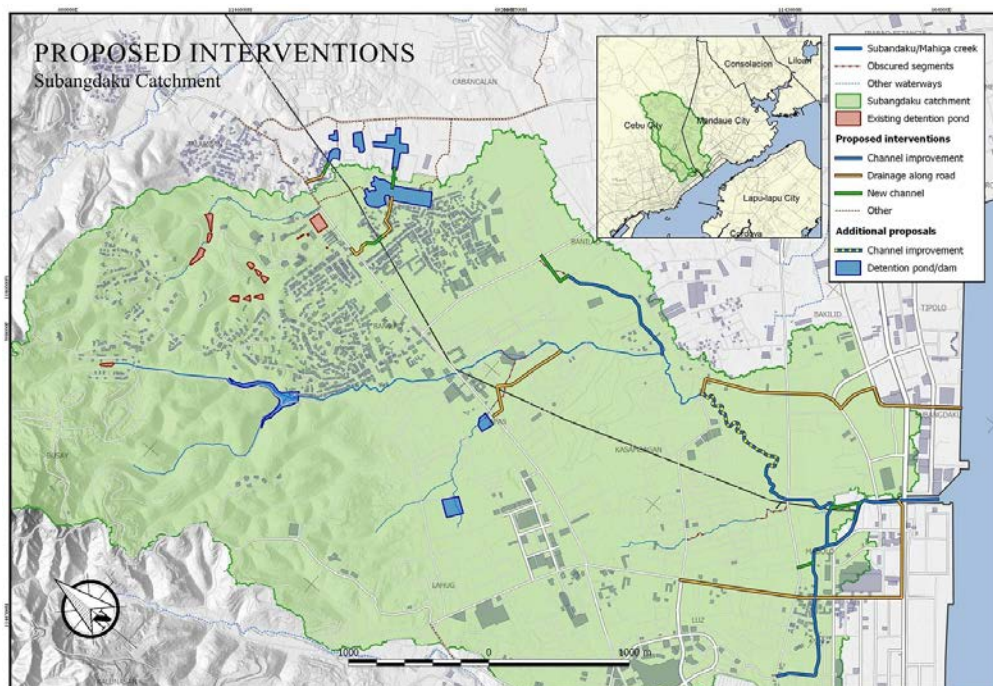


**Figure 2.** Flood Mitigation Program for Subangdaku catchments.

### 3.1 Alternative 1: Proposed river improvement program

The alternative proposed program for flood mitigation involves mainly the improvement of Subangdaku river, construction of drainage mains, and detention system at source. For the river improvement, the flood frequency of 25 years was selected, while drainage mains adopted 10 years return period. Detention system takes the form of cistern at household level and in commercial and industrial development areas. As already known, rivers and creeks have existing capacity of runoff with 2 years return period, hence, major river works are needed. The improvement involves river widening, provision of river easement, which entail the removal of structures along the banks. From the technical perspective, it is a simple task in determining the extent and sizes of the channel to meet the desired flood frequency. However, the political and social dimension may not necessarily subscribe to the simplistic technical recommendations. What can be offered as a common ground and compromise is quite trivial and depends mainly on the local chief executive. Shown below is the Subangdaku River with informal settlers living along the riverbanks.



**Photo 2.** Structures along the Subangdaku River.

### 3.2 Alternative Program 2: Diversion channel

Another alternative was explored to minimize disturbance of residents along the river. Among the technical possibilities include the construction of a diversion channel to divert flood flows that exceeds the 5 year return period. The proposed diversion channel will be laid along major roads going to the coasts as shown in the map above. This option faces overwhelming challenges by commuters and motorist on the already traffic congestion of the City roads due to the limited road-width. The existing vehicle speed at present is estimated at 10kph. Hence, this is a critical consideration aside from the cost of the drainage infrastructure.

### 3.3 Alternative Program 3: Construction of major detention basin upstream

This alternative proposed the construction of detention basin or a lagoon at the upstream section of the catchment. The program was designed to reduce flood peaks by 40%. It also allows for long-term groundwater replenishment. However, a closer look at the upstream condition, the cost of such structure is also enormous having to deal with land acquisition, relocation of affected residents and willingness of the owner to allow the government to use the land. Although an eminent domain can be used as legal means of acquiring the property, the process may also take time.

Summary of the three alternatives is presented in Table 2 below.

**Table 2.** Summary of alternatives on identified intervention program.

N	Flood control Program	Program Alternative 1	Program Alternative 2	Program Alternative 3
1	Description	River improvement with drainage mains and source control	Diversion channel with minimal river improvement (5-year return period)	Detention basin with minimal river improvement (5-year return period)
2	Dimensions	River improvement Q = 293m <sup>3</sup> /s - Width: 14 – 16m - Length: 3,200m	River improvement (Q=183) - Width: 10-12m, - Length: 3200m Diversion (Q=110m <sup>3</sup> /s) - Width: 4m - Length: 2,250m	River improvement (Q=183) -Width: 10-12m - Length: 3200m Detention/lagoon basin: - Area; 12 hectares
2	Social consideration	Need to relocate 660 households	Need to relocate around 368 households	Need to relocate around 390 households
2	Cost of infrastructure	P865.00 M	River: P672.00 M + Diversion: P481.00 M	River: P672.00M + Lagoon/detention: 780 M
3	Estimated cost of relocation	P297.00 M	P165.00 M	P175.50 M
4	Socio-political Support	Resistance from informal settlers, support of program dependent on local chief and political will	Results in high traffic congestion throughout duration (1 to 2 years)	Difficulty in identifying suitable and adequate size for detention basin
6	Implementation duration	Delay due to social resistance weak enforcement of laws	Delay is still expected due to resistance of residence but may be shorter with lesser number of households	Delay is still expected due to resistance of residence but may be shorter with lesser number of households
7	Other considerations	Compliance of the national laws- on river easement Rivers can be monitored and maintained appropriately	Does not comply with easement law as stated in Water Code Inaccessible river prone to pollution	Does not comply with easement law stated in Water Code Inaccessible river prone to pollution

Note: 1US\$ = P50

Given the above consideration, it is clear that a full river improvement should be pursued to allow for safe passage of flood waters. Relocation of housing structures along the river is necessary for safety of residents, proper maintenance of river system, and ecological reason. Thus, the City will have to face the reality of moving or relocating their constituents to a safer ground in the future.

#### 3.4 Non-structural intervention program

The non-structural program to reduce flood magnitude and frequency, as well as ensuring the sustainability of engineering program is still at a primordial stage in many cities in the Philippines, and thus, was not considered as part of the intervention in many programs in the past.

In the case of Metro Cebu, such program is currently being pursued as part of “sustainable drainage system”. This program was incorporated in the current drainage master planning and it involved the regulation of land use for housing and commercial/industrial development, legislation on the utilization of rainwater, watershed protection and management, and solid waste management. A framework of the program is shown in Figure 3, highlighting the policy issuance as the basic foundation of the program. Such policy should be based on technical studies that will suit to the local practices.

While such program is currently being adopted and finds acceptance by many lawmakers, the realization of its impact to the urban center is still far from reality.

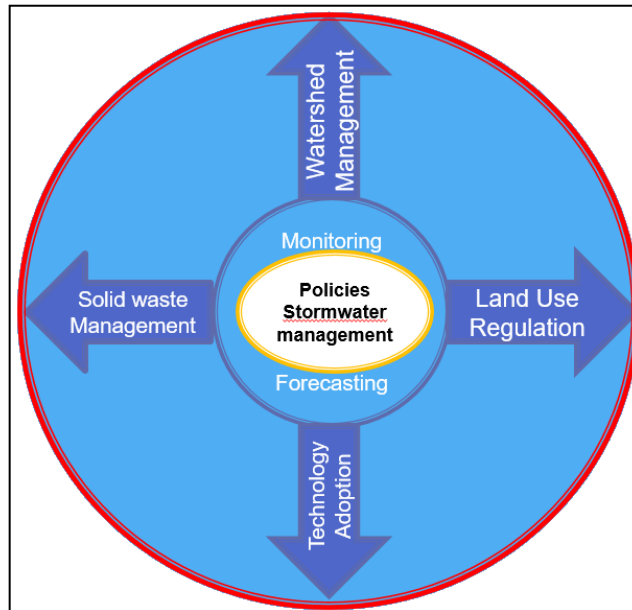


**Figure 3.** Non-structural measures adopted for Metro Cebu.

#### 4 TECHNICAL AND INSTITUTIONAL CHALLENGES

##### 4.1 Technical design challenges

The new design guidelines of the Department of Public Works and Highways (DPWH) require higher return period; thus, renders the old drainage system inadequate. Subscription to the new guidelines implies that new lines will be installed to augment the capacity of the old ones. This has become a major challenge to the planners. However, on a closer look, the problem of flooding is not necessarily the issue of design return period but the efficiency of the existing system in which the capacity are reduced significantly due to siltation and clogging of garbage. Thus, maintaining the existing drainage line could be a cheaper way of solving the problem. In addition, incorporating upstream control by constructing lagoon, mini-dams and similar structure could be the more appropriate and cost-effective solution.

##### 4.2 Institutional challenges

To address the flooding problems, large investment is required to improve the drainage system. However, the sustainability of the drainage system designed for a given return period cannot be ensured without enforcement of stormwater management that is consistent across political boundaries. The situation is aggravated by the institutional weaknesses, particularly in the area of local legislation. There is also the lack of educational program, weak enforcement of drainage system plans and programs and national laws. Implementation of a local legislative agenda on drainage necessitates the creation of a body to implement the drainage program. Table 3 below shows the functional matrix of various stakeholders.

The roles of key players in drainage show that DPWH and the city (municipal) government play a principal role in policy formulation, planning, implementation, repair and maintenance. The civil society and the private sector play a supportive role in the implementation, and repair and maintenance.

**Table 3.** Functional matrix of various entity.

Entity	Policy/Planning	Implementation	Repair & Maintenance
DPWH	P	P	P
LGUs	P	P	P
Civil Society		S	S
Private Sector		S	S

Legend: P – Principal role; S – Supporting role

Implementing agency (office) of the project depends on the size (cost) of projects as defined by the DPWH Secretary. The cost ceiling of its regional offices is P200 Million whereas its district engineering offices has a cost ceiling of P50 Million. The limit of delegated authority of DPWH Region Directors is likewise set at P200 Million. Pursuant to the DPWH Department Order No. 140, Series of 2014, the limit was the result of the assessments conducted by the Bureau of Design and the Bureau of Construction on the design and estimating capability of DPWH regional offices. There are three aspects that are relevant and worth mentioning.

- **Public Awareness.** Flooding occurrences are common sight during rainy season. However, people do not seem to connect the cause-effect of one's actions. For drainage program to be successful, the mandated agencies need to develop program of public awareness to internalize the consequences of some practices such as indiscriminate dumping of garbage on the streets and waterways affecting the overall function of drainage facilities. Awareness should also reach the household level not only touching on the cognitive faculties of the individual but compelled by actions. Reaching people through media and other means of communications should be a priority.
- **Public Education.** A more aggressive stance is for the City and DPWH to develop programs to educate the community particularly the leaders of the community and the business sectors. It is unfortunate that some of the developers are contented with compliance rather than full reliance of moral and ethical requirements to preserve and conserve nature. The City and DPWH may tap existing institutions such as schools (through DepEd), public forum and similar activities.
- **Public Participation.** Organizing the Community into groups that conduct community works relevant to river protection and similar activities would be beneficial. Once the groups are organized (Youth Groups, NGOs, etc.), activities such as River Clean Up, and watershed protection through tree planting program can be organized. The City should look into ways to encourage these groups to fulfill important tasks that will result into greater awareness of the general public.

#### 4.3 Creation of a project management office (PMO)

The creation of a PMO within the DPWH Regional Offices is recommended since most of the project gets muddled by the so many concerns of the agency. The creation of a PMO highlights the importance and urgency of the matter. The task of PMOs is to manage the implementation of the Drainage Investment Program, consisting of various packages.

#### 4.4 Creation of a drainage task force (DTF) in each LGU

The proposed DTF shall be tasked to manage and monitor the implementation of drainage program within its jurisdiction. The management and the maintenance of the drainage facility of each LGU will be under the auspices of the Office of the City/municipal Mayor through a local task force which shall be created by the City for the given purpose. Coordination with other agencies is critical. The proposed structure is shown below.

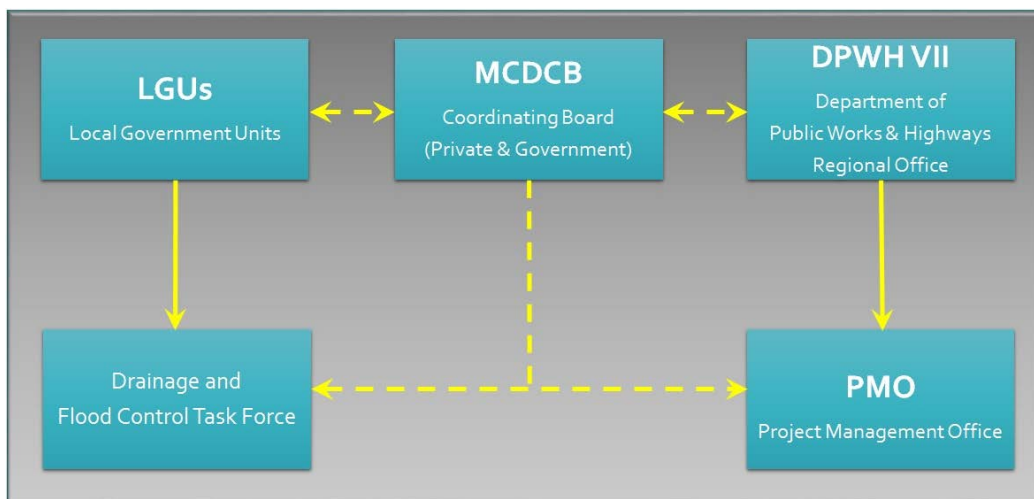


**Figure 4.** Institutional program and relationship with other sectors.

The “Drainage and Flood Control Task Force (DFCTF), as shown in Figure 4 will be created specifically to oversee the implementation, protection, and maintenance of the LGU drainage system and flood control facilities. Members of the task force shall include key personnel from various departments of the local government with the support of local private organizations and representatives from DPWH. The inclusion of the private sector in the task force is aimed at promoting public and private partnership.

The Local Government, through its task force, undertakes/initiates monitoring activities, as well as the following activities. Expanded roles may be discussed and clarified during the formation and institutionalization of the Task Force. Program of activities shall include the following:

- (1) Provide Database of Drainage Plans
  - Obtain and provide data relevant to drainage and flooding to serve as database for further planning and review of existing facilities

- Provide database of as-built plans and drawings of drainage system
- Update finish grade elevations of road networks
- (2) Enact Ordinances and Laws
  - Pass and enforce ordinance requiring new development to construct storm water detention/retention basin
  - Recommended sizes of stormwater collection system such as cistern, detention or retention basin and ditches which are incorporated into the stormwater – Best Management Practices
  - Develop mechanism to enforce the laws and deputize civilians to assist the law enforcement officers
- (3) Allocate Areas for Stormwater Detention
  - Negotiate with existing establishments and identify suitable sites to serve as stormwater retention areas. These establishments include the military camps, school grounds, government centers and parks and playgrounds, as well as subdivisions and commercial establishments.
  - Utilize parking lots as infiltration beds by using concrete blocks, macadam or similar structures and/or materials that allow water to seep into the ground.
- (4) Review Solid Waste Management Program
  - Garbage trapped in drainage lines are among the key issues resulting in flooding. The City needs to evaluate and recommend strategies to minimize if not eradicate this problem.

The role of MDCDCB has its legal basis from Section 33 of the Local Government Code which states, inter-alia: “Local government units may, through appropriate ordinances, group themselves, consolidate, or coordinate their efforts, services, and resources for purposes commonly beneficial to them.”

## 5 CONCLUSIONS

An integrated drainage and flood mitigation program supported by local policies and legislation on stormwater management to control and regulate the surface runoff are key factors that will address perennial flooding in vulnerable urban centers. In Metro Cebu, the non-implementation of the drainage infrastructure program as well as the weak policies on stormwater management contributes to the present and increasing flooding woes in the City. It is thus necessary to implement river improvement program using Alternative 1 which provides a cost efficient means of addressing flooding problems. This program involves full implementation of river improvement, requiring relation of informal settlers along the river. The program also proves to be sustainable and ecologically advantageous compared with other options. Due to the high cost of land acquisition and the huge number of informal settler families living along the river/channels, the tasks seem enormous and necessitate the support of the local and national government to provide the necessary funds for the relocation.

## ACKNOWLEDGEMENT

The research is part and parcel of the Metro Cebu Drainage Master Planning Study which is funded by Department of Public Works and Highways (DPWH)-Philippines and implemented by Woodfields Engineers (2016) and is realized through the support of Local Government Units in Metro Cebu.

## REFERENCES

- Andjelkovic, I. (2001). *Guidelines on the Non-Structural Measures in Urban Flood Management*, Technical Document on Hydrology No. 5 UNESCO, Paris.
- Cebu City Government (2005). *Flood Mitigation and Drainage Study for Cebu City*, Joint Study conducted by GENSON-TCGI-WOODFIELDS and SPACES.
- Department of Public Works and Highways, (2016). *Comprehensive Study for a Metro Cebu Integrated Flood and Drainage System Master Plan*, September 2016.
- Japan International Cooperating Agency, (JICA). (2014). *The Roadmap Study for Sustainable Development for Metro Cebu*, Metro Cebu Development Coordinating Board. ALMEC Corporation, Metro Cebu.
- Japan International Cooperating Agency, (JICA). (1995). *Study on the Flood Control for Rivers in the Selected Urban Centers*, CTI Engineering Co. LTD in association with Pacific Consultants International.

## HYDRAULIC DESIGN OF HONG KONG WEST DRAINAGE TUNNEL

ANIL KUMAR <sup>(1)</sup>, WONG CHIN TO LOUIS <sup>(2)</sup> & RAYMOND TAI <sup>(3)</sup>

<sup>(1,2)</sup> ARUP, Level 5, Festival Walk, 80 Tat Chee Avenue, Kowloon Tong, Kowloon, Hong Kong,

<sup>(3)</sup> Drainage Services Department, the Government of the Hong Kong Special Administrative Region, 42/F Revenue Tower,  
5 Gloucester Road, Wan Chai, Hong Kong

anil.kumar@arup.com; louis.wong@arup.com; wmtai@dsd.gov.hk

### ABSTRACT

The Hong Kong West Drainage Tunnel (HKWDT) meets the major social and business needs by preventing flood damage to the most densely urbanized areas of the Northern Hong Kong (HK) Island. The HKWDT comprises approximately 11km of drainage tunnel with internal diameter varying from 6.25m to 7.25m from Tai Hang to Cyberport, about 8km of associated connection adits, 34 no. intake structures and two portals. The majority of intakes are located in the upper catchment intercepting flows from streams, nullahs, box culverts and pipes. The supercritical flow from upstream catchment is diverted to the drainage tunnel through a uniquely designed intake structure focusing on space saving. The intake structure consists of a bottom rack, a bottom rack chamber and connection to a spiral vortex inlet through a link channel, and a dropshaft. An InfoWorks CS model was used for the overall hydraulic design of the HKWDT and to assess the hydraulic performance of the tunnel under a range of rainfall events. However, the InfoWorks CS model has its limitation in assessing the hydraulic behavior of the portals and intake structures. Therefore, physical modelling was used for the hydraulic design of intake structures and portals. Due to the site constraints, two typical intake structures were selected and developed through extensive physical modelling for maximum design discharge. The design of individual intake was developed based upon geometrical similarity using Froude's Law. Furthermore, it was difficult to construct a completely vertical shaft and therefore Computational Fluid Dynamics (CFD) modelling was carried out by using an inclined shaft with a gradient 1 in 200 to assess the hydraulic performance of intake structure. This paper describes the hydraulic design process involved in optimizing the arrangement of the various components of the HKWDT.

**Keywords:** Flood protection; intake structure; bottom rack; drop shaft; hydraulic modelling.

### 1 PROJECT BACKGROUND

The HKWDT meets the major social and business needs by preventing flood damage to the most densely urbanized residential and commercial areas of the Northern HK Island. Most of the existing drainage systems in the lower catchment of the Northern HK Island were built more than 50 years ago and do not meet the current design standard of 200-year flood protection, and they can no longer cope with the increased stormwater runoff resulting from rapid urbanization and climatic change. In recent years, flooding in the rainy seasons has caused severe disruption to the urban areas in the Northern HK Island.



**Figure 1.** Flooding in the Northern HK Island.

The Drainage Services Department (DSD) of the Government of the Hong Kong Special Administrative Region (HKSAR) opted for an interception approach to collect stormwater flows from upstream catchment and convey the intercepted flows via a system of adits and tunnels to the sea. The possibility of major improvement works to the lower drainage catchment was ruled out due to traffic disruption, land acquisition, disruption to normal life of the general public and the associated environmental impact in the heart of the urban area.

Ove Arup & Partners HK Limited (Arup) were commissioned by DSD in March 2006 to undertake the design, tendering and construction supervision of the HKWDT. The construction commenced in November 2007 and the drainage tunnel was commissioned in 2012.

The general alignment of the main drainage tunnel starts at Tai Hang in the center of HK Island and discharges the collected stormwater runoff 10.7km away through an outfall located at Cyberport on the south-west coast of HK Island.



Figure 2. The location plan of HKWDT and intakes.

The HKWDT is the longest stormwater drainage tunnel in HK and has two different diameters of 6.25m and 7.25m for upstream and downstream respectively. The main drainage tunnel branches into over 8km of 2.8m diameter horseshoe-shaped horizontal adits, which in turn link to the vertical dropshafts up to 180m deep. The top of the dropshaft is connected to an intake structure intercepting the stormwater runoff from existing stream courses and culverts.

The whole system is capable of discharging stormwater runoff under a 200-year rainstorm event. The peak discharge will be increasing from upstream to downstream along the drainage tunnel with maximum estimated discharge of 135 m<sup>3</sup>/s under a 200-year rainstorm event near the western portal before discharging into the sea near Cyberport.

## 2 DESIGN CRITERIA AND METHODOLOGY

The hydraulic design was carried out in accordance with the guidelines contained in the “Stormwater Drainage Manual” (SDM) 3<sup>rd</sup> edition published by DSD. There are five key elements of the whole system namely main tunnel, adits, intakes, eastern portal and western portal. The main objective of the eastern portal is to divert large magnitude of stormwater flow at the inlet/start of drainage tunnel from the existing stream course, whereas that of the western portal is to dissipate the flow energy before its final discharge into the sea so as to minimise any erosion and any adverse impact to the marine environment. Figure 3 below shows the catchment plan for various intakes intercepting the stormwater flow from upstream catchment.

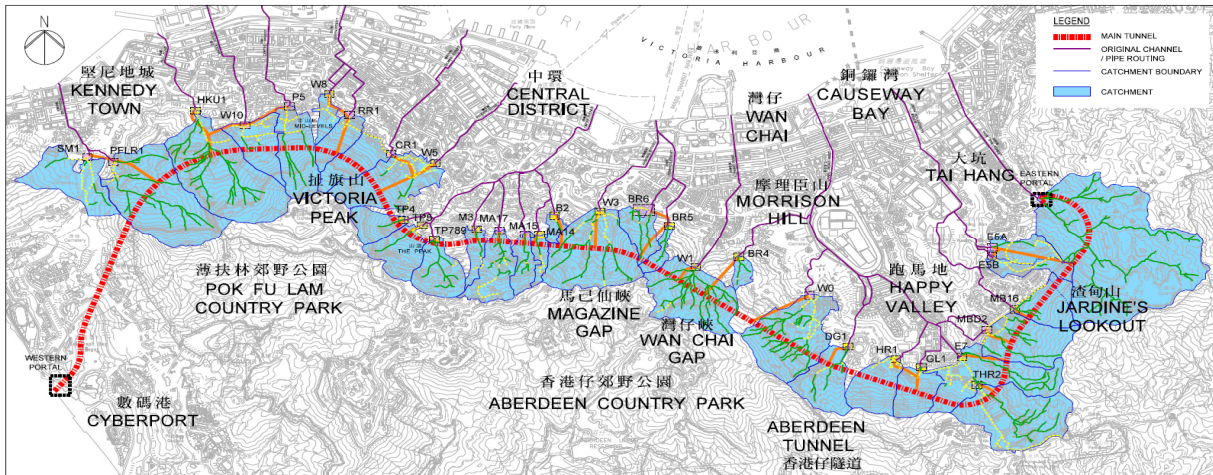


**Figure 3.** Catchment plan for HKWDT.

An in-depth review of previous works on the intake design was carried out to prepare for the detailed design of intakes under this project. Due to the complex hydraulic behaviour of the intakes and portals, the hydraulic design was prepared using empirical equations developed from a similar type of works and then further verified using physical models to ensure that the intakes/portals could convey peak flow under a 200-year rainstorm event. The following are the key design parameters for the design of tunnel, adits, intakes and portals:

### 2.1 Design rainstorm profile

The design rainstorm profiles were in accordance with the requirements of the SDM. A single rainstorm of 4-hour duration was used for all catchments to intercept all stormwater flows within the catchment. The 4-hour rainstorm duration was used to assess the hydraulic performance of the tunnel under 1 in 10 years, 50 years and 200 years return period rainstorm events. The rainstorm profiles were synthetic, peaked and symmetrically distributed.

### 2.2 Design sea levels

The HKWDT discharges the stormwater runoff into the sea near Cyberport and the nearest and representative tide gauge is Chi Ma Wan. However, the invert of drainage tunnel at the outfall is higher than the 200-year return period for the design extreme sea level at Chi Ma Wan of 3.75mPD and therefore the hydraulic performance of drainage tunnel is not affected by the tidal levels.

### 2.3 Roughness values

The main tunnel was designed with 6mm roughness for bottom third and 1.5mm roughness for the remaining two third of tunnel. However, sensitivity tests were performed to ensure the adequacy of tunnel passing peak flow for a 200-year rainstorm event with higher roughness.

### 2.4 Head losses

The head losses occur at bends and junctions apart from friction along the drainage tunnel. The head losses due to bend along the tunnel and adit were neglected because the ratio of radius of curvature to the tunnel diameter is larger than 10. To model the head losses at junction of tunnel and adit, a higher head loss coefficient in InfoWorks CS model was used to assess the overall performance of drainage tunnel. However, head losses due to junction and other transition are negligible as compared to friction losses along the system.

### 2.5 Siltation

The drainage tunnel was designed well above the tidal influenced zone whereas the intakes were designed with proper desilting facilities in the form of bottom rack to prevent entry of trash and to minimize entry of silt into the tunnel. During severe rain storms, flow velocity inside the tunnel would be high and the deposited silt/sediment in the drainage tunnel, if any, would be re-suspended and flushed to the sea by the high velocity flow. Therefore, it was envisaged that the amount of siltation would be very limited under severe rain storm events which would be removed regularly as part of regular operation and maintenance of the drainage tunnel. Figure 4 below shows the hydraulic profile along the main tunnel under a 200-year rainstorm event. It shows that the tunnel would not be surcharged under peak flows and hydraulics performance would not be influenced by tidal condition at downstream where siltation would happen.



## 4 PHYSICAL MODELLING

### 4.1 Intake structure

The intake structures were designed to divert the supercritical flow through a compact, space saving bottom intake structure that consists of four key elements (i) bottom rack; (ii) bottom rack chamber and connection to the vortex inlet through a link channel; (iii) spiral vortex inlet; and, (iv) dropshaft.

The width, length and height of the intake structure would influence the air and water flow behaviour. A comprehensive physical model study was carried out to determine the hydraulic behaviour of the complex three dimensional two phase flow in the intake structure. Extensive experiments were performed to establish the key performance characteristics of various designs including (i) the maximum standing wave height in the vortex inlet and (ii) the minimum air core ratio in the dropshaft. The test for spiral vortex, tangential slot and link channel were carried out on 1:24.5 scale, whereas the bottom rack was tested on 1:9.5 scale. After optimization, the integrated intake structure comprising the bottom rack, link channel and spiral vortex inlet with dropshaft was tested on 1:9.5 scale for a range of flow with a maximum flow of  $18\text{m}^3/\text{s}$ . A minimum air core ratio 0.41 was measured for the maximum flow  $18\text{m}^3/\text{s}$  which was more than 0.25 recommended to preserve the hydraulic capacity of shaft. It was found that the flow stability and the key performance characteristics were strongly dependent on the geometry of the bottom rack, link channel and vortex inlet. Based on the model tests, an optimised design of the bottom rack structure connected to a spiral vortex inlet, with warped invert or tapering tangential slot intake was recommended. As there was significant variation in the design flow for various intakes, it was not cost effective to adopt a typical intake design for all intakes. In this regard, sizing of individual intake was determined based upon the geometrical similarity using Froude's Law.

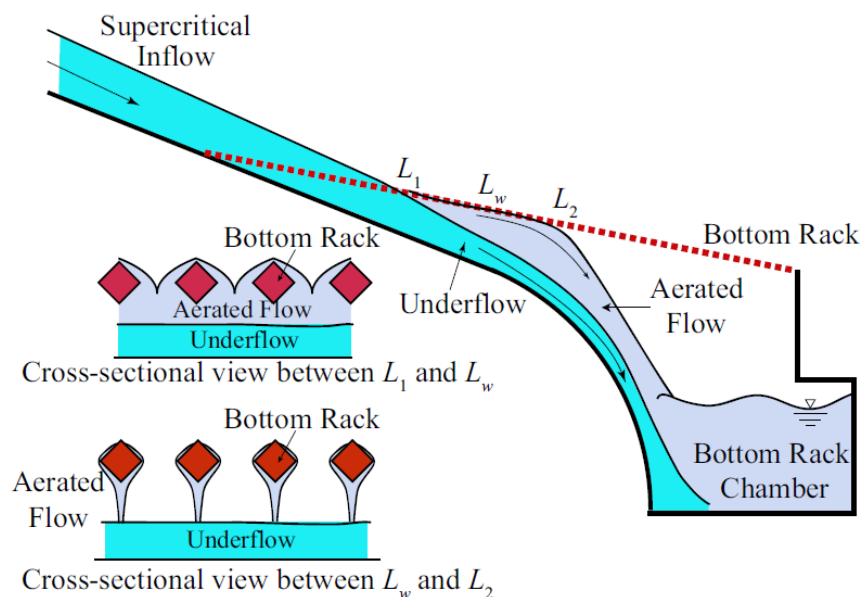


**Figure 7.** Flow condition along bottom rack and in bottom rack chamber.

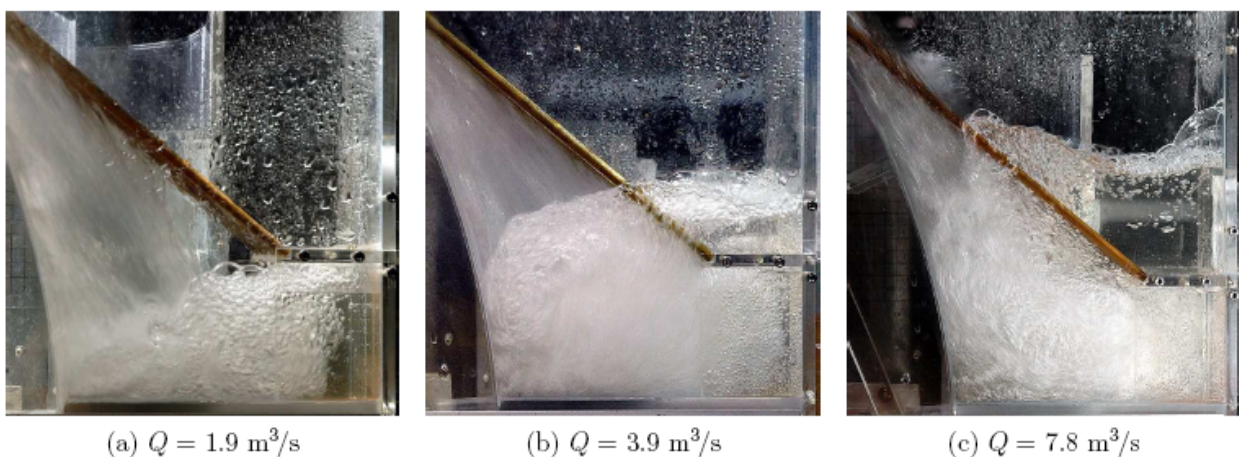


**Figure 8.** Flow condition in bottom rack chamber with different design flow.

Physical modelling was also carried out to find out how the lateral flow would affect the flow pattern within the bottom rack chamber. One of the important aspects affecting the hydraulic performance of the intake was the merging of the lateral flow with the main flow. To minimise the turbulence at the confluence of both flow elements, a curved variation to the invert of lateral flow was adopted. This arrangement reduced the direct interaction of the main flow with the lateral flow and hence the water depth within the bottom rack chamber.

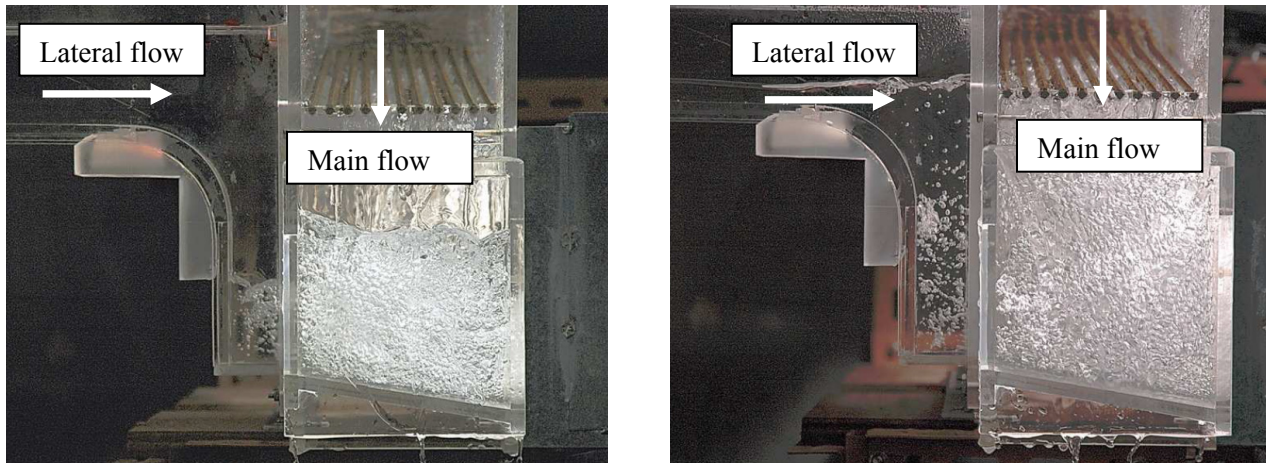


**Figure 9.** Flow pattern in bottom rack chamber with lateral flow at different design flow.

#### 4.2 Eastern and Western Portal

The eastern portal was designed to dissipate the flow energy and divert the stormwater flow at the entrance of main drainage tunnel from a steep natural stream. The portal comprised of a stepped chute, a stilling basin and a link channel. Physical modelling was carried out to ensure that the flow was evenly distributed in chute from the entry to the stilling basin, and the hydraulic jump was contained within the stilling basin to minimize wave action against the downstream wall to prevent premature overflow. The model showed that the hydraulic jump could be contained within the stilling basin with slightly rough water surface. However, a vortex was formed at junction of the link channel and the stilling basin due to abrupt change in the flow direction. The original design of orifice to link channel was modified with curved transition to avoid vortex formation.

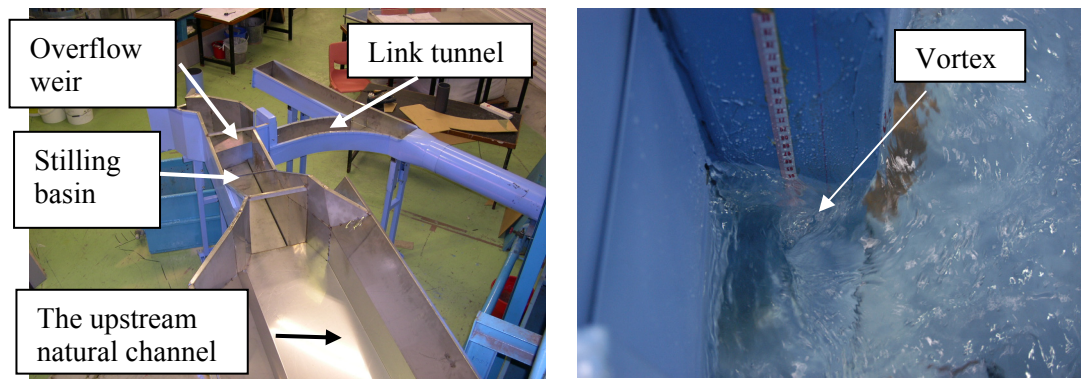


**Figure 10.** General arrangement of eastern portal in physical model and vortex formation.

The western portal at downstream end of the drainage tunnel was constructed to dissipate the flow energy before discharging into the sea at the existing coast line. The portal comprised approximately a 90m transition section from 7.25m diameter tunnel to 18m rectangular section and a stilling basin. The main objective of the transition section was to lower the flow velocity before reaching the stilling basin to minimise the length of stilling basin and contain the hydraulic jump within the basin to minimise impact to marine environment along the shore line. Hydraulic performance of the western portal was assessed by constructing an undistorted 1:48 scale model. The main objective of physical model was to ensure that the flow smoothly developed through the transition section of tunnel to the portal, with no flow separation from the tunnel to the stilling basin, with inclined water surface drop clinged onto nappe smoothly, and with hydraulic jump contained within the stilling basin. For transition sections, straight and curved expansions were tested and wavy water surface was found within the straight expansion. However, flow conditions were nearly the same in the stilling basin. As such, a straight expansion was adopted in the final design due to its simplicity of construction of expansion of tunnel through transition section.

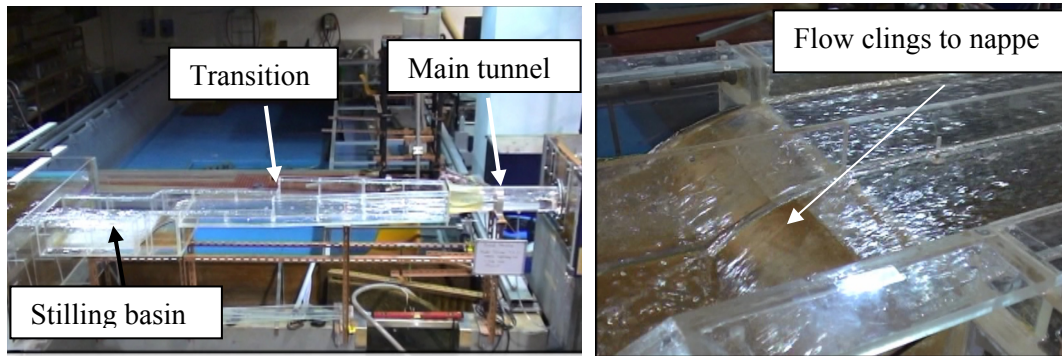


**Figure 11.** General arrangement of western portal and transition from tunnel to stilling basin in physical model.

## 5 COMPUTATIONAL FLUID DYNAMICS (CFD) MODELLING

There were a number of dropshafts up to 180m in depth. Although some of them were excavated using raised boring method, they could not be excavated to a totally vertical alignment. The air core ratio was one of the main parameters affecting the hydraulic capacity of the dropshaft. A CFD modelling was carried out to assess the impact of non-verticality of the dropshaft on the air core ratio. The CFD model comprised of the vortex chamber, dropshaft and stilling basin.



Vortex and Dropshaft General Arrangement

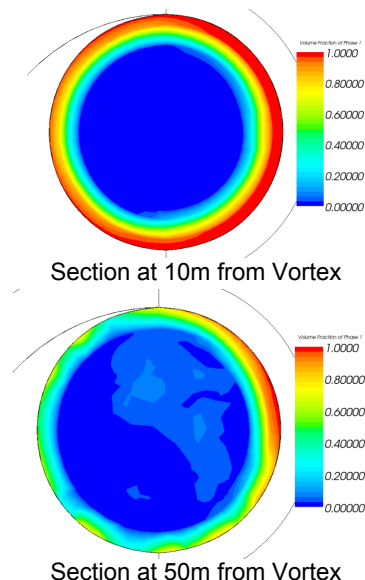


**Figure 12.** Vortex/dropshaft general arrangement and water/control volume fraction ratio along drop shaft.

The air core ratio was determined by comparing the fraction of water volume to the total control volume, with zero referring to total air and one referring to total water. The figure above shows the vortex/dropshaft general arrangement in the CFD model and also the water to total control volume fraction ratio along the dropshaft at 10m and 50m depth from the ground surface. It can be seen that air fraction reduced with depth with the minimum near to the stilling basin. The minimum air fraction was estimated to be 0.40 near the stilling chamber which was more than 0.25 recommended to preserve the hydraulic capacity of dropshaft.

Figure 13 below shows the water to control volume fraction ratio along the shaft and within the stilling chamber. It can be seen from volume fractions that air core fraction always maintained more than 0.25 with the minimum at junction of dropshaft with vortex chamber which should have minimum impact due to tilting of drop shaft. In summary, a 2% tilting of dropshaft had minimal impact on hydraulic capacity of the intake structure.

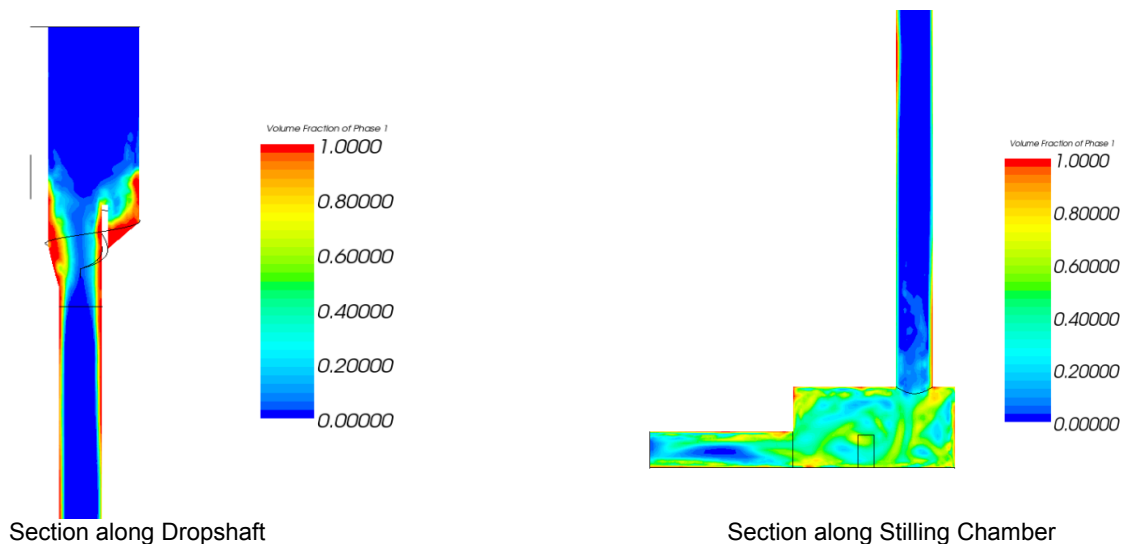


**Figure 13.** Section along drop shaft and stilling basin.

## 6 CONCLUSIONS

To alleviate flooding problems in the Northern HK Island and to meet current flood protection standards, a storm water interception scheme was commissioned in 2012. This scheme involves the interception of storm water flows through a series of intake structures in upper reaches of catchment above the urban districts of the Northern HK Island and transfer the stormwater flow to the HKWDT for its final discharge to the sea at Cyberport. The HKWDT involves approximately 11km of drainage tunnel of 6.25m to 7.25m diameter, 34 no. intake structures and two portals.

The hydraulic performance of the main tunnels and adits were assessed using the InfoWorks CS model under a range of rainstorm events. Due to the limitation of the existing hydraulic tools, the hydraulic design of intake structures and portals were verified using the physical modelling. The design of intake structures was optimized based upon findings from the physical model and geometrical similarity principal was used for design discharge of particular intake. It was difficult to construct a completely vertical dropshaft and therefore CFD modelling was carried out using the inclined dropshaft with a gradient 1 in 200 to assess the hydraulic performance of dropshaft. The CFD modelling concluded that the design air core ratio was maintained in the dropshaft during design flows.

The main tunnel, adits, intake structures and portals can convey runoff from a 200-year rainstorm event without any overflow to the downstream drainage system or surcharging the main drainage tunnel. Regular operation and maintenance of main tunnel and adits are planned to ensure their satisfactory hydraulic performance during the design life. With the commissioning of the HKWDT, the flood risk to downstream urban areas in the Northern HK Island has been reduced significantly.

## ACKNOWLEDGEMENTS

This paper was based upon findings undertaken as part of the consultancy under Agreement No. CE 17/2005 (DS) Tender and Construction of Hong Kong West Drainage Tunnel – Design and Construction, commissioned by the Drainage Services Department (DSD), the Government of the Hong Kong Special Administrative Region, China.

## REFERENCES

Stormwater Drainage Manual, (1995). *Planning, Design and Management*, Drainage Services Department, Government of the Hong Kong Special Administrative Region.

## MODELLING TSUNAMI-GENERATED DEBRIS FLOW IN URBAN ENVIRONMENTS

RICARDO B. CANELAS<sup>(1)</sup>, DANIEL CONDE<sup>(2)</sup>, ORLANDO GARCIA FEAL<sup>(3)</sup> & RUI M.L. FERREIRA<sup>(4)</sup>

<sup>(1,4)</sup> CERIS, Instituto Superior Técnico, Universidade de Lisboa, Lisbon, Portugal,  
ricardo.canelas@ist.utl.pt, ruif@civil.ist.utl.pt

<sup>(2)</sup> Instituto Superior Técnico, Universidade de Lisboa, Lisbon, Portugal,  
daniel.conde@ist.utl.pt

<sup>(3)</sup> Environmental Physics Technologies SL., Spain,  
rodland@gmail.com

### ABSTRACT

Tsunamis incorporate solids as they propagate in urban environments. Two-dimensional (2D) models have been used to assess its propagation even in dense urban fronts. The objective of this work is to introduce computational advances in tsunami modelling in urban areas. These include a fully lagrangian, three-dimensional (3D) description of the fluid-solid flow, coupled with a high performance meshless implementation, capable of dealing with large domains and fine discretizations. A Smoothed Particle Hydrodynamics (SPH) Navier Stokes discretization and a Distributed Contact Discrete Element Method (DCDEM) description of solid-solid interactions provide state-of the-art fluid-solid flow descriptions. High resolution simulations of a city section in Lisbon downtown are presented. It is shown that the incoming wave is able to mobilize and incorporate standing vehicles and other urban hardware. Such fully detailed (3D) simulation provides explicit description of the interactions among fluid, floating debris, the buildings and the pavement. The proposed model presents both an interesting research tool for the study of these flows and an innovative tool for civil protection authorities to design and test mitigation solutions.

**Keywords:** Tsunami; urban debris; dual SPHysics; STAV2D.

### 1 INTRODUCTION

As it propagates in urban areas, tsunamis incorporate debris from the remains of buildings or infrastructures. Such debris modifies flow rheology and the presence of solids in the tsunami wave-front will add extra complexity to the interaction between the run-up flow and the built structures that survived the earthquake. Two-dimensional (2D) shallow-water models have been used to assess the propagation of tsunamis even in dense urban fronts (Conde et al., 2015) and mobile complex geometries (Conde et al., 2013). However, this may compromise phenomenological description. Complex three-dimensional (3D) models incur in larger computational times but may express wake and separated flow phenomena.

In this work 3D computational advances are introduced. These include a fully lagrangian, 3D description of the fluid-solid flow, coupled with a high performance meshless implementation capable of dealing with large domains and fine discretizations. A Smoothed Particle Hydrodynamics (SPH) Navier Stokes discretization and a Distributed Contact Discrete Element Method (DCDEM) description of solid-solid interactions provide a state-of the-art fluid-solid flow description. Together with support for arbitrary geometries, centimeter scale resolution simulations of a city section in Lisbon downtown are presented. It is shown that the incoming bore is able to mobilize and incorporate standing vehicles and other urban hardware. Such fully featured simulation provides explicit description of the interactions among fluid, floating debris, the buildings and the pavement.

The application is in Praça do Comércio, Lisbon, Portugal, an urban area known to have been stricken by tsunamic in the past (Baptista et al., 2009). The computational domain for the 3D simulations, including the river front, as shown in Figure 1.

The developed work shows the advantages of considering hybrid 2D/3D modelling for highly non-linear cases and inherently multi-scale problems. While 2D simulations are fundamental for the propagation of the wave to the vicinity of interest area, highly resolved fully coupled 3D models can provide a meaningful solution due to the complex geometries and possible mobile objects that make up the urban scenario.

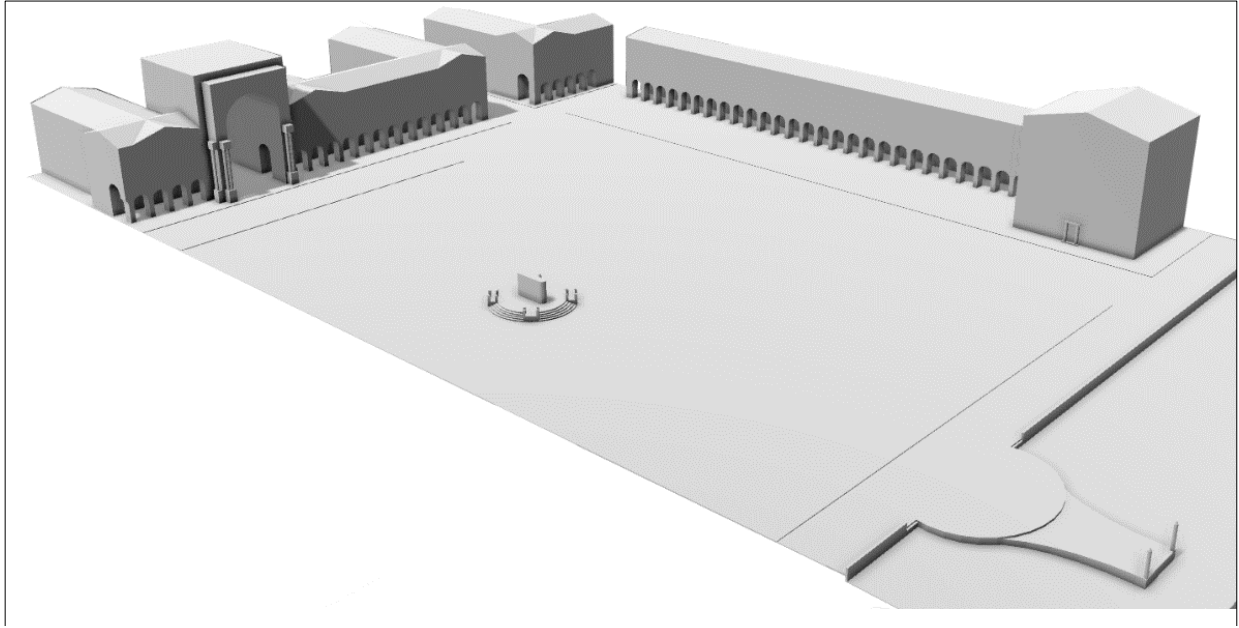


Figure 1. 3D model of Praça do Comércio, downtown Lisbon - the domain of 3D simulations.

## 2 MODELLING TSUNAMI PROPAGATION AS A SHALLOW FLOW WITH STAV2D

### 2.1 Conceptual model of STAV2D

STAV2D is a 2DH (two-dimensional-horizontal) mathematical model suitable for the simulation of discontinuous shallow flows over irregular surfaces, such as the case of a tsunami propagating overland. The governing system of conservation equations was composed of total mass, total momentum, sediment mass transported in the water column and sediment mass lying on the riverbed. In this paper, a non-stratified version of the model was used. The hyperbolic and non-homogeneous system of conservation laws is

$$\partial_t h + \partial_x(hu) + \partial_y(hv) = -\partial_t Z_b \quad (1)$$

$$\partial_t(uh) + \partial_x\left(u^2h + \frac{1}{2}gh^2\right) + \partial_y(uvh) = -gh\partial_x Z_b - \frac{1}{\rho_m}\partial_x hT_{xx} - \frac{1}{\rho_m}\partial_y hT_{xy} - \frac{\tau_{b,x}}{\rho_m} \quad (2)$$

$$\partial_t(vh) + \partial_x(uvh) + \partial_y\left(v^2h + \frac{1}{2}gh^2\right) = -gh\partial_y Z_b - \frac{1}{\rho_m}\partial_y hT_{yy} - \frac{1}{\rho_m}\partial_x hT_{yx} - \frac{\tau_{b,y}}{\rho_m} \quad (3)$$

$$\partial_t(C_m h) + \partial_x(C_m hu) + \partial_y(C_m hv) = -(1-p)\partial_t Z_b \quad (4)$$

$$(1-p)\partial_t Z_b = (q_s - q_s^*) / \Lambda \quad (5)$$

where  $t$  denotes time;  $x$  and  $y$  are the 2D coordinates;  $h$  is the flow depth;  $u$  and  $v$  are the depth-averaged velocities;  $Z_b$  is the bed elevation;  $\rho_m$  and  $C_m$  are the depth-averaged density and sediment concentration of the water-sediment mixture;  $T_{ij}$  is the depth-averaged stress tensor;  $\tau_b$  is the bed shear stress;  $q_s$  is the solid discharge; and  $q_s^*$  is its equilibrium value. The difference between the actual and equilibrium sediment discharge was proportional to the vertical sediment mass exchanges (in volume per unit area in equation 5) where, the inverse of the adaptation length,  $\Lambda$ , is the proportionality constant. Further closure equations regarding resistance, turbulence and solid transport can be found in Ferreira et al. (2009).

The employed discretization was based on a first order Godunov Finite-Volume approach, where the previous system was integrated over triangular cells of varying size and the fluxes between these cells were computed according to a revised version of the Roe-Riemann solver. Further details on the numerical implementation and validation of STAV-2D can be found in Canelas et al. (2013).

### 2.2 Two-dimensional simulation set-up

STAV2D was employed to simulate a tsunami in the present-day Lisbon and Tagus estuary, similar to the one that struck the Portuguese coast on the 1st of November of 1755. The initial estuarine conditions are set in a worst-case tide scenario, fully described in Conde et al. (2015), featuring a spring tide of +2.3m.



**Figure 2.** 2D simulation domain and boundary conditions.

The simulation domain has two open boundaries, namely at the Tagus valley and at the Atlantic reach (Figure 1). The Tagus boundary features constant discharge compatible with a 100-year flood. In the Atlantic boundary it is imposed a water elevation time series, corresponding to the wave train of the 1755 event (Conde et al., 2015). The main feature of these series is a 5.5m amplitude peak (Baptista et al., 2009). STAV-2D employs adaptable triangular meshes in order to balance an acceptable computational workload and different refinement levels. The computational domain depicted in Figure 1 is discretized into approximately 4 million cells, explicitly defining streets, prescribed over the urban mesh across the riverfront. The mesh gradually coarsens up to 20.0m over the inner and deeper areas of the estuary.

### 2.3 Overview of tsunami impacts on Lisbon's waterfront

Figure 3 depicts some of the results obtained with STAV2D. A 1775-like tsunami would have a devastating impact across Lisbon's riverfront areas. The inundation would reach over 1 km in Alcântara and nearly 500m in the Downtown (Terreiro do Paço). Almost all locations in the south riverfront, including the Downtown area, are classified as extremely dangerous in a tsunami scenario (Conde et al., 2015) with flow depths reaching over 5m and velocities reaching over 6m/s.

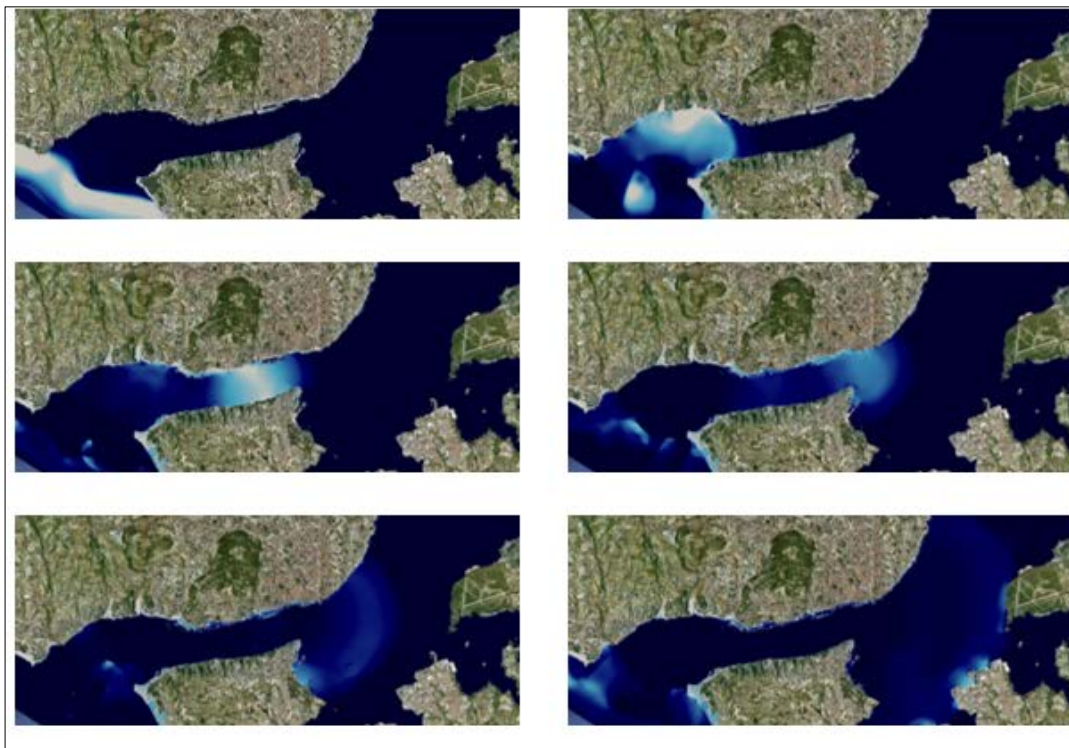


**Figure 3.** Propagation along the estuary for the first tsunami wave. From top left to bottom right: Tagus mouth approach (520s), first impact at Algés (800s), reaching Alcântara (1080s), flooding the Downtown area (1200s), spreading out through the estuary (1320s); impacting the left bank of the Tagus (1600s).

In the Downtown, an area that is given particular emphasis in this work, a time series of unit discharges was obtained and used as open boundary condition for the 3D SPH simulations presented in the following sections.

### 3 3D TSUNAMI SIMULATION WITH DUALSPHYSICS

#### 3.1 Conceptual model and discretization technique of DualSPHysics

In SPH, the fluid domain is represented by a set of nodal points where physical quantities such as position, velocity, density and pressure are approximated. These points move with the fluid in a Lagrangian manner and their properties change with time due to the interactions with neighboring nodes. The method relies heavily on integral interpolant theory (Monaghan, 2005). An approximation to discrete Lagrangian points can be made, by a proper discretisation of the continuous integral by

$$A_i \approx \sum_j A_j W(\mathbf{r}_{ij}, h) V_j, \quad (6)$$

called the summation interpolant, extended to all particles  $j$ , where  $\mathbf{r}_{ij}$  is the distance between  $i$  and  $j$ ,  $V_j$  is the volume of particle  $j$ ,  $A_i$  is the approximated variable at particle  $i$  and  $W$  is the weight, or kernel, function.

The proposed SPH formulation relies on the discretization of the Navier-Stokes (NS) and continuity equations. Written for a variable density and neglecting the divergence of the velocity field in the NS equations, these are

$$\frac{d\mathbf{v}}{dt} = -\frac{\nabla p}{\rho} + \frac{\mu}{\rho} \nabla^2 \mathbf{v} + \mathbf{g} \quad (7)$$

$$\frac{d\rho}{dt} = -\rho \nabla \mathbf{v}, \quad (8)$$

where  $\mathbf{v}$  is the velocity field,  $p$  is the pressure,  $\rho$  is the density and  $\mu$  and  $\mathbf{g}$  are the kinematic viscosity and body forces per unit mass, respectively.

Solving these Equations in a Lagrangian framework allows for the simple imposition of solid boundaries through an equivalent Immersed Boundary Method, as well as the consideration of 6 degrees of freedom for a defined rigid body.

#### 3.2 3D simulation set-up

The computational domain for the 3D simulations represents a section of downtown Lisbon. Part of Praça do Comércio and the surroundings was reproduced in a 3D geometry, including the river front, as shown in Figure 1. The streets between the buildings are kept as open boundaries, where the fluid leaves the domain, while all others were modelled as solid walls, simplifying the simulation by taking advantage of a somewhat symmetrical configuration of the square. All geometrical detail was included, such as the height of the sidewalks and the square itself and small columns on building fronts. For traditional, 2DH simulations, these details are not important, but in the present case, assuming the simulation is well resolved, all of the details may have relevant consequences. The sidewalks provide tipping points for dragged structures.

The domain was populated with a distribution of buses, trams and cars on the transit streets, as visible in Figure 6. These were attributed properties of steel for the bodies, with a low restitution coefficient to somewhat account for deformation in contacts, and rubber for the tires. The fixed background boundaries were treated as lime-stone.

The incoming wave was defined using the hyrogram produced with the 2D propagation simulations. The wave has a 20 degrees NE direction. The results are shown using post-processing techniques, specifically, particles were replaced with a meshed iso-surface of the mass for the fluid. This allows for a more natural visualization, even though some artefacts may be introduced due to the employed algorithm. Solid bodies are rendered using the original 3D models that originated them, mapped to the respective particle system.

#### 3.3 Results of 3D detailed tsunami propagation in Lisbon's downtown

The incident wave immediately submerges the river front, including the pier aligned with the square. In Figure 4, 5 s after the start of the simulation, the influence of the columns in the pier is evident by the two large wakes being generated. The incoming wave is now starting to propagate as a bore, after breaking.

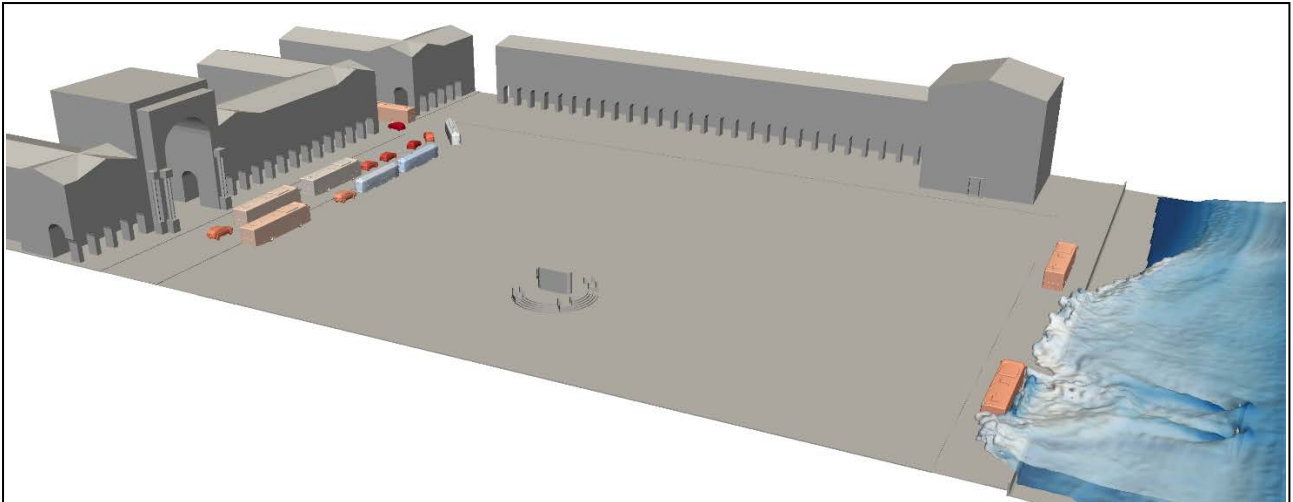


**Figure 4.** Results of the 3D simulation for  $t = 5s$ .

At 20s, the fluid reaches the end of the square, even if highly deformed by the geometry and the obstacles, as seen in Figure 5. The buses that were initially between the square and the river are now dragged by the wave. Both of them have tipped over their side and the motion is a combination of translation by action of the drag forces and rotation due to friction with the bottom.

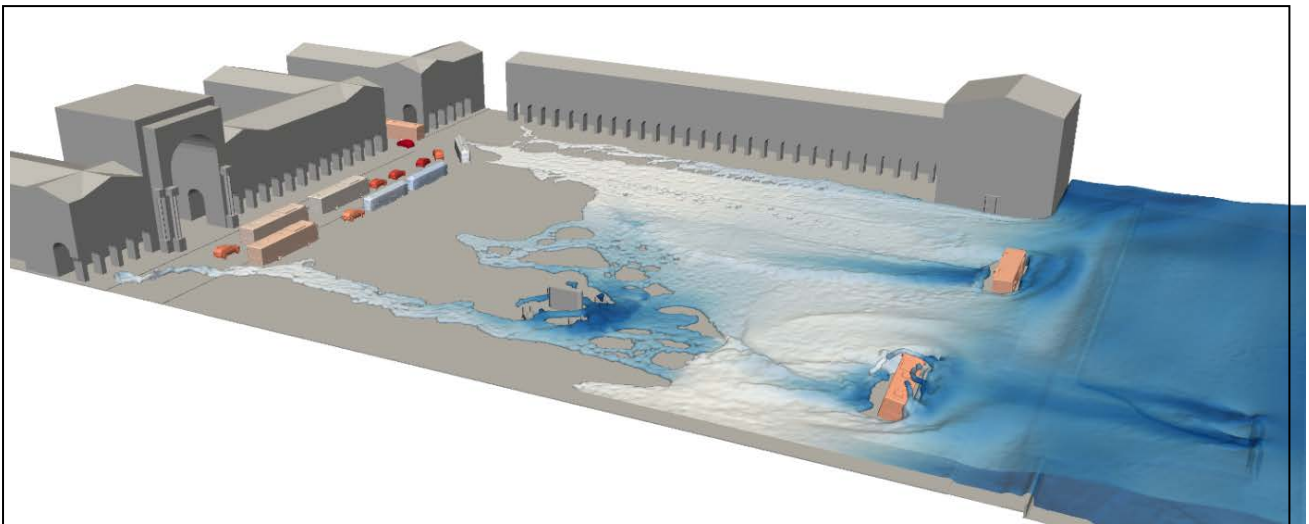


**Figure 5.** Results of the 3D simulation for  $t = 20s$ .

Thirty seconds after the beginning of the simulation, (Figure 6) the wave has hit all of the structures opposed to the river, and mobilizes the second set of vehicles. Flow under the building galleries is registered.

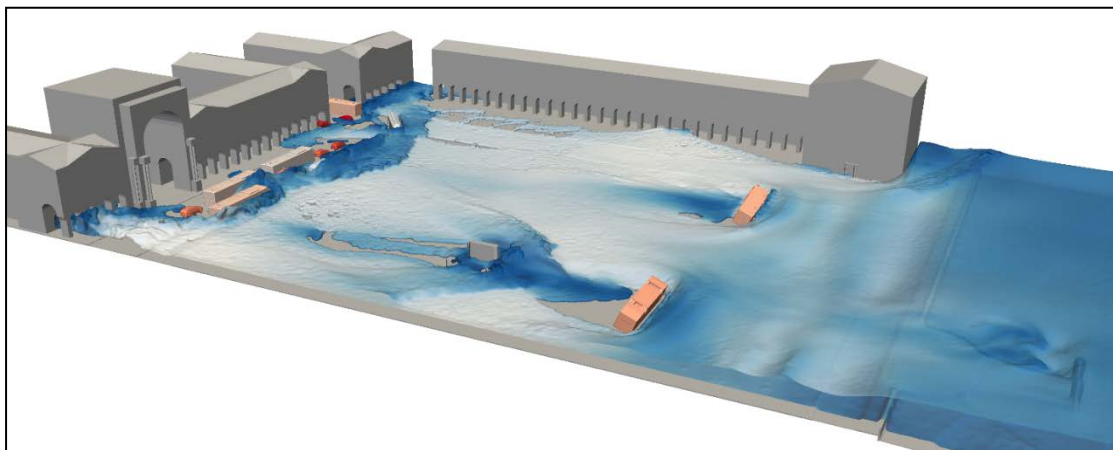


**Figure 6.** Results of the 3D simulation for  $t = 30s$ .

Figure 7 shows further details of the simulation. Some vehicles at the far end of the square do not show violent motions, mainly due to loss of energy of the wave as it crosses the square. On the east side, however, where the wave is mostly unobstructed, cars, buses and trams are dragged with ease against the buildings. Water accumulation is also notorious, already reaching the top of the galleries. This is due to the dense urban geometry creating sudden contractions for the flow, leading to increased local flow depths. The complete simulation can be seen in [www.fluidmechenv.tk](http://www.fluidmechenv.tk).

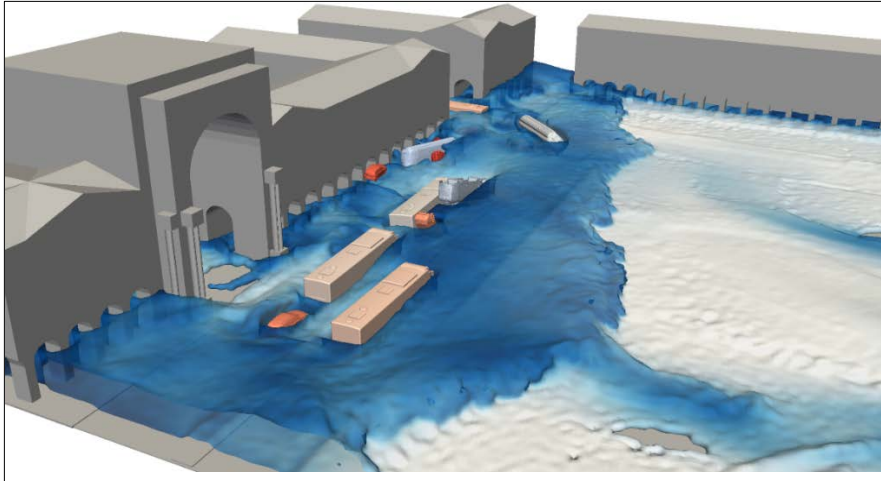


**Figure 7.** Results of the 3D simulation for  $t = 65s$ .

This simulation tool has obvious potential for civil protection agencies. 3D simulations can inform managers on mitigating strategies, test, refine them and simultaneously show the expected outcomes to the population through appealing high quality renders, promoting civil engagement.

#### 4 CONCLUSIONS

This work shows the advantages of considering 2D/3D modelling for highly non-linear cases and inherently multi-scale problems. The proposed hybrid modelling approach presented in this work is based on a 2DH shallow water model, STAV2D, and a fully 3D hydrodynamic and solid transport model, DualSPHysics. Together they constitute both an interesting research tool for the study of tsunami propagation in complex geometries and a powerful and innovative tool to design and test mitigation solutions at the local scale. While 2D simulations are fundamental for the propagation of wave conditions to the interest area, highly resolving fully coupled 3D models can provide a meaningful solution due to the complex geometries and possible mobile objects that make up the urban scenario.

Concerning this last aspect, the potential for civil protection agencies is very high. 3D simulations can inform managers on mitigating strategies, test, refine them and simultaneously show the expected outcomes to the population through appealing high quality renders, promoting civil engagement.

Future work should focus on the coupling of these two modeling strategies under a unified platform, with a common and intuitive interface, allowing the managers to focus on the results and its contextualization and not on the details of the simulation set-up.

#### ACKNOWLEDGEMENTS

This research is partially supported by Portuguese and European funds, within programs COMPETE2020 and PORN-FEDER, through project PTDC/ECM-HID/6387/2014 granted by the National Foundation for Science and Technology (FCT).

#### REFERENCES

- Baptista, M.A. & Miranda, J.M. (2009). Revision of the Portuguese Catalog of Tsunamis. *Nat. Hazards Earth Syst. Sci.*, 9(1), 25-42.
- Canelas, R.B., Crespo, A.J.C., Domínguez, J.M., Ferreira, R.M.L. & Gómez-Gesteira, M. (2016). SPH-DCDEM Model for Arbitrary Geometries in Free Surface Solid-Fluid Flows. *Computer Physics Communications*, 202, 131-140.
- Canelas, R.B., Domínguez, J.M., Crespo, A.J.C., Gómez-Gesteira, M. & Ferreira, R.M.L. (2015). A Smooth Particle Hydrodynamics Discretization for the Modelling of Free Surface Flows and Rigid Body Dynamics. *International Journal for Numerical Methods in Fluids*, 78(9), 581-593.

- Conde, D.A.S., Baptista M.A.V., Oliveira C.S. & Ferreira R.M.L. (2013). A Shallow-Flow Model for the Propagation of Tsunamis over Complex Geometries and Mobile Beds. *Natural Hazards Earth System Science*, 13(10), 2533–2542.
- Conde, D.; Telhado, M.J.; Baptista, M.A.V. & Ferreira, R.M.L. (2015). Severity and Exposure Associated with Tsunami Actions in Urban Waterfronts: The Case of Lisbon, Portugal. *Natural Hazards*, 79(3), 2125-2144.
- Crespo, A.J.C., Domínguez, J.M., Rogers, B., Gómez-Gesteira, M., Longshaw, S., Canelas, R.; Vacondio, R.; Barreiro, A. & García-Feal, O. (2015). DualSPHysics: Open-Source Parallel CFD Solver based on Smoothed Particle Hydrodynamics (SPH). *Computer Physics Communications*, 187, 204-216.
- Ferreira, R.M.L.; Franca, M.J.; Leal, J.G. & Cardoso, .A.H. (2009). Mathematical Modelling of Shallow Flows: Closure Models Drawn from Grain-Scale Mechanics of Sediment Transport and Flow Hydrodynamics. *Can. J. Civ. Eng.*, 36(10), 1605–1621.
- Monaghan, J. (2005). Smoothed Particle Hydrodynamics. *Reports on Progress in Physics*, 68(8), 1703-1759.

## SUDS IN THE UK AND SPONGE CITIES IN CHINA – WHAT PROGRESS IS BEING ACHIEVED IN URBAN FLOOD RISK MANAGEMENT?

RICHARD KELLAGHER<sup>(1)</sup>, BRIDGET WOODS-BALLARD<sup>(2)</sup>, JUAN GUTIERREZ-ANDRES<sup>(3)</sup> & VIVIAN DOU<sup>(4)</sup>

<sup>(1,2,3)</sup> HR Wallingford Ltd, Howbery Park, Wallingford, OX10 8BA, UK  
e-mail: r.kellagher@hrwallingford.com

<sup>(4)</sup> Hydraulic Environment Technology Consulting (Shanghai) Ltd, Shanghai - 200135, PR China  
e-mail: V.dou@hrwallingford.com.cn

### ABSTRACT

The rate of urbanisation in China is higher than anywhere in the world. More than 40,000km<sup>2</sup> of land has been developed over the last 35 years, with the number of cities increasing from 193 to 653 and urban populations rising from 170 to 750 million. The Chinese acknowledge that their cities have grown too fast without adequate consideration of vital environmental risks. Beijing's drainage system was built to serve rainfall runoff based on a 1:1 year or 1:2 year pipe-full capacity. Water management and pollution from urban runoff was not included in rainfall runoff design criteria. The outcome from this is that flooding and river pollution have become urgent issues: annually more than 100 cities are affected by floods; 234 cities suffered from flooding in 2013 alone. In 2014, direct economic losses from flooding were estimated as RMB 157.4 billion (£17.3 billion). The aim of settling an additional 100 million migrant workers in cities over the next 5 years, combined with likely climate change impacts on increasing rainfall intensities, means that economic consequences are significant if these drainage issues are not tackled. Three years ago, the Chinese President announced that new cities and redevelopment would conform to a surface water management 'sponge-city' paradigm and China's state council announced a new set of urbanisation guidelines. This paper compares and contrasts the expectations of moving to new sponge city criteria in China with the sustainable drainage criteria used in the UK. The paper details the requirements for each country and then provides illustrations of the performance of sustainable drainage systems in both the UK and China based on applying the respective criteria. Conclusions are drawn on the current state of surface water management in each country and the changes that might lie ahead.

**Keywords:** LID; SuDS; sponge cities.

## 1 DRAINAGE INSTITUTIONAL STRUCTURES AND LEGISLATION

### 1.1 UK institutional structures and legislation

In England, the government have drawn back on a commitment to legislate within the Flood & Water Management Act (2010) to deliver statutory national standards for making sustainable drainage systems (SuDS) mandatory for any drainage scheme. The original intention, as recommended in the Pitt review (2008), was that there would be national SuDS Standards enacted in law with the intention of creating a new body within the local authority - the SAB (SuDS Approving Body) for approving drainage proposals and adopting and maintaining these surface water drainage systems. Following a number of years of discussions, the SuDS Standards were developed, but the government did not pass this into legislation and decided not to create the SAB entities. The ownership of SuDS systems therefore remains unresolved as water companies are generally not prepared to adopt them. As a result, private management companies are being created to own and manage SuDS surface water systems.

Guidance on how to design SuDS systems has been produced, but these standards are advisory and not enacted in law. In England, these non-statutory standards (Defra, 2015) are primarily focused at flood protection and not their other multiple benefits associated with SuDS. These guideline standards officially only apply to developments of more than 10 properties, though fortunately most authorities are applying them to all planning applications whatever the number of properties or type of development. As a result of the relatively luke-warm position on applying SuDS taken by the government, the application of SuDS in new developments is not maximising the opportunity that they offer.

The UK actually comprises of 4 countries (England, Wales, Scotland and Northern Ireland). The subject of drainage has been devolved to each country, so there are actually a range of slightly different criteria applied in each country with these differences mainly relating to the water quality and other benefits associated with SuDS. The standards for Wales (Welsh Government, 2016) and Scotland (SUDSWP, 2016) also extend the requirements in England by adding guidance on prioritising the runoff destination based on a hierarchy of preferred destination (preferring rainwater harvesting and infiltration over runoff directed to surface water

systems). In terms of water quality treatment, specific guidance is given on preventing any runoff from taking place from a new site for a significant proportion of all frequent rainfall events, and this is called Interception. The objective of this Interception criteria is to maximize the protection of the morphology of receiving surface waters. Interception is recommended to be the prevention of any runoff for the first 5mm of any rainfall event. To account for the variability of catchment wetness, this criterion has a probabilistic application which allows 20% failure of meeting this target for summer months and 50% failure to comply in winter months. At present, although the benefits of Interception is promoted and known about, it is rarely asked for by planning authorities or designed for by drainage engineers.

## 1.2 China institutional structures and legislation

China has now recognised that its rapid urbanisation is environmentally unsustainable and potentially detrimental to future economic security. China's New Urbanisation Planning Guidance (2014-2020) (State Council of the PRC, 2014) clearly sets out that the country must enter a new era of quality-oriented transformation, ensuring that development does not occur at the expense of natural resources, environmental pollution and ecological degradation. The Conference Report at the 18th Communist Party of China congress (Jin, 2012) promotes a requirement for an 'ecological civilisation' concept – with the construction of 'sponge cities' as a key to sustainability. A 'sponge city' is defined as development that prioritises the natural attenuation, infiltration and purification of stormwater runoff, using systems that are resilient and adaptable, that absorb (and can then release) water for use and in so doing reduce flood risk, protect water resources and enhance ecological systems. The sponge city principles are stated as "infiltrate, detain, store, cleanse, use and drain". The SuDS terminology used in China is 'Low Impact Development' (LID) (a term created in the USA several years ago) and the design objectives for such development are presented in Figure 1. LIDs in USA and SuDS in UK are effectively the same approach to achieve sustainable drainage management though LID can be considered to have greater emphasis at plot scale drainage elements.

New cities in China are now required to consider using LIDs at all stages in their development; integrating stormwater control with public and private space design, architectural building design, transportation networks, drainage and water supply infrastructure. Regional planning controls must set LID objectives for surface water management and the design criteria should reflect local objectives, hydrology, weather and land use conditions. The aim is to ensure city specific goals are optimised both technically and economically so that solutions provide 'efficient investment' for the region.

Local government urban construction bureau or other government bodies will normally approve LID designs in order to facilitate the implementation process. Local government will also take ownership of these systems with funding secured from a range of sources including central and local government, private-public partnership initiatives, and non-government funds or grants.

During 2015/2016, the China Ministry of Finance selected 30 cities to be pilot sites under the Sponge City Plan. Each city receives between 400 and 600 million RMB (£47-£70 million) annually for 3 years, with the total investment estimated to be about 42.3 billion RMB (£5 billion). Local supporting funding is required and public-private partnerships (PPP) are being actively encouraged; cities receiving a 10% funding bonus from central government if the PPP contribution exceeds a certain percentage of the overall budget. Preliminary estimates put total investment on Sponge City implementation at 100-150 million RMB/km<sup>2</sup> (£120,000/ha - £170,000/ha).

## 2 SURFACE WATER DESIGN CRITERIA

### 2.1 UK SuDS surface water design criteria

In the UK, the spectrum of design criteria for SuDS/LID broadly fit into four categories: water quantity, water quality, amenity and biodiversity (see Figure 2). The SuDS Manual (Wood-Ballard, 2015) is the principal document from which the individual country guidance is based. This has ensured consistency on design criteria between all the regulatory guidance that has been issued.

The surface water drainage design criteria in England has two objectives; managing the runoff from new development so that it minimises any additional flood risk in areas downstream of the site created by the construction of additional paved surfaces, and secondly, drainage criteria is defined to set a minimum standard for the frequency of flooding. For flood risk protection downstream, the focus is on peak flow control based on greenfield conditions (pre-development runoff) for the 1:1 year and 1:100 year return period events and volume control associated with pre-development runoff for the 1:100 year, 6 hour event. Flood risk protection on the development site itself aims to provide no flooding for the 1:30 year event and no property flooding internally for the 1:100 year event.

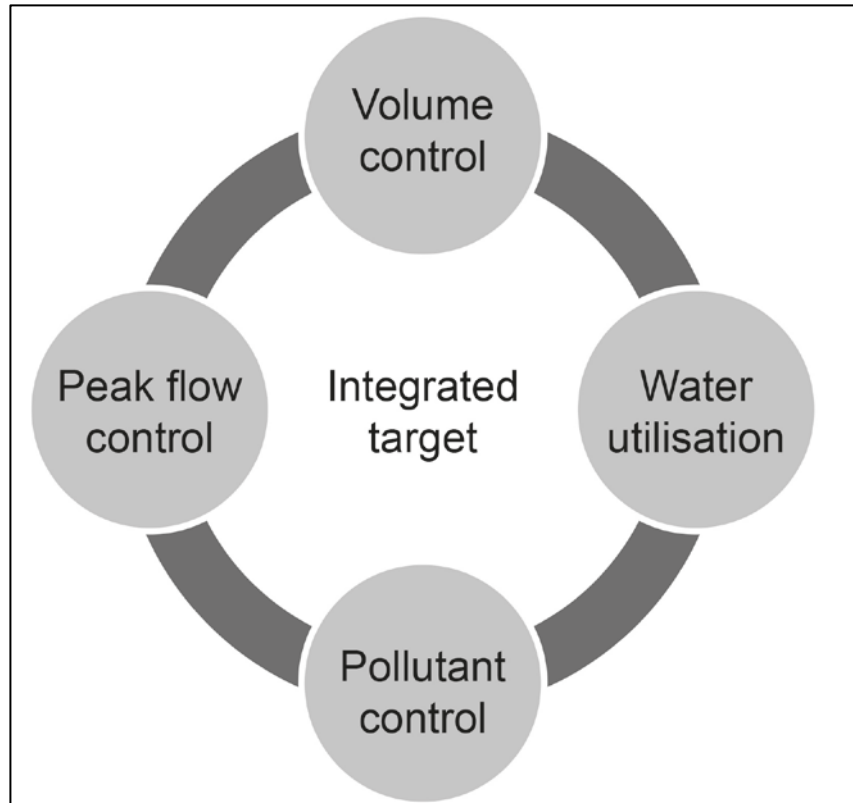


**Figure 1.** Diagram showing China's LID Control Objectives

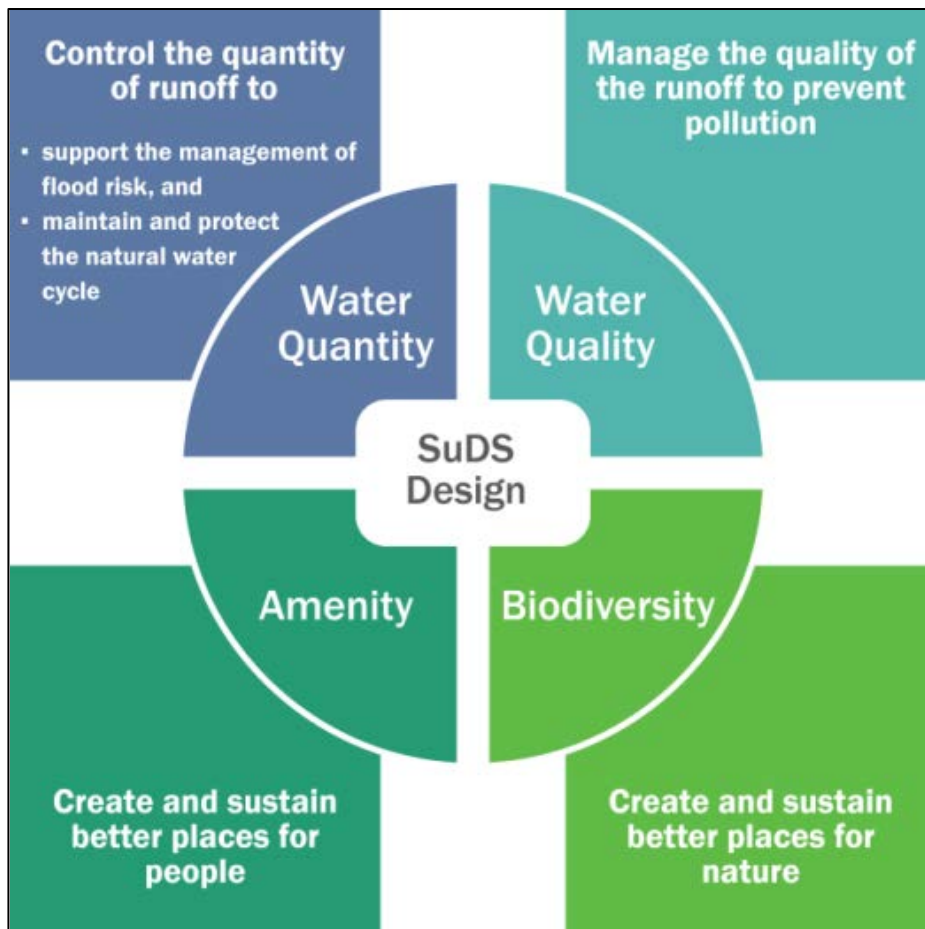


**Figure 2.** The UK design objectives for SuDS (Woods Ballard et al., 2015)

## 2.2 China Sponge city surface water design criteria

In China, sponge city projects need to comply with the “Sponge City Construction Technical Guidance” (Ministry of Housing, PRC 2014) which specifies the following key objectives:

- Total Annual Runoff Volume Control Rate - the proportion of the total rainfall volume that should be infiltrated, used or otherwise retained on site. The target of 60-90% retention is a variable based on city specific conditions.
- Peak Flow Control – requiring compliance with Outdoor Drainage Design Specifications (GB50014) (Mouhurd, 2006) for city flood risk management and drainage system standard of service design.
- Rainwater Harvesting – the proportion of rainfall across the year (a value set by each city) that should be harvested to support local water resource needs.
- Runoff Pollution Control – LID delivery of suspended solids removal rates of 40-60%.
- Standard for flood protection - has been raised to 1:5 years for no flooding on the surface.

Other supporting objectives include the ecological remediation of land adjacent to natural water bodies, the maintenance and protection of stable long term groundwater levels, and the alleviation of potential negative urban heat island effects resulting from the development.

Interpretation of the annual volume control of runoff has been developed based on a similar concept to that of Interception. While Interception in the UK is set at an event of 5mm with a seasonal probabilistic level of compliance, in China, a design rainfall event of a specific depth is obtained from a table provided by the guidance for implementing the sponge city concept. The depth of the design event is a variable derived for each city and linked to the proportion of runoff (between 60% and 85%) that is to be achieved. The design rainfall depths range from 4mm through to 14mm for a 60% volume reduction and 9mm through to 34mm for 85% reduction. The analysis carried out for deriving these rainfall depths was based on assessing the total annual rainfall volume for all events greater than 2mm and selecting the rainfall depth that gave a cumulative rainfall volume for the target reduction.

The interpretation of 60% – 90% volume reduction is not based on the volume that would runoff from a traditional pipe drainage system, but is based on the gross rainfall depth across the whole area; whether it is paved or vegetated.

## 3 DELIVERING TOTAL RUNOFF VOLUME CONTROL AND SURFACE WATER USE

HR Wallingford carried out an analysis of the impact of applying the Interception criteria in the UK and also was involved in supporting a volume reduction analysis for a sponge city in China. While the study in the UK was applied at a micro scale for theoretical application of SuDS on a development, the study in China was carried out using LIDs at the macro scale for 10 pilot areas across the city. These two studies assessing the reductions in the volume of runoff are first detailed and then compared.

### 3.1 UK surface water runoff management for Interception

As outlined earlier, a probabilistic approach to Interception with a target retention of 5mm for all rainfall events is the design criterion used in the UK. Both the probabilistic seasonal targets and minimum rainfall depth are potential variables depending on the location and the impact of the runoff, but unlike China where the target design criteria is chosen based on city specific requirements, the UK criterion is the same across the whole country. Five millimetres of rainfall may seem very unambitious, but in the UK for most urban areas, this represents the majority of the number of rainfall events (based on an inter-event period of 6 to 12 hours). In practice, the constraints of soils with low infiltration rates, unsuitability of infiltration, and the limited use of rainwater harvesting, means that even this target criterion is seen as being quite challenging.

The only accurate way to assess compliance with this criterion is to run a model of the system using continuous time series rainfall. The model needs to represent runoff from all surfaces with an appropriate model – taking into account the increase in runoff with wetness and also explicitly modelling the effects of depression storage on paved surfaces and soil moisture for vegetated areas. A fixed percentage runoff factor is therefore not really appropriate as the proportion of runoff for the many small events will be quite low compared to larger events. Each SuDS unit must be represented for all the relevant processes of soil moisture, evaporation and infiltration. Even very low infiltration rates can be very effective in reducing the volume of runoff through the year.

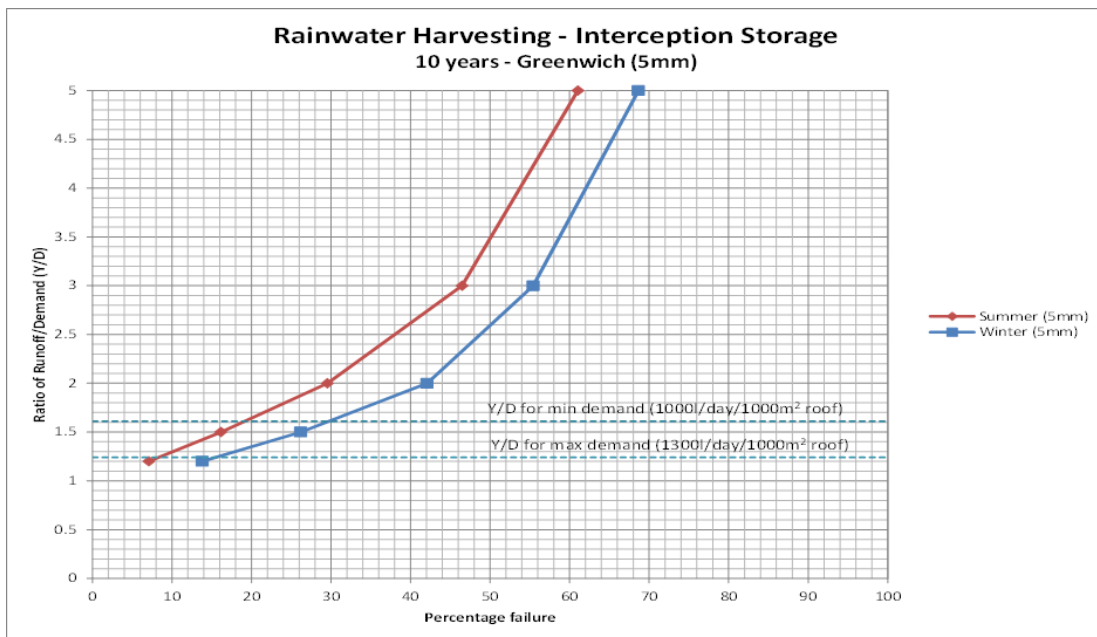
A study was carried out on Interception by HR Wallingford (2014) to look at the relative effectiveness of different SuDS. Various assumptions were made on the design of each type of SuDS unit and the results were processed to provide monthly performance of volume reduction and compliance to meet the probabilistic based Interception criteria of 5mm. This analysis used continuous 5 minute resolution rainfall for a 10 year period.

Taking an example of a typical rainwater harvesting system: the Yield / Depth (Y/D) ratio represents the relationship between the average roof water yield (Y) over the year and the average demand (D) for non-potable water by the property. It can be seen in Figure 3 that a Y/D loading factor of around 1.5 ensures more than 80% compliance in summer and more than 70% compliance in winter. This fits well with the design

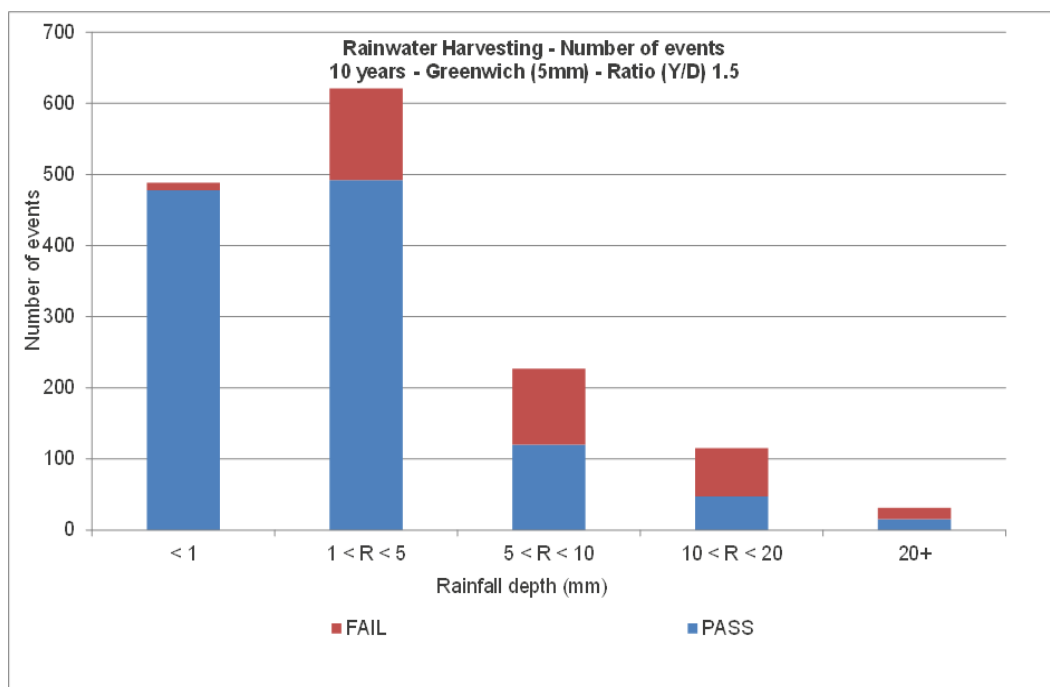
approach to toilet flushing used by supermarkets of Y/D ratio ranging from 1.25 to 1.6. However, if the roof area increases relative to the demand for non-potable water, (the Y/D ratio becomes larger) compliance to the seasonal probabilistic criteria drops off for the proportion of events for which the first 5mm is retained.

Figure 4 breaks down the rainfall events into depth categories which illustrate that even very small events can “Fail” to store the design 5mm rainfall depth. This happens when the roof has recently had rainfall which has filled the storage tank of the rainwater harvesting system. By inspection of the graph in Figure 3, it can be seen that the total compliance of 100% in both seasons would be achieved if Y/D is 1.0 or less.

Figure illustrates a volumetric assessment of the amount of rainfall retained on site and the amount discharged off site. It can be seen that even though 5mm might be considered to be a very unambitious target to be used to protect stream morphology, it is extremely effective in preventing the majority of the rainfall through the year from leaving the site. It is only in the wetter periods in autumn and winter as well as larger events, that significant amounts of runoff leaves the site. The reduction in the volume of runoff can be seen to be of the order of 67% of the net rainfall for the year for a Y/D ratio of 1.5.



**Figure 3.** Performance of rainwater harvesting for Interception storage of 5mm



**Figure 4.** Rainwater harvesting: Number of events that Pass or Fail retention of 5mm – Y/D of 1.5.

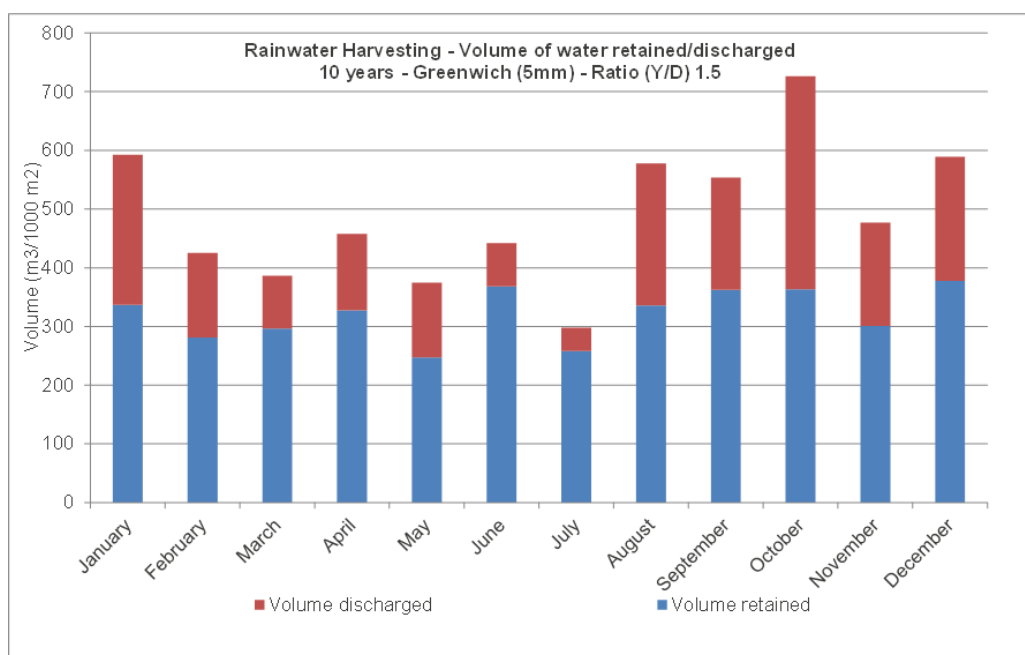


**Figure 5.** Rainwater harvesting: Volumes of runoff retained on site and discharged off site – Y/D factor 1.5.

It is important to recognize that different types of SuDS are effective in different ways. Those that depend on evaporation will be more effective in summer than winter compared to constant loss models such as rainwater harvesting or infiltration systems. Figure 6 shows the results of the analysis for a swale which has both evapotranspiration and infiltration modelled. Evapotranspiration varies from 3mm/day in mid-summer to 0.5mm/day for mid-winter. Infiltration was assumed to be  $1 \times 10^{-5}$  m/s which was the minimum rate of infiltration that would normally be considered for the use of soakaways. A soil store of 50mm was assumed along with an above surface temporary store of 200mm before flows pass forward and discharge from the site. The loading condition for this example shown here was 50 to 1 i.e.  $50 \text{ m}^2$  of paved area running off to  $1 \text{ m}^2$  of swale.

Analysis of the results showed that the probabilistic compliance to retaining the first 5mm was 97% in summer and 88% in winter. It can be seen from Figure 6 that the larger storms in August and October generate more runoff from the site, but very little runoff takes place through the rest of the year.

This swale arrangement shows that the volume of runoff through the whole year can be reduced by 80%. The effectiveness for protecting the river from pollution and other morphological damage is therefore very high. What is remarkable is that this only requires 2% of the land to be allocated to a vegetated system where it is designed to maximize its potential and effectively utilise even low rates of infiltration.

#### 4.1 China surface water runoff management for Interception

The China sponge city LID analysis was based on building models of 9 pilot areas across the city and assessing the performance of traditional pipe drainage and LID systems for both flood protection effectiveness, runoff volume reduction and pollution loading on receiving waters.

Although the key drivers in China are environmental protection and water resource resilience, it is early for the implementation of the new Chinese policy, so it remains to be seen which types of SuDS will be most used. However, assuming the policies result in widespread stormwater control using source control approaches, the benefits related to the hydraulic capacity of sewerage systems and the quality and morphology of receiving waters will be significant.

Although the Chinese method is based on the use of a design storm of a small depth ranging from 4mm through to 34mm depending on the volume reduction target and the city it is applied to, the HR Wallingford study used the approach of using a continuous rainfall time series, to obtain a performance assessment for the nine pilot areas of various LID configurations. Figure 7 illustrates the conceptual modelling approach taken for the analyses of these pilots.

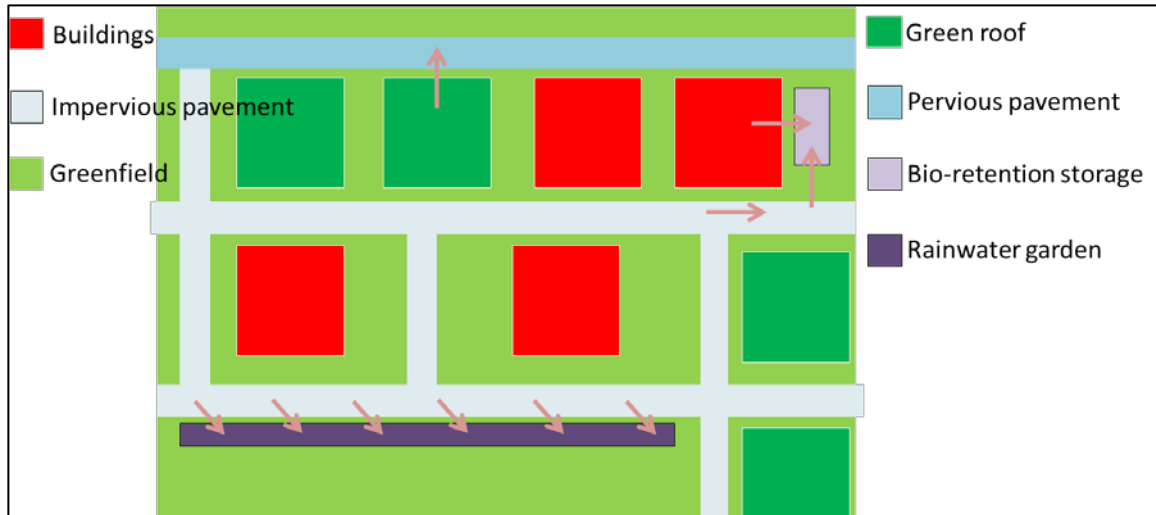


**Figure 7.** Structure of a LID/sponge city subcatchment model

For carrying out the analysis of annual runoff volume reduction, a period of 10 years was assessed for annual rainfall depth and from this, a typical year was selected for the analysis. In practice, a detailed study would consider multiple years and look at seasonal periods to see if there were particular months in which river pollution was taking place, or demand on non-potable water could not be met. 2010 was fairly close to being an average year based on total rainfall depth.

Having selected 2010, the rainfall for the whole year was applied continuously at a 5 minute resolution. Figure 8 shows the 2010 rainfall data that was used. It can be seen that there is a strong seasonal aspect with much of the rainfall taking place in August and with very little rainfall taking place for 9 months of the year.

This information not only illustrates the contrast to the conditions in the UK where rainfall is spread fairly evenly through the year, but also draws attention to the less advantageous use of rainwater harvesting as a cost-effective runoff control mechanism as this will be largely ineffective in providing non-potable water for the majority of the year.

The LIDs modelled included green roofs, permeable pavements, bio-retention systems and swales. Infiltration rates were taken to be equal to the soil characteristics for the city and this was taken to be  $6 \times 10^{-5}$  m/s. The modelling was carried out in Infoworks ICM which has the ability to represent all aspects of LID characteristics.

Various combinations of LIDs were applied for each of the nine pilot areas. Table 1 shows the performance of these pilot areas for both traditional pipe based drainage systems and LID arrangements. It should be noted that the reduction in volume is based against the total gross rainfall and therefore losses associated with traditional drainage is a function of the runoff model and the assumption of the fixed percentage runoff used for paved and pervious surfaces.

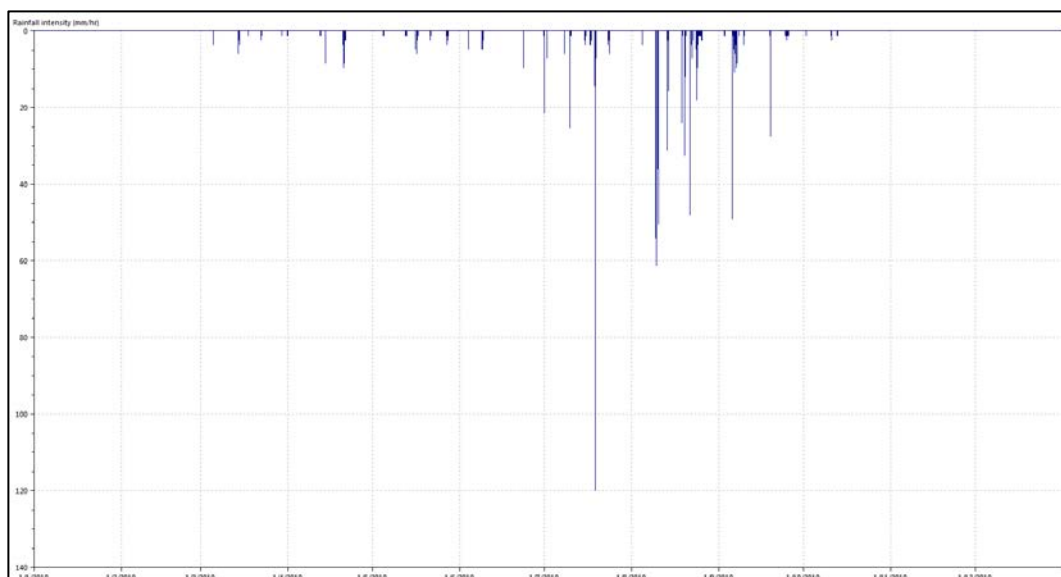


**Figure 8.** Annual rainfall for 2010

**Table 1.** Performance of pilot catchments for traditional drainage and LID systems

Pilot site	Rainfall volume (m <sup>3</sup> )	Volume of runoff	Volume of runoff	Storage in landscape	Percentage retention	Percentage retention
		Traditional drainage (m <sup>3</sup> )	LID drainage (m <sup>3</sup> )	water bodies (m <sup>3</sup> )	Traditional drainage	LID drainage
1	8,750,855	4,313,836	1,906,593	154,210	51%	78%
2	3,427,125	1,715,065	818,988	51,470	50%	76%
3	6,350,335	3,177,269	1,471,832	62,400	50%	77%
4	9,227,297	4,040,639	1,960,463	184,286	56%	79%
5	9,793,443	4,788,218	2,653,456	172,340	51%	73%
6	660,817	395,852	174,659	0	40%	74%
7	3,450,652	1,784,935	748,537	0	48%	78%
8	21,336,448	9,978,947	4,168,018	428,288	53%	80%
9	21,866,445	9,289,269	3,953,564	637,447	58%	82%

The pilot sites demonstrate that there is quite a high level of reduction in runoff volume compared to the gross rainfall even for traditional pipework systems with retained rainfall volumes ranging from 40-58%. However, the use of LIDs increases this to losses of between 74% and 85% depending on the pilot area and the use of LIDs.

From this study, it can be seen that sufficient application of LIDs across a city can achieve between 70% and 85% reduction in runoff volume compared to the gross rainfall falling on the area. This represents a 50% increase in the reduction of runoff compared to volumes of runoff from traditional drainage systems.

## 5 CONCLUSIONS & CHALLENGES

The sponge city aspirations of China can be said to lead the world in terms of aspiring to having sustainable drainage systems at the city scale focused at surface water volume reduction.

The concept of using a design rainfall depth to design LIDs to meet volume reduction targets aims to be a short cut to avoid the use of time series rainfall, but such analysis provides the engineer with little understanding of relative SuDS performance and does not provide evidence of compliance to the standard. These two studies do show that, even though climate and weather conditions are very different in the UK and

China, the effectiveness of SuDS / LIDs in removing runoff volume is very great and similar levels of reduction in runoff volume can be achieved.

What remains uncertain is whether the UK will progress down the route of designing for Interception without a strong lead from regulatory authorities seeking to improve water course quality. It is hoped that the lead taken by China and the similar approaches now being pursued in other countries will lead to increased pressure on improved SuDS implementation in the UK.

In the case of China, there appears to be the will to progress the use of LIDs at a national scale to protect the environment from the polluting impact of cities, but the details as to what LIDs will be used is still to be established along with the development of effective drainage design procedures.

To secure significant economic impacts from the use of LIDs (e.g. through water quality improvement, CSO spill reduction etc.) requires their widespread implementation and, for this, retrofit strategies will be required alongside this new policy of sponge cities.

Although the inertia UK on the best practice use of SuDS is not reflected in China, the lack of incentives for change and the need for inter-agency and multi-stakeholder coordination at local levels is limiting the progress. Although China also has a need to ensure cross-stakeholder collaboration, this does not seem to be the impediment to LID take-up as it is in the UK.

## REFERENCES

- China Ministry of Housing and Urban-Rural Construction (MHURC) (2014). *Technical guidelines on Sponge City construction—Low impact development stormwater management system*. 2014.
- Defra (2015) *Non-statutory technical standards for the design, maintenance and operation of sustainable drainage systems to drain surface water, PB14308*, Department for the Environment, Food and Rural Affairs, London, UK

- Floods and Water Management Act (2010). UK Government.
- Jin T, Hu (2012). *Conference Report, The 18th National Congress of the Communist Party of China*, Beijing, Nov. 8, 2012
- MOUHURD (2006), *Outdoor Drainage Design Specs (GB50014)*, Beijing, 2006
- Pitt, M (chair) (2008). Learning Lessons from the 2007 Floods.
- State Council of the P.R.C, (2014), *China's New Urbanisation Planning Guidance (2014-2020)*, State Council of the P.R.C, Beijing, 2014
- SUDSWP (2016) *Water Assessment and Drainage Assessment Guide*, Sustainable Urban Drainage Scottish Working Party.
- Welsh Government (2016) *Recommended Non-Statutory Standards For Sustainable Drainage (Suds) In Wales - Designing, Constructing, Operating And Maintaining Surface Water Drainage Systems*, January 2016. Welsh Government.
- Woods Ballard, B, Wilson, S, Udale-Clarke, H, Illman, S, Scott, T, Ashley, R & Kellagher, R (2015) *The SuDS Manual, C753*, CIRIA, London, UK. ISBN 978-0-86017-760-9.
- Kellagher R. (2014) *Supermarket Representation For Suds Guidance: Interception Storage Analysis. MAM7091*. HR Wallingford.

